Simulation of Complete Geobag Revetment Failure Processes

By

Leila Khajenoori

Submitted for the degree of **Doctor of Philosophy** in

Civil Engineering

Heriot-Watt University

Energy, Geoscience, Infrastructure and Society / Institute of Infrastructure and environment

July. 2019

Abstract

Geobag revetments have recently emerged as long-term riverbank protection measures in developing countries, however, their performance is still not well understood. According to previous research by Heriot-Watt University and The University of Edinburgh, the initial failure mechanisms associated with simple geobag riverbank revetments are now relatively well understood and numerical modelling has advanced to the stage where incipient failure can be simulated using Discrete Element Modelling (DEM). However, to develop the type of robust design standards needed to improve the effectiveness and durability of geobag installations, the essential next step is to develop numerical techniques to efficiently simulate the complete failure of geobag structures.

In order to improve our understanding of geobag–water flow interactions and gather the data required to calibrate and validate the numerical model, a comprehensive programme of small-scale experimental tests was undertaken. Comparison of a range of different construction methods and revetment side slopes subjected to different flow loading was carried out. The results indicate that whilst failure mechanisms are highly dependent on water depth and revetment slope, the construction method had no noticeable impact and it was concluded that the dominating factor is the friction between individual geobags, which itself is dependent on bag overlap rather than specific construction method. Furthermore, flow velocity measurements taken during both the pre-failure and post-failure stages indicated that the formation of failure zones leads to a decrease in turbulence, and a subsequent stabilization of the failure process.

In the second part of the research a Discrete Element Method (DEM) model was constructed using the LIGGGHTS open source software with drag and lift models applied to a multi sphere simulation of the laboratory model geobags. The validated DEM model could reproduce very well the complete failure processes of the geobag revetment, mounted on a fixed bed and also on a mobile sediment bed. Finally, it is found that the DEM model could provide more details on the performance of geobag revetment in riverbanks.

Based on the results found, it can be concluded that the developed DEM model can satisfactorily simulate the complete failure of geobag revetments and hence be the basis for the development of future deign guides. Finally, recommendations on the application of DEM model for design guidelines of geobag revetment are outlined.

DEDICATION

To my parents, my husband and my lovely son for their patience and continuous support throughout my study.

ACKNOWLEDGMENTS

This work was performed with the help and support of many people. I would like to thank them from the bottom of my heart:

First of all, I would like to acknowledge Heriot Watt University for providing funding for this study.

My deep gratitude goes to Dr. Grant Wright and Professor Martin Crapper for selecting me as the recipient of the scholarship and providing me an excellent opportunity to work in the rewarding working environment of the Institute for Infrastructure and Environment at Heriot Watt University. Without proper guidance, advice and suggestions from them, this research would have never been completed.

I would also like to thank Mr. Tom Ferguson for the technical support during my work in the Hydraulic laboratory at Heriot Watt University. Also, the logistic support I received from the other school staff, namely Mr. James Maguire and Mr. Alastair Macfarlane are highly appreciated.

I thank all my friends from both Heriot Watt University and the University of Edinburgh. Their love and compassion are the most valuable treasures in my life.

Thanks to my parents, who have always supported me and despite the thousands of kilometres that we were apart, made me feel that they were always near to me.

Lastly, but with my most sincere love and gratitude, I would like to thank my dear husband Mehrzad and our lovely son Amir for their unconditional love and support during my study. Mehrzad has always inspired me, kept me motivated and his strong support has helped me to overcome crucial moments not only during this PhD journey but also in my life. His love and comprehension are the most valuable treasures in my life.

HERIOT WATT UNIVERSITY

Research Thesis Submission

Please note this form should be bound into the submitted thesis.

Name:	Leila Khajenoori		
School:	School of Energy, Geoscience, Infrastructure and Society (EGIS)		
Version: *(i.e. First, Resubmission, Final)*	Final	Degree Sought:	PhD in Civil Engineering

Declaration

In accordance with the appropriate regulations I hereby submit my thesis and I declare that:

1. The thesis embodies the results of my own work and has been composed by myself
2. Where appropriate, I have made acknowledgement of the work of others
3. The thesis is the correct version for submission and is the same version as any electronic versions submitted*.
4. My thesis for the award referred to, deposited in the Heriot-Watt University Library, should be made available for loan or photocopying and be available via the Institutional Repository, subject to such conditions as the Librarian may require
5. I understand that as a student of the University I am required to abide by the Regulations of the University and to conform to its discipline.
6. I confirm that the thesis has been verified against plagiarism via an approved plagiarism detection application e.g. Turnitin.

ONLY for submissions including published works

Please note you are only required to complete the Inclusion of Published Works Form (page 2) if your thesis contains published works)

7. Where the thesis contains published outputs under Regulation 6 (9.1.2) or Regulation 43 (9) these are accompanied by a critical review which accurately describes my contribution to the research and, for multi-author outputs, a signed declaration indicating the contribution of each author (complete)
8. Inclusion of published outputs under Regulation 6 (9.1.2) or Regulation 43 (9) shall not constitute plagiarism.

* *Please note that it is the responsibility of the candidate to ensure that the correct version of the thesis is submitted.*

Signature of Candidate:	*Leila Khajenoori*	Date:	27/05/2020

Submission

Submitted By *(name in capitals)*:	LEILA KHAJENOORI
Signature of Individual Submitting:	
Date Submitted:	

For Completion in the Student Service Centre (SSC)

Limited Access	Requested	Yes		No		Approved	Yes		No	
E-thesis Submitted (mandatory for final theses)										
Received in the SSC by *(name in capitals)*:						Date:				

TABLE OF CONTENTS

LISTS OF TABLES

LISTS OF FIGURES

LIST OF PUBLICATIONS

- Khajenoori L., Wright G., Crapper M.," SIMULATING GEOBAG REVETMENT FAILURE PROCESSES" 37th IAHR World Congress, August 13 – 18, 2017, Kuala Lumpur, Malaysia

- Khajenoori L., Crapper M., Wright G.," Evaluating the performance of Geobag revetment using DEM method", to be submitted.

- Khajenoori L., Wright G., Crapper M.," Laboratory investigation of geobag revetment failure processes", under review.

List of Symbols

Nomenclature

F_L: Lift force

F_D: Drag force

F_G: Gravitational force

C_L: Coefficients of lift force

C_D: Coefficients of drag force

C_M: Coefficients of inertia

α: Slope angle of the revetment

D_{50}: Average soil particle size

m: Mass

P: Interaction force between two particles in Hertz contact model

Y: Young's Modulus

R: Radius

υ: Poisson's ratio

E: Stiffness

ξ_0: Surface energy

G: Shear modulus

Kn: Elastic constant for normal contact

Kt: Elastic constant for tangential contact

e: Coefficient of restitution

L: length of geobag

x: x direction

y: y direction

z: z direction

u: Stream-wise velocity

v: Transverse velocity

w: vertical velocity

TKE: Turbulent kinetic energy

τ: Reynolds shear stresses

TI: Turbulence intensity

μ: viscosity

ρ: density

Subscript

ave: average

HW: horizontal well

x: x-direction

y: y-direction

z: z-direction

Abbreviations

ADV: Acoustic Doppler Velocimetry

DEM: Discrete Element Method

CFD: Computational Fluid Dynamics

Chapter 1. INTRODUCTION

1.1. Motivation

Since the beginning of history, people have tended to live in riverside areas. Hence, protecting riverside areas has been a significant concern for most human societies. One of the most common problems in rivers which flow through low-lying alluvial plains is riverbank erosion. Morphologically, riverbank erosion can lead to changes in the characteristics of river channels and flood zones, which in turn can lead to the loss of fertile agricultural land, damage to properties and danger to human and animal life. For example, more than 8,000 hectares of riverside lands are lost due to bank erosion annually in Bangladesh (Rahman, 2010). On the other hand, riverside zones are one of the most valuable and sensitive ecosystems. Therefore hard protection measures need to be minimised. In recent years, investigating new sustainable alternatives for riverbank protection which retain visual harmony with the environment as well as the reversibility of engineering measures has received much attention.

Geobag (sand-filled geotextile bags) revetments have recently emerged as long-term riverbank protection measures in developing countries, primarily due to their effectiveness, low cost and ready availability (Zhu *et al.*, 2004; JMREM, 2006; NHC, 2006; Akter *et al.*, 2011; Oberhagemann and Hossain, 2011). Since standard bank protective structures tend to be expensive, large in scale and incompatible with the environment, geotextile bags filled with locally available sand can be a suitable substitution for other countermeasures such as riprap or concrete units which are generally used to protect riverbanks from erosion (Figure 1.1)

The application of geobags to protect coastline has been proven to be environmentally and economically advantageous (Recio and Oumeraci, 2009a). The potential advantages and disadvantages of applying geobag structures to protect riverbank are listed as follow:

Advantages:

- Geobag revetments can be successfully applied as riverbank protection structures to counter conventional river problems.
- Geobag revetments are resistant against river-related natural hazards specifically during the flood season.

- Geobags can provide the necessary flexibility to respond adaptively to different site conditions and changes of the morphological foundation.
- The use of geobag compared to traditional materials could significantly reduce the total costs of construction and life cycle. This benefit can be due to the possibility of using locally available sand, less work volume and decrease of sophisticated equipment and high-skilled labour requirement.
- Geobag revetments have shown flexibility to deal with cyclic hydrodynamic loads because of unpredictable river behaviour.
- Sand or local flora usually cover geobags, and consequently, structures would have a pleasant and "natural" appearance.
- In the case of unsuccessful engineering measures, geobags can be easily removed.
- Compared with traditional hard, geobags are extremely user-friendly, they add to local amenity and reduce the potential for injury and public liability.
- The flexibility of geobag structures allows improved environmental amenity, through focussed planting or integration with the surrounding environment.

Disadvantages:

- Specific site conditions are required to design and construct geobag structures.
- Lack of deep understanding of the performance of geobag structures under different hydraulic conditions.
- Lack of comprehensive design guideline which can deliver the safety requirements under different conditions.

The performance of geobag revetments and their stability are affected by several factors which cause the failure process of geobag revetment to become a complex mechanism. Figure 1.2 demonstrates different failure zones in a geobag revetment in the Jamuna river due to different failure mechanisms. As a result of previous research, the failure mechanisms associated with geobag revetments are well understood, and numerical modelling has advanced to the stage where incipient geobag displacement can be simulated using Discrete Element Modelling (DEM).

Notwithstanding recent advances, additional research is still required to better understand the performance of geobag revetments in the fluvial environment and to provide the necessary data to inform the development of a numerical model capable of

simulating complete revetment failure, both of which are required to develop much-needed revetment design guidelines.

(a) Mechanically installation - Sungai Tenglu River, Johor Malaysia. (TenCate, 2018)

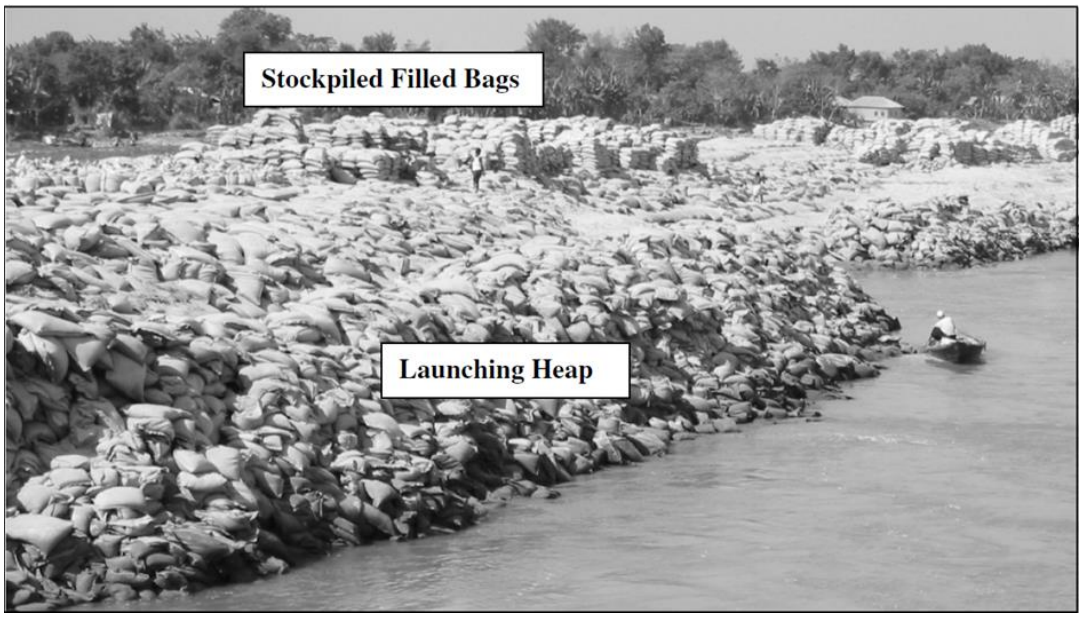

(b) Dumped from launching heap - Pirdp 2002. (Oberhagemann *et al.*, 2006)

Figure 1.1: Geobags for riverbank erosion protection.

(A)

(B)

Figure 1.2: (A, B) Failure zones in geobag revetment using in the Jamuna riverbank (Akter *et al.*, 2009)

1.2. Research Aim and Objectives

The topic of this research is the simulation of the complete geobag revetment failure processes. Based on this topic, research questions have been determined, and the research aim, and objectives have been recognised in this section.

1.2.1. *Research Question*

According to the topic of this research and the literature gaps identified in Section 2, the main research questions are formulated as follows:

1. How changes in water flow conditions due to geobag displacements, or vice versa, lead to the complete failure processes of geobag revetment?
2. At what stage of the failure process of geobag revetments does the role of hydrodynamic forces (drag forces and lift forces) become more significant?
3. How can complete failure processes, incorporating geobag/water feedback mechanisms, be efficiently simulated?
4. How to use the numerical model as a tool to develop design guidelines?

1.2.2. *Aim and Objectives*

In order to answer the research questions, the research aim is identified, and research objectives are classified. The main aim of this research is to:

"Fully predict failure processes of geobag revetments in a river through both physical and numerical model studies".

Concerning this aim, the objectives of this research are defined as follows:

i. Conduct a quasi-physical model study to both improve understanding of the complete failure processes of geobag revetments as riverbank protection under hydrodynamic loadings, and to collect data to validate related numerical models.
ii. Determine the most appropriate numerical techniques to simulate the complete failure processes of geobag revetments as riverbank protection
iii. Develop a numerical model capable of simulating the complete failure processes of geobag revetments as riverbank protection
iv. Propose and develop the tools required to develop and improve design guidelines

1.3. Thesis structure

In order to achieve the aim and objectives of the research project, the adopted methodology in this study is briefly illustrated in a conceptual chart presented in Figure 1.3.

In Chapter 2, literature covering different aspects of the hydraulic stability of geobag structures used in coastal and rivers is reviewed and analysed with the purpose of recognising the most important physical factors and hydraulic properties which may influence the stability of geobag structures and ultimately leading to them failing.

In Chapter 3, the adopted methodology is discussed and detailed more precisely.

In Chapter 4, a variety of laboratory tests using a quasi-physical model of geobags revetment are conducted with the intention of identifying, understanding and analysing the failure mechanism of geobag structure, mainly focusing on investigating the impact of the hydrodynamic forces. The investigated features of the geobag revetment in this chapter are (i) failure modes, (ii) hydraulic parameters of the flow, (iii) construction method i.e., running bond and stack bond (iv) revetment side slope (v) the magnitude of failure in each condition (vi) the turbulent properties of flow in pre- and post-failure conditions.

In Chapter 5, available open source Discrete Element Model (DEM) codes (LIGGGHTS) are developed to the stage that complete failure processes of geobag revetment are successfully simulated. In this numerical approach a one–way coupling method is employed to link depth-average velocities, measured in the laboratory, to the DEM calculation applying a drag model for non–spherical particles (Hölzer and Sommerfeld, 2008) and a separate lift model (Yin *et al.*, 2003). DEM model is calibrated and validated to replicate the quasi-physical model features. The DEM model is also further developed to represent the impact of toe scour phenomena on the progression of failure mechanism and outcomes of the model are validated against laboratory result presented by Akter *et al.* (2013).

In Chapter 6, the knowledge obtained from the quasi-physical model tested in the laboratory and the numerical study are used to develop available design guidelines for geobag riverbank protections. Observations and findings analysed and presented throughout Chapter 4, and 5 are elaborated in order to show the application of this research project in the context of evaluating the performance of riverbank geobag revetment. The applicability of this thesis to develop the design guidelines for the geobag revetment preparation in riverbank are discussed, and the relevant comments are finally made.

In Chapter 7, the final conclusions are presented. Furthermore, in case of possible future research, some recommendations are made.

Figure 1.3 below shows the overall methodology used for the completion of this research study.

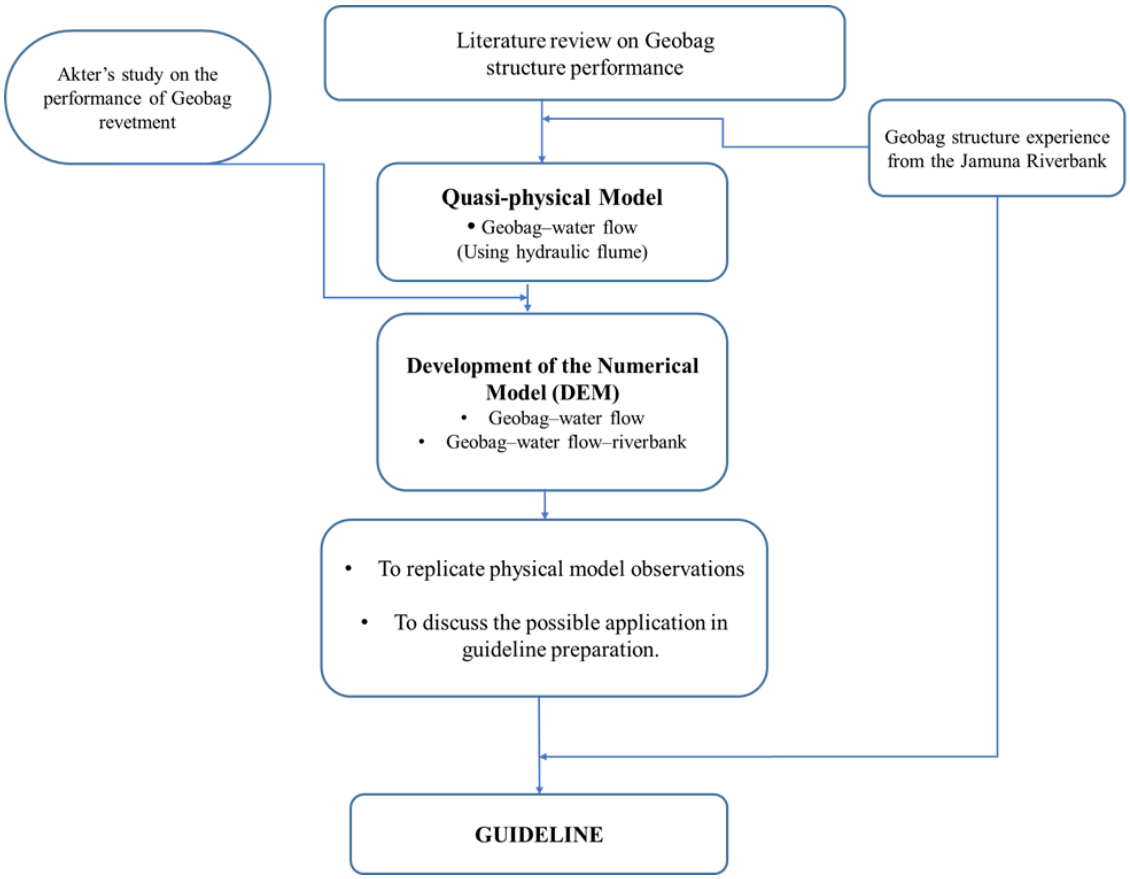

Figure 1.3: Flowchart of the research outline

Chapter 2. STATE OF THE ART REVIEW

In this chapter, the available publications and research which represent the latest findings and knowledge relevant to the hydraulic stability of geobag structures are discussed. Literature related to coastal and riverbank protection work is reviewed and analysed separately, mainly focusing on the details formulated in Chapter 1 as the objectives and methodology of the present study. This chapter is divided into two main sections:

Firstly, a summary of the state-of-the-art knowledge related to the studies investigated geobag for coastal protection is presented.

Secondly, available published research and practical works related to geobag structures used for river protection are reviewed, and accordingly, the state of the relevant knowledge is classified.

2.1. Introduction

Over the past decades, coastal and riverbank protection structures made from sand-filled geotextile bags (geobags) have been used commonly as a substitution for traditional, hard (rock/concrete) structures (Heibaum, 1999; Pilarczyk, 2000). Also, geobags have been widely applied as scouring protections in bulkheads[a] and revetments in coastal, island and bridge abutment applications (Gutman, 1979; Gadd, 1988; Korkut *et al.*, 2007). Geobag protection has been used to control erosion in several parts of the world. Some areas like Yangtze River (Yang *et al.*, 2008) and Changjiang River (Zhu *et al.*, 2004) in China and the Jamuna and Meghna Rivers in Bangladesh (JMREM, 2006) are successful examples of geobag protection to control erosion. As a case study, the Jamuna River in Bangladesh was an object for several studies that have investigated geobag revetment performance using both laboratory and field observations (JMREM, 2006; NHC, 2006).

2.1.1. *Revetments*

A revetment is a type of bank protection measure which is made of erosion-resistant materials to protect bank slopes. For the construction of a revetment, a suitable hard material needs to be employed to reduce the hydraulic load acting on the slope and toe of the river bank and help to stabilise soil against erosive forces of highly turbulent flow and dynamic actions of waves (Rahman, 2010).

Different types of materials are used to construct revetments. In general, the most popular construction materials can be listed as follow: all kinds of rip-rap protection using stones and concrete blocks, articulated blocks and slabs concrete block layers without interlocking, sand-filled geotextiles bags and geo-tubes (Rahman, 2010; Sadik *et al.*, 2011).

[a] The function of a bulkhead is, in protected environments, to retain or prevent the sliding of land at the transition between the land and sea.

2.1.2. *Advantages of geobag revetments*

Among all these materials, since 1999, the emerged technology of geobags has started being popular particularlty in developing countries. Easier installation, cost-effectiveness and technical efficiency are the main reasons that make geobag an ideal substitute for conventional materials such as concrete block, gravel and hard rock.

Compared with rigid conventional materials, geobags reduce the cost of revetment construction by 40% to 60% (Sadik *et al.*, 2011). This reduction is due to less transportation, installation and maintenance cost (Artieres *et al.*, 2010) as well as lightweight equipment and less construction work requirements. In addition, locally available filled material of geobag (sand), easier manufacturing and quality control are their major advantages that facilitate easier implementation of geobags compared to the concrete blocks and boulders (Sadik *et al.*, 2011).

Up to the present time, most of the previous work has studied geobag performance in coastal protection works. The next subsections separately review the key field, laboratory and numerical studies that have been undertaken on geobag revetment performance in coastal and riverbank contexts.

2.2. Geobag coastal structures

There is a history of 50 years of applying sand containers and geobags as hydraulic and marine protection structures. A successful example of coastal protection structures using geobags can be found in several parts of the world, especially in Germany and Australia (Heerten, Jackson, Restall and Stelljes, 2000; Restall *et al.*, 2002, 2005) (Figure 2.1).

Understanding the performance of sandbags (Venis, 1968a; Porraz *et al.*, 1979; Kobayashi and Jacobs, 1985) and geobags (Bezuijen *et al.*, 2004; Recio and Oumeraci, 2009a, 2009c; Recio *et al.*, 2010) in coastal applications has been investigated by several field studies (Heerten, Jackson, Restall and Saathoff, 2000; Heerten, Jackson, Restall and Stelljes, 2000; Pilarczyk, 2000; Bezuijen *et al.*, 2004; Saathoff *et al.*, 2007; Enrica Mori *et al.*, 2008; Heerten *et al.*, 2008), physical modeling (Venis, 1968a; Porraz *et al.*, 1979; Kobayashi and Jacobs, 1985; Gadd, 1988; Grüne *et al.*, 2007; Krahn *et al.*, 2007; E Mori *et al.*, 2008; Recio and Oumeraci, 2009a, 2009c; Dassanayake and Oumeraci, 2012a;

Mudiyanselage, 2013) and numerical modelling (Recio *et al.*, 2010; Mudiyanselage, 2013).

(a) Jumaira Beach Revetment (2003)

(b) Maroochy Groyne (2002)

(c) Narrowneck Artificial Reef (2000)

(d) Stockton Seawall

Figure 2.1: Different applications of geobags as coastal structures all over the world (Restall et al., 2002, 2005; Saathoff et al., 2007).

Stability of geobag structures was the subject of several hydraulic physical model studies for more than 40 years. Mostly, these model tests investigated the hydraulic stability of geobag revetments and geobag-breakwaters exposed to wave attack (e.g. Hudson (1959), Kobayashi and Jacobs (1985); Odgaard and Bergs (1988), Porraz *et al* (1979), Ray (1977), Venis (1968a, 1968b), Pilarczyk, (2000), Oumeraci, (2004) and Recio (2008)).

According to the obtained results from previous studies, the main factors influencing the hydraulic stability of geobag structure related to the hydro-geotechnical processes are presented in Figure 2.2. The most critical factors have been recognised: (i) Displacement of slope-geobag, (ii) wave pressures on geobag structures, (iii) internal movement of sand inside geobags, (iv) permeability of the geobag structure and (v) wave-induced

deformations of geobags (Recio, 2008). However, many uncertainties still exist, thus more investigations are still required.

Findings from these studies have been classified in the following subsections.

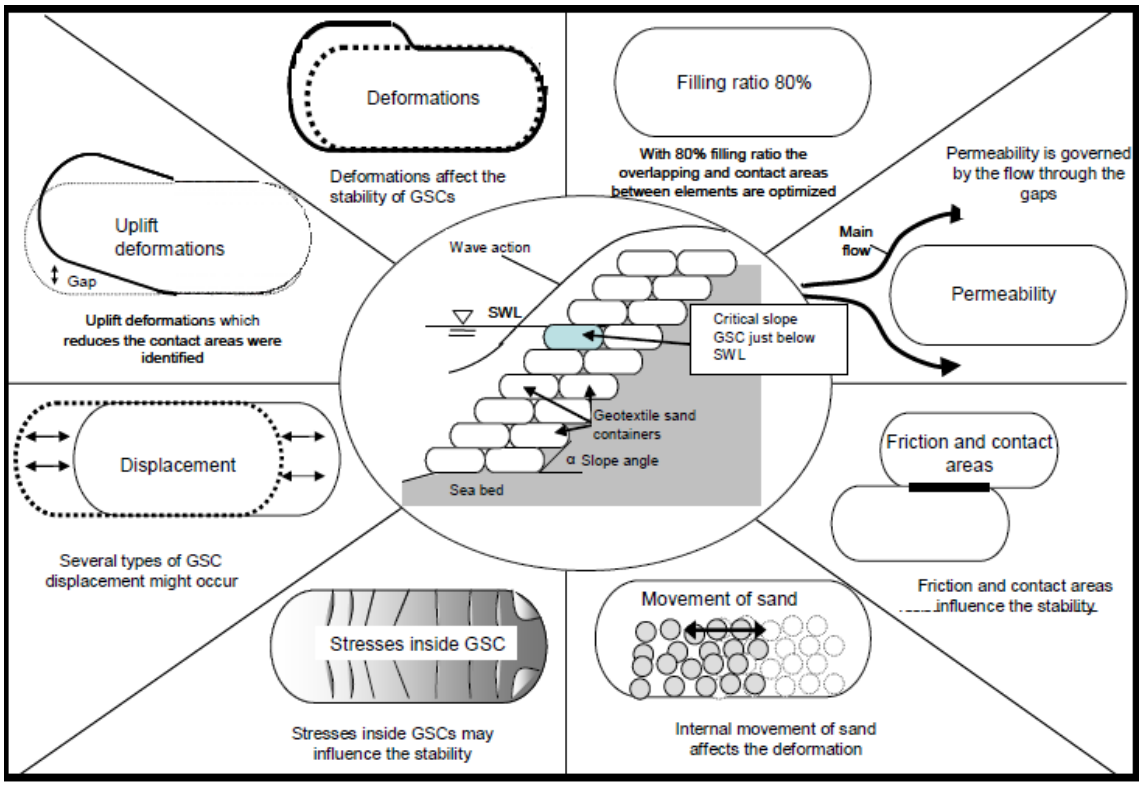

Figure 2.2: Factors which affect the stability of geobag structures (Recio, 2008)

2.2.1. *Physical properties of geobags*

The physical properties of geobags, which influence the hydraulic stability are described in the following sections.

2.2.1.1. Properties of Geotextile Material

The geotextile material which is commonly employed to manufacture geobags has a significant impact on the geobag performance and consequently the stability of geobag-structures. Geotextile materials can be divided into three main types which are knitted geotextiles, woven geotextiles and non-woven geotextiles (PIANC, 2011). In cases that geobag structures are in high tensile strength, woven and knitted geotextiles are recommended. On the other hand, non-woven geotextiles are employed once geobags require deformation abilities, sturdiness and porosity for filtration efficacy (PIANC,

2011). Furthermore, because of the higher roughness of non-woven needle- punched fabrics, a better interlocking is expected between bags made from this type of fabrics (Saathoff *et al.*, 2007).

Therefore, due to the advantages of non-woven geotextile properties, they are efficient in sand container applications for example geobags, so non-woven needle–punched geotextile is widely used in several investigations which consider geobags structures performance (Brand and Pang, 1991; Heerten, Jackson, Restall and Saathoff, 2000; Heerten *et al.*, 2008).

The geotextile fabrics must have sufficient tensile strength and also necessarily need to show enough UV-abrasion and damage resistance to tolerate different environmental conditions (Restall *et al.*, 2002). Gadd (1988) and Saathoff *et al.* (2007) have recommended seam strength to be no less than 80 – 90% of the tensile strength of the material because several loadings (during filling, placement and in-service under wave attack) have to be endured by seams. However, depending on the environmental conditions that geobags need to withstand, geotextiles could be customised during the manufacturing process with the required characteristics.

2.2.1.2. Properties of fill Material

Despite the widely use of sand as the fill materials of geobags in field and laboratory (

Table 2-1), Saathoff *et al.* (2007) suggested using a mixed gravel filter with grain sizes range between 0.1 to 100mm (D_{50} must be between 15 to 25 mm), in the case of employing geobag protection structures in field. This packing of the mixed gravel is filter resistance towards basis embankment soil and could prevent the material from being decomposed.

The degree of saturation affects the geobag weight and the falling velocity during placement (dropping). The intensity of impact on the bottom of the bag decreases with lesser degrees of saturation (i.e. dry sand-fill), due to the increasing capability of the sand to absorb energy during the impact (Bezuijen *et al.*, 2004). On the other hand, moisture content associated with other properties such as grain size and grain distribution can affect the degree of compaction which has been found as an important factor affecting the movement of the material inside the geobag and eventually causes geobag deformation. Fill material with a higher proportion of fine particles and cohesive properties need more time to be fully compacted. Furthermore, the properties of the fill material can

significantly influence the deformability of geobags when they are subject to confined load. Therefore, a stress-strain relationship for woven sandbags was developed by Matsuoka *et al.*, (2001) considering the properties of the fill material and the geotextile material.

2.2.1.3. Geobag size and Sand fill ratio

Several studies have shown that the sand fill ratio of geobags is a significant parameter in the hydraulic stability of geobag-structures (Venis, 1968a; Dassanayake and Oumeraci, 2007; Grüne *et al.*, 2007; Oumeraci and Recio, 2010; Grima and Wypych, 2011). It plays a vital role in the sand's internal movement, and subsequently in the deformability of containers and on how they resist against sliding. It straightly affects the hydraulic stability of a geobag structure.

Table 2-1 summarises the bag size used in different experimental studies with respect to the applied fill ratio. In general, the empty bag size is displayed by the length and width but for filled bag, the thickness might vary with the fill ratio. As Table 2-1 presents, usually the length of 80% filled geobags is twice larger than its width and five times larger than its height (Mudiyanselage, 2013). In the field, in different protection works such as Stockton beach revetment, Maroochy groynes, Jumaira beach revetment, Eider storm surge barrier (Saathoff *et al.*, 2007) and Marina di Ronchi (submerged groin) (Enrica Mori *et al.*, 2008), the length of used bags was 1.22 to 2 times its width.

According to previous studies the typical geobag sand fill ratio used in the field (Pilarczyk, 2000; Oumeraci *et al.*, 2003; Recio and Oumeraci, 2009c; PIANC, 2011) and laboratory (Table 2-1) is 80% and the values of sand fill ratio directly influence the dimensions of filled geobag (Figure 2.3). Oumeraci *et al.* (2009) carried out experimental work to find the optimal fill ratio for the geobags that are employed for protection against scouring phenomena in offshore environments. In their study, they have shown that increasing the sand-fill ratio leads to enhanced hydraulic stability.

Oumeraci and Recio (2010) postulated that the impact of the sand fill ratio on the hydraulic failure of geobag should be systematically investigated. Hence, Dassanayake and Oumeraci (2012) conducted physical model tests to determine which sand fill ratio was optimal for avoiding pullout of geobags (lateral sliding displacement of geobags) from revetment due to wave attack. They tested the hydraulic stability of geobags at different fill ratios and finally they determined the optimum sand-fill ratio to resist against

pullout of the geobags is between 90%-100%. Their result contradicted the findings of previous studies which recommend the fill ratio should not be more than 80%, because stiff geobags are not be able to adjust to the sand bed or surrounding geobags (PIANC, 2011). Dassanayake and Oumeraci (2012) clarified that regarding the pullout, the higher weight and the higher permeability due to greater sand fill ratios (100%) make geobag structures hydraulically more stable than those made with moderate sand fill ratio (80%) (Table 2-1). Therefore, defining an optimum value for sand fill ratio ought to be the subject of future research, and because of its significant impact on the hydraulic stability and the longstanding performance, forthcoming standards and strategies need to investigate the subject of the sand-fill ratio of geobag (Oumeraci and Recio, 2010; Dassanayake and Oumeraci, 2012a).

In Figure 2.3, the dimensions of a flat empty bag are shown by the length (a) and width (b). If used fabric could not stretch and shear, the thickness of the bag varies with the fill ratio. Robin (2004) introduced Equation 2.1 to approximate the maximum theoretical volume (Vmax) of a closed bag which when fully inflated, is given by:

$$V_{max} = a^3 \left[\frac{b}{\pi a} - 0.142\left(1 - 10^{-b/a}\right)\right] \qquad \text{Equation 2.1}$$

Moreover, the sand fill ratio can be estimated based on this theoretical maximum volume (Dassanayake and Oumeraci, 2012a).

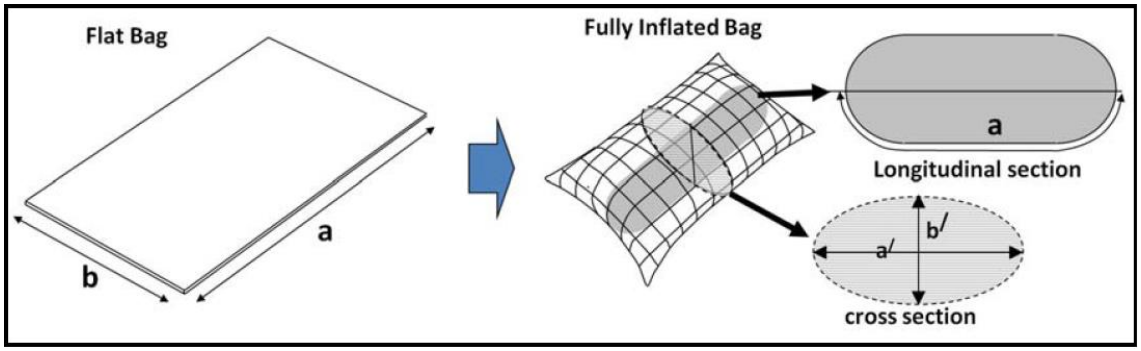

Figure 2.3: Calculation of initial theoretical volume of a geobags (Dassanayake and Oumeraci, 2012a)

On the other hand, to control sand fill ratio in the Jamuna-Meghna River Erosion Mitigation Project, it was found that a bag filled with sand fill ratio of 80% covers 80% of its unfilled (flatter shape) area (length ×width), whereas when fully inflated with the

fill ratio of 100 % (rounded shape, Figure 2.3) it covers only 75 % of its unfilled area (Oberhagemann *et al.*, 2006).

Table 2-1 Physical properties of geobag used in previous coastal experimental studies

Author and Year	Container dimensions Length ×Width ×Height	Filling Material	Filling ratio
(Ray, 1977)	Without filling 2.44 × 1.52m Full 2.15×1.2×0.33	Wet sand, ρs=2000 kg/m^3	75%
(Kobayashi and Jacobs, 1985; Odgaard and Bergs, 1988)	Without filling 12.7×8.9cm; Full 12.4×6.2×3.3cm	Dry & wet sand, ρs=1699 kg/m^3 & 1955 kg/m^3	Unknown
(Oumeraci *et al.*, 2003) (small scale)	Without filling 0.31×0.15 Full 0.25×0.1×0.06m	Sand	80%
(Recio and Oumeraci, 2009c) (2008) and (2009b)	Full 0.25×0.1×0.06m; 0.26 × 0.13×0.052m; 0.35×0.24×0.09m; 0.48×0.24×0.11m;	Sand, ρs=1800 kg/m3	80%
(Coghlan *et al.*, 2009)	0.165 × 0.14 ×0.043m	sand	100%
(Das Neves *et al.*, 2012)	0.13×0.065m 0.24×0.12 m 0.38×0.19m	sand	80%
(Dassanayake and Oumeraci, 2012a)	Full: 0.14×0.07×0.028m 0.14×0.07×0.04m 0.18×0.07×0.024m	Washed sand	80 and 100%

2.2.2. *Mechanical properties*

Many authors have highlighted the importance of the mechanical properties of geobags. However, there has been little work on the impact of the different geobags' properties on the hydraulic stability of geobag structures. In this section, the mechanical properties of geobags, such as permeability, the internal friction between geotextile-geotextile and geotextile-sand, which can affect the hydraulic stability of the geobag structure are the objectives of the literature review. The interdependence of these properties is fundamental as it could considerably influence the stability of geobag structures.

2.2.2.1. Frictional resistance

Kim *et al.* (2004) and Krahn *et al.* (2007) studied the interface shear strength of a pile of sandbags. Krahn *et al.* (2007) conducted an experimental study in which they used a

large shear box to estimate the friction angle under different loads. Their research study has also demonstrated the interface shear strength between the geotextile materials alone is less than that of sand-filled bags. However, the direct shear test with geotextile samples is not a precise way to estimate interface friction between sandbags. Their findings give a better understanding of interface shear properties of geobags. Finally, Recio (2008) listed friction angles for non-woven and woven geotextile shown in Table 2-2. Akter (2011) showed that the average friction angle between geobags, which applied during the majority of studies investigating the performance of geobag structures, was 30° (Figure 2.4). However, more future works need to be implemented to investigate the friction angle between geobags and its impact on the hydraulic stability of geobag structures.

2.2.2.2. Permeability

Another mechanical property which significantly influences the stability of geobag structures is permeability. Permeability herein is defined as the internal gaps between bags. Recio, (2008) studied the effect of structure permeability on the total forces and moments for geobag displacement in a structure under wave conditions. This process depends on the wave pressure propagation inside the gaps. The contact areas with the neighbouring bags decrease because the infill sand in the bags accumulates at the seaward end and leads to the deformation of the latter part of the bag. The impact of sand fill ratio on the total permeability of geobag structure has been intensively studied by Dassanayake and Oumeraci, (2012). They found that increasing the sand fill ratio to 100% resulted in higher permeability of geobag structure and consequently 30-50% higher resistance against pullout.

Table 2-2 Friction Angles and Friction Factors (Recio, 2008)

	Interface Materials	Friction Angle ϕ	Friction Factor $\tan\phi$
Nonwoven Geotextile	Terrafix 1200R (mechanical nonwoven) vs. Sand	30.11	0.57
	Terrafix 1200R (mechanical nonwoven) vs. Terrafix 1200RP	25.97	0.48
	Terrafix 1200RP (mechanical nonwoven) vs. Terrafix 1200RP	22.53	0.41
Woven Geotextile	Geolon PP120S (woven) vs. Geolon PP120S	20.38	0.37
	Mirafi GT1000 (woven) vs. Mirafi GT1000	14.80	0.26
	Mirafi GT500 (woven) vs. Mirafi GT500	11.91	0.21

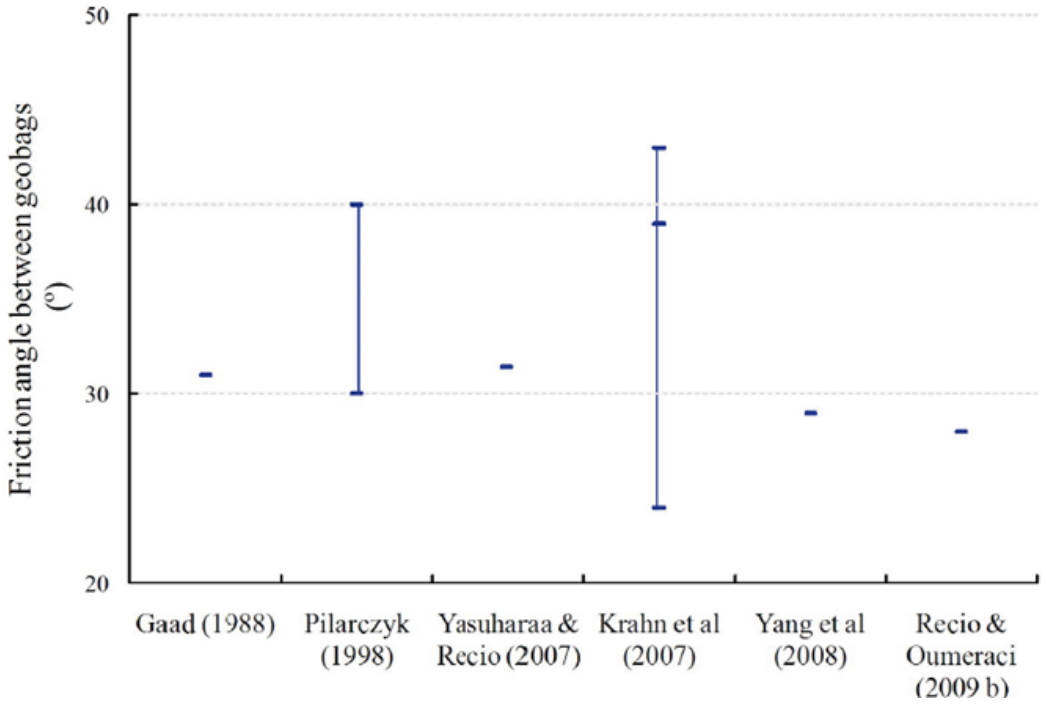

Figure 2.4: Published geobag–geobag friction angle (Akter, 2011)

2.2.3. *Revetment construction*

To obtain the desired stability of the geobag structure, the addressed specifications for construction of geobag structures should delineate the thickness of protection work, bag placement (concerning coast/bank line) and the slope of the structure. According to previous research, bag placement parallel to the flow direction (relative to the coast/bank line) is found to be the most effective bag configuration.

Furthermore, laboratory experiments demonstrated that irrespective of the initial orientation, geobags move in water with the largest axis parallel to streamwise direction if sufficient water depth is available (Dassanayake and Oumeraci, 2012a). Bezuijen *et al.*(2004), during a field study, determined that in a water depth between 15 m to 22 m, accurate placement of geocontainers is a function of water depth, and a standard deviation of less than 1 m can only be expectable in launching accuracy if water depth is less than 10 m.

The extent of spatial geobag overlapping affects the stability of geobag structures by controlling the structure slope. Figure 2.5 shows different 50% overlapping conditions. In Table 2-3 construction specifications of different geobag structure tested in previous laboratory studies are presented. Overlapping has a significant impact on the stability of geobag structure as increasing the overlapping will increase the stability . In terms of total failure, when a coastal geobag revetment is subjected to wave attack, comparison of two different tested side slopes of 1V:1.5H and 1V:2H, Coghlan *et al.*, (2009) showed that the revetment with side slope 1V:1.5H was more stable and less vulnerable as it had the maximum potential overlapping (Table 2-3). Evaluation of different layer to layer overlapping condition showed that a 50% overlapping arrangement was optimum (Porraz *et al.*, 1979; Kobayashi and Jacobs, 1985; Gadd, 1988; Recio and Oumeraci, 2009a).

In the Stockton beach revetment, the double layer bag thickness and the running bond (Figure 2.5) bag setup was innovative as there were no guidelines for bag placement available at this time (Saathoff *et al.*, 2007). It should be noted that running bond bag setup, the geobags are laid longitudinally, in a typical brick wall pattern (Figure 2.5 a), with the geobag joints laying in the middle of the bags in the layers directly above and below.

(a) Running bond

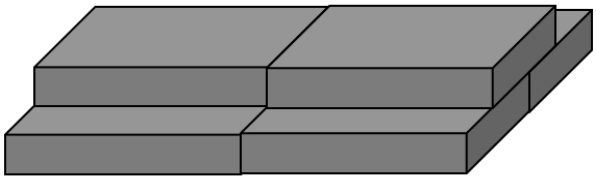

(b) Stack bond

Figure 2.5: Different construction method with 50% overlapping

The most common slope employed in previous research is between 1V: 1H to 1V: 3H (Table 2-3). Practically in field design, wave height and the pattern of erosion or scour hole play a significant role in the determination of a suitable slope (Heibaum, 1999). To achieve the design slope, a mechanical device should be used during the geobag placement process, as in manual bag drop there is uncertainty in achieved geobag position (Akter, 2011). GeoCoPS (2.0) is a well-known computer software package which is applied for simulating the theoretical shape of geobag on the seabed after installation by using a mechanical device (Hornsey *et al.*, 2003).

Table 2-3 Construction specifications of different geobag structure tested in previous laboratory studies

Author and Year	Type of Structure	slope	Overlapping
Porraz *et al.*, (1979)	Breakwater	(1V:1 and 2H)	Unknown
(Kobayashi and Jacobs, 1985; Odgaard and Bergs, 1988)	Revetment	(1V:3H)	50%
Oumeraci (2003) (small scale)	The protection of dune, revetment & submerged breakwater	(1V:1;1.5; 3H)	<=50%
Oumeraci (2003) (large scale)	Revetment	(1V:1H)	<=50%
Kim et al., (2004) (large scale)	Revetment	(1V:1and 2.5H)	<=50%
Coghlan *et al.*, (2009)	Geobag revetment	(1V:1.5 and 2H)	Varies
(Recio, 2008; Recio and Oumeraci, 2009a, 2009c)	Coastal-geobag structures	(1V:1H)	50-100%
Das Neves et al., (2012)	Breakwater and revetment	(1V:1H)	60%

2.2.4. *Failure mechanism*

The hydraulic stability of geobag structures is affected by many complex factors which may create a number of different failure modes (Jackson *et al.*, 2006). Although preliminary studies of failure modes started in 1979 by Porraz *et al.* , so far only a few studies have been conducted to understand the failure mechanism of geobag structures (Table 2-4). Figure 2.6 schematically shows the most common potential failure modes that have been identified during laboratory and field studies of coastal geobag structures. These potential failure modes are: puncturing, sliding, overtopping, pullout/dislodgement and toe scour (Table 2-4). Detailed information of the failure modes of geobag structures observed in the laboratory performed by Oumeraci *et al.*, (2003); Jackson *et al.*, (2006); Mori *et al.*, (2008); Lawson, (2008); Recio, (2008); Van Steeg and Klein Breteler, (2008); Oumeraci and Recio, (2009b); Dassanayake and Oumeraci, (2012b) are summerised in Table 2-4. According to these experimental works, failures of geobag structure is mainly due to friction, inertia, drag and lift forces. There is no available standard for determining coefficient of friction needed for force calculations when considering the whole structure. To date direct shear test is the only method addressed to determine this value (Kim et al., (2004; Krahn et al., 2007). A physical model with consideration to inertia, drag and lift forces was introduced by Recio and Oumeraci (2009 a, b). This experimental study was conducted in a wave flume with emphasis on wave loading. Therefore, the force coefficients obtained by Recio and Oumeraci (2009 a, b) could not be applied to underlying hydraulic loading.

2.2.4.1. Failure due to pullout

"Pullout" represents one of the main hydraulic failure modes of geobags. Although Jackson *et al.* (2006) addressed the most important factors which influence the pullout of geobags from revetment, they did not consider the deformation of geobags due to the internal sand movement (Figure 2.7). "Pullout" mechanisms of geobags due to wave attack was investigated, by Oumeraci *et al.* (2003) and Recio (2008) through a series of laboratory tests. During an experimental and numerical investigation, Recio (2008) attempted to understand the process of the pullout of geobags from a geobag revetment because of wave attack and the research showed that the hydraulic stability of geobag structures is considerably influenced by the interface friction between geobags. They also investigated the internal movement of sand due to uprush and downrush wave that caused the sand container to deform. According to their finding, compared with a normal geobag,

a deformed bag has a smaller contact area with neighbouring bags, therefore, has smaller resisting forces and larger wave- induced mobilising forces. Eventually, these processes result in the pullout of geobag from revetment.

Dassanayake and Oumeraci (2012) conducted pullout tests in a wave flume to determine the significance of geobags' properties (i.e., sand fill ratio and interface friction) and their impact on the hydraulic stability of geobags structures. Additionally, the sensitivity of each of the geobag's property on its hydraulic stability, and as a result new hydraulic stability nomogram have been developed as an outcome of their investigations.

2.2.4.2. Failure due to deformation and sliding of geobags

Sliding of geobag is one of the most common failure modes which could cause failure processes to progress more quickly. An extensive laboratory study conducted by Recio and Oumeraci, (2009b) to investigate the impact of geobag deformation on the progression of geobag failure subjected to wave attack. Different formulae were suggested to predict different failure modes such as sliding. They found that during a wave attack uprush of the wave could lead to uplift the front part of geobag and reduce the effective contact area between geobags. The deformation due to the uplift of the geobag bag and internal movement of sand into geobag eventually result in the sliding of geobag either towards the seaward direction (geobag at the slope or the crest) or towards the landwards direction (only geobags at the crest). Therefore, to consider the effect of deformation on the sliding of geobag, Recio (2008) suggested applying correction factors to the sliding formulae.

Hydraulically the location of the centroid (centre of gravity) of geobags changes as a result of deformation, so the moment due to drag force and inertia force increase while the moment due to lift force decreases. Moreover, the pressure exerted on the deformed section of the geobag result in additional vertical force component which needs to be considered predicting geobag sliding (Mudiyanselage, 2013).

2.2.4.3. Failure due to Overturning of geobags

Commonly, in geobag structure failures due to overturning are observed for geobags at the crest of the structure. Thus, for a low-crested geobag structure, the crest geobags are the critical elements of structure in the process of failure (Oumeraci *et al.,* 2003).

According to Recio (2008), in the same wave conditions, to increase the stability of the geobag structure, the recommended weight of a crest geobag needs to be up to 8 times greater than the required weight of slope geobags. However, during extremely high wave conditions, both the crest geobags and also the slope ones are exposed to failure due to overturning.

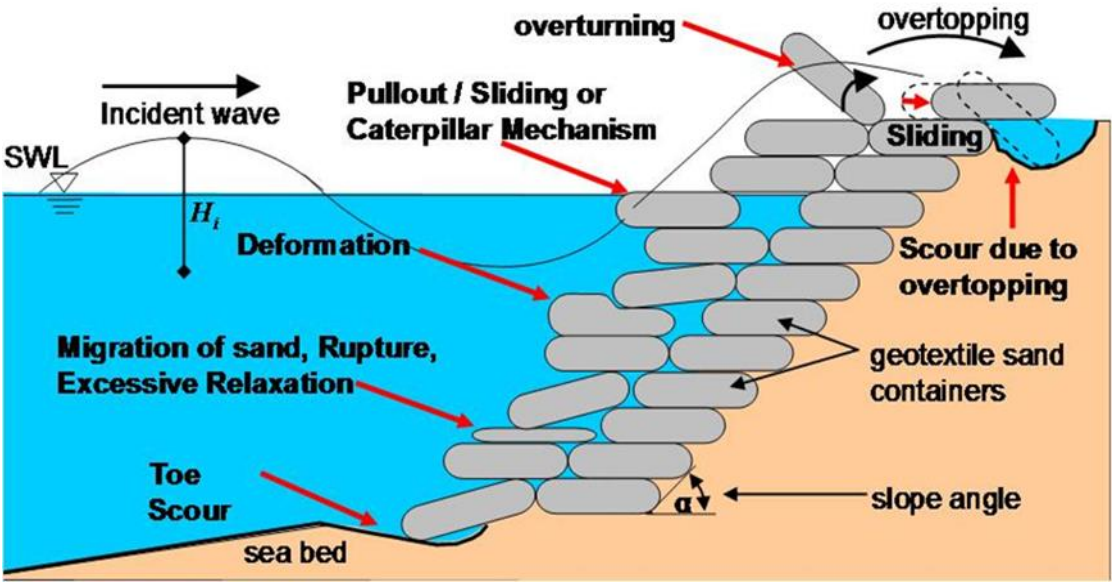

Figure 2.6: Potential Failure Modes of a geobag revetment (Mudiyanselage, 2013)

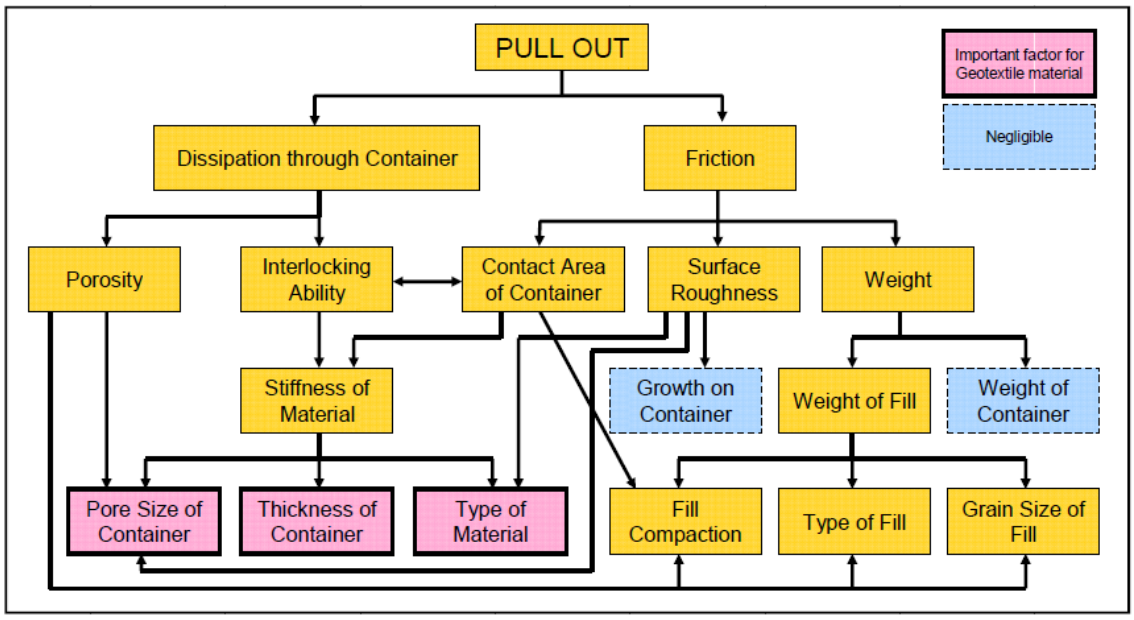

Figure 2.7 Factors influencing pullout of geobags (Jackson *et al.*, 2006; Mudiyanselage, 2013)

Table 2-4 Published failure mode observation in physical modeling (updated from Akter, 2011)

YEAR	AUTHORS	FAILURE MODE	FAILURE REASON
1979	Porraz *et al*	Slide	Friction.
		Push	Thrust force due to waves current.
		Pullout	Uplift pressure and wave current.
1985	Kobayashi and Jacobs	Plugging, collapsing and surging	The combined effect of slope angle, wave steepness and wave period.
1988	Gadd	Dislodgement	Wave impact and physical property
2004	Kim *et al.*	Slide, overturn and pullout	Friction
2006	Jackson *et al.*	Pullout/dislodgement	The physical property of bags; and Geobag–geobag friction.
2007	Saathoff *et al.*,	Overtopping	Wave run–up and freeboard.
		Uplift	Wave run–down.
2008	Van Steeg and Klein Breteler	Sliding and caterpillar mechanism	migration of sand in the geocontainers
2008	Mori *et al.*	Whole structure failure	Hydraulic stresses in bags due to wave load.
		Overturning	Wave height; and Wave period.
2008 and 2009b	Recio and Oumeraci	Slide	Bag submerged weight and lift force; Friction; Deformation.
		Pullout effect	Several wave cycles on the structure; Relatively longer experimental time.
		Uplifting/ overturn	Drag and inertia force.
2012b	Dassanayake and Oumeraci	Pullout	Mechanical properties of sandbags: sand fill ratio, the type of geotextile material and the interface friction

2.2.5. *Hydraulic stability formulae*

Hydraulic processes which influence the stability of geobag structures have been widely investigated by (Oumeraci *et al.*, 2003; Grüne *et al.*, 2007) and Recio (2008). As geobag structures is an emerging technology, comprehensive design strategies are needed for designing geobag structures (Dassanayake and Oumeraci, 2009; Oumeraci and Recio, 2010). Compared with rock or concrete units, the behaviour of geobag because of their lower specific gravity and lower rigidity are entirely different therefore the distinct design formulae for geobags structure should be established.

Failure mechanisms of geobag structures can be governed by friction, inertia, drag and lift forces. Available stability formulae are used to calculate the stability number and are based on the balance of flow forces acting on a geobag exposed to wave actions. The total wave-induced force on geobags could be decomposed as a drag force, a lift force and an inertia force. The gravitational force is considered as the stabilising force. Although, a direct shear test is typically used to estimate the coefficient of friction needed for force calculations (Kim *et al.*, 2004; Krahn *et al.*, 2007; Matsushima *et al.*, 2008) the results of this test are not applicable when considering the whole structure. During an experimental study in a wave flume, Recio and Oumeraci, (2009a) found the coefficient of drag and lift forces are a function of Reynolds numbers and the roughness of geobags. They estimated these coefficients as a function of (i) Keulegan–Carpenter KC and (ii) Reynolds number. The tests were conducted with shallow water conditions therefore, the horizontal particle velocity was equal to the wave celerity (Table 2-5).

Table 2-5 Coefficient of drag and lift forces related to wave loading on geobag

Authors and year	Drag Coefficient C_D	Lift Coefficient C_L	Reynolds Number Re	Remarks	
Bezuijen et al. (2001)	1	–	–	Field study	
Kim et al. (2004)	1	–	–	Laboratory test	
Recio and Oumeraci (2009)	0.5-3	0.3-1.2	8×104–1.8×105	Bottom Layer bag	Laboratory test
	2.5-9	0.3-1.2		Middle bag	
	4-15	0.3-1.2	8×10^4–2×10^5	Top layer bag	

2.2.5.1. Stability Formula of Hudson (1959)

Hudson's stability formula (1956) for stone armour layers has been commonly used to design geobag structures. The formula is based on geometrical considerations of the balance of wave-generated flow forces acting on an armour stone in a slope of a breakwater.

Stability Formula suggested by Hudson (1956) is as follows:

$$N_s = \frac{H}{\Delta D_n} = (K_D \cot\alpha)^{1/3} \qquad \text{Equation 2.2}$$

$$W_{50}=\frac{\rho_s g H^3}{K_D(\rho_s/\rho_w\text{-}1)^3 \cot\alpha}$$ Equation 2.3

where N_s is the stability number, α is the slope angle of the revetment, K_D is a stability coefficient which is obtained experimentally, H is wave height, $\rho_s$is the density of the armour unit, Δ is $(\rho_s/\rho_w - 1)$ and W_{50} is the average weight of the element.The simplicity of Hudson formula and its applicability for different types of armour units and configurations make it advantageous.

2.2.5.2. Wouters (1998)

Wouters formula was presented to describe the relationship between the stability number of geobags and the surf similarity parameter which includes the wave period. Wouters stability formula is based on the balance of moments of the lift force F_L, the drag force F_D and the stabilising gravitational force FG.

In this formula instead of the typical required weight of the geobags, the thickness *D* of the cover layer calculated as:

$$D = l \sin\alpha$$ Equation 2.4

the porosity *n* should be adapted to obtain a more realistic density of the geobag:

$$\rho_E = (1 - n).\rho_S + \rho_W.n$$ Equation 2.5

where *n* is the porosity of the filling material (sand). The stability number can then be determined with (Wouters, 1998):

$$N_S = \frac{H_S}{\left(\frac{\rho_E}{\rho_W} - 1\right).D} = \frac{C_W}{\sqrt{\xi_0}}$$ Equation 2.6

where ρ_W is the density of water, ρ_E is the density of geobag, C_W is an empirical parameter based on laboratory experiments, a value of C_W= 2.0 was proposed by Wouters (1998).

$\xi_0 = tan\alpha \Big/ \sqrt{\frac{H_0}{L_0}}$ is the surf similarity parameter, where α is the slope angle of the revetment and *Ho /Lo* the deepwater wave steepness.

The main advantages of this formula are the consideration of the porosity of the filling material and wave period. The applicability of the formula is limited to slope geobag revetments and not sufficiently validated with experimental results or field data (Recio, 2008; Mudiyanselage, 2013).

2.2.5.3. Oumeraci et al. (2003)

Based on Hudson's formula for the hydraulic stability of rock armour units (non-deformable) a stability number is formulated and postulated to be a function of surf similarity. Oumeraci *et al.* (2003) proposed two different formulae for slope and crest geobags for high overtopping revetments and low-crested structures based on small and large-scale experiments which are as follows:

$$N_{s,slope} = \frac{H}{\Delta D_n} < \frac{2.75}{\sqrt{\xi_0}} \qquad \text{Equation 2.7}$$

$$N_{s,crest} = \frac{H}{\Delta D_n} < 0.79 + 0.09\frac{R_c}{H} \qquad \text{Equation 2.8}$$

Where N_S is the stability number for slope and crest elements while ξ_0 is Iribarren number[b] and *Rc* is the crest freeboard of the revetment (Recio, 2008).

2.2.5.4. Recio and Oumeraci, (2009b)

Process-based stability formulae for different types of geobag structures considering two principal hydraulic failure modes are sliding and overturning were purposed by Recio and Oumeraci, (2009b) these are represented by Equation 2.9 and Equation 2.10 respectively. Force coefficients were found by conducting several small-scale experiments.

[b] also known as the surf similarity parameter and breaker parameter – is a dimensionless parameter used to model several effects of (breaking) surface gravity waves on beaches and coastal structures.

$$l_{C(sliding)} \geq u^2 \frac{[0.5KS_{CD}C_D + 2.5KS_{CL}C_L\mu]}{\left[\mu KS_R\Delta g - KS_{CM}C_M\frac{\partial u}{\partial t}\right]}$$ Equation 2.9

$$l_{C(overturning)} \geq u^2 \frac{[0.5KO_{CD}C_D + 1.25KO_{CL}C_L]}{\left[0.5KO_R\Delta g - 0.1KO_{CM}C_M\frac{\partial u}{\partial t}\right]}$$ Equation 2.10

Where l_c length of the geobag, u is horizontal velocity, C_D, C_L and C_M are the drag, lift and inertia coefficients respectively. *KS* and *KO* are coefficients of deformation during sliding and overturning respectively, $\frac{\partial u}{\partial t}$ is horizontal acceleration and μ is friction factor between geotextile.

Furthermore, Recio *et al.* (2010) designed stability nomograms based on Recio and Oumeraci, (2009b) formulae to design prototype structures and these nomograms also could be used for different types of geobag coastal structures. These stability nomograms were also developed by Coghlan *et al.* (2009) and Hornsey *et al.* (2011) for two specific geobag geometries using empirical data.

2.2.6. *Available numerical studies*

Recio and Oumeraci, (2009a) studied the effect of frictional forces and deformation on the stability of geobag structures by applying a computational fluid dynamic model (COBRAS) and two computational structural dynamic models (UDEC). COBRAS is a fluid dynamic base model which was utilised to calculate the wave-induced forces on geobags, while the UDEC model consists of a Finite Element Model (FEM) that simulated the total stresses and deformations for each geobag and a Discrete Element model (DEM) that used to simulate the displacement of each geobag. COBRAS-UDEC were partially coupled to represent a 2D numerical model of a geobag structure which showed the consequent forces and displacements due to wave action. Ultimately their findings demonstrated the smaller friction angle could cause larger displacement. Mudiyanselage (2013) numerically simulated a 2D model of geobag structures affected by wave actions using coupled RANS-VOF model and FEM-DEM models (COBRAS-UC/UDEC) and developed stability curves and a simple formula for the hydraulic stability of crest geobags used for coastal protection.

2.3. Geobag riverbank protection

To date, the vast majority of previous research has been focused on geobag performance in coastal situations (Bezuijen *et al.*, 2004; Saathoff *et al.*, 2007; Recio and Oumeraci, 2009a; Dassanayake and Oumeraci, 2012a, 2012b). However, the perpendicular wave action found in coastal scenarios is not significant in fluvial applications, where the flow direction is generally parallel to riverbank revetments, so the performance and failure mechanisms of geobag revetments in rivers are considerably different from that of coastal structures. Although coastal-based studies provide essential background knowledge of physical and mechanical properties of geobags, due to the difference hydraulic loads, hydrostatic forces, and active shear stresses on the geobags in river their results of are not practically applicable to analyse the behaviour of geobags in riverbank revetments.

Since the late 1990s, in Bangladesh riverbank revetments constructed of sand-filled geotextile bags have been developed in response to the lack of traditional erosion-protection materials mainly rock. Due to an emerged technology of using geobag structures as riverbank protection few available published studies are investigating geobag structures in the river. One study that has looked at the use of geobags in the fluvial environment was conducted as part of the wider Jamuna–Meghna River erosion protection scheme in Bangladesh (NHC 2006). Furthermore, Akter *et al.* (2011) undertook an extensive experimental and numerical programme, to investigate the failure processes of geobag revetments in the fluvial environment.

2.3.1. *Physical properties of geobags*

2.3.1.1. Properties of geotextile material

According to JMREM (2006), geotextile bags which are fabricated from engineered geosynthetic materials must be produced under controlled conditions. Since the top surface of the geotextile bags is usually exposed to river drag forces and sediment transport, to assure the long-term stability of the geotextile in the given environment, a modified form of an abrasion test was introduced by adding an additional O_{90}[c] criterion

[c] O90 describe the opening size of geotextile which corresponds with average sand diameter of sand fraction of which 10% escapes through the geotextile opening (Mudiyanselage, 2013).

for containing the sand fill (Restall *et al.*, 2002; Heibaum *et al.*, 2008). The typical geotextile used to manufacture geobags in JMREM project was polypropylene or polyester textile fabric, which was non-woven, needle-punched and not thermally bonded. The density of geotextile was about 400 g/m^2 with a tensile strength of more than 20 kN/m. With an EN ISO 12956 test, an opening size of 0.06mm<O_{90} <0.08mm was determined for this type of geotextile. (NHC, 2006; Oberhagemann and Hossain, 2011).

2.3.1.2. Properties of fill material

Practical considerations and experience from the JMREM project (2006) showed that when considering the fineness of the locally available sand, the most suitable fill material is non–plastic, non–saline, free from silt, clay, roots, and other organic materials. As the minimum available of non-woven geotextile has an O_{90} of around 0.08 mm, the sand D_{50} of about 0.2 mm with the minimum grain size O_{90} of 0.08 mm and the range of Fineness Modulus from 1 to1.3 is recommended as the most suitable fill material for geobags used to protect riverbank in Bangladesh. The woven material commonly has an O_{90} of above 0.1 mm, which was recognised to be too porous in JMREM project (Oberhagemann and Hossain, 2011).

2.3.1.3. Geobag size and fill ratio

Due to the difficulty of filling, storing, and mixing a larger number of bags of different sizes at the site, during JMREM project (2006), two sizes were found to be more stable under the higher flow velocities with their details listed in Table 2-6. Usually to cover one square meter of the riverbank with one layer of geobags, two filled 126 kg bags, or three filled 78 kg bags are required. To achieve fully covered slopes and falling aprons usually three or four layers of geobags are needed. Bag size of 1.03 m × 0.70 m with 80% fill ratio results in a weight of 126 kg. The area of a fully filled bag (fill ratio of 100%) is about 75% of the area of an empty bag (Oberhagemann and Hossain, 2011).

Table 2-6 Geobag dimensions used in JMREM project (2006)

The weight of bag (kg)	Empty bag size (mm)	Area of the empty bag (m2)	Area of fully filled bag (m2)	Number of bags per m3
126	1030×700	0.72	0.54	14.3
78 kg	830×600	0.50	0.37	23.1

2.3.2. *Revetment construction*

In order to provide more insight into issues of geobag placement for revetment structures in Jamuna – Meghna River erosion protection scheme, NHC (2006) conducted laboratory tests using 1:20 scale models in four categories of test including drop, launch, incipient motion and mega container. The bag-drop test showed that, when dropped, dry bags travel longer than wet bags before settling on the bed because of their lower weight. In the laboratory, when launched, slightly steeper revetment slopes are produced by mixed size geobags compared to the typical 1V:2H slopes that usually produce by single 126 kg size bags. With the same test, it was also shown that bags of 126 kg are the optimum weight for bags (more stable structures) under high flow velocities (up to 4.5 m/s). The incipient motion test (when ten geobags are displaced, the incipient motion has started) showed that failure started at a prototype velocity of 2.9 m/s when side slope is 1V: 2H.

Zhu et al., 2004 attempted to predict the horizontal settling distance of sandbags, and critical flow velocity at incipient sandbag motion in open channel flows by undertaking a laboratory study and field observations. They observed that 60% of the total number of bags settled onto the channel bed with the longest axis in the streamwise direction. They also presented two formulae, one for predicting settling distance and one for computing the critical flow velocity for geobag incipient motion. Their suggested formulas were described as a function of two hydrodynamic forces (drag and lift).

2.3.3. *Failure mechanism*

In terms of failure modes NHC (2006) reported that inadequate bag coverage and toe scour are the main reasons for failure due to sliding/slip and slumping. During a field study in 2009, the observed failure mechanisms of geobag revetments in the Jamuna River showed hydraulic loading, toe scouring and management as three main factors which influenced the performance geobag revetment (Akter, 2011), as follows (Figure 2.8):

a) Hydraulic loading; the rapid drawdown during flood season can cause failure due to slump and/or pullout and sliding (Figure 2.9 a).
b) Hydraulic loading and toe scour failure; when the impacts of undeveloped scour and rapid drawdown are combined both crest bags and slope bags are displaced by a slip circle formation (Figure 2.9 b).

c) Management; since the performance of geobag revetments depends on human contribution in operation and maintenance levels, poor maintenance can result in insufficient thickness at the revetment top (Figure 2.9 c).

Figure 2.8: Failure modes in geobag revetment (JMREM, 2006; Akter, 2011): 1: Pullout; 2: Slump; 3: Dislodgement of the top bag; 4: Slide; 5: Physically damaged

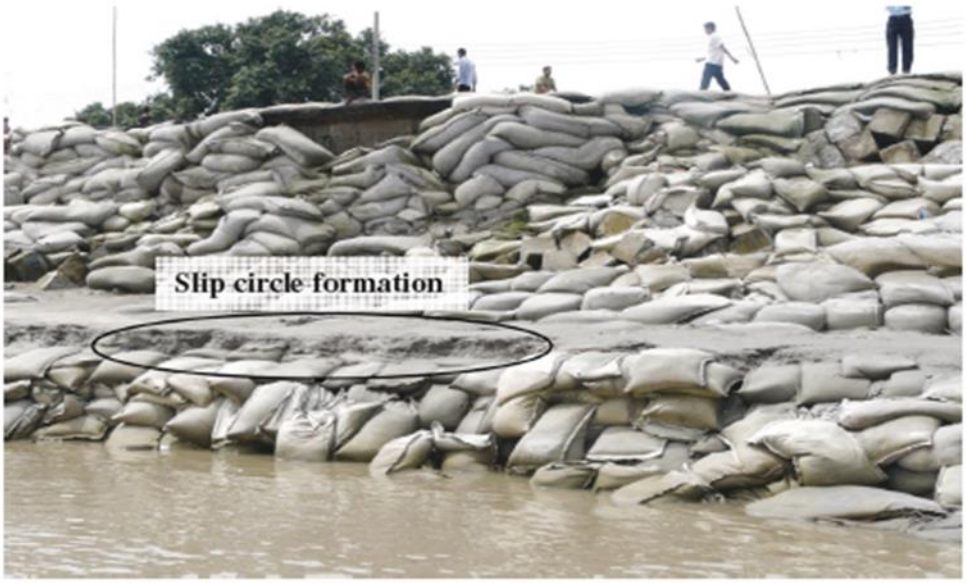

(a 1) Displacement due to rapid drawdown

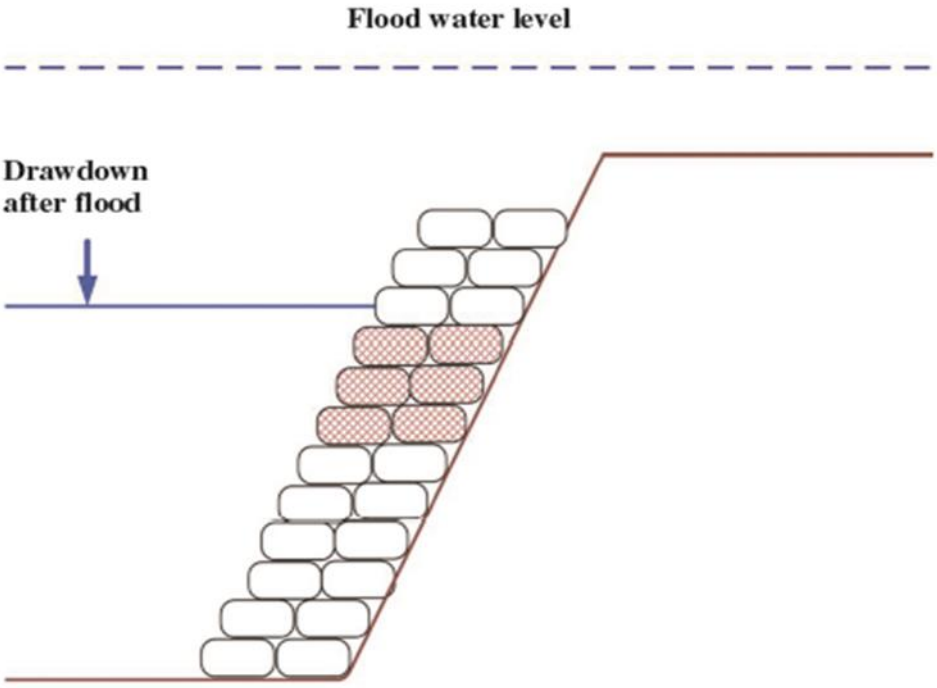

(a 2) Schematic of displacement due to rapid drawdown

Figure 2.9 a: Geobag displacement, Jamuna River (Akter, 2011) (Cont'd)

(b 1) Bag displacement due to combined effect of retarded scour and drawdown

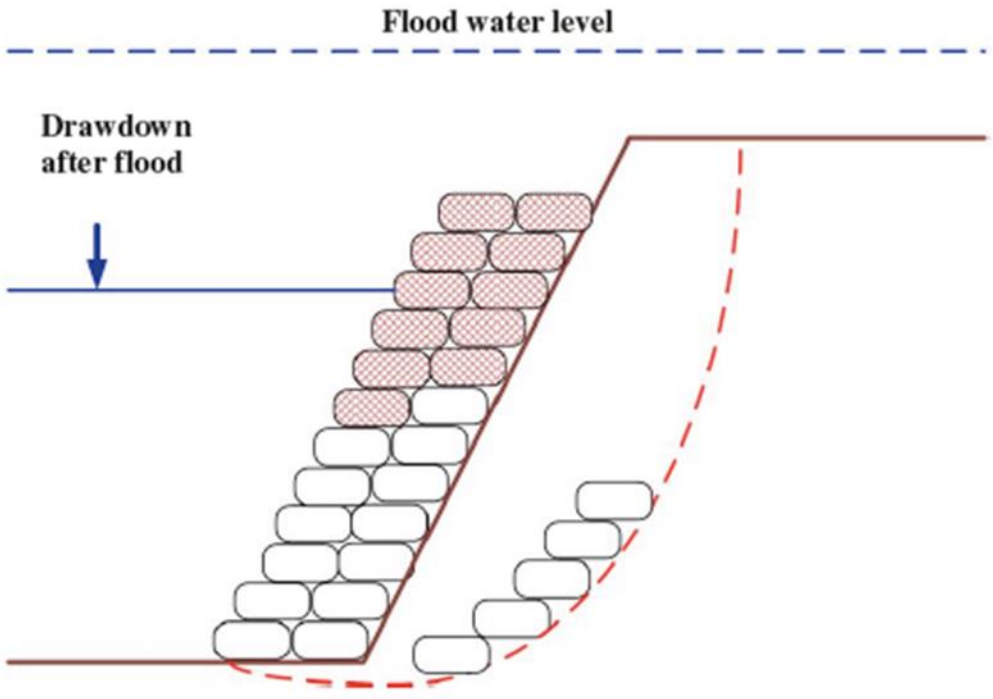

(b 2) Schematic of the combined effect of retarded scour and drawdown

Figure 2.9 b: Geobag displacement, Jamuna River (Akter, 2011) (Cont'd)

(c 1) Inadequate thickness of geobag revetment

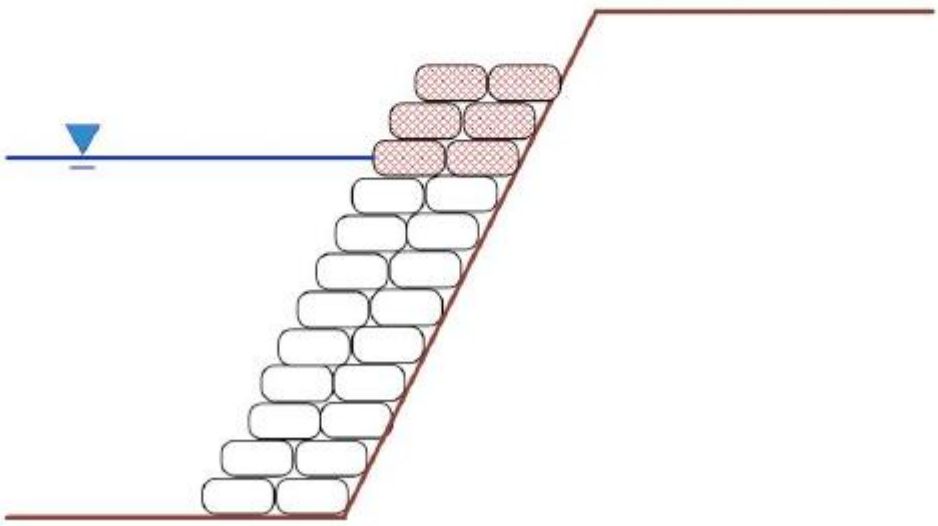

(c 2) Schematic of bags prone to displacement due to inadequate thickness of revetment

Figure 2.9 c: Geobag displacement, Jamuna River (Akter, 2011)

To date, the only significant laboratory work investigating geobag revetment performance in rivers has been undertaken by Akter (2011). Akter (2011) attempted to numerically and experimentally investigate the behaviour of a geobag revetment under different hydrodynamic loads and toe scour conditions and it was found that failure

mechanism of geobag revetment could be initiated due to overtopping, sliding, puncturing and pull-out/dislodgement.

During an extensive experimental programme, using a quasi-physical model study, this work further developed an upgraded conception of geobag stability under frictional, horizontal and vertical loadings, and provided the data required to validate a numerical model capable of simulating the incipient motion of geobags. Using a laboratory flume, fixed, and mobile beds were considered to investigate the initial failure modes in geobag revetment experimentally. A CES model was initially validated alongside the fixed-bed experimental results. The validated CES model was applied to determine the Froude number and the active shear stress that is required for the initiation of the bag movement. Ultimately, a failure diagram was developed for the geobag–water flow interface. It was also found the CES model is a useful tool for demonstrations of bed formation and it was highlighted that bed changes against different water depths.

2.3.4. *Hydraulic stability formulae for geobag riverbank structures*

To date there are no available formulas for calculating the stability of geobags against flow forces in rivers, as exist for riprap. Existing riprap formulas should be modified and verified to be adapted to the specific characteristics of geotextile bags. In JMREM project, revetments constructed of 126 kg geobags are considered to be stable for a depth-averaged flow velocity of 3 m/s, based on laboratory studies and field investigations conducted by NHC (2006) that mentioned earlier (Oberhagemann and Hossain, 2011).

2.3.5. *Numerical Studies*

Akter et al. (2011) applied a mapped velocity field, obtained by CES for the Discrete Element Method (DEM) to simulate incipient geobag revetment failure modes (one-way coupling method). The one-way coupled numerical models (EDEM-CES) were validated and could determine the initial displacement of bags in varying water depths and with varying bed formations. To represent the interaction of geobags with flow, an external flow field was imported from CES into the DEM system. The DEM model also represented the incipient movement of geobags due to toe scour. According to their work, using a DEM model will provide a way to explore more details of geobag revetment

performance in rivers. However, the processes which are involved in the complete failure of geobag revetments still need to be investigated.

2.4. Published geobag guidelines

Although the first work on sand filled bags for coastal bank protection was published in 1968 by Venis, geotextile sand-filled containers have been employed as permanent construction means in coastal protection works for more than 30 years. In Bangladesh since the late 1990s riverbank revetments constructed of sand-filled geotextile bags (geobags) have been commonly used due to the lack of traditional materials/solutions particularly rock for erosion-protection. On the other hand, for emergency flood protection, geobags can be applied as emergency measures since they can be filled with locally available sand and used as a quick response to dynamic river changes. Thus, regarding temporary use of geobags, there are many available guidelines on bag design specifications, construction method and placement. However, this thesis aims to evaluate the performance of geobag revetment as a long-term protection means so the existing emergency sandbag guidelines are not taken into account for protecting riverbanks which are subjected to a significant amount of hydraulic forces.

Although, the first guideline was published in Germany in 1994 and probably for large-scale coastal protection works. A comprehensive design guideline for permanent use of geobag structure in coastal or riverbank protection is still not available. German Geotechnical Society (DGGT) recommended 'EAG–CON' which is developing to describe the principles of geobag application and system requirements i.e. material properties, design, quality assurance, construction, installation possibilities and bag filling method towards the final bag positioned and prefilled bag handling (Saathoff *et al.*, 2007). **Error! Reference source not found.** highlights a more detailed guidance which is described by the Australian guidelines on the application of geobag structures in coastal protection (NSW, 2011). Furthermore, some guidance was developed in UK and USA on bag design and revetment construction specifications (Scottish Natural Heritage, 2000; US Army Corps of Engineers, 2004; Coastal Area Management Act (CAMA), 2008; Hellevang (NDSU & U.S. Department of Agriculture), 2011; GEOFABRICS, 2018) (Table 2-7 and Table 2-8).

Although in 1993, the first design guidelines titled “Guide to planning and design of river training and bank protection works” was published in Bangladesh. In 1999, critical riverbank erosion that was threatening two large irrigation projects in Asia, one located on the west bank of the lower Brahmaputra (called Jamuna in Bangladesh) and the other on east bank at the confluence of Upper Meghna and the Padma which carries the combined flow of the Brahmaputra and Ganges (ADB, 2002). The requirement of large river bank protection -which needs to be economically feasible led to use of sand-filled geotextile bags which previously had been applied for emergency protection since the mid-1990s. Experience in emergency works was used to establish the main design and construction phase of the project from 2003 to 2006. This continued experience with geotextile bags led to improving understanding about failure mechanisms of riverbank protection and an updated “Guidelines for Riverbank Protection” in 2008 was published, which was supported by the Bangladesh University of Engineering and Technology (BUET) (Oberhagemann and Hossain, 2011). However, earlier in 2007 a guideline for ‘Design of riverbank protection and manual’ had been published under Jamuna Meghna River Erosion Mitigation (JMREM) project.

To achieve long-term reliability of the geobag revetment, JMREM, (2006), developed a modified “adaptive” approach based on phased planning and implementation. This approach provides the necessary flexibility actions needed to respond to the largely unpredictable river behaviour. Core principles of the adaptive approach are: (i) erosion prediction during the dry season to provide data for constructing revetment in an emergency, (ii) the first level protection are provided by first major construction that need to complete usually in two years, (iii) extensive river surveys during the flood season to identify the river erosion nature and estimate the length of the monitoring and adaption phase, (iv) if river attack continues, provide the second level of adaptive protection to extend the existing protection to deeper levels and (v) monitoring on a regular basis and normal maintenance need to be conducted on the protected riverbank (Akter, 2011).

Therefore, after the first major construction the knowledge of failure mechanisms of the geobag revetment is needed to provide information for the rest of the adaptive approach. The performance of the designed geobag revetment strongly depends on their hydraulic stability. In addition to the acquired experience from laboratory geobag revetment and field to develop knowledge on failure modes in geobag revetment Akter, (2011), used a 3D numerical model for predicting initial failure mechanism of geobags in a revetment.

However, additional research is still required to achieve the desired performance of geobag revetments in the fluvial environment and to provide the necessary data to inform the development of a numerical model capable of simulating complete revetment failure which is required to develop much-needed revetment design guidelines.

Table 2-7: Published geobag guideline obtained for coastal protection works (developed from Akter, (2011))

Structure zone	Bag Design Specification				Construction Specification				cycle (Year)	Maintenance and Inspection	Labour Safety	Year	Reference
	d50 (mm)	Fabric (Thickness)	Fill ratio (%)	Bag size Weight Volume	Bond bag-bag	Thickness	Placement (streamwise)	Slope					
Coastal	–	Geotextile	–	3m ×1.5m × 0.5m, 3 tonnes	Running bond	2–3bag widths	Parallel	≤1:1.5	5–10	Adaptive management	≤ 50 kg	2000	Scottish Natural Heritage
	–	–	–	2–4.5m × 1–1.5 m	–	–	Parallel	≤1:3.3	2–5	Following standards 15A NCAC 7H Section .0308(a)		2008	CAMA[d]
	0.15–0.5	Woven polypropylene fabric or Geotextile (5 mm)	67–100	≥ 18 kg 0.75 m^3	Running bond	2 layers	Perpendicular	1:1.5	–	Coastal protection Act 1979 Section 55R(1)(c)		2011	NSW
	–	Geotextile	80	40-100kg	Running bond	–	Perpendicular or Parallel	–	≥20	–		2018	GEOFABRICS

[d]Coastal Area Management Act (CAMA)

Table 2-8: Published geobag guideline obtained for riverbank protection works (developed from Akter, (2011))

Structure zone	Bag Design Specification				Construction Specification				cycle (Year)	Maintenance and Inspection	Labour Safety	Year	Reference
	d50 (mm)	Fabric (Thickness)	Fill ratio (%)	Bag size Weight Volume	Bond bag-bag	Thickness	Placement (streamwise)	Slope					
Riverbank	–	Burlap and plastic	50 – 67	0.61 m × 0.36m – –	–	–	– –	1V:1H	–	–	–	2004	US Army Corps of Engineers
	0.2	non-woven Geotextile	80%	1.03 m × 0.70 m 126 kg.	Running bond	3 layers	Parallel	1V:2H	30	Maintenance and Evaluation division of Bangladesh Water Development Board (BWDB)		2007	Jamuna Meghna River Erosion Mitigation (JMREM)
	–	Woven polypropylene	50	0.61 m × 0.36m 16–18 kg – –	Running bond	–	Parallel	1V:2H 1V:3H	–	–	–	2010	NDSU & U.S. Dept. of Agri.

2.5. Discussion and implication for the present study

As the main result from literature review has shown, that so far several attempts have been undertaken to determine the factors which affect the stability of geobag structures. These are physical properties (i.e., filling ratio, fabric), mechanical properties (friction between geobags), hydraulic properties (i.e., force acting on the revetment under different water depth) and construction specifications (i.e. the steepness of the slope, orientation of the bag with respect to flow).

However, it can be seen that the vast majority of these works is allocated to marine and coastal geobag structures. Due to substantial different hydraulic conditions that are dominant in rivers and acting on geobags in the riverbanks, the performance of geobag revetments in rivers and their failure mechanism are noticeably different.

To date, only a few researchers have studied the parameters affecting geobag revetment performance in a riverbank protection context and, through these studies, only Akter (2011) considered the hydrodynamic forces associated with varying water depth and toe scouring phenomena. Akter also successfully simulated the initial movement of geobag in the revetments using EDEM software by the one-way coupling method. However, details of complete failure process in the riverbank protection context are still unknown. Although results obtained by Akter (2011) represent an excellent starting point for this research project, both experimental and numerical investigation are essential to evaluate the geobag structure performance in river engineering completely.

Factors that affect the hydraulic stability of geobag revetment in a riverbank protection context need to be explored concerning the hydrodynamic forces associated with different construction specifications (e.g. different revetment side slopes and geobags configurations in the revetment). To design a guideline for constructing geobag revetments in the riverbank protection works, these factors need to be profoundly understood. The necessity to thoroughly understand the impact of these parameters shows the importance of laboratory experiments to investigate the performance of geobag revetment at the local scale. To encounter scale effects and experimental limitations which influence laboratory measurements, numerical modeling approach should be employed to observe the behaviour of each individual/discrete geobag under hydraulic loading as prevailing water flow condition can influence geobags displacement and failure mode significantly. To fully realise this potential impact, it is essential to couple hydraulic and geobag conditions. To achieve this, and to be able to predict the complete

failure processes, it is proposed to develop the existing DEM modeling further to incorporate geobag/water feedback mechanism and to efficiently simulate the complete failure of geobag structures.

Chapter 3. **METHODOLOGY**

After the review of the state of the knowledge related to the hydraulic stability of geobags, the methodology presented in Chapter 2 has been discussed and detailed more precisely in this Chapter. According to the aim and objectives defined for this study, this work will consist of lab experimental work to support later numerical model development.

3.1. Experimental methodology

Well-designed laboratory experiments are one of the best approaches to clarify the processes affecting the stability of geobag revetments. Several types of laboratory tests were conducted with the following main objectives: (i) to understand the process affect displacements of geobags under different types of failure modes, (ii) to analysis of the flow-induced pressures and forces on geobags, (iii) to better understand the flow characteristics and flow interaction with a geobag revetment and (iv) to collect data for a numerical model development.

3.1.1. *Quasi-Physical model scale*

Froude similarity is typically applied for physical hydraulic model studies in open-channel hydraulics, where friction effects are negligible or highly turbulent phenomena exist. Using Froude scaling method help to have a statistically correct scaled turbulent shear stress terms and consequently the energy dissipation, even though the fine turbulent structures and the average velocity distribution of the model flows are different to prototype flows (Hughes, 1993). Therefore, in order to minimise scale effects produced by non-satisfied similarity and also to obtain results of highest possible accuracy, in this study a scale of 1:10 (L) was selected based on Froude scaling criteria and the available laboratory flume facilities. Considering the prototype characteristics, the selected geometric scale parameter, L=10, was set to obtain the largest possible model which could be accommodated by the available facilities. From the Froude criteria, the velocity scale relates to the geometric scale in the proportion $L^{1/2}$, so the relevant scale ratio was 3.17. Thus, other relevant scales were computed as shown in Table 3-1

In addition, Reynolds-number similarity (Dynamic similarity) is satisfied since flows in both model and prototype are fully turbulent (see Table 4-1).

Table 3-1 Scale ratio for the experimental setup

Quantity	Dimension	Scale ratio
Length, breadth	L	1:10
Bag volume/mass	L^3	1:1,000
Velocity	$L^{1/2}$	1:3.17
Discharge	$L^{5/2}$	1:316

One of the main challenges in modelling geobag on a small scale is to scale down the geotextile properties. Due to practical limitations, using different scaling criteria should be used for various properties of geotextile (Pilarczyk, 2000). Although, in small scale models using a thinner suitable geotextile was recommended to warrant sufficient rigidity and flexibility of geobag (Mudiyanselage, 2013). Van Steeg and Vastenburg (2010) using a scale of 1:4, studied the scaling problem of geotextile and fill materials during an experimental study investigating hydraulic stability of geotextile tubes, but could not obtain a proper conclusion.

To date there are not available defined scaling rules regarding geotextile and fill materials in small scale geobag structure models. Since it was not practical to manufacture a scaled down model of the constituent materials within the geobags and satisfy other model parameters such as the interface friction, the hydraulic conductivity of geotextile and the properties of fill material (sand), it is clear that some material distortion exists in the study. In the present study, models of geobag were constructed from a realistic and commercially available nonwoven geotextile (Secutex® 401 GRK 5 C 4) filled with fine sand with a Fineness Modulus of 1.72, D_{50} of 0.2 mm and a dry density of 1.83.

In Jamuna riverbank protection work, the recommended field characteristics by NHC (2006) were geobags of dimensions 1.03 × 0.7 m and 126 kg mass which offered the best performance (see chapter 2). Therefore, for the laboratory experiments, this size considered to be scaled down applying the 1:10 scale and to achieve the purposed size of small scaled sand-filled bags, the empty flat geotextile bag (unfilled) dimensions were set to 113× 80 mm which after filling to 80% of its capacity should have covered 80% of its unfilled area (length × width) (Oberhagemann *et al.*, 2006). Eventually, models of geobag which with 80% filling ratio represented a sand-filled bag of 0.126kg mass and

dimensions of 103 × 70 mm were prepared for the laboratory tests. The density of the dry geobag was found as 1596 kg/m^3.

Since the hydraulic permeability of a geobag revetment mainly depends on the void size between neighbouring geobags (Recio, 2008) with a proper scaled down geometry, the model of geobag revetment should represent adequate permeability as the prototype.

3.1.2. *Experimental setup*

Experimental tests were performed in a hydraulic flume (22m long, 0.75m wide, 0.50m deep). The channel bed slope was set to 5.5×10^{-3} which replicates that in the Jamuna River, where the present geobag revetment exists, making the present work directly comparable to previous similar studies (NHC, 2006; Akter, Crapper, *et al.*, 2013). Two pumps were employed to generate the required flow at the upstream end of the flume, while each of them provided a maximum pumping rate of 75 l/s. Since construction geobag revetment along the whole length of the flume was not feasible, based on some primary runs, a 3m long prototype geobag revetment was placed within the quasi-uniform flow zone within the flume (Figure 3.1). Depending on the specific design criteria (slope and bond, see below), the prototype geobag revetment consisted of 600-800 geobags.

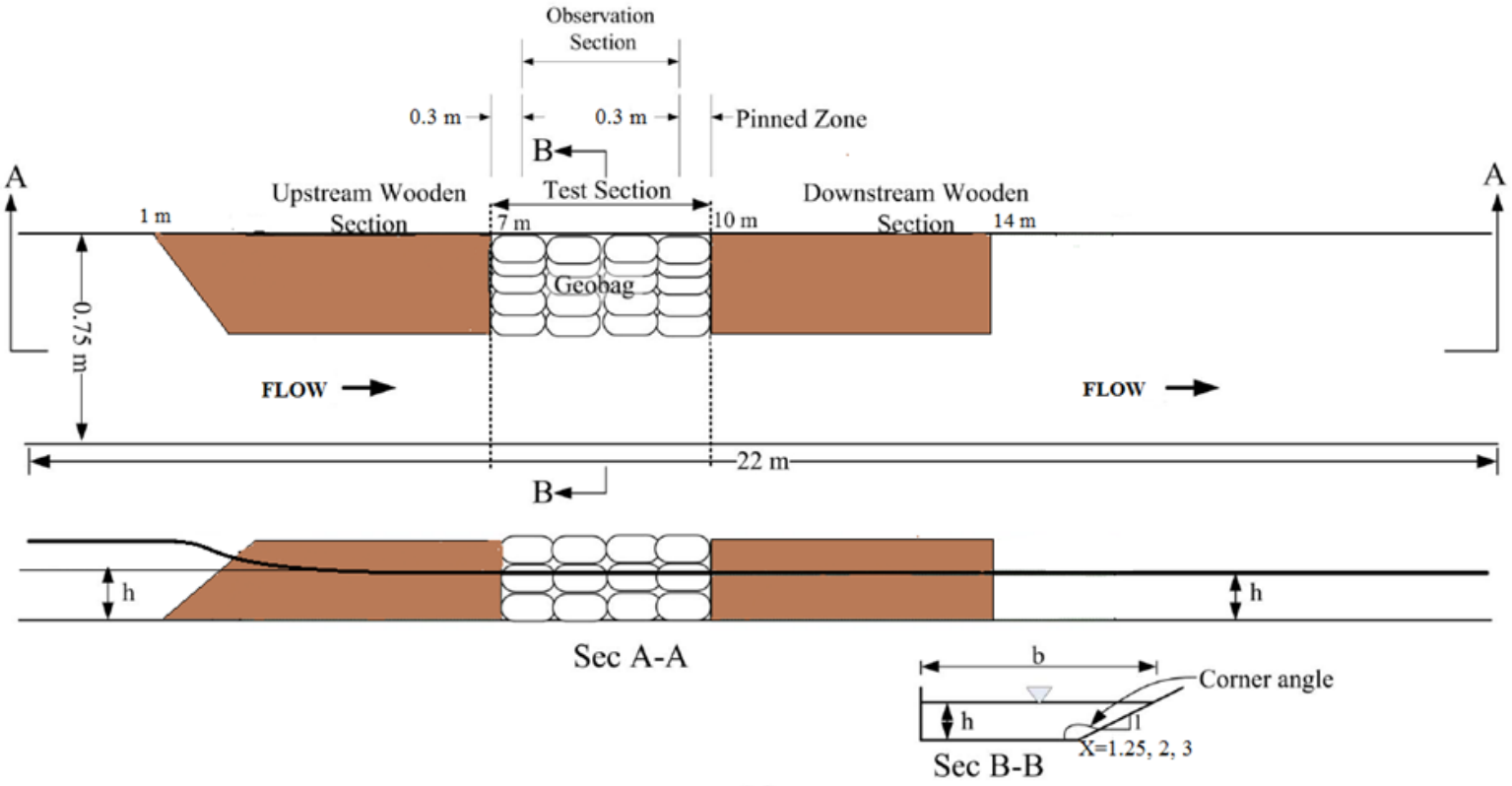

Figure 3.1: Experimental apparatus

3.1.2.1. Flow transitions

To minimise the impact of the unavoidable flow contraction and expansion, tapered wooden sections were installed at the upstream and downstream ends of the observation section. Additionally, to avoid turbulence driven effects at the interface between the wooden tapers and the geobag structure and reduce the edge effect due to discontinuity (model limitation), the surface geobags were pinned down for a distance of 0.3m of the test section at either end. Both of these measures help better replicate field conditions, where sections of geobags are typically flanked by firmer (soil or rock) conditions.

To observe the performance of the geobag revetment under hydrodynamic loads, and to avoid the impact of toe scouring on the process of failure, the experiments were conducted under a fixed-bed (non-erodible) condition. Experiments ran for approximately seven hours, which was sufficient for the failure processes to stabilise, i.e. there was no significant further change in revetment structure. From previous studies (Akter, Pender, *et al.*, 2013), it was observed that specific failure modes tend to occur in different ranges of water depth. Thus, experiments were run under steady/quasi-steady conditions with low, medium and high-water depths as follows:

a. Condition A: water level up to 49% of revetment height (low-level);
b. Condition B: water level between 50-60% of revetment height (medium-level) and
c. Condition C: water level between 60-80% of revetment height (high-level).

However, to keep flow Froude numbers as constant as possible and hence enable comparison of all results, water depths for the steepest side slope configuration were 0-30%, 30-40% and 40-50% of revetment height.

3.1.2.2. Revetment side slopes

According to previous experimental work (NHC, 2006), manually dropping 126kg bags into place from the riverbank or from dumping pontoons located on the river produces typical revetment side slopes of 1V:2H. However, it seems reasonable to assume that the existing (pre-revetment) side slope of any riverbank will play a significant role in the final revetment side slope and that the final revetment slope may influence the overall stability of a geobag revetment. Hence, three different side slopes (1V:1.25H, 1V:2H, 1V:3H), which were practically feasible to be constructed within the flume, were tested to investigate the impact of side slope on stability and failure mode. These side slopes

gave revetment dimensions of 0.375 m width and 0.30, 0.18, 0.125 m height respectively. For both construction bonds (see below), the number of geobags used for each revetment were 620, 730 and 810 respectively (Figure 3.2(a to c)).

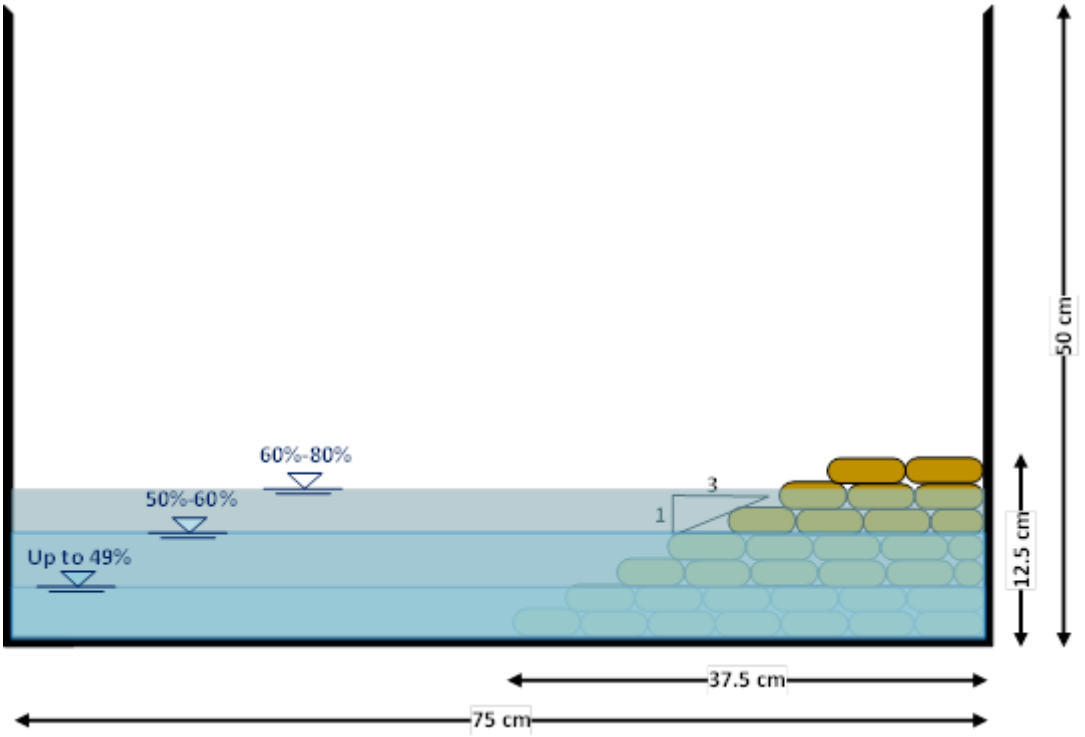

(a) Side slope: 1V:2H

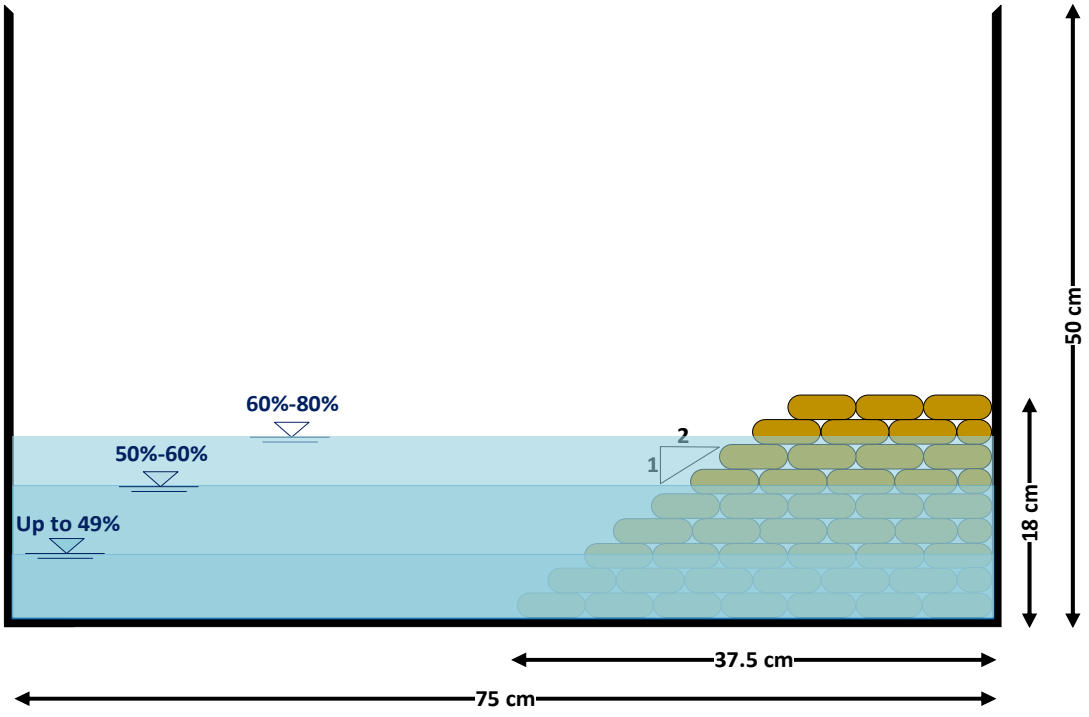

(b) Side slope: 1V:2H

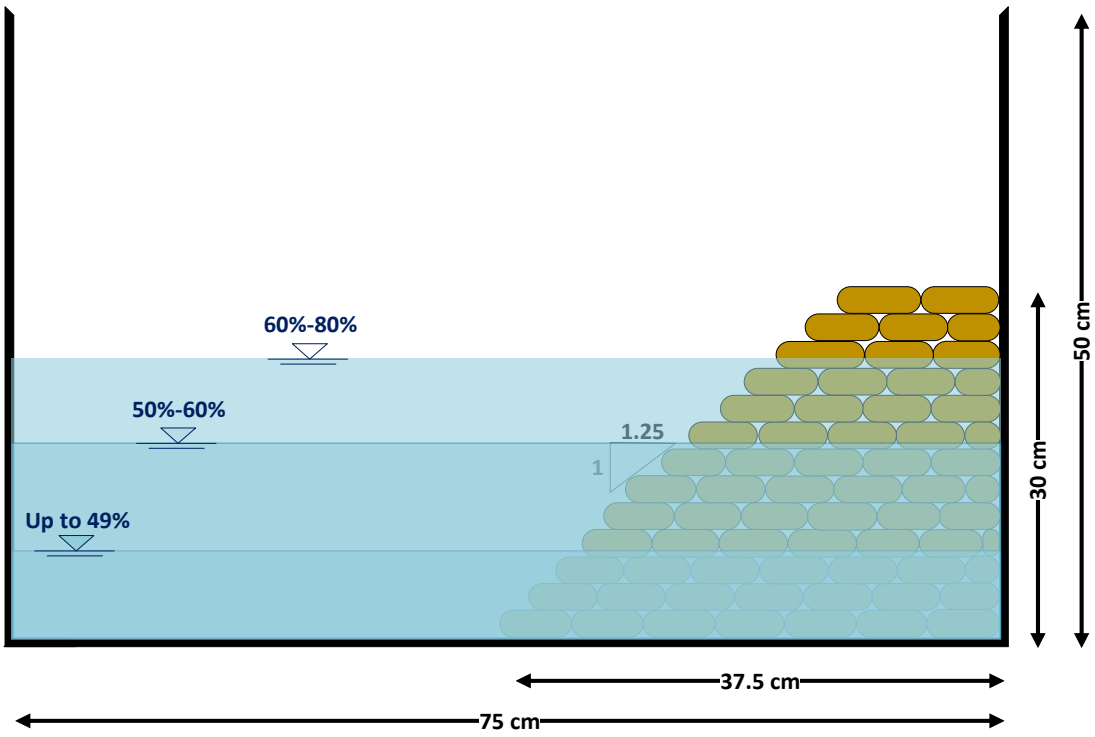

(c) Side slope: 1V:1.25H

Figure 3.2 (a to c): Water depth conditions, revetment side slopes: (a)1V:3H, (b)1V:2H, (c)1V:1.25H

3.1.2.3. Construction bond

In the field, different placement methods (e.g. riverbank launching, pontoon launching) can lead to a wide range of different construction bonds due to random placement

(Oberhagemann and Hossain, 2011). To determine the impact of construction bonds on revetment performance, two possible different bonds were tested (Figure 3.3a, b), namely a stack bond (0% longitudinal overlap) and a running bond (50% longitudinal overlap). In accordance with accepted practice and the results of previous field studies (Zhu et al., 2004), geobags were placed with the longest axis in the streamwise direction for both construction methods, and with transverse overlaps varying between 50% and 60% depending on revetment slope.

(a) stack bond

(b) running bond

Figure 3.3 (a,b): Revetment construction - stack bond (a), running bond (b)

3.1.3. *Data collection*

In this study, using different revetment side slopes and construction methods associated with varying water depths, laboratory experiments on hydrodynamic forces were conducted to acquire (i) observations of complete failure processes, (ii) velocity measurements of flow, (iii) effect of failure on flow conditions close to revetment and (iv) three-dimensional velocities analysis.

Along with the three side slopes and two construction bonds, this resulted in a total of 18 separate experimental scenarios. Prior to the commencement of each test, the weights of the individual surface geobags were measured to ensure that all individual experiments run with relatively dry bags (moisture content less than 0.5%). At the end of each test, the number of bags that were displaced from the revetment and settled at the end of the flume (washed away geobags) was recorded. To ensure representative results, each test was repeated at least 2 times, with a third test undertaken if the results from the first two differed significantly.

Experiments were run under steady/quasi-steady flow conditions and each model run was recorded by a video camera from the beginning of revetment construction until the

end of the model test to capture the performance of geobag revetment under different conditions.

3.1.3.1. ADV Measurements

Nowadays in fluid dynamics water velocity needs to be measured in laboratory and field research with a high temporal and spatial resolution. Although some technique like Laser Doppler velocimetry (LDV) and particle image velocimetry (PIV) commonly used as reliable measuring techniques which satisfy such requirements some restrictions reduce the feasibility of these techniques when the scale of the experiment increases or in the case of flow with suspended sediment. In most of these cases, Acoustic Doppler Velocimetry (ADV) could be an alternative technique due to its lower cost, its capability of recording data at a relatively high frequency (up to 100 Hz) and its relatively small sampling volume (according to the instrument selected, it could vary from 0.09 to 2 cm^3). Acoustic Doppler velocimeters could accurately record mean values of 3-dimensional water velocity (Lohrmann *et al.*, 1994; García *et al.*, 2005, 2007) even in low flow velocities (Lohrmann *et al.*, 1994). Although Lohrmann *et al.* (1994) reasoned that the acoustic Doppler velocimeters provide enough resolution to capture a considerable fraction of the Turbulent Kinetic Energy (TKE) of the flow, they found that the Doppler noise could cause the TKE to show an inclination toward a high value. To define the optimal flow and sampling conditions for turbulence measurements using ADVs, the acoustic Doppler velocimeter performance curves (APCs) were introduced by (García *et al.*, 2005) as a new tool to assess the capability of acoustic Doppler velocimeters to resolve flow turbulence.

3.1.3.2. ADV Performance Curves

The parameter F shows the capability of an ADV to resolve flow turbulence and is defined as:

$$F = \frac{f_R L}{U_c} = \frac{f_R}{f_T} = \frac{L}{d_R} \qquad \text{Equation 3.1}$$

where L = length scale of the energy containing eddies (here taken as equal to the water depth, h), f_R = ADV user set frequency (here 25 Hz), Uc = convective velocity (approximately U_{avg}), f_T = characteristic frequency of large eddies presents in the flow and d_R = diameter of the sampled volume (set by flow and sampling characteristics).

A higher value of F indicates a better description of the turbulence that can be achieved with a specific instrument (García *et al.*, 2005). With values of $F > 20$, the turbulence scale is well described, but for lower values, $F < 20$, smoothing out of portions of the turbulent motion by the ADV results in lowered second- and fourth-order moments, lowered energy in the power spectrum and increased integral time scales. García *et al.* (2005) demonstrated these reductions as functions of F in the concept of "ADV performance curves."

In the present study, as the sampling volume is clearly not a point, so using d_R to calculate F is the method recommended by García *et al.* (2005). Furthermore, in the case of the 10 MHz Nortek ADV used in the laboratory tests, the diameter of the measurement volume is d=6 mm and represents the minimum value of d_R according to García *et al.* (2005). With f_R=25 and U_c (~U_{avg}) higher than 15 cm/s, using the average water depth at the flume, h=0.1 shows that the time series had F values <20, and F_{min}=16. According to the ADV performance curves of García *et al.* (2005) this would lead to an average decrease of the second-order moments by approximately 16% relative to their true values. This shows that, even though the ADV performance curve indicates that the measurement conditions in the laboratory were not optimal for turbulence measurement the velocity data still contains useful information about the flow around the revetment.

3.1.3.3. Velocity measurement

General velocity data were collected using a side-looking Acoustic Doppler Velocimeter (ADV) at 0.10 m intervals in the streamwise direction, at 20%, 40%, 60% and 80% of the water depth below the surface. This data was used to calculate mean velocities using the three-point method (British Standards Institution (BSI), 2007), i.e. the average of the values at 0.2, 0.6, and 0.8 of the depth.

As this and other studies (Akter, 2011) have identified the significance of flow conditions on revetment failure mechanisms and additional velocity data was collected to better understand hydraulic conditions during failure progression. Because for a side-looking ADV, the transmit pulse is typically directed away from the bottom boundary, it makes this type of AVD a better alternative than the down-looking for measuring flow velocity in shallower flow (NORTEK, 2018). Therefore, using a side looking ADV, detailed three-dimensional velocity measurements were taken for the most likely occurring revetment configuration (side slope of 1V:2H, medium water depth and stack bond construction). With the ADV probe positioned at 0.5h=4.5cm (where h is the total

water depth) above the bed of flume at each point (Figure 3.4), the duration of sampling was set to 120 s, which gave 2,000 data samples for each velocity component at a frequency of 25 Hz.

As the sampling volume was 5 cm from the probe, measurements could be taken immediately adjacent to the revetment with minimal disturbance to the flow. Velocity measurements were taken during both the pre-failure and post-failure stages. During the pre-failure stage, the surface layers of geobags were pinned down to ensure they did not move during the measurement period, and the velocities were measured at 104 different nodal points, covering 60cm of the test section or approximately half the length of the failure zone (Figure 3.5a). Velocity measurements during the post-failure stage were undertaken when the revetment had stabilised, i.e. after there was no significant further change in revetment structure. To avoid minor bag movements affecting measurement accuracy, all of the geobags on the remaining surface of the failed revetment were again pinned down in situ. To cover the failure zone for the post-failure condition, a section of 130cm was chosen to measure velocities (Figure 3.5b), resulting in 183 different nodal points.

WinADV32-version 2.028 software was used to de-spike each set of obtained ADV measurements. For the present study, the Phase space threshold de-spiking filter was applied to filter the output data from the ADV. This filter was provided by Goring and Nikora (2002), and it has been employed in WinADV32 Software.

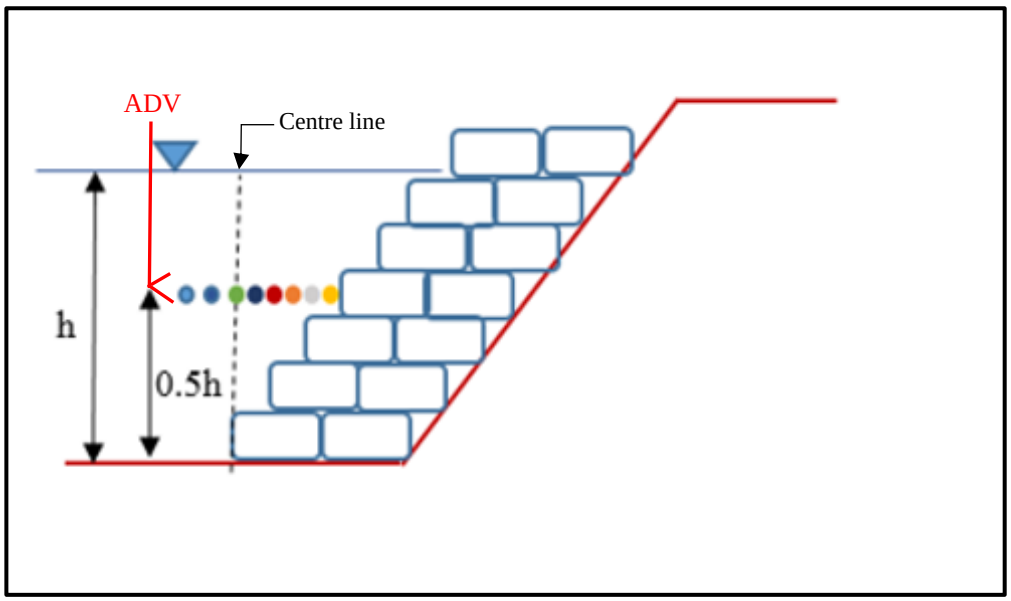

Figure 3.4: ADV probe location for both pre- and post-failure conditions

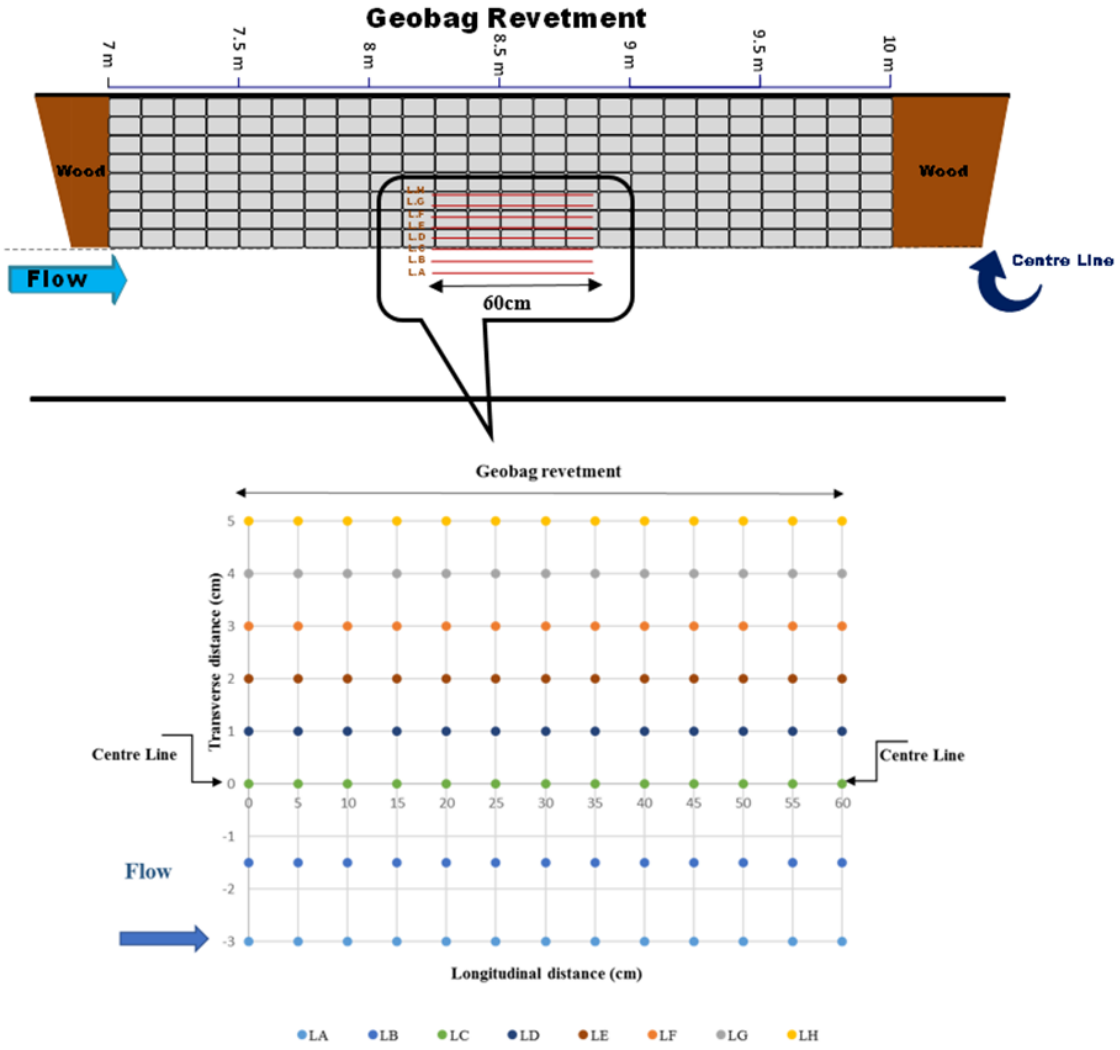
Geobag Revetment
7 m
7.5 m
8 m
8.5 m
9 m
9.5 m
10 m
Wood
Wood
Flow
Centre Line
60cm
LH
LG
LF
LE
LD
LC
LB
LA
Geobag revetment
Transverse distance (cm)
Longitudinal distance (cm)
Centre Line
Centre Line
Flow
LA
LB
LC
LD
LE
LF
LG
LH

(a)

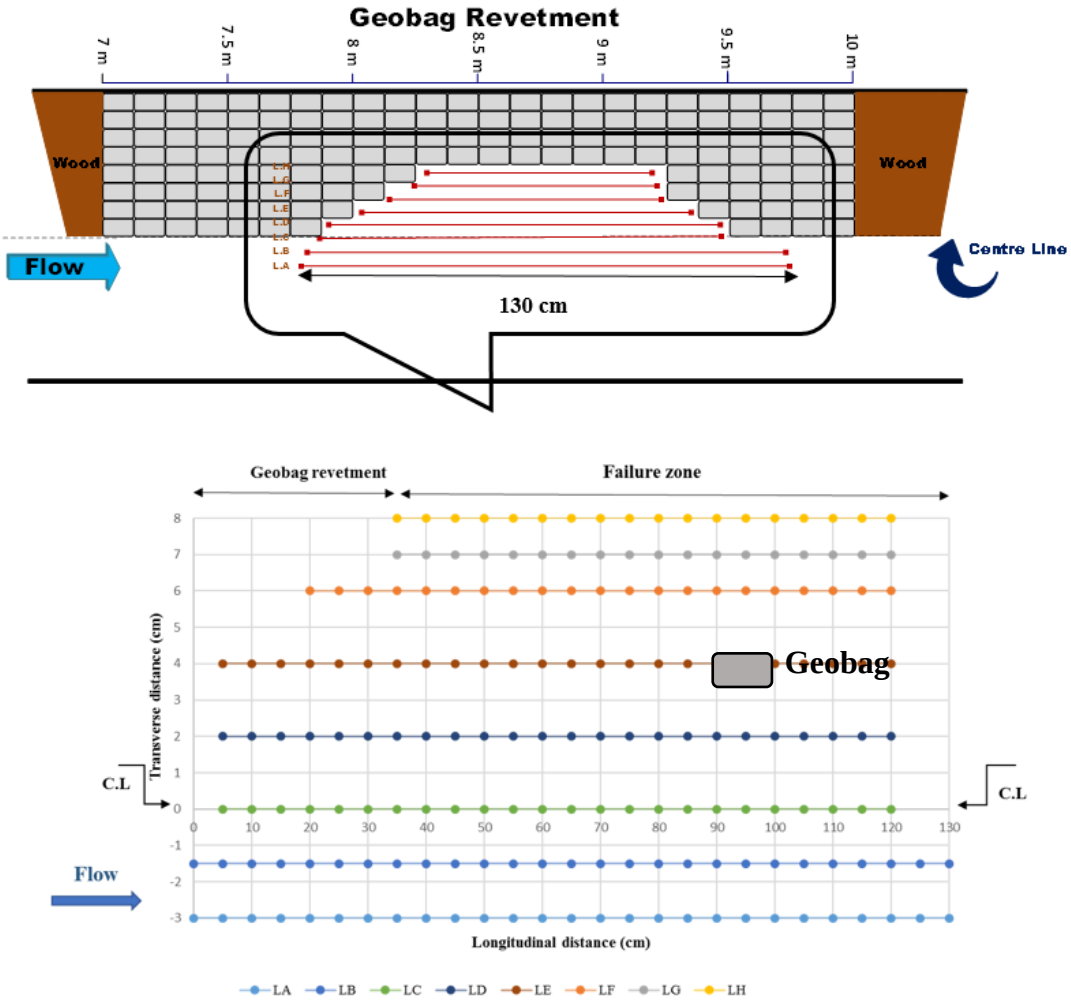

(b)

Figure 3.5: Velocity measurement locations for (a) pre-failure and (b) post-failure conditions.

3.1.4. *Experimental limitations*

In this phase of the research the distorted-scale model used in laboratory experiments has the following restrictions:

- Physical model-scale effects: Due to the material distortion a scale effect that might be noticeable is that -compared with the prototypes, the scale models of geobag were quite stiff and could not deform sufficiently to affect the contact area and consequently bag-on-bag friction (Neill *et al.*, 2008). Bag-on-bag friction might be relatively insignificant for initial bag displacement, where the lift force is the main hydrodynamic force (see chapter 4 and 5) that causes to displace geobags from the surface of revetment, but it might become important during the processes of failure;
- In the laboratory, the flow has a higher level of turbulence than flows in the real river, although the higher turbulent flow could provide easier observation of the failure modes(Akter, Pender, *et al.*, 2013).

Considering these limitations, the distorted model offers a good basis for the DEM model setup detailed in following subsections.

3.2. Numerical methodology

A Discrete Element Model (DEM) is further developed and validated to simulate the geobag structure and its behaviour under the range of the different conditions tested in the laboratory. The hydraulic scale-model tests conducted (see section 3.1) towards a full understanding of the complete failure processes involved in the geobag revetment. The stability of the geobag-structure is tested by the available Discrete Element model code "LIGGGHTS" which has been extended/adopted for this study.

3.2.1. *Development of the DEM model*

In order to work towards our aim of developing design guidelines for geobag revetments in rivers, numerical simulations were attempted using the Discrete Element Method (DEM). The Discrete Element Method is a numerical method used to simulate the movement and interaction of a large number of rigid or deformable discontinues elements either sphere or arbitrary shaped particles subjected to external stresses or forces (Mustoe and Miyata, 2001; Crapper et al., 2005, Akter et al. 2013). In particular, DEM is suitable for granular media as it is known for modeling particles, so each simulated particle could be either a single element or discretised into particle shaped elements (Padrós, 2014). Therefore, DEM is a useful numerical technique for tracking the movement of each element in this case, an individual geobag, according to Newton's Laws of Motion, accounting for collisional and frictional forces between elements and between elements and boundaries and in case of hydraulic forces, in particular, drag, lift and buoyancy.

Recio and Oumeraci, (2009a) used a UDEC model consists of a Finite Element Model (FEM) that simulated the total stresses and deformations for each geobag and a Discrete Element model (DEM) that used to simulate the displacement of each geobag. UDEC were partially coupled with COBRAS (a fluid dynamic base model) to represent a 2D numerical model of a geobag structure. The aim their study was investigation the effect of frictional forces and deformation on the stability of geobag structures. Mudiyanselage (2013) developed a 2D numerical model of geobag structures affected by wave actions using coupled RANS-VOF model and FEM-DEM models (COBRAS-UC/UDEC) and studied the impact of deformation on the hydraulic stability of crest geobags. Since FEM deals with continuum problems while DEM deals with discontinues problems. In both above studies FEM method was applied on deformable geobag which were divided into a mesh of finite difference elements. The deformation of geobag were simulated by

responding each element to the linear or nonlinear stress-strain law. In contrast DEM simulates the behaviour of discontinuous objects (geobags in revetment) exposed to either static or dynamic loading(fluids). The relative motion of the discrete elements is calculated based on linear or nonlinear force displacement relations in both normal and shear directions.

Akter, (2011) previously used a simple DEM-CES model for simulating the initial bag movement in the revetment. DEM model presented by Akter simulated the critical location for bag instability in the revetment based on the initial response of any layer of geobags in the revetment. Therefore, simulation of different failure modes and failure processes in a geobag revetment using an applicable numerical model was still a challenge before conducting the present study.

Considering the three interactions that govern the failure processes of geobags, i.e., geobag–geobag, geobag–water flow, and geobag–water flow–riverbank, the DEM solver can calculate the particle positions and velocities used for individual particles (geobag and sediment particles in scour situations) and its interaction with other particles (geobag to geobag) and boundary surfaces (geobag to riverbank material). In this study, one of the main objectives was to model the distinctive shape of the geobag and to reproduce a three-dimensional DEM setup of geobag revetment. This was achieved using the open source DEM code LIGGGHTS (*DCS Computing*, 2018). LIGGGHTS is an open source, C++, MPI parallel DEM code for modelling granular materials. LIGGGHTS stands for LAMMPS Improved for simulating General Granular and Granular-heat transfer. LIGGGHTS was developed and distributed by Sandia National Labs (*DCS Computing*, 2018) and it is based on the Open Source MD code LAMMPS. LIGGGHTS now brings DEM features of LAMMPS to an advance level. Additional characteristic features have been implemented on top of the LIGGGHTS "GRANULAR" features are as follow:

- The capability of importing and handling complex geometry and triangular meshes from computer-aided design (CAD) into a LIGGGHTS simulation;
- Pair style parameters like stiffness and damping can be linked to material properties that can be derived from lab experiments (e.g. density, Young's Modulus, Poison's ratio and coefficient of restitution);
- The possibility of re-write contact formulations, such as define macroscopic particle cohesion;
- A moving mesh features.
- Dynamic load balancing feature.

- Improved particle insertion.

More features, such as improved handling for non-spherical particles, 6 degrees of freedom solver for arbitrarily shaped bodies, and wall stress analysis have also been developed (Padrós, 2014)

Furthermore, LIGGGHTS is part of the CFDEM project with the goal to develop a new CFD-DEM approach and provides the potential for modelling soft materials, solid-state materials and coarse-grained granular materials. The open source LIGGGHT model has the capability of the creation of non- spherical particles by linking and overlapping spheres of differing sizes. As the principal goal of this study was to track the geobags' movement under different hydraulic loading and toe scour conditions, hence LIGGGHTS can be regarded as the most appropriate and feasible tool to simulate the failure mechanisms of geobag revetment through the objectives defined for this project (see chapter 1).

In addition to hydraulic forces, the DEM model accounted for geobag self-weight under gravity, sliding friction and tangential and normal forces in collisions using a Hertz-Mindlin soft-sphere collision model which it has implemented in LIGGGHTS.

3.2.1.1. Hertz-Mindlin (HM) Granular Contact Model

The Hertz-Mindlin model is the most commonly used within DEM simulations. It is a non-linear elastic model and one of the most suitable computational models to present the non-cohesive interactions. According to this model the contact force depends on the local contact law. Therefore, when two particles establish contact, the result of contact force will be the total of normal forces and tangential forces. The value of the contact force is described by Equation 3.2.

$$F = \underbrace{\left(K_n \underbrace{\delta n_{ij}}_{\substack{normal\\ overlap}} - \gamma_n \underbrace{Vn_{ij}}_{\substack{normal\\ relative\ vel.}} \right)}_{normal\ force} + \underbrace{\left(K_t \underbrace{\delta t_{ij}}_{\substack{tangential\\ overlap}} - \gamma_t \underbrace{Vt_{ij}}_{\substack{tangential\\ relative\ vel.}} \right)}_{tangential\ force} \quad \text{Equation 3.2}$$

The normal force is a function of normal overlap $K_n \delta n_{ij}$, normal component of the relative velocity $\gamma_n Vn_{ij}$ and K_n is given by:

$$K_n = \frac{4}{3} Y^* \sqrt{R^* \delta_n} \quad \text{Equation 3.3}$$

Where Y^* and R^* are the equivalent of Young's Modulus and the equivalent radius respectively and are defined as:

$$\frac{1}{Y^*} = \frac{(1-v_i^2)}{Y_i} + \frac{(1-v_j^2)}{Y_j} \quad \text{Equation 3.4}$$

$$\frac{1}{R^*} = \frac{1}{R_i} + \frac{1}{R_j} \quad \text{Equation 3.5}$$

With Y_i, R_i, v_i and Y_j, R_j, v_j being the Young's Modulus, Poisson's ratio and radius of each sphere in contact. γ_n is given by:

$$\gamma_n = -2\sqrt{\frac{5}{6}}\,\beta\sqrt{S_n m^*} \geq 0 \quad \text{Equation 3.6}$$

$$\frac{1}{m^*} = \frac{1}{m_i} + \frac{1}{m_j} \quad \text{Equation 3.7}$$

Where m^* is the equivalent mass. S_n and β (the normal stiffness) are given by:

$$S_n = 2Y^*\sqrt{R^*\delta_n} \quad \text{Equation 3.8}$$

$$\beta = \frac{ln(e)}{\sqrt{ln^2(e)+\pi^2}} \quad \text{Equation 3.9}$$

With *e as* the coefficient of restitution. The tangential force is a function of tangential overlap $K_t\delta t_{ij}$ and the relative tangential velocity $\gamma_t V t_{ij}$. Where K_t and γ_t are given by:

$$K_t = 8G^*\sqrt{R^*\delta_n} \quad \text{Equation 3.10}$$

$$\gamma_t = -2\sqrt{\frac{5}{6}}\,\beta\sqrt{S_t m^*} \geq 0 \quad \text{Equation 3.11}$$

Where G^* is the equivalent shear modulus and is given by:

$$\frac{1}{G^*} = \frac{2(2-v_i)(1-v_i)}{Y_i} + \frac{2(2-v_j)(1-v_j)}{Y_j} \quad \text{Equation 3.12}$$

Also, Coulomb friction is described by $\mu_s F_n$ and is applied to limit the tangential force by the coefficient of static frictionμ_s.

For this contact model three mechanical properties for each material (Young's modulus, Poisson's ratio, and density) and two-particle interaction properties (the coefficient of restitution and Coulomb or static friction coefficient) are required for a simulation. Verifying the output of EDEM model runs with the dry experimental results, Akter, Pender, *et al.*, (2013) determined the coefficient of static friction of 0.55. They also recommended using the minimum value of the coefficient of restitution (0.0001) to reflect the low "bounce" nature of the bags (Table 3-2). Furthermore, the initial model run with arrange of different combinations of mentioned parameters to handle the sensitivity of the model.

The numerical model has been developed in a Linux machine, with Ubuntu 14.04. The LIGGGHTS-PUBLIC package version 3.3.1 was downloaded and compiled on a desktop system with 20GB of RAM memory and a quad core processor at 3.2GHz. This package prepared to run simulations in parallel.

Table 3-2 Required Material and Interaction Properties for LIGGGHTS Geobag Revetment Model

Material properties			**Interaction properties**	
Details	**Geobags**	**Flume bed (Iron)**	**Details**	**Value**
Modulus of rigidity (G)(pa)	1.1×10^{6}[e] - 1.9×10^{6}[f]	8.16×10^{10}[g]	Coefficient of static friction	0.55[h]
Poisson's ratio (υ)	0.42[i]	0.293[e]	Coefficient of restitution	0.0001
Density (ρ) (kg/m^3)	1596[j]	7852[e]		

3.2.2. *Hydrodynamic forces on geobags*

Hydraulic forces in DEM depend on a formulation to describe them regarding the surrounding fluid. This can come directly from experimental measurements or from a modelling approach such as CES used by Akter (2011) or from CFD simulations. In the latter case, the link between the DEM and the CFD can be one-way coupling in which the discrete elements (geobags) have no impact on the flow field or fully-coupled, in which the momentum and/or volume of the geobags are used in the CFD and updated at every CFD time step. The latter is theoretically more accurate but requires a vastly more computational resource to transfer data between the DEM and CFD aspects of the simulation.

The approach followed herein was to use a one-way coupled approach for initial model runs, with additional comparisons to a fully-coupled approach to determine whether the additional computational expense was warranted.

[e] Data from Recio and Oumeraci (2009c)

[f] Geobag in shearbox experiment was carried out following BSI (1991)

[g] Data from Tilley (2004)

[h] Data from Akter (2011)

[i] Young's modulus was obtained for only geotextile following(British Standards Institution (BSI), 1992).

[j] Considering geobag as coarse aggregate, experiment carried out following BSI (1995)

Although drag is the significant and dominant force in the dynamics of spherical particles in a fluid, Yin *et al.* (2003) showed that when the spheres are in the high–shear region, lift forces and Magnus forces become important. For non–spherical particles, the lift force is also influential at lower shear because of the aspect ratio of the particle shapes.

Tran-Cong *et al.*, (2004) conducted laboratory measurements to determine the terminal velocity of irregularly shaped agglomerates of spheres. The drag coefficients are reported for six different geometrical shapes. A new and accurate empirical correlation for the drag coefficient, C_D, of irregularly shaped particles was developed. They observed a good agreement for the variously shaped agglomerates of spheres as well as for the regular shape particles, over the ranges $0.15 < Re < 1500$. Akter (2011) approximated the hydrodynamic forces and torques acting on a non–spherical particle in a non–uniform flow field by using a new simple DEM model. In this case, the geobags are approximated as a number of interconnected, simple rectangular flat plates. Drag and lift are calculated for each plate based on semi-empirical drag models. Then, the drag and lift coefficients were set manually by the user in the model to replicate the observation.

The one-way coupling is a simple, yet highly computationally efficient, method of simulation. Constant drag and lift forces were applied using traditional formulations which are adopted from Yin *et al.* (2003) as in equations Equation 3.13 and Equation 3.14:

$$F_D = 0.5 C_D \rho_w A_S \vec{V} |V| \qquad \text{Equation 3.13}$$

$$F_L = 0.5 C_L \rho_w A_T \frac{\vec{z}.V}{|V|} [\vec{z} \times V] \times V \qquad \text{Equation 3.14}$$

Here, ρ_w is the density of the water, C_D and C_L are drag and lift coefficients, V is the velocity of the geobag relative to the water, A_S is the cross-section area normal to the flow, A_T the cross-sectional area tangential to the flow and $\vec{z}$ is geobag major axis direction. Drag and lift forces are calculated for each primary sphere base on Equation 3.13 and Equation 3.14 then the total force is summed up for all spheres. The total torque acting on the particle (multi-sphere model of the geobag) is determined by summating the

torque produced by the total of the hydrodynamic forces acting on each discretised sphere with respect to the centre of gravity of the particle (geobag). The buoyancy force is included in the calculations.

3.2.3. *Geobag revetment representation in DEM model*

Numerical activities initially focused on evaluating the suitability of different simulation methodologies, ranging from simpler DEM-only simulations through to fully coupled CFD/DEM approaches. In the current study, a primary fully coupled simulation was conducted using LIGGGHTS as an open source DEM software and Open FOAM as an open source CFD solver. The model run with two geobags which each one consisted 178 spheres. The CPU time required to finish the simulation was about seven days for two bags. The computational demands associated with fully coupled modelling, and the promising early results obtained from simpler approaches, indicated that DEM-only simulations (with CPU time of about 1 minutes for two bags) presented the best way forward. Similarly, the open source nature of the LIGGGHTS software made it the ideal candidate for model development, with the non-spherical geobags being modelled using the multi-sphere method (see Chapter 5).

3.2.3.1. Fixed bed

To reproduce the laboratory observations a 3D DEM model of the quasi-physical model was created using the LIGGGHTS. Using the same configuration, the LIGGGHTS model of geobag revetment setup in the flume was build up (as described in Section 3.1). With this setup, models of geobag revetment for two different construction bonds (running bonds and stack bonds) and three different side slopes of 1V:2H, 1V:1.25H and 1V:3H were made. (Figure 3.6 and Figure 3.7). The interaction properties are tabulated in Table 3-2. The simulation was run for 200 s to allow the failure processes completely. For each setup, the mean velocity in x, y, and z-direction measured in the laboratory was used as a basis for calculating the drag and lift forces on the geobags. Figure 3.6 and Figure 3.7 show the numerical model setups of geobag revetment for two different construction methods and three different side slopes respectively (see Figure 3.1 for the experimental equivalent).

To understand the applicability of the DEM model to predict the failure processes of geobag revetment, under different construction conditions, the numerical model was applied to simulate the response to different side slopes. The numerical model setups of geobag revetment for side slope 1V:2H was previously presented in Figure 3.6. Moreover

Figure 3.7 (A1 to A3) demonstrate DEM models of revetment for milder slope (1V: 3H), (1V:2H) and steeper slope (1V: 1.25H) respectively.

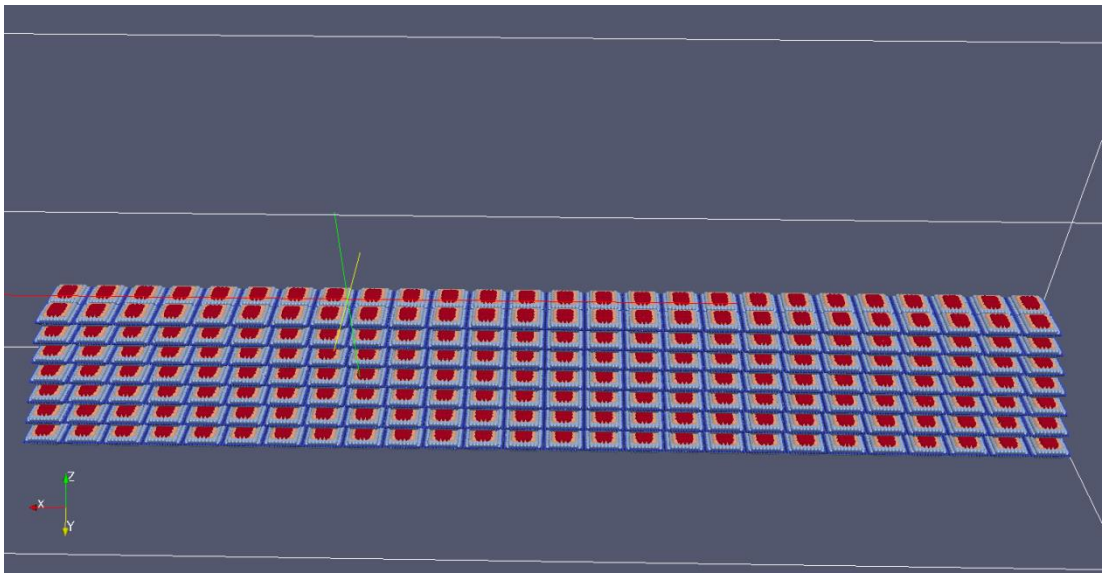

(A1) Stack Bond Construction

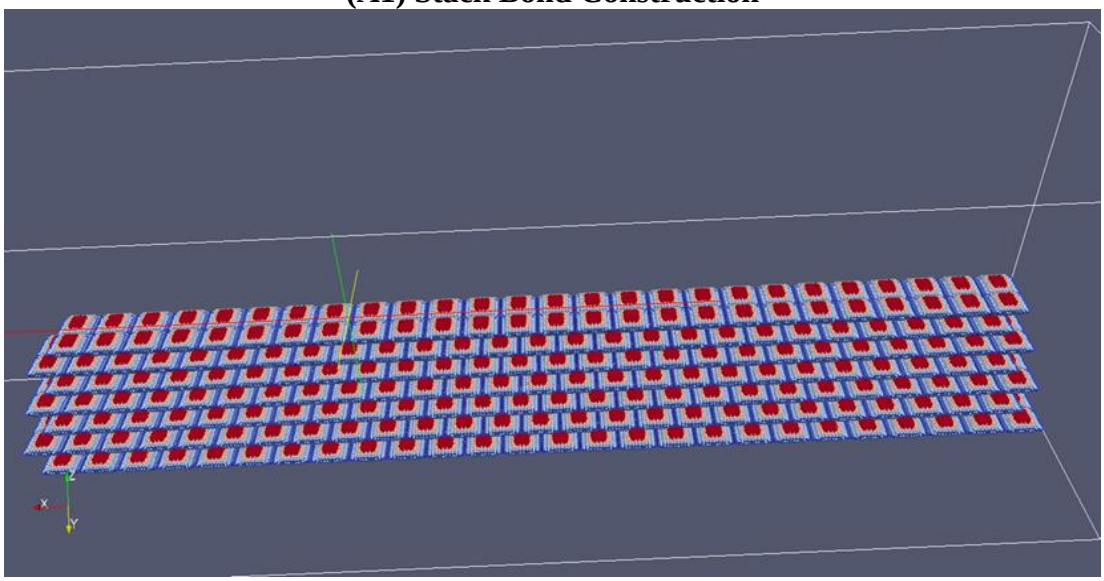

(A2) Running Bond Construction

Figure 3.6 (**A1** and **A2**): Model setup for the geobag revetment in the flume (different construction bonds)

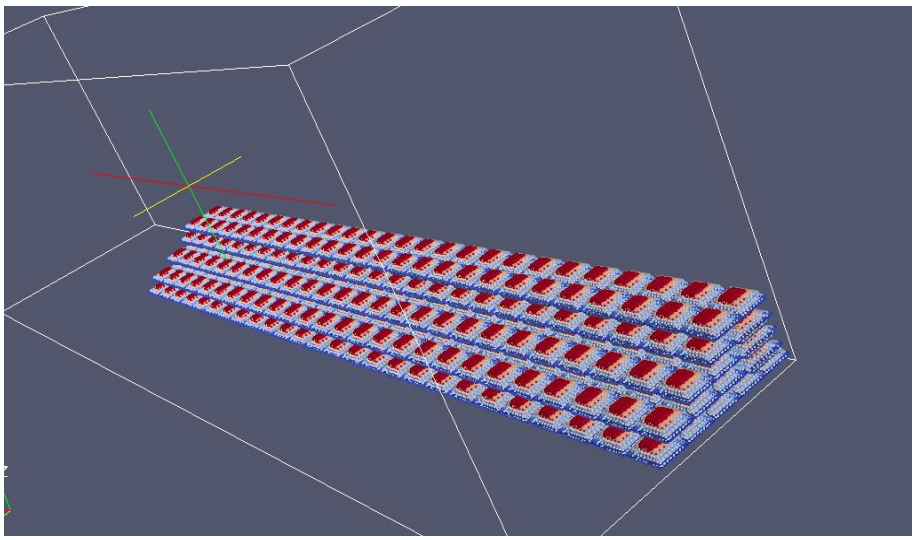

(A1) side slope 1V:3H

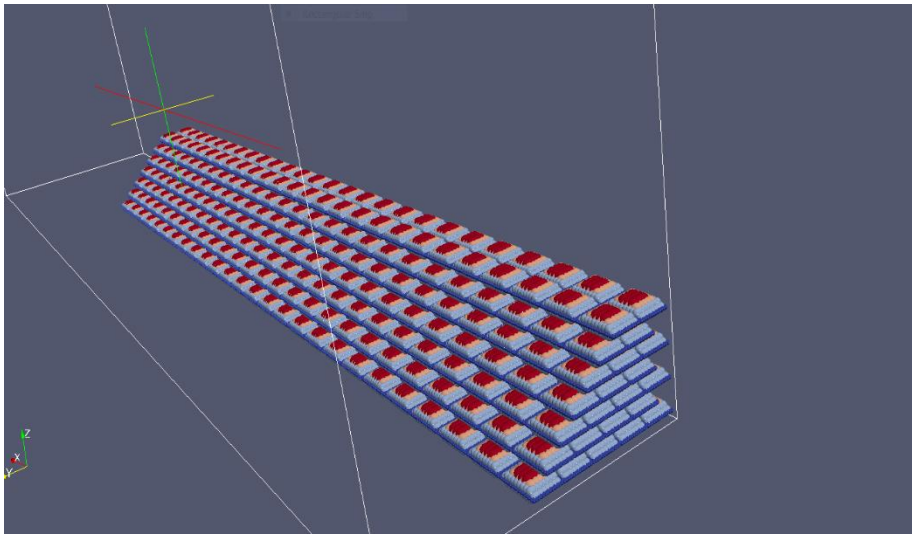

(A2) side slope 1V:3H

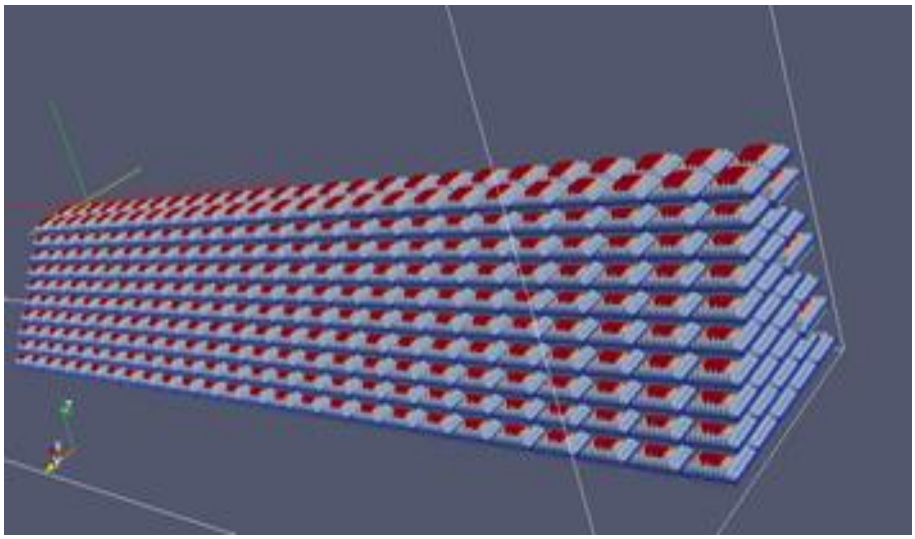

(A3) side slope 1V:1.25H

Figure 3.7 (A1to A3): Model setup for the geobag revetment in the flume (different side slopes)

3.2.3.2. Mobile bed

In this session an attempt was made to evaluate the response of the DEM model to bed erosion and toe-scouring. Thus, the DEM model was developed to simulate the sand bed underneath the geobag revetment. The simulation was carried out using the same experimental setup followed by Akter, Crapper, *et al.*(2013) and Akter, Pender, *et al.*(2013) and obtained result visually validated using their collected experimental data. Furthermore, numerical results were compared with the outcome of EDEM® applied by Akter, Crapper, *et al.*(2013) to confirm the advancement of the DEM model used in the current study.

In the case of mobile-bed, Akter, Pender, *et al.*(2013) applied 0.10-m-deep sand bed underneath the geobag test section with no upstream sediment supply or recirculation (Figure 3.8). Since experimental results for the fixed bed condition showed that the failure processes were not affected by specific geobag bond configuration, only stack bond construction was used for this simulation. According to referred work, the performance of geobag revetment over a sand bed was tested under four different water-level conditions. The conditions were as follows:

- Condition A (up to 49% of the geobag revetment height)
- Condition B (50–64% of the geobag revetment height)
- Condition C (65–84% of the geobag revetment height)
- Condition D (85–100% of the geobag revetment height)

Since no bag displacement was observed in condition A and B (Akter, Pender, *et al.*, 2013), in this study the simulation was just carried out for condition C and D (Table 3-3). shows the required input values for the DEM model.

In the model setup a mesh consisted of three separate pieces represented the 3 m long, 0.75 m wide sand bed. The middle piece was movable and giving a distance of 0.10 m to the bottom boundary of domain, representing the thickness of sand bed. This allowed it to move downward with the degree of freedom equal to maximum scour depth and the vertical velocity of 0.06 m/s reported in the mentioned study. This movable mesh was located underneath the toe area of revetment as the most scour prone location (Figure 3.9).

Table 3-3 Flow conditions at different water depths (Akter, Crapper, *et al.*, 2013)

Condition	Water depth % revetment height	Maximum scour depth (m)	Mean water level (m)	Mean velocity (m/s)	Flow rate (m3/s)	Froude number	Reynolds number
C	60-80%	0.03	0.01	0.76	0.0315	0.69	83665
D	80-100%	0.05	0.014	1.05	0.0712	0.79	189110

Table 3-4 Required material and interaction values for LIGGGHTS geobag revetment model on mobile sand bed (Akter, Crapper, *et al.*, 2013)

Material properties			Interaction properties	
Details	**Geobags**	**Flume bed (Sand)**	**Details**	**Value**
Modulus of rigidity (G)(pa)	1.1×10^6 1.9×10^6	1.25×10^7[k]	The coefficient of static friction	0.55
Poisson's ratio (υ)	0.42	0.2[i]	Coefficient of restitution	0.0001
Density (ρ) (kg/m^3)	1596	1830[l]		

[k]For Jamuna riverbed Tomlinson and Woodward (2007)

[l]Experiment carried out for the sand used in flume following the BSI (1995)

The DEM simulation was carried out applying the same practice as done for fixed bed programme. In order to the simulate the incipient failure mode, simulation runs for 100 seconds which allowed to initiate bag motion. The mapped streamwise velocity field of 0.05 m intervals provided by Akter *et al.* (2013) using the CES method, was applied (described later in subsection 4.4.2). The mean lateral and vertical component of the mapped velocity field was determined as 2.4% and 0.5% of the mean streamwise velocity respectively (Akter, Pender, *et al.*, 2013).

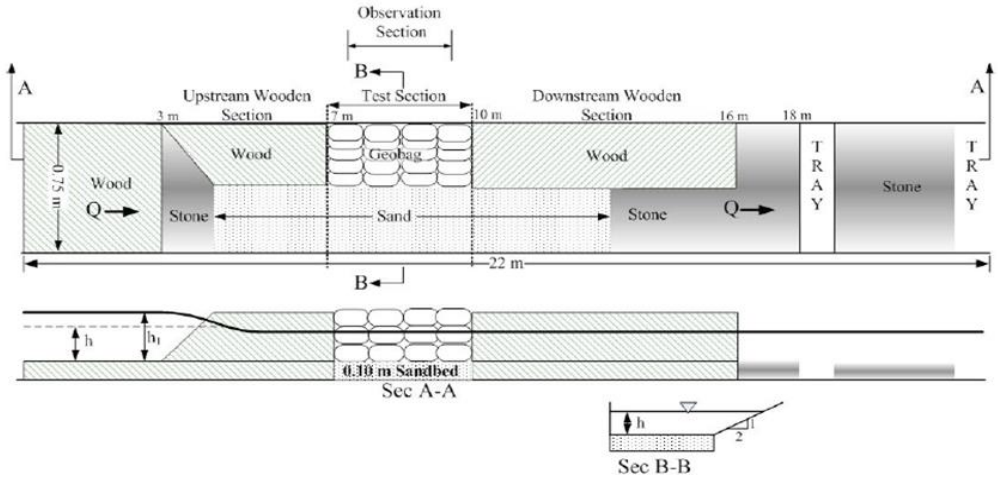

(A1) Schematic of mobile flume bed experiment setup

(A2) Geobag revetment on the sandbed

Figure 3.8(A1, A2): Experimental setup for mobile bed condition (Akter, 2011)

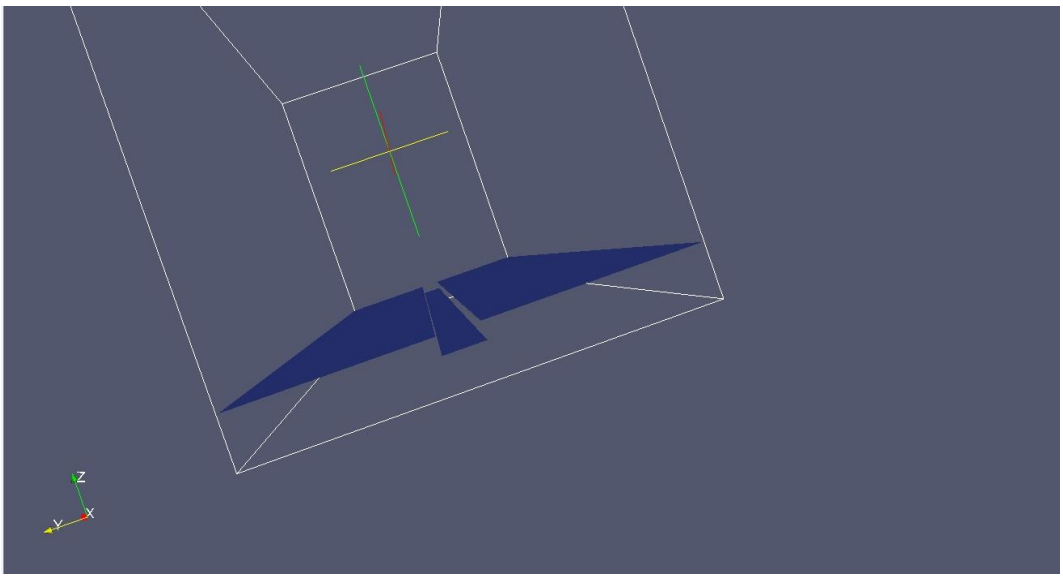

(A1) Representation of the sandbed and toe scour

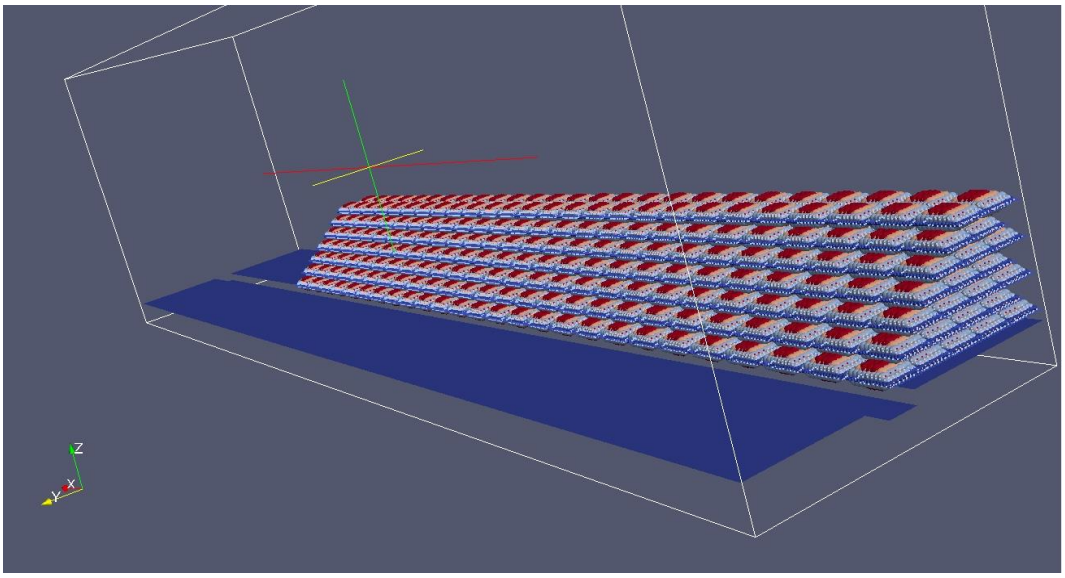

(A2) Model of geobag revetment over a sandbed

Figure 3.9 **(A1, A2):** Model setup of geobag revetment using LIGGGHTS

3.2.4 Validation process

Validation of a DEM model requires an evaluation of model performance in comparison to experimental data. This is considered as an essential step in any DEM modelling to confirm that the numerical results have a strong basis. The DEM model presented here was supported by undertaking a laboratory-scale validation. the validation approaches adopted in this study, are as follows:

- Qualitative approach: The experimental method is a very popular validation method used to validate numerical models (Abbaspour-Fard, 2004) and visual comparison, using experimental data, is the most common, and often the only available technique for validating DEM models (Yang *et al.*, 2008; Grima and Wypych, 2011; Obermayr *et al.*, 2014).
- Quantitative validation: A good measure for quantifying the behaviour of geobags in response to flow, neighbouring geobags and boundaries is the consideration of the time-averaged positions of a geobag in horizontal(x) and vertical (z). To use this approach position of bag removed and / or extent of uplifting was quantified (see results in chapter 5).

3.2.4. *Numerical model limitations*

In this phase of the research the numerical model has the following restrictions:

- Tolerance limits of bags in their initial placement might differ with the experiment. Therefore, the initiation time of bag movement in numerical model might disagree with the observations in the laboratory.
- The bag permeability and the state of wetness are disregarded in numerical model.
- Bag stiffness: the numerical models of geobag were assumed to be stiff and could not deform. Due to the small-scale physical model of geobag, similar limitation exists for the physical model.
- Post-failure flow conditions: In the one-way DEM-CFD model the impact of geobag displacements cannot be fed back into the prevailing water flow. conditions.

Considering these limitations, the numerical model offers a good representation of the experimental setup detailed in section 3.1.

3.3. Summary

In this chapter the methodology presented in chapter 1 was discussed and specified in more detailed. Whilst the work undertaken focused on the development of efficient numerical simulation techniques, it was necessary to undertake a comprehensive programme of small-scale experimental tests in order to improve our understanding of geobag–water flow interactions and gather the data required to calibrate and validate the numerical model. These tests were undertaken in a recirculation flume (23m long, 0.75m wide and 0.5m deep) containing a 3m long geobag revetment test section made up of ~800 model geobags (1:10 scale) on a fixed (non-erodible) bed. The failure processes were studied for a range of different construction methods, side slopes and water depths.

To Extend the knowledge gained from the laboratory experiments a Discrete Element Method (DEM) model was constructed using the LIGGGHTS open source software with drag and lift models applied to a multi-sphere simulation of the laboratory model geobags.

Chapter 4. **EXPERIMENTAL RESULTS**

This chapter represents the results of several laboratory experiments conducted to identify and understand the processes involved in the complete failure of the geobag revetment.

Firstly, to enrich the fundamental understanding of geobag–water flow interactions, some small-scale experimental tests were conducted using a hydraulic flume to observe complete failure processes under different water depths with fixed bed condition. The studied features are (i) failure modes in a geobag revetment, (ii) hydraulic parameters of the flow and (iii) the influence of different revetment side slopes and construction bonds along with varying water depth on the hydraulic stability of geobag revetment.

Secondly, a set of velocity measurements for pre- and post-failure conditions were undertaken to analyse the velocity components and calculate the characteristics of the prevailing flows.

4.1. Geobag revetment failure processes

Failure processes for the combination of three side slopes and two construction methods were observed through 18 experimental runs under different flow conditions, with the purpose of evaluating the hydraulic stability of a revetment as a function of water level and flow velocity. Table 4-1 details the general flow conditions for each of the water depths and side slopes.

Table 4-1: Flow conditions at different water depths

a. Side slope 1V:3H

Condition	Water level	Water depth %revetment height	Mean water level (m)	Mean streamwise velocity(m/s)	Percentage of mean streamwise velocity		Flow rate(m^3/s)	Froude number	Reynolds number
					Transverse velocity	Vertical velocity			
Stack bond									
A	Low	0-49%	0.055	0.95	2.8	0.8	0.024	1.41	158801
B	Medium	50-60%	0.077	1.1	2.34	0.65	0.041	1.39	235568
C	High	60-80%	0.09	1.2	2.2	0.4	0.054	1.41	287864
Running bond									
A	Low	0-49%	0.054	0.92	2.42	0.82	0.023	1.39	153241
B	Medium	50-60%	0.08	1.1	2.14	0.52	0.044	1.40	248345
C	High	60-80%	0.091	1.18	2.38	0.26	0.055	1.41	291576

b. M, Side slope 1V:2H

Condition	Water level	Water depth %revetment height	Mean water level (m)	Mean streamwise velocity (m/s)	Percentage of mean streamwise velocity		Flow rate(m^3/s)	Froude number	Reynolds number
					Transverse velocity	Vertical velocity			
Stack bond									
A	Low	0-49%	0.071	1. 12	2.24	0.16	0.035	1.43	231265
B	Medium	50-60%	0.095	1.26	1.93	0.38	0.055	1.40	322057
C	High	60-80%	0.115	1.39	2.07	0.47	0.075	1.39	401126
Running bond									
A	Low	0-49%	0.074	1.15	2.54	0.33	0.037	1.41	240618
B	Medium	50-60%	0.095	1.26	2.25	0.38	0.055	1.40	322057
C	High	60-80%	0.113	1.35	2.15	0.65	0.073	1.40	393841

c. Side slope 1V:1.25H

Condition	Water level	Water depth %revetment height	Mean water level (m)	Mean streamwise velocity (m/s)	Percentage of mean streamwise velocity		Flow rate (m^3/s)	Froude number	Reynolds number
					Transverse velocity	Vertical velocity			
Stack bond									
A	Low	0- 30%	0.085	1.25	6.1	1.92	0.044	1.40	294974
B	Medium	30-40%	0.105	1.41	6.7	2.5	0.061	1.39	376119
C	High	40-50%	0.122	1.50	5.9	1.9	0.078	1.40	450225
Running bond									
A	Low	0- 30%	0.084	1.27	5.7	2.23	0.043	1.40	289533
B	Medium	30-40%	0.108	1.42	6.52	2.1	0.064	1.40	389923
C	High	40-50%	0.121	1.53	5.9	1.95	0.078	1.42	451922

4.1.1. *General failure mechanisms*

Failure mechanisms progressed with increasing flow velocity in and around the bag voids, which led to an increase in associated hydrodynamic forces (drag force, lift force), subtly altering the balance with the other forces (buoyancy, bag self-weight) as shown in Figure 4.1.

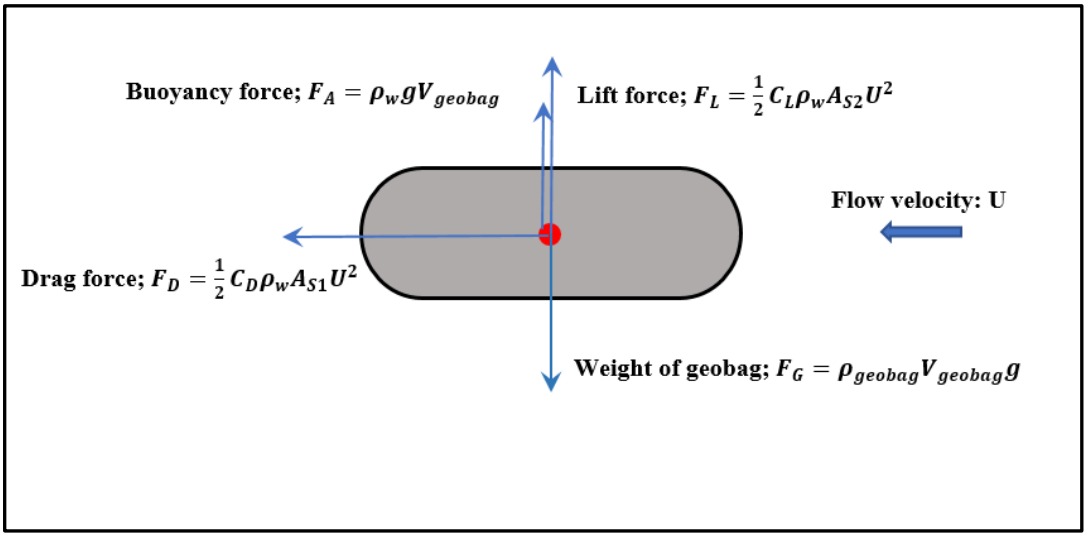

Figure 4.1: Forces acting on a submerged geobag

4.1.1.1. Mobilising and Resisting Forces on submerged geobags

To understand the mechanisms which affect the hydraulic stability of a geobag revetment, the balance of forces that are acting on a geobag needs to be considered. (Figure 4.1). However, herein due to the complexity of the stability problem of geobag structures, the impact of geobag deformation on the hydraulic stability is neglected by assuming stiff geobags.

The flow on and around a geobag with horizontal velocity U in a steady flow condition with associated acceleration $\frac{\partial u}{\partial t} = 0$ results in three types of forces as explained by Equation 4.1 to Equation 4.3:

Drag force: $$F_D = \frac{1}{2} C_D \rho_w A_S U^2$$ Equation 4.1

Where C_D is a drag coefficient which depends on the shape and roughness of the geobags ρ_w is the density of water (kg/m^3), U is the horizontal flow velocity (m/s) and A_S is the cross area normal to the flow.

Lift Force: $$F_L = \frac{1}{2} C_L \rho_w A_t U^2$$ Equation 4.2

Where C_L is the lift coefficient, and A_t is the projected area of the geobag in the flow direction (m).

Buoyancy Force: $$F_A = \rho_w g V_{geobag}$$ Equation 4.3

Where g is the gravitational acceleration (m/s^2) and V_{geobag} is the volume of geobag (m^3).

The resisting forces are essentially due to the weight of the geobag under buoyancy:

Weight of geobag $$F_G = \rho_{geobag} V_{geobag} g$$ Equation 4.4

The resisting force on the submerged container can be defined as:

where $\rho_{geobag} = \rho_s - \rho_w$ is the submerged density of the geobags, ρ_s and ρ_w are the density of dry geobag and water respectively.

In the current study, depending on construction specification of geobag revetment, i.e. side slope, length of overlap and the way geobags were placed to build the revetment (stack bond or running bond), three main types of displacements are observed: (a) uplifting (b) pullout and (c) sliding.

4.1.1.2. Failure due to uplifting

Generally uplifting is a rotational displacement of geobags in the upward direction. According to Equation 4.5, uplifting of a geobag occurs, when mobilising moments (due to hydrodynamic forces) around the rotation point are large enough to overcome the resisting moments (due to the weight of geobag). The rotation point is a virtual point (in the vertical plane) which is located at the end edge of the contact area of the geobag with adjacent geobag underneath or bed of the flume. Uplifting of the geobag can be described as (Figure 4.2):

Mobilising moments ≥Resisting moments.

$$\underbrace{(F_D \,.\, m_s) + (F_L \,.\, r_s)}_{Destabilising\ Moment} \geq \underbrace{(F_G . r_s)}_{Stabilising\ moment} \qquad \text{Equation 4.5}$$

Where rs is the horizontal distance between the centre of gravity of the geobag and the rotation point. m_s is the vertical the distance between the centre of gravity of the geobag and the rotation point (Figure 4.2).

When destabilising moments on the left side of Equation 4.5 increases; that could be due to turbulent bursting–induced flow through the revetment voids (Figure 4.3) or an increase in flow velocity and water depth; partial or full uplifting occurs which result in instability of the geobag (Figure 4.4). Partial uplifting is normally observed when mobilising moments (right hand side in equation 4.5) are great enough to just raise head edge of the bag. Therefore, partial uplifting is basically a partial bag displacement that means bag remains in its own location in the test section with an upward movement (Figure 4.4). Full uplifting occurs when flow-induced loads on geobags are much larger than the resisting force that results in dislodgment of the bag from test section.

Uplifting directly depends on water level and also the area of overlaps (Equation 4.5). Therefore at relatively low water levels or bag arrangements with less overlaps, e.g. Side slope 1V:3H, bag displacements were usually due to turbulent bursting–induced flow through the revetment voids (Figure 4.3 and Figure 4.4) which lead to partial uplifting. Whereas increasing water level, full uplifting associated with local vortices were the typically observed failure modes. Partial uplifting normally is one of the main initial failure modes which is commonly seen in very bottom layer of revetment in low to medium water levels. Whereas increasing water level, full uplifting associated with local

vortices were the typical observed failure modes which contributes to the completion of failure processes.

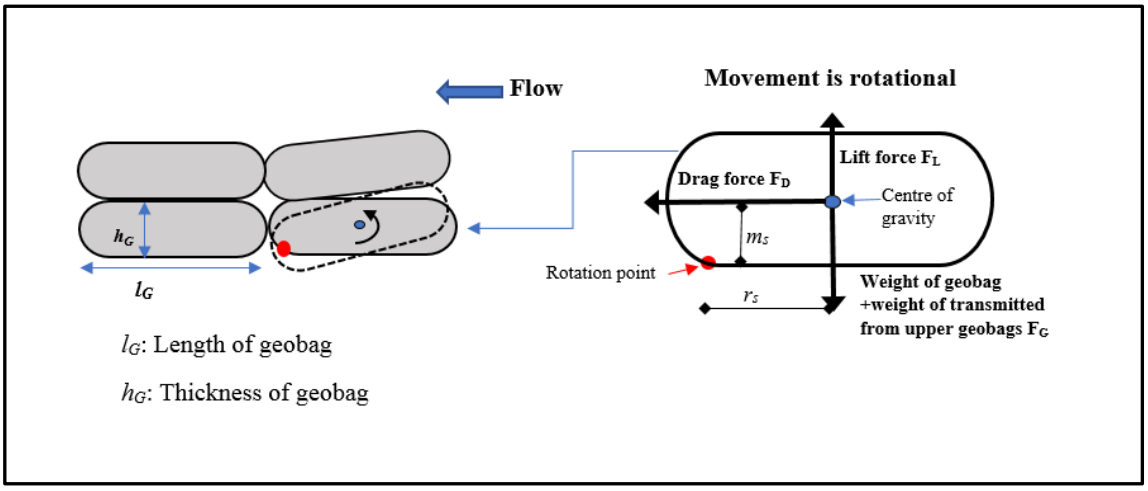

Figure 4.2: Definition sketch for Uplifting of a geobag

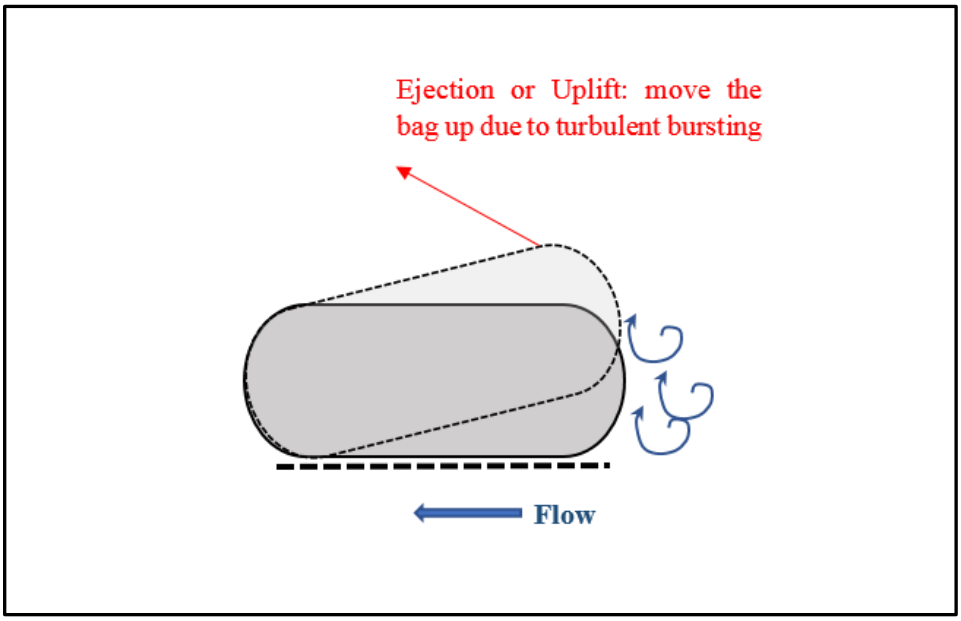

Figure 4.3: Definition sketch for Ejection or Uplifting of a geobag due to turbulent bursting

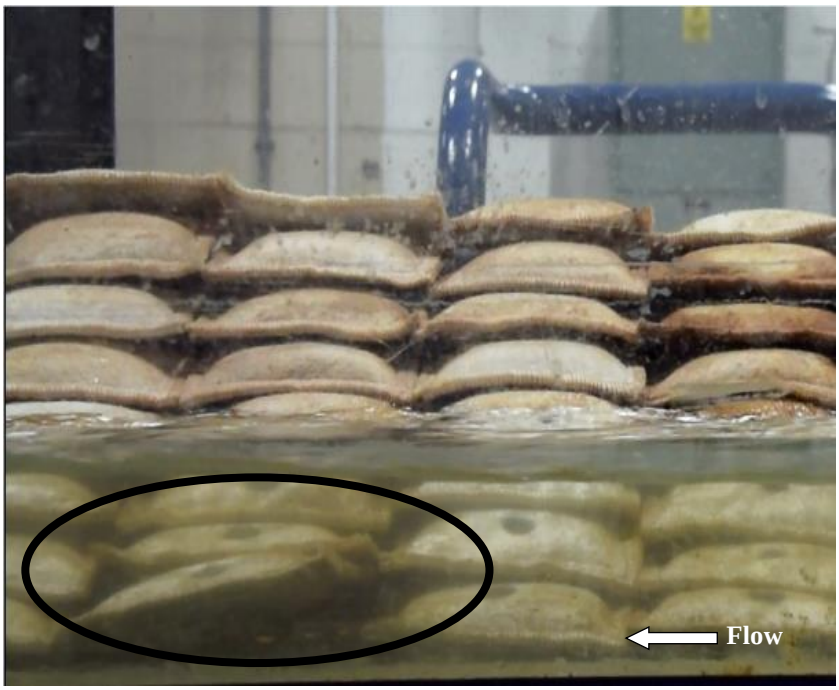

(a)

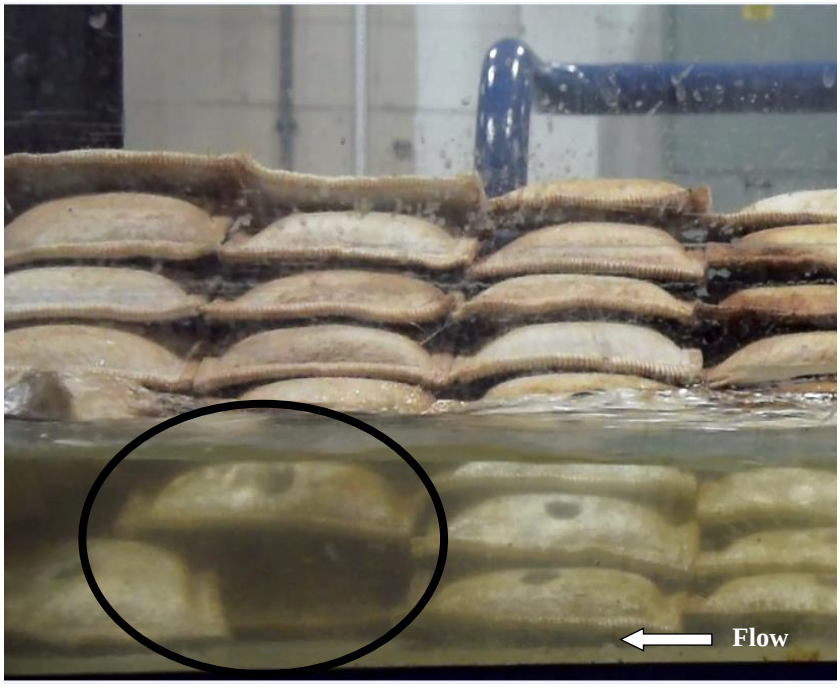

(b)

Figure 4.4: Displacement due to (a) partial uplifting (b) pressure difference between the main flow and void flow.

4.1.1.3. Failure due to pullout

Pull-out was the most common failure mode which was observed during the whole processes of failure and almost in all cases. Pullout frequently occurred with geobags located near the water surface where higher flow velocities caused the incident hydrodynamic forces to become large enough to displace the geobags and typically manifested itself in a clockwise rotation in the horizontal plane (Figure 4.5 and **Error! Reference source not found.**). This type of displacement occurred only if the flow-induced loads on the geobags were much larger than the resisting force. According to Mudiyanselage (2013) this resisting force is highly dependent on the weight and frictional properties of geobags, i.e. surface roughness and the contact area between geobags.

Equation 4.6 addresses the friction force as a function of normal loads and also proportional to the friction coefficients (μ) measured from direct shear tests (Mudiyanselage 2013).This force acts as a resisting force against pullout forces. According to Equation 4.6, pullout of a geobag occurs, when mobilising moments (due to hydrodynamic forces) around the rotation point (**Error! Reference source not found.**) are large enough to encounter the resisting moments (due to friction forces). In the case of pullout, rotation point is a virtual point (in the horizontal plane) which is located at the inner edge of the contact area of the geobag with adjacent geobag underneath or bed of the flume. Pullout of the geobag can be described as Equation 4.6.

$$Friction{=}F_{Resisting} = \mu(F_G - F_L) \qquad \text{Equation 4.6}$$

$$\underbrace{(F_D \,.\, n_s)}_{Destabilising\ Moment} \geq \underbrace{(\mu(F_G - F_L).\, n_s)}_{Stabilising\ moment} \qquad \text{Equation 4.7}$$

where n_s is the transverse distance between the centre of gravity of the geobag and the rotation point (Figure 4.5 and **Error! Reference source not found.**).

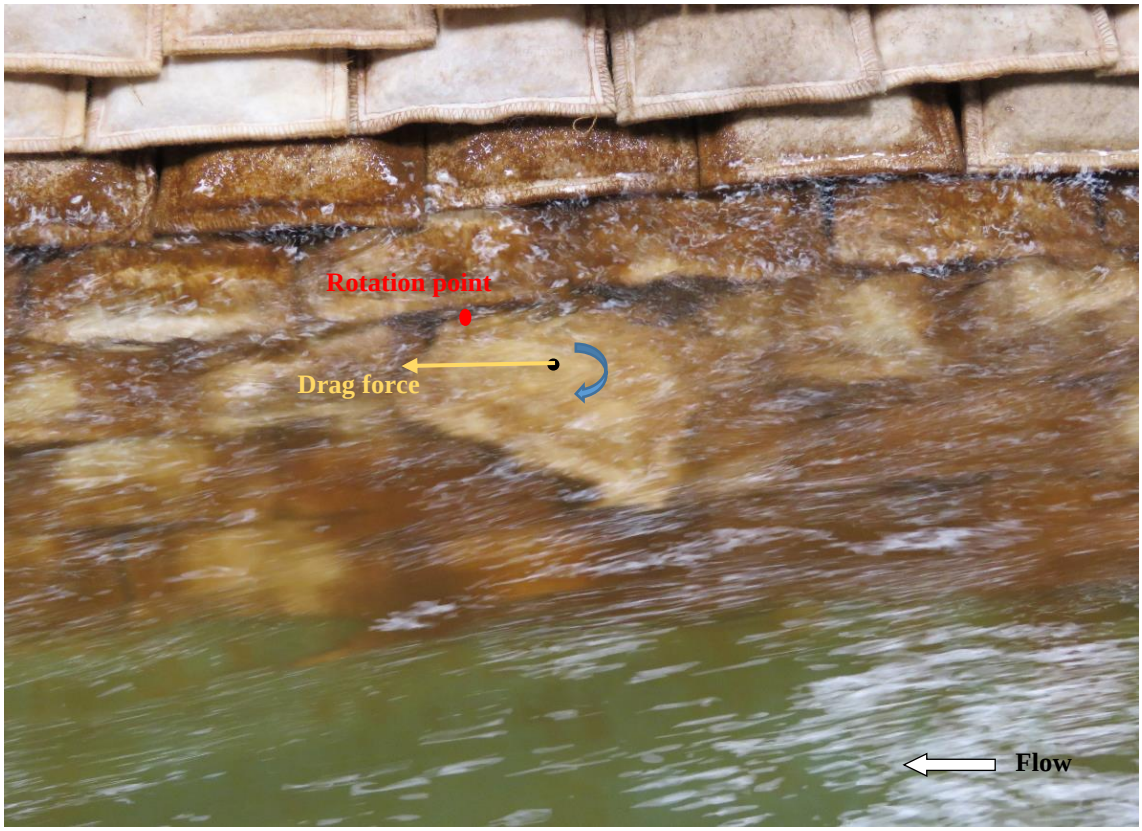

Figure 4.5: Pullout of a geobag

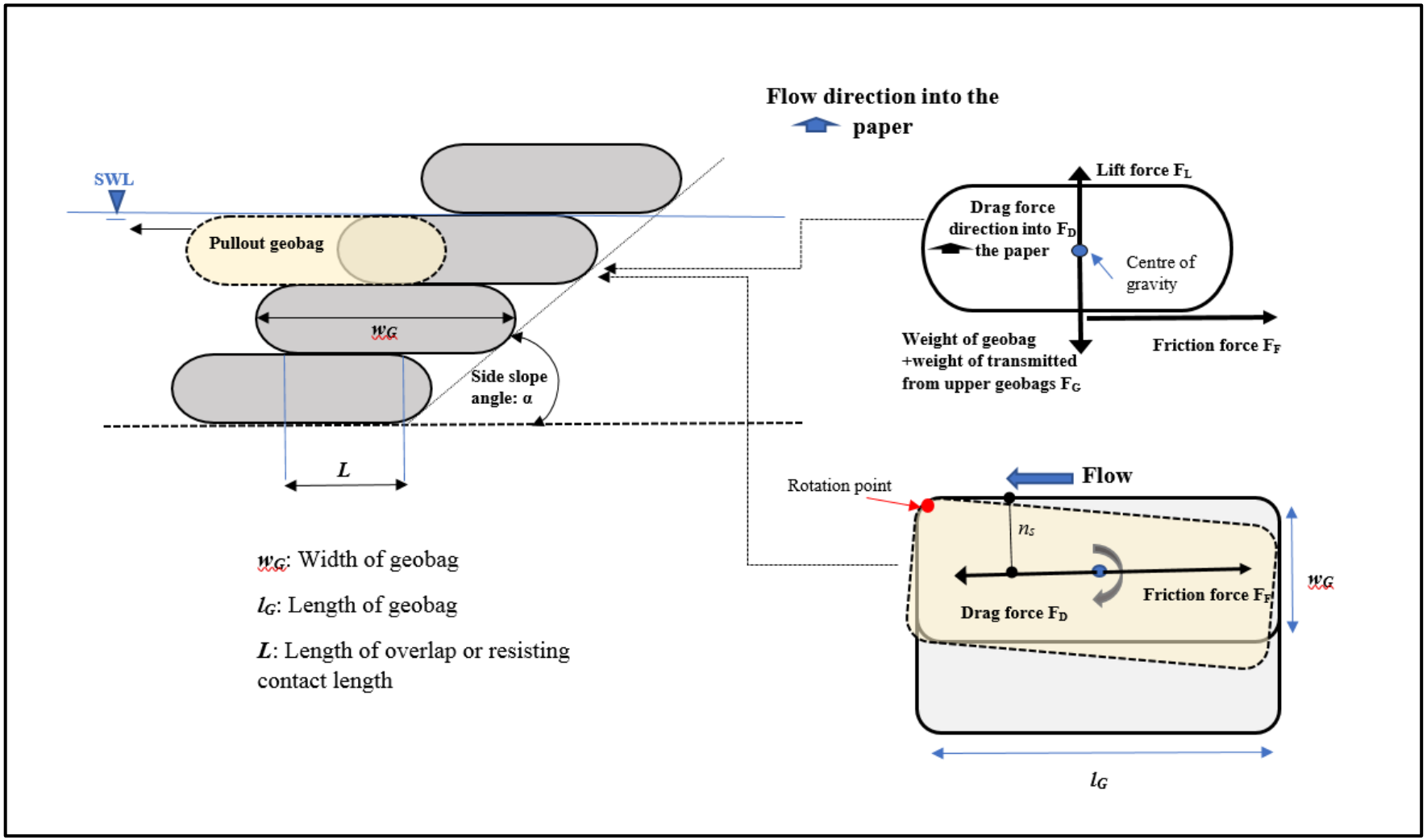

Figure 4.6 Definition sketch for Pullout of a geobag

4.1.1.4. Failure due to sliding

Sliding and slumping were observed in all cases but were most prominent in the failure processes for high water level conditions and steepest side slope 1V:1.25H. These types of displacement were highly progressive and occurred when the gravitational force on a bag (i.e. geobag weight) was higher than the resisting force on a bag (i.e. friction). Typically, geobags above the water surface were most vulnerable to sliding, both because of higher normal loads and also the failure of submerged supporting bags.

Due to the difference in normal loads, sliding under dry (above the water surface) and submerged conditions are different. When geobags are submerged, due to buoyancy, normal loads are small, and consequently sliding forces are also smaller.

As expected, geobags in revetments with steeper side slope showed lower resistance to sliding forces. This is mainly because mobilising force (geobag weight component in parallel to the slope) is more in line with the centre of gravity, so it overcomes friction and sliding is more probable. In contrast, slumping was mostly seen in the case of milder side slope (1V:3H) where the perpendicular component of the geobag weight vector was large enough to let geobag vertically collapse. In this case, geobag weight component in parallel to the slope is not in line with the centre of gravity (Figure 4.8b, c and Figure 4.9b, c).

Figure 4.7: shows the definition sketch for sliding of geobag used to protect the riverbank. In this figure the flow direction is into the paper.

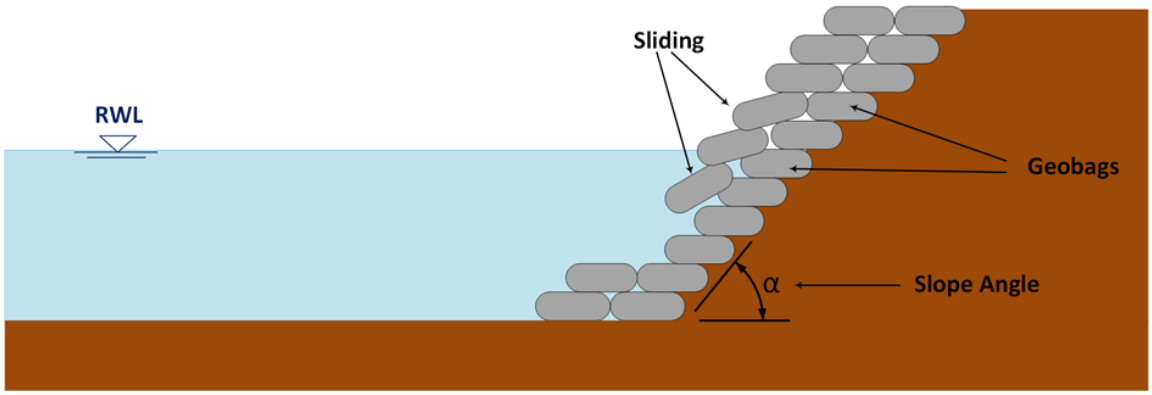

Figure 4.7: Definition sketch for Sliding of a geobag

4.1.2. *Impact of varying hydrodynamic Load (water depth)*

In general, the failure processes for all experimental runs and for varying water depths were completed through combinations of failure modes such as, turbulent bursting–induced flow through the revetment voids (usually outward movements of bags), partial or full uplifting, pull out (ejections of bags), and internal sliding (Figure 4.8 to Figure 4.18).

Observations indicated that failure mechanisms were significantly influenced by water level. At relatively low water levels bag displacements were usually due to turbulent bursting–induced flow through the revetment voids which tended to lead to partial uplifting (Figure 4.8a, Figure 4.9a, Figure 4.11a and Figure 4.14a), whilst in moderate to high water levels the typical observed failure modes were: full uplifting associated with local vortices or/and pullout processes (Figure 4.12a, Figure 4.15a).

Sliding was commonly seen in all cases. However, it characterised the failure process in high water level condition where bottom layer bags were washed away quickly from the test section and upper layer bags collapse due to sliding (Figure 4.13a and Figure 4.16a).

4.1.3. *Impact of side slope*

4.1.3.1. Side slope 1V:3H

The experimental data indicate that revetment stability is strongly dependent on the side slope. The mildest side slope revetments (1V:3H) were noticeably more stable, to the extent that bag movement was not observed for low and medium water levels. Although the failure of the mildest sloped revetments under high depth conditions was observed to initiate in the layer of bags at the water surface, no bags were washed away from the bottommost layer. Typically, in the case of the mildest side slope, and for both construction methods, partial and full uplifting associated with pull-out were the most common initial failure modes (Figure 4.8a and Figure 4.9a). Interestingly, as failure progressed, the slump of the top layers of bags over the bottom layer appeared to help the revetment remain stable and prevent the failure zone expanding despite the generally disordered structure of revetment (Figure 4.8b,c and Figure 4.9b,c). Figure 4.10 shows a temporal analysis of events and failures, in the form of a hydrograph. In this figure, flow initialisation, steady state flow achieved, failure initialisation, modes of failure, end of

failure, number of bags washed away from test are demonstrated. This figure displays a delay in initiation of failure which prove more hydraulic stability for this side slope.

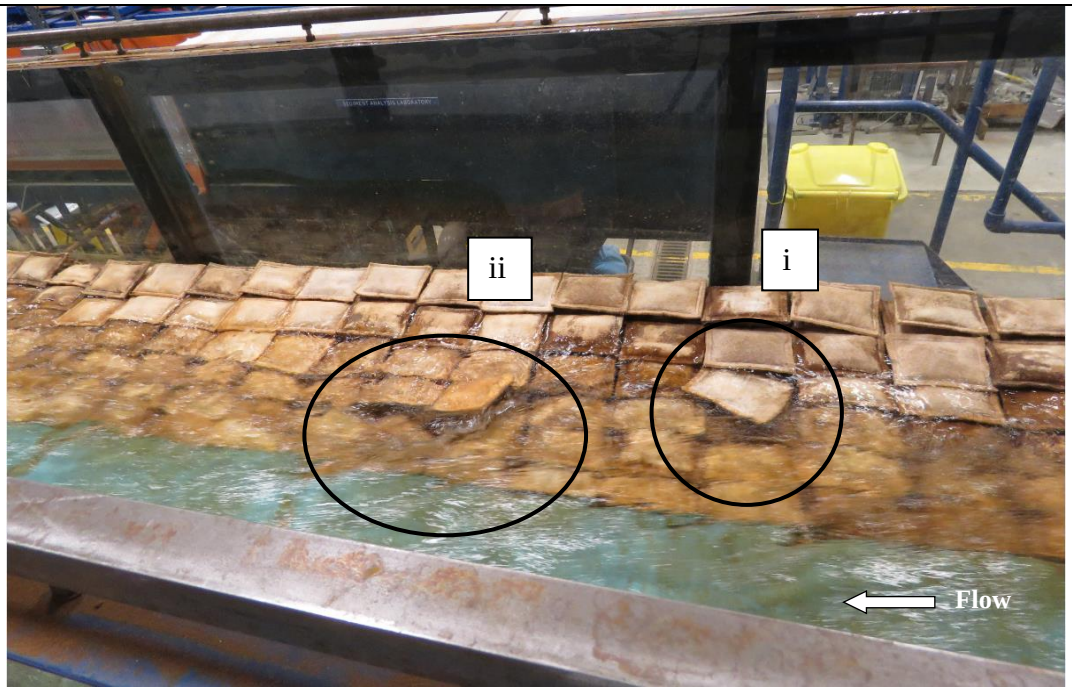

(a) Initial displacement due to (i) pullout, (ii) partial uplifting.

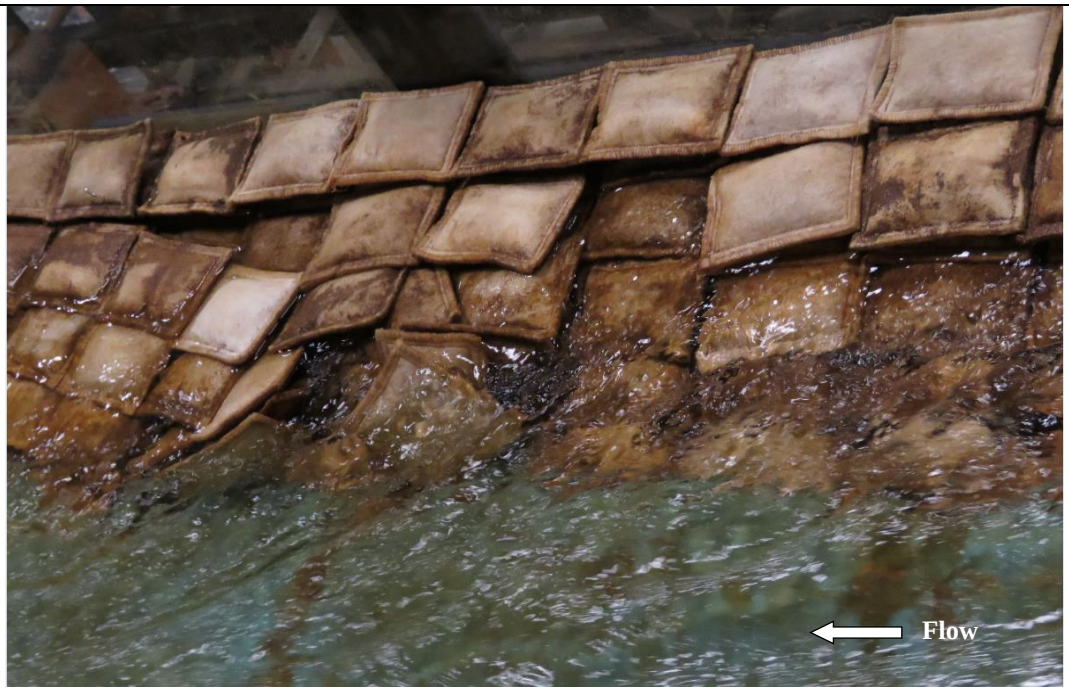

(b) The slump of upper layer bags on the bottom layer

Figure 4.8 (a to c): Detail of different failure modes in geobag revetment for mild side slope (1V:3H), stack bond (Cont'd)

(c) Slump and slide zones

Figure 4.8(a to c): Detail of different failure modes in geobag revetment for mild side slope (1V:3H), stack bond.

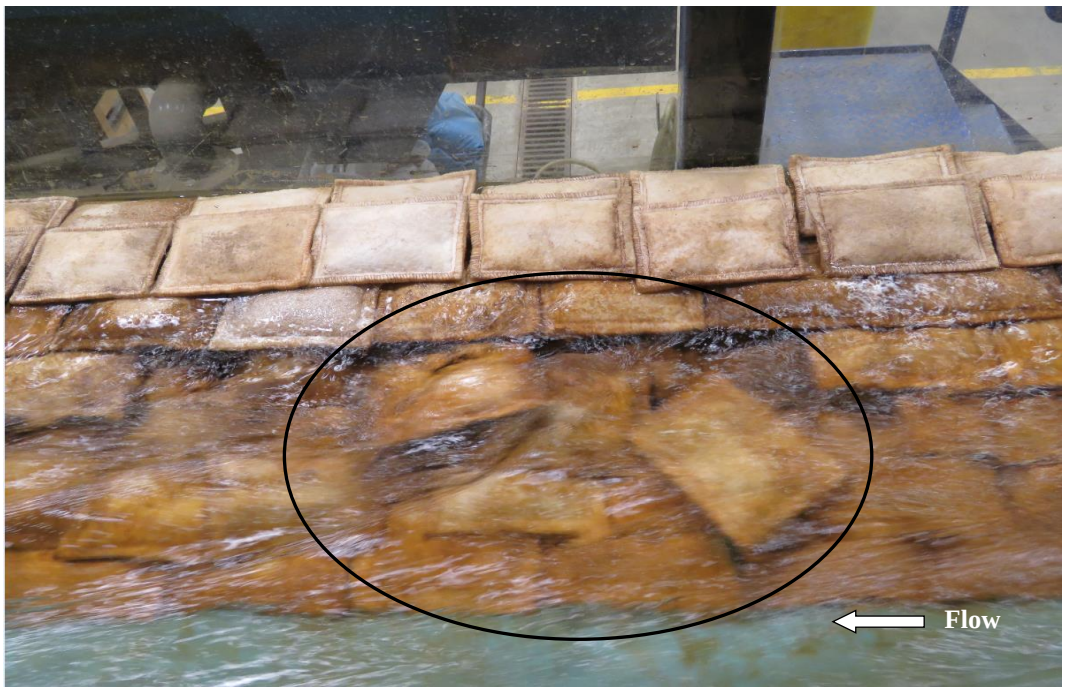

(a) initial displacement due to pullout, partial uplifting and turbulent bursting

(b) The slump of upper layer bags on the bottom layer

(c) Slump zones

Figure 4.9 (a to c): Detail of different failure modes in geobag revetment for milder side slope (1V:3H), running bond.

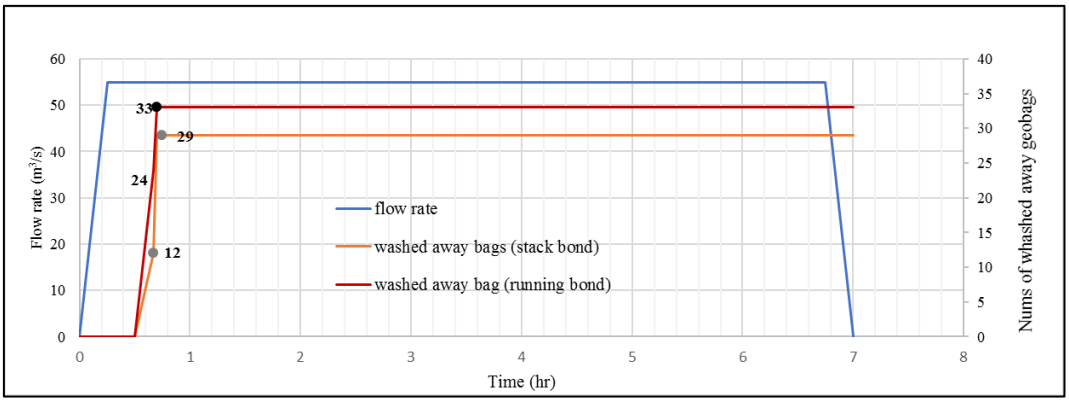

	Initial failure mode	Complete failure mechanisms
Stack bond	Turbulent bursting, Partial uplifting, Pull-out	Pull-out, Slumping
Running bond	Turbulent bursting, Partial uplifting, Pull-out	Pull-out, Slumping

Figure 4.10: Temporal analysis of failure processes, and steady state flow achieved, side slope (1V:3H) and for high-water depths.

4.1.3.2. Side slope 1V:2H

As shown in Figure 4.11a, Figure 4.12a, Figure 4.14 and Figure 4.15a for both construction bonds with a side slope of 1V:2H and low to medium water depth the geobag layers below the water surface tended to fail due to pull out, uplifting and turbulent bursting, and followed a similar process to that observed for initial revetment failure by Akter, Pender, *et al.* (2013). Vertical sliding which was initiated with the failure of the submerged supporting bags, was also observed in the layers above the water surface for the high-water level condition (Figure 4.13a and Figure 4.16a). Also, for low to medium water depths and for both construction bonds the failure process created a clump of collapsed bags which itself led to a localised increase in upstream water depth. Whilst this phenomenon exposed the upper layers of the geobags to the flow it also decreased local flow velocities in this area which seemed to prevent more upstream bags from being washed away (Figure 4.11b, Figure 4.12a and Figure 4.14a,b). Moreover, this failure mechanism affected downstream flow conditions by reducing flow acceleration in front of the revetment, hence helping downstream geobags to remain stable. A temporal analysis of failure processes was presented in Figure 4.17. This figure shows that failure initialisation and failure modes and the end of failure, number of bags washed away from test section were highly dependent on water depth. Compering the processes of failure in different hydraulic conditions shows that failure initiated later and takes longer to be completed for low water depth. In contrast failure progressed rapidly in the case of high-water level conditions.

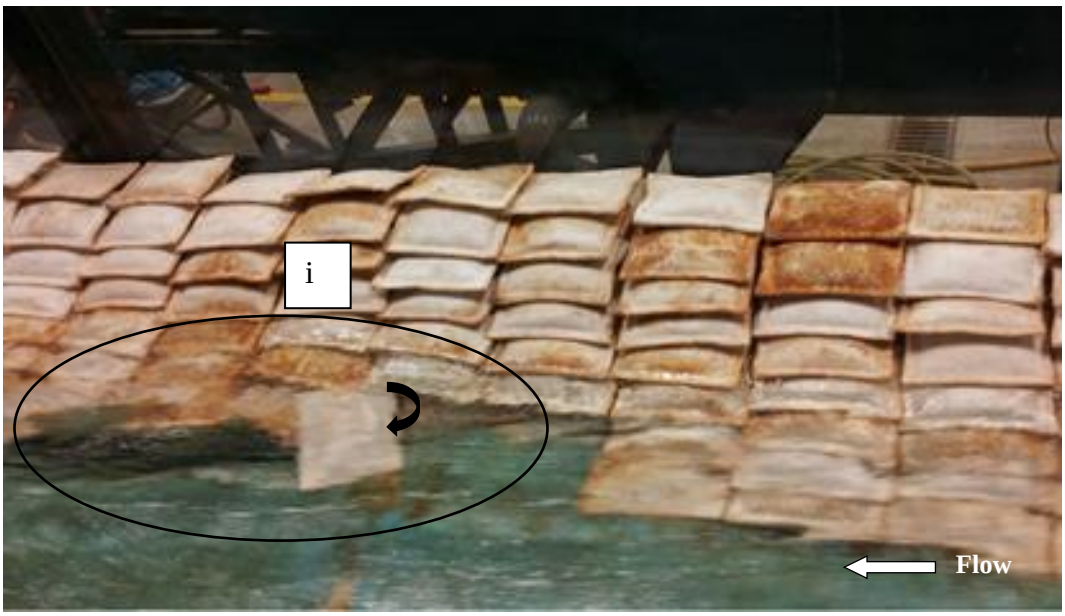

(a) partial uplifting and pullout

(b) A clump of collapsed bags

Figure 4.11 (a,b): Failure processes and detail of different failure modes in geobag revetment for stack bond construction, side slope (1V:2H) and for condition A: low-water depth.

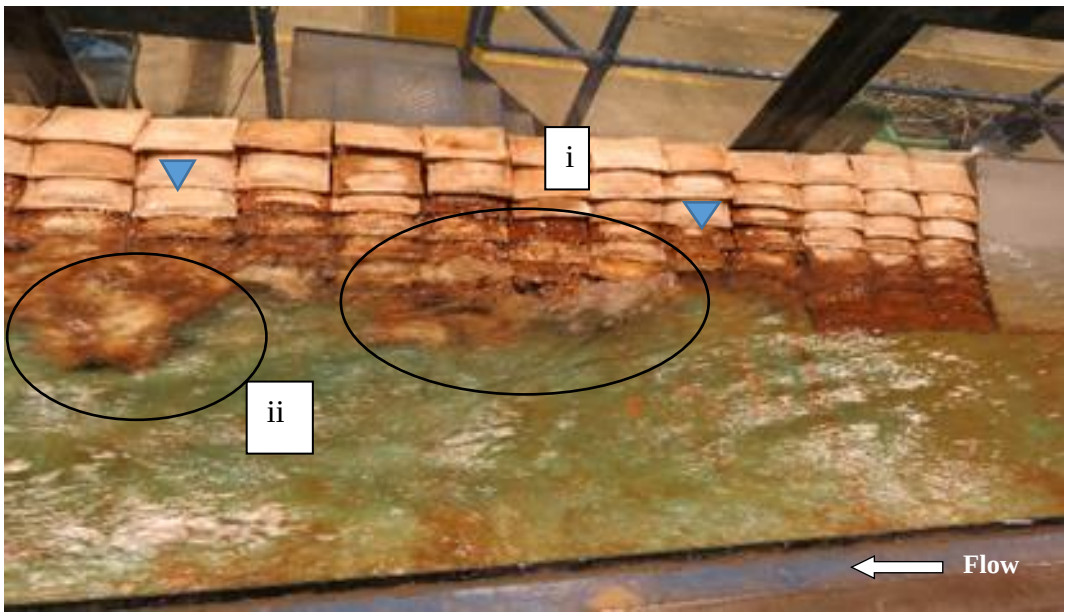

(a) Displacement due to (i)pressure differences between the main and void flow and full uplift, (ii) pullout.

(b) Failure zone

Figure 4.12 (a, b): Failure processes and detail of different failure modes in geobag revetment for stack bond construction, side slope (1V:2H) and for condition B: medium -water depth.

(a) Turbulent bursting–induced flow through revetment voids and sliding

(b) Complete failure: sliding and pullout geobags

Figure 4.13 (a, b): Failure processes and detail of different failure modes in geobag revetment for stack bond construction, side slope (1V:2H) and for condition C: high - water depth.

(a) Full uplifting

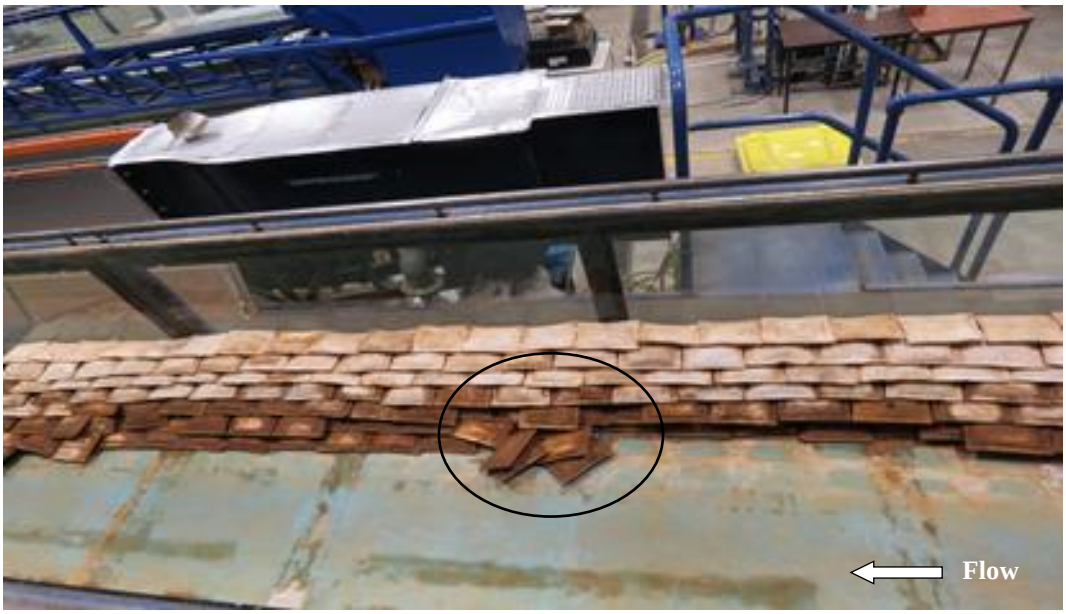

(b) A clump of collapsed bags

Figure 4.14 (a, b): Failure processes and detail of different failure modes in geobag revetment for running bond construction, side slope (1V:2H) and for low-water depth.

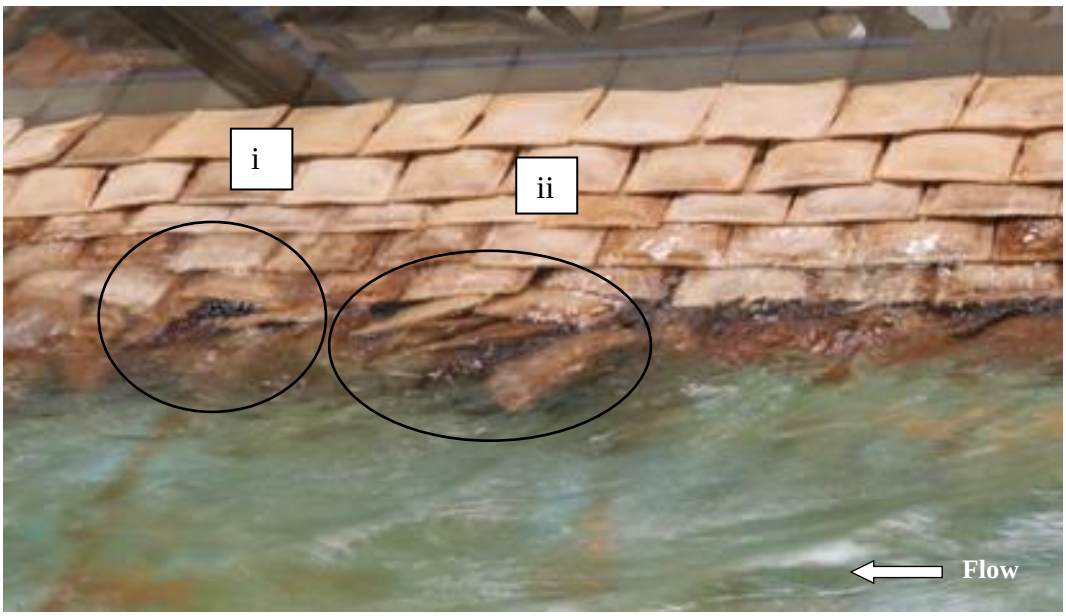

(a) Displacement due to (i) pressure differences between the main and void flow and full uplift, (ii) pullout

(b) Failure Zone: pullout and dislodging

Figure 4.15 (a, b): Failure processes and detail of different failure modes in geobag revetment for running bond construction, side slope (1V:2H) and for medium-water depth.

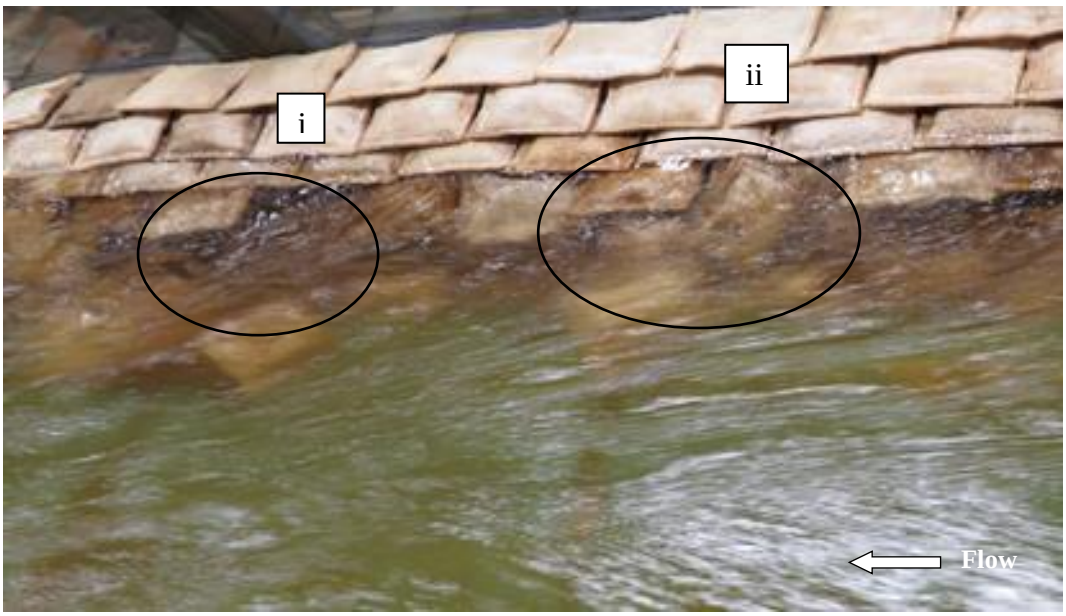

(a) Displacement due to (i) turbulent bursting–induced flow through revetment voids, (ii) sliding.

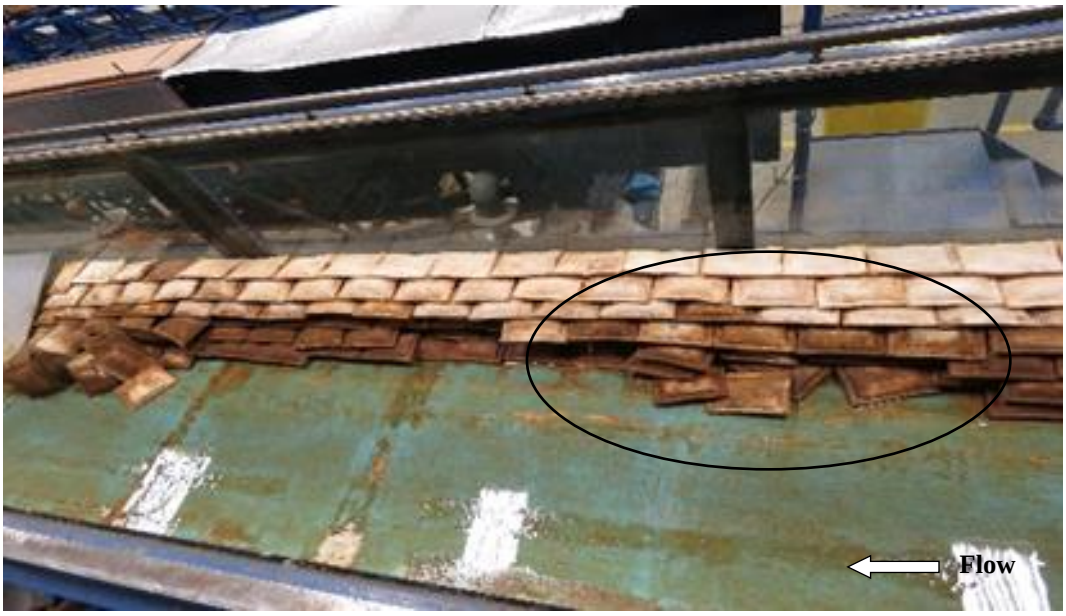

(b) Sliding zone

Figure 4.16 (a, b): Failure processes and detail of different failure modes in geobag revetment for running bond construction, side slope (1V:2H) and for high-water depths.

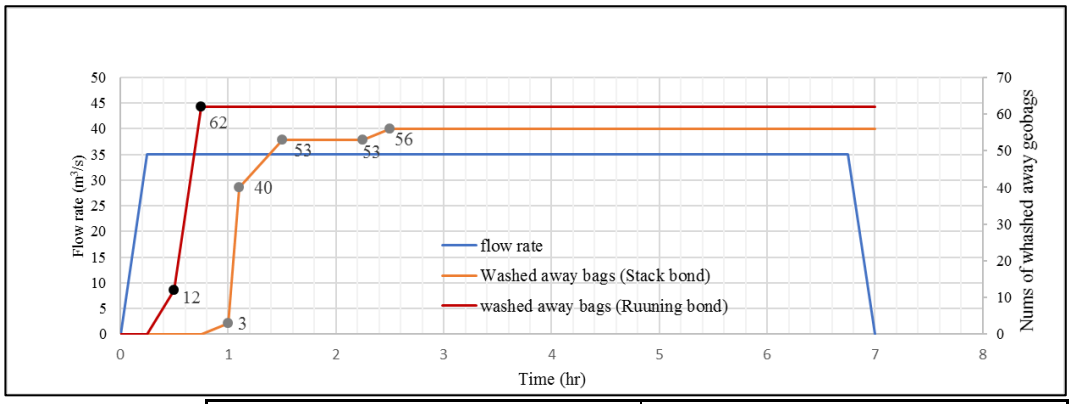

	Initial failure mode	Complete failure mechanisms
Stack bond	Turbulent bursting, Partial uplifting	Full-uplifting, internal sliding
Running bond	Turbulent bursting, Partial uplifting	Full-uplifting, internal sliding

(a1)

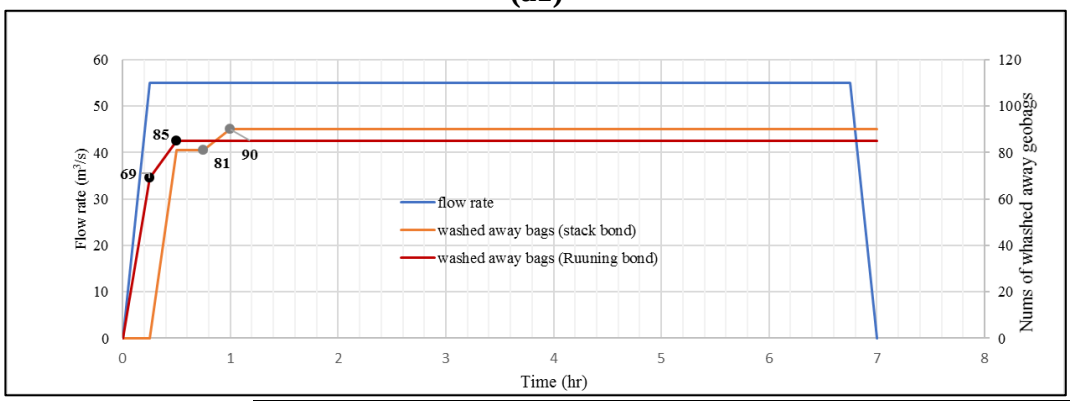

	Initial failure mode	Complete failure mechanisms
Stack bond	Pull-out, Full uplifting	Pull-out, internal sliding
Running bond	Pull-out, Full uplifting	Pull-out, internal sliding

(a2)

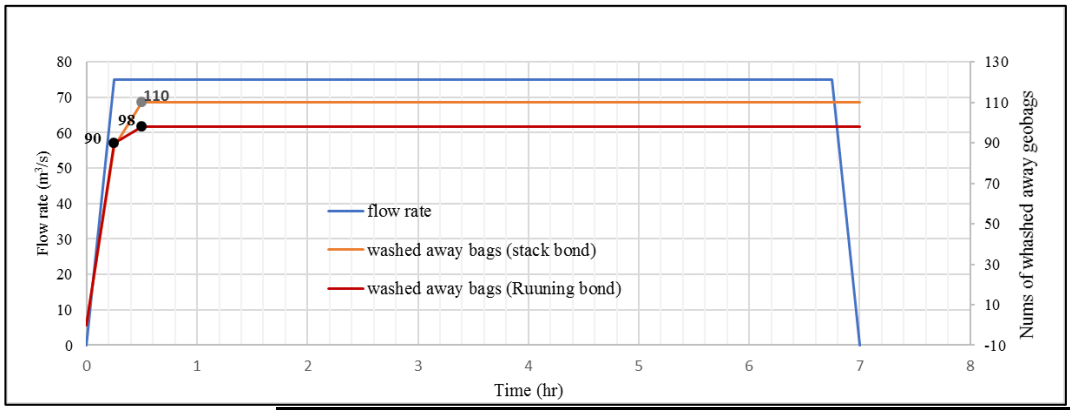

	Initial failure mode	Complete failure mechanisms
Stack bond	Pull-out, Sliding	Pull-out, Sliding
Running bond	Pull-out, Sliding	Pull-out, Sliding

(a3)

Figure 4.17: Temporal analysis of failure processes, and steady state flow achieved, side slope (1V:2H) and for (a1) low, (a2) medium and (a3) high-water depths.

4.1.3.3. Side slope 1V:1.25H

In comparison with the other side slopes, the failure processes for revetments with the steepest slope (1V:1.25H) progressed rapidly. As an example, Figure 4.18b shows a large number of bags which were washed away at the beginning of a test and resulted in a large and deep failure zone (Figure 4.18 c). Although, with relatively dry geobags, failure usually started with the bag pullout processes associated with higher streamwise velocities. Vertical sliding played a significant role in failure progression in the case of the steepest slope. Moreover, turbulent bursting–induced flow through the revetment voids as a result of the water-pressure differences between the channel side and the geobag lee side and other failure modes (e.g. uplifting) were commonly observed during the failure process in almost all water level conditions (Figure 4.18a) Figure 4.19 shows that failure initiated and progressed through a combination of uplifting , pull-out and sliding but sliding played the main role in completing the failure processes for the side slope of 1V:1.25H.

(a) Initial displacement due to turbulent bursting–induced flow through revetment voids and sliding, low water level

Figure 4.18(a to c): Failure processes and detail of different failure modes in geobag revetment for side slope (1V:1.25H) and for low (a); and high-water depths (b and c) (Cont'd)

(b) Magnitude of the revetment failure at the beginning of the test due to vertical sliding, high water level

(c) Failure zone (slide zone) after high-water depth condition test

Figure 4.16 (a to c): Failure processes and detail of different failure modes in geobag revetment for side slope (1V:1.25H) and low (a); and high-water depths (b).

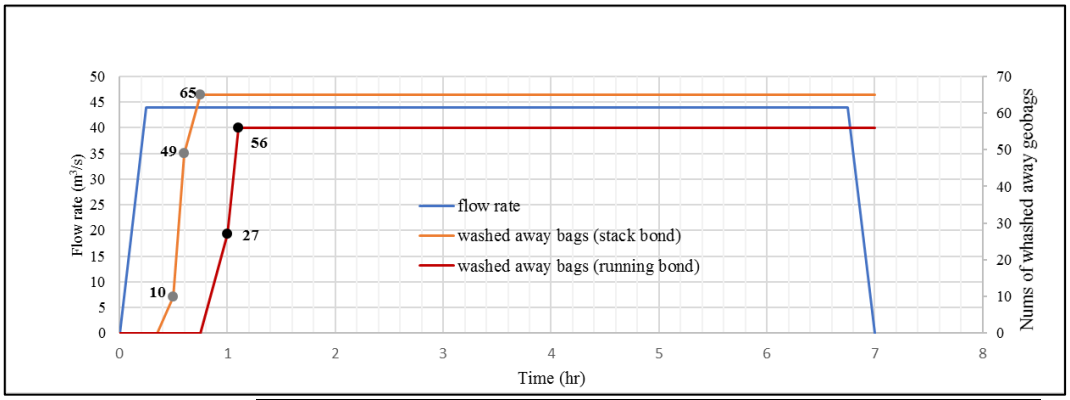

	Initial failure mode	Complete failure mechanisms
Stack bond	Uplifting, Pull-out	Pull-out, Vertical sliding
Running bond	Uplifting, Pull-out	Pull-out, Vertical sliding

(a1)

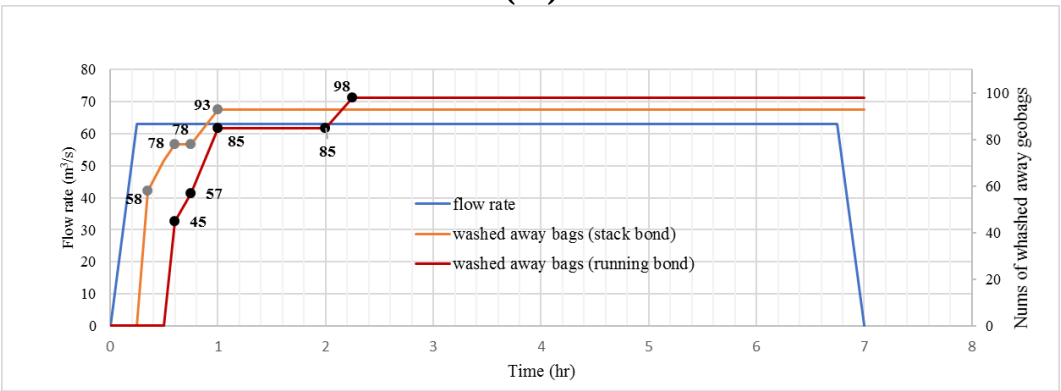

	Initial failure mode	Complete failure mechanisms
Stack bond	Pull-out, Vertical sliding	Pull-out, Vertical sliding, Uplifting
Running bond	Pull-out, Vertical sliding	Pull-out, Vertical sliding, uplifting

(a2)

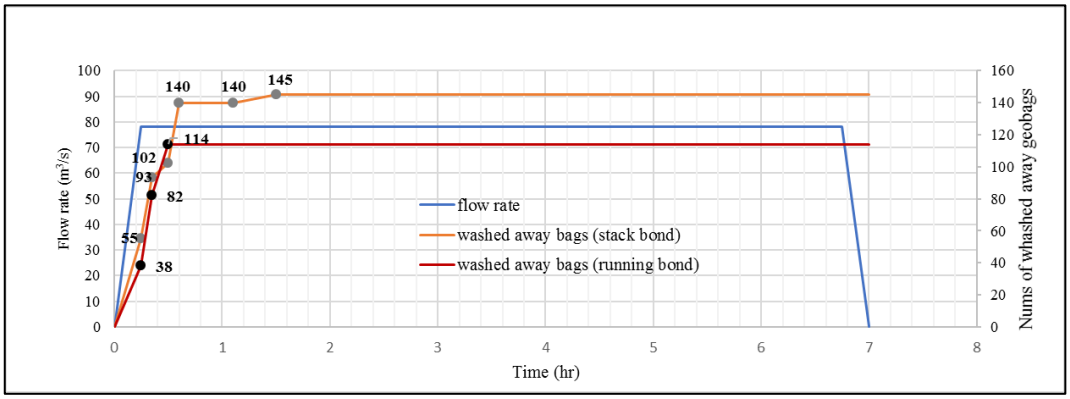

	Initial failure mode	Complete failure mechanisms
Stack bond	Pull-out, Vertical sliding	Pull-out, Vertical sliding, Uplifting
Running bond	Pull-out, Vertical sliding	Pull-out, Vertical sliding, uplifting

(a3)

Figure 4.19: Temporal analysis of failure processes, and steady state flow achieved, side slope (1V:1.25H) and for (a1) low, (a2) medium and (a3) high-water depths.

4.1.4. *Impact of construction bond*

Experimental results indicate that failure mechanisms depend on both water depth and revetment slope. However, somewhat surprisingly, they were found to be generally independent of the specific geobag bond configuration. With no mortar-like bonding between individual geobags, the integrity of a revetment under any particular slope/depth scenario was found to be dependent on the contact area between individual geobags, which can be considered a proxy for frictional resistance, rather than the precise bond configuration. Figure 4.20:, Figure 4.21: and Figure 4.22: illustrate this finding by showing that the number of bags displaced from the revetment was relatively unaffected by the construction bond.

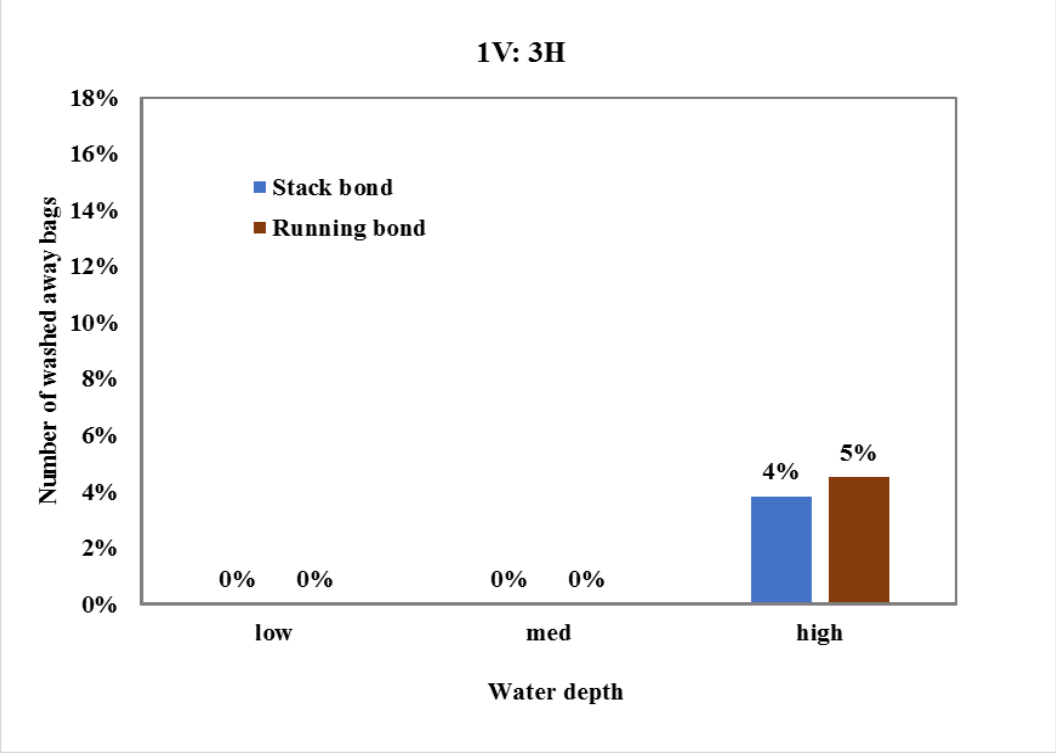

Figure 4.20: Average percentage of washed away bags at the end of each test for two different bonds and side slope 1V:3H.

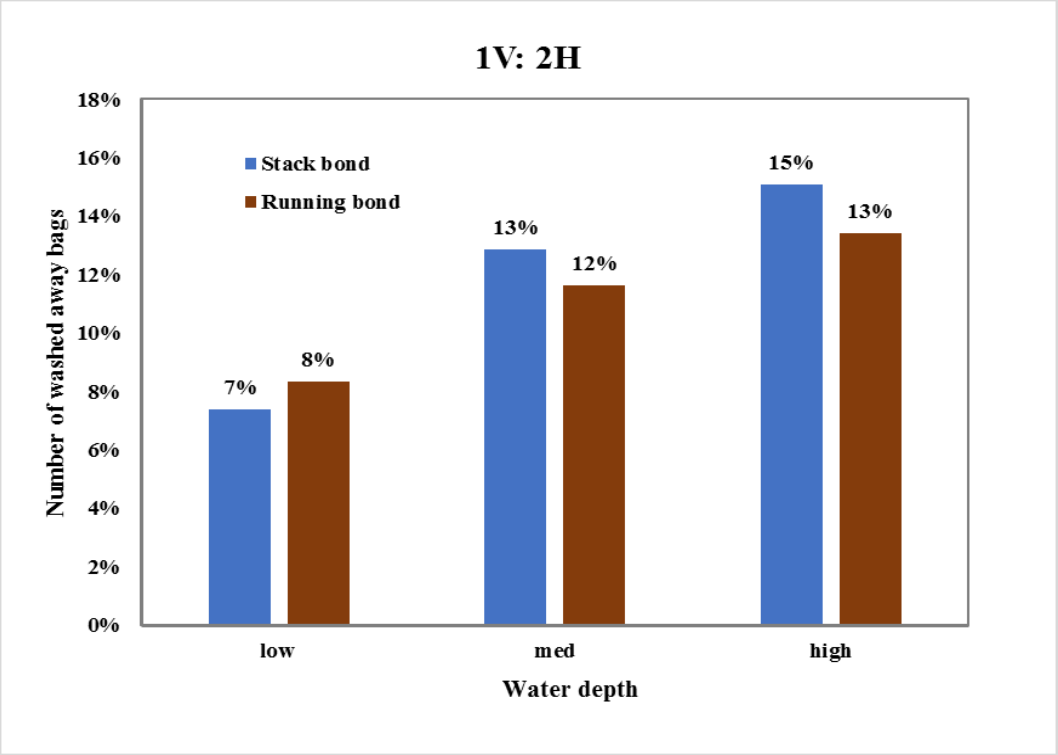

Figure 4.21: Average percentage of washed away bags at the end of each test for two different bonds and side slope 1V:2H.

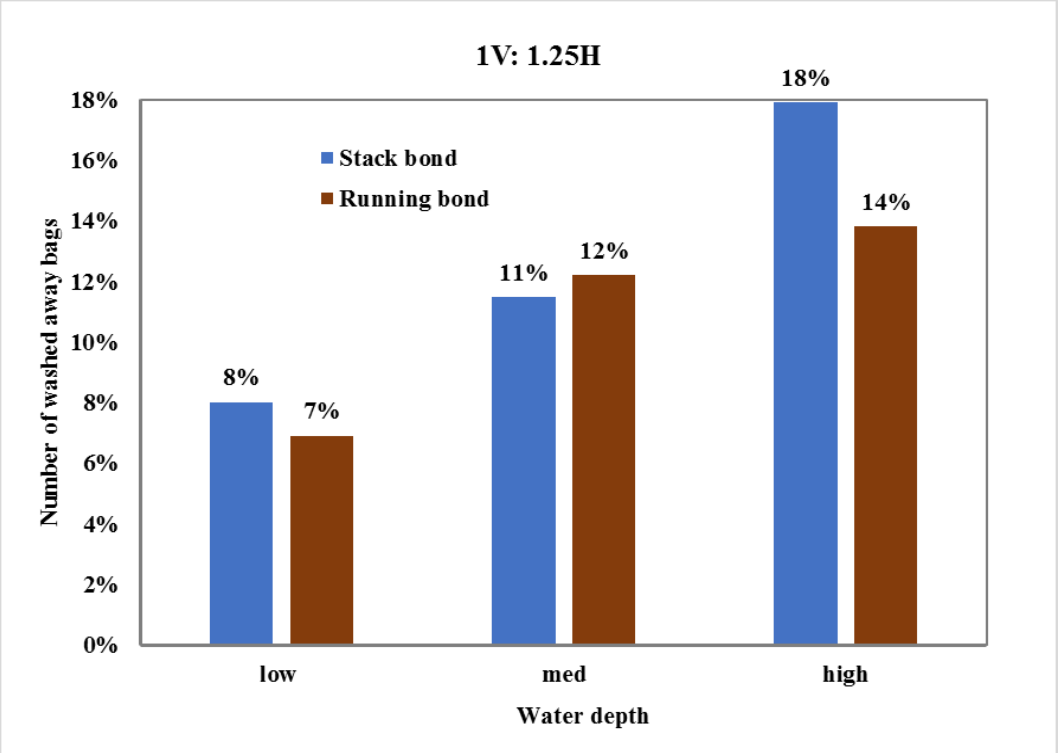

Figure 4.22: Average percentage of washed away bags for at the end of each test for two different bonds and side slope 1V:1.25H.

4.1.5. *Internal Sand movement in the geobag*

Moreover, during the model test runs it was commonly observed that the height of the geobags and consequently the height of the geobag revetment was reduced due to the saturation of the sand material inside the geotextile bag. For the tested geobag revetment, the height of both geobags and geobag revetment decreased approximately 5% from dry to wet conditions (Figure 4.23) which is close to the result obtained by Recio (2008). Recio (2008) analysed the movement of sand inside the geobag and found that the reduction of the height of the geobag (and consequently the total height of geobag structure) was affected by the internal movement of sand inside the geobags.

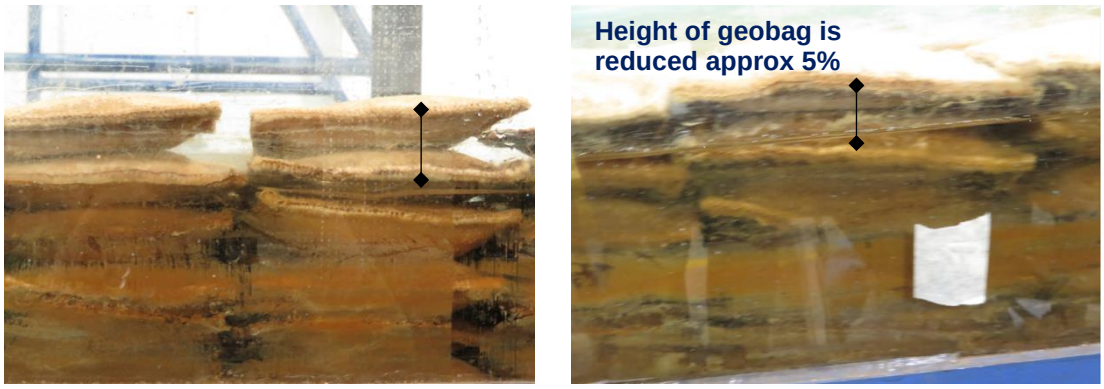

(a) the distance between edges of geobags at the start of a test run

(b) the distance between edges of geobags during a test run

Figure 4.23 (a and b): Reduction of the height of the geobag revetment due to internal movement of sand

4.1.6. *Failure zones*

The failure zone for any revetment can be defined as the area of the revetment influenced by failure processes and the dimensions of a failure zone can be used to estimate the magnitude of damage. Figure 4.24 shows the worst-case scenario for each revetment side slope (under the high-water level condition) based on the size of the failure zone. These images were produced using photogrammetry software to analyse ~100 digital photos to develop a mesh-based image of the revetments after failure, which could be used to identify the failure-induced change in revetment geometry. As shown in Figure 4.24c, a steeper side slope results in a larger and deeper failure zone.

Note that the "holes" shown in the meshes are due to the lack of sufficient image overlap.

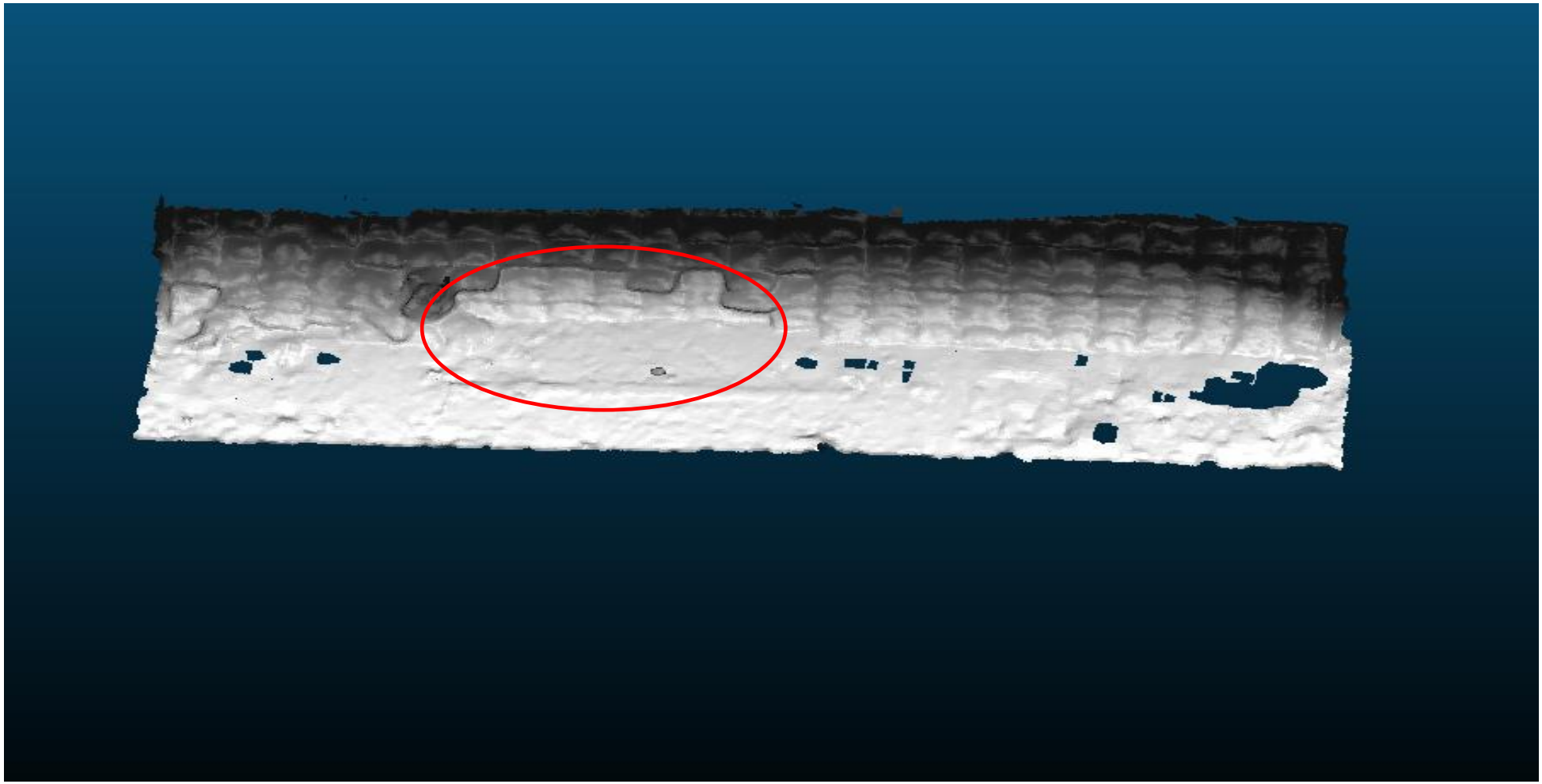

Figure 4.24 (a): Failure zones for 1V: 3H side slope

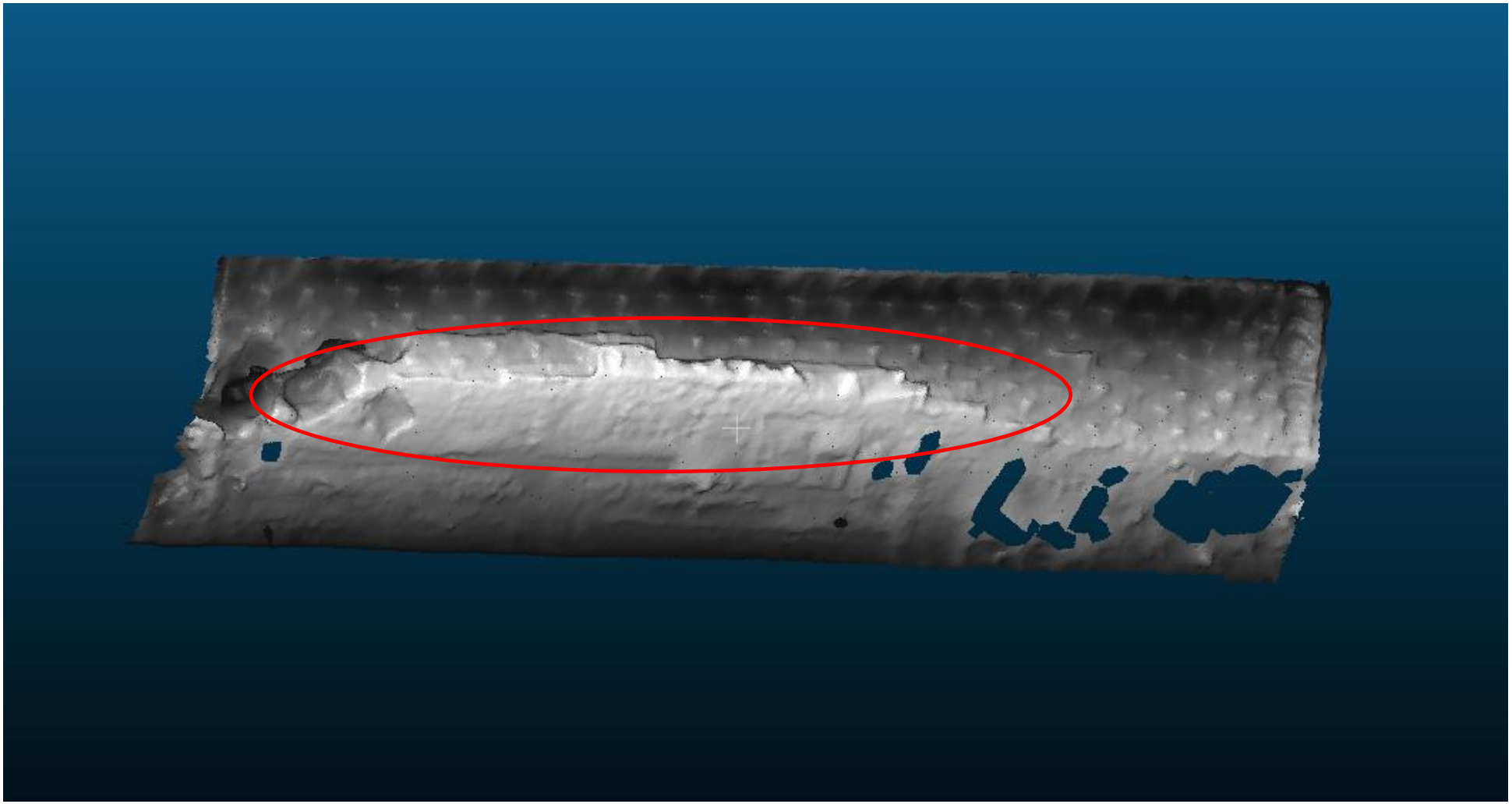

Figure 4.24 (b): Failure zones for (b) 1V: 2H side slope.

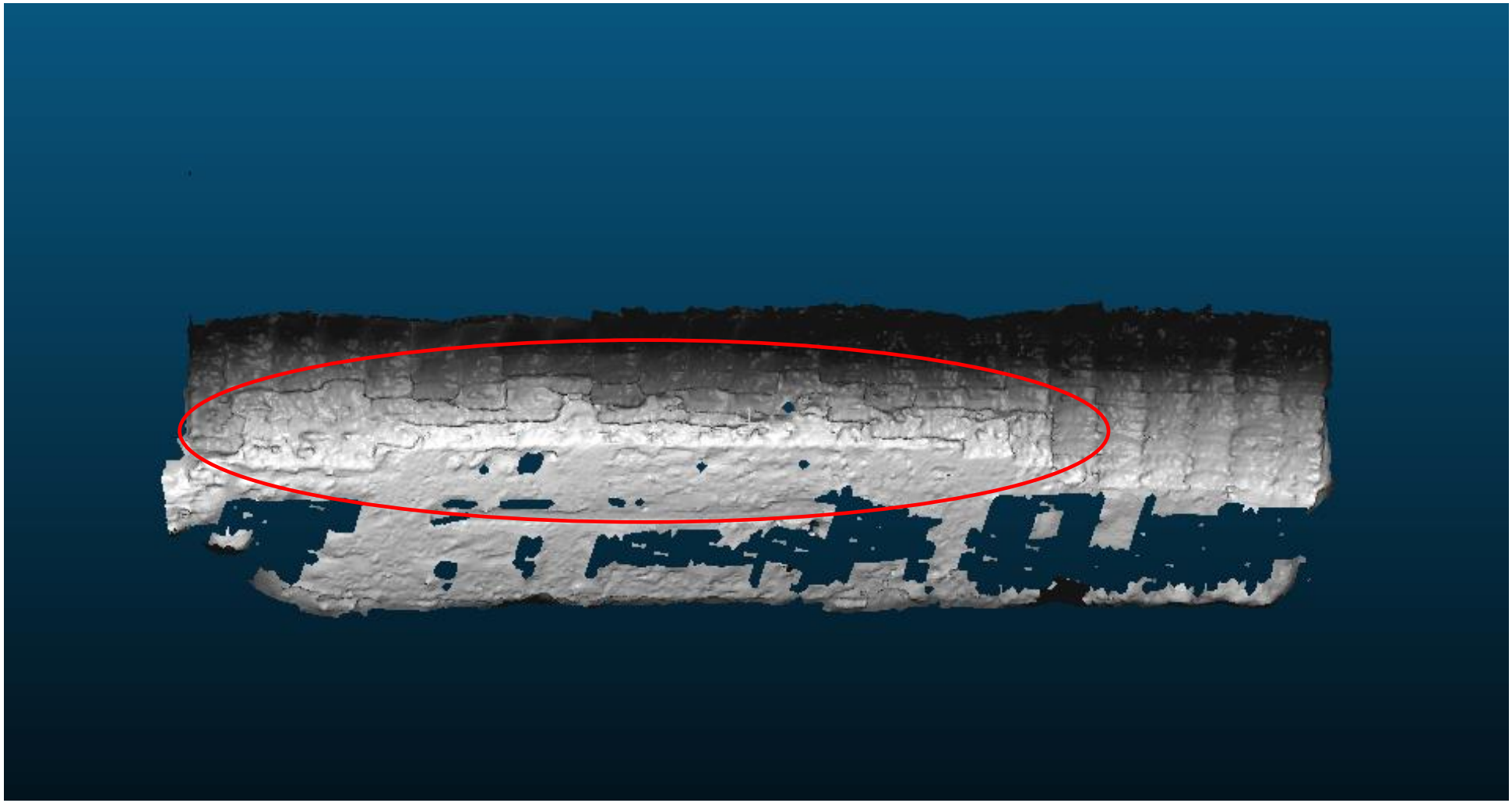

Figure 4.24 (c): Failure zones for 1V:1.25H side slope.

4.1.7. *Summary of experimental results*

Concerning the hydraulic stability of geobag revetment the main results can be summarised as follows:

- According to the Froude and Reynolds numbers outlined in Table 4-1, during all model test runs the flow in the flume was supercritical and turbulent in nature.
- The most critical location for the stability of slope geobags is for the geobags placed just below the water surface level.
- The internal movement of sand inside the geobags resulted in a height reduction of revetment approximately to 5%.
- Bag movements usually initiated within a clockwise direction with regard to the streamwise direction, regardless of water depth.

Throughout the complete failure processes the observed failure modes for each condition were:

(1) Side slope 1V:2H: for both construction bonds and low to medium water depth conditions A and B), the geobag layers tended to fail due to pullout, dislodgement, uplifting and turbulent bursting. Vertical sliding failure initiated with the failure of the submerged supporting bags was also observed in the layers above the water surface for the high-water level condition.

(1) Side slope 1V:3H: Typically, in the case of mildest side slope, and for both construction methods partial and full uplifting associated with pullout were the most common initial failure modes.

(1) Side slope 1V:1.25H: vertical sliding played an important role in failure progression in the case of the steepest slope. Moreover, turbulent bursting–induced flow through the revetment voids combined with other failure modes (e.g. uplifting) were commonly observed during the failure process in almost all water level conditions.

The results also indicate that whilst failure mechanisms are highly dependent on water depth and revetment slope the construction method had no noticeable impact and it was concluded that the dominating factor is the friction between individual geobags which itself is dependent on bag overlap rather than specific construction method.

Experimental results indicate that failure mechanisms depend on both water depth and revetment slope but, somewhat surprisingly, were found to be generally independent of the specific geobag bond configuration

4.2. Velocity analysis

As this and other studies (e.g. Akter *et al.*, 2013) have identified the significance of flow conditions on revetment failure mechanisms, it is informative to undertake an analysis of the velocity components of the prevailing flows. In the following sections, firstly ADV data assessment will be presented then the flow characteristics in pre- and post-failure conditions in front of revetment will be analysed.

4.2.1. *Power Spectral Density*

The power spectral density shows the distribution of energy over a range of time scales or frequencies (Strom and Papanicolaou, 2007). Figure 4.25 (a and b) represents the power spectral density at one point before and after the failure. For both conditions, the most substantial portion of the energy is contained in frequencies < 2 Hz. Since the large scale flow structures have been documented as having a frequency $f_L = (3-5)\ h\ /U_{avg} \approx$ 0.6–1Hz (Roy *et al.*, 2004), Figure 4.25 indicates that the dominant frequencies of motion (0.5–1 Hz) are comparable with the frequency of large scale turbulent structures (0.6–1 Hz).

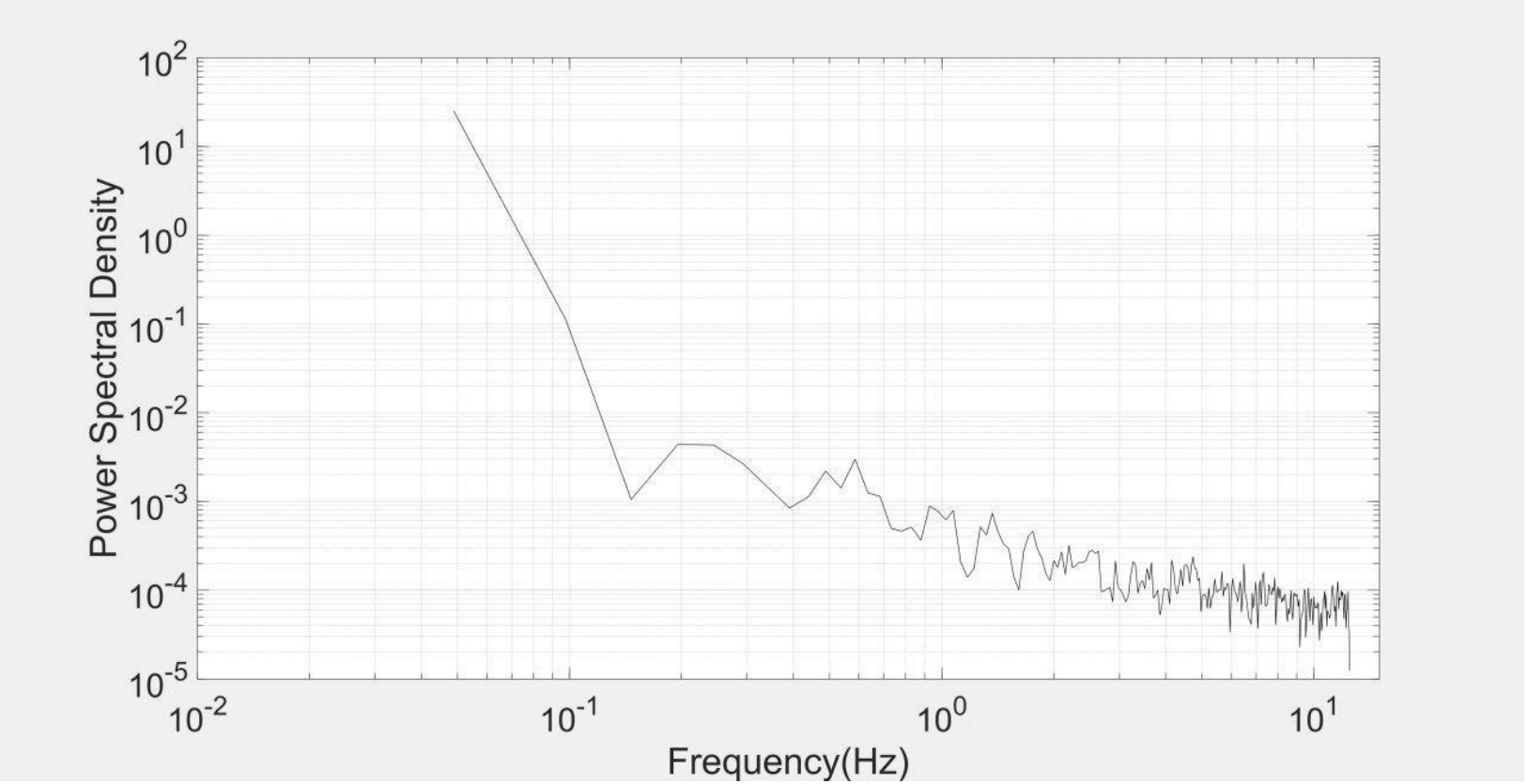

(a)

Figure 4.25 (a, b): Power spectral density in front of revetment and 5cm above the bed (a) pre-failure condition and (b) post-failure condition (Cont'd)

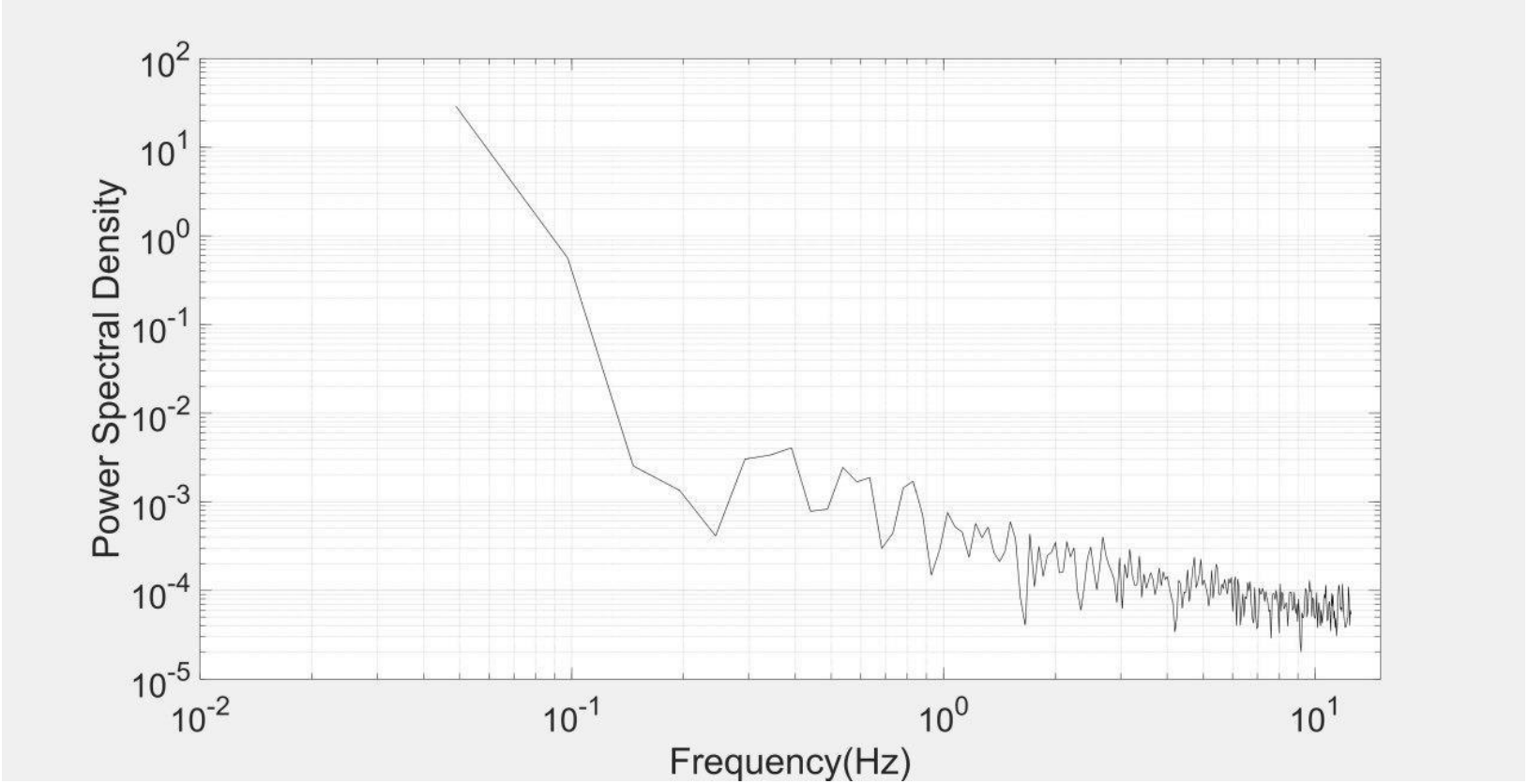

(b)

Figure 4.25 (a, b): Power spectral density in front of revetment and 5cm above the bed (a) pre-failure condition and (b) post-failure condition.

4.2.2. *Analysis of Mean Velocity Profiles*

Two locations in the middle of the test section were chosen to measure mean velocity profiles in pre-and post-failure conditions. These locations were the same for both pre- and post-failure conditions (Figure 4.26), one was close to the midpoint of a geobag (GTS - Geobag Transect Section) and the other was in a void between two geobags (VTS - Void Transect Section).

Figure 4.27 and Figure 4.28 show the distribution of the mean streamwise velocity (u) and Turbulence Intensity (TI) at GTS and VTS. The transverse distance to the revetment is normalised applying the geobag width W and due to the difficulty in accurately determining u* over geobags, the local depth-averaged velocity V was used as the most relevant velocity scale to normalise the terms of velocity. The profiles in Figure 4.27 and Figure 4.28 represent two average flow regions. GTS and VTS represent average flow conditions close to a geobag and void between two geobags respectively. Although both velocity profiles are almost identical and show the same rising trend with X/W (transverse distance to the revetment), differences can be observed in the near revetment region, where the velocity profiles are influenced by the roughness of the boundary. This is representative of the high spatial heterogeneity of the flow and its dependence on both the roughness layer and the height of the prominent part of each individual surface geobag in the revetment.

In general, since measured velocity distribution and Turbulence Intensity profile shown in Figure 4.27a were S-shaped, the flow over the revetment can be said to have two main zones (Kouwen *et al.*, 1969; Ikeda and Kanazawa, 1996) as follows:

- Zone I ($X/W<0.85$) is characterised by steep, positive velocity gradients that follow a logarithmic trend, increasing with distance from the revetment. In this Zone, the velocity values become small, but the measured velocity distribution follows a vertical profile and shows a high-velocity gradient. Here the measured velocities profile seems to follow a logarithmic trend. In Zone I the velocity profiles are concave upward and tends asymptotically, for $(u/V)\rightarrow 0$ to the vertical axis. Moving toward revetment the velocity values rapidly decrease, and the velocity gradient along the vertical assumes its maximum value. Moreover, in this Zone Turbulence Intensity values dramatically increase due to the higher velocity fluctuation in the near revetment region.

- In Zone II (X/W>0.85), here higher velocity values exist. This zone is characterised by shallow positive velocity gradients that decrease with distance from revetment and become almost horizontal in the "free-stream zone" (Carollo *et al.*, 2002). In Zone II where the velocity profile becomes horizontal, with distance from the revetment turbulence intensity becomes almost null and the thickness of the free-stream zone increases.

Figure 4.28 (a,b) shows the GTS and VTS velocity profile and Turbulence Intensity profile for the post-failure condition. Both profiles are almost identical, and their horizontal nature confirms that there is a significant decrease in mean velocity fluctuation, and consequently turbulence intensity, in the failure zones.

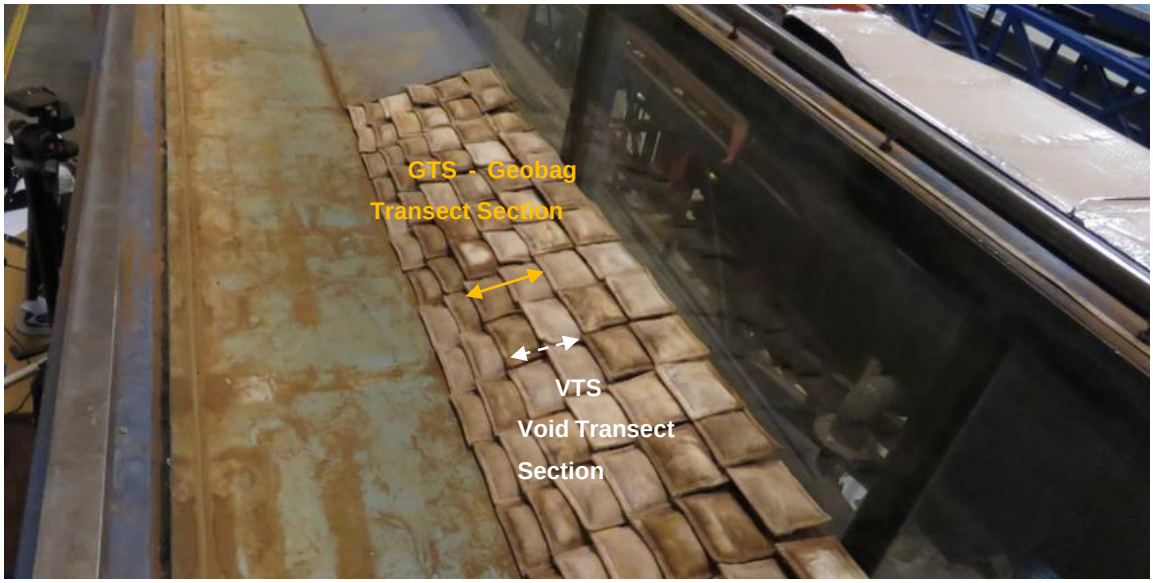

Figure 4.26 GTS (Geobag Transect, cross Section) and VTS (void Transect, Cross Section)

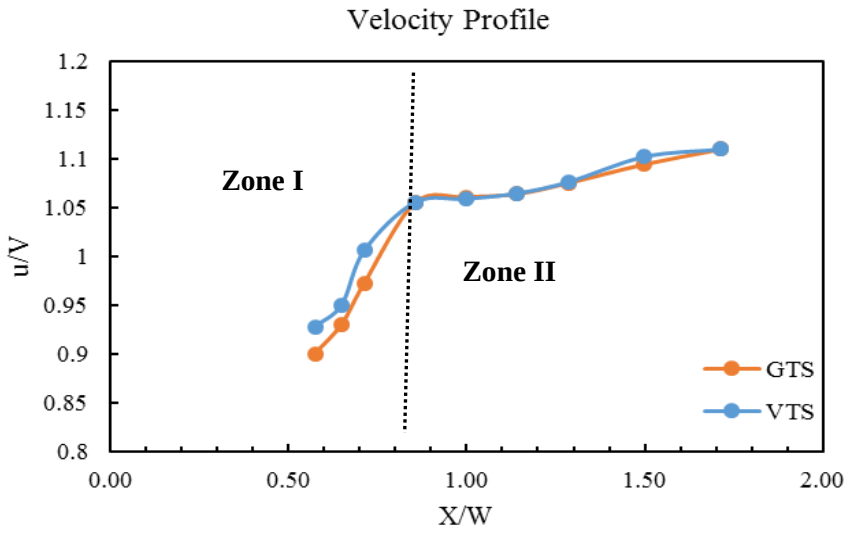

(a)

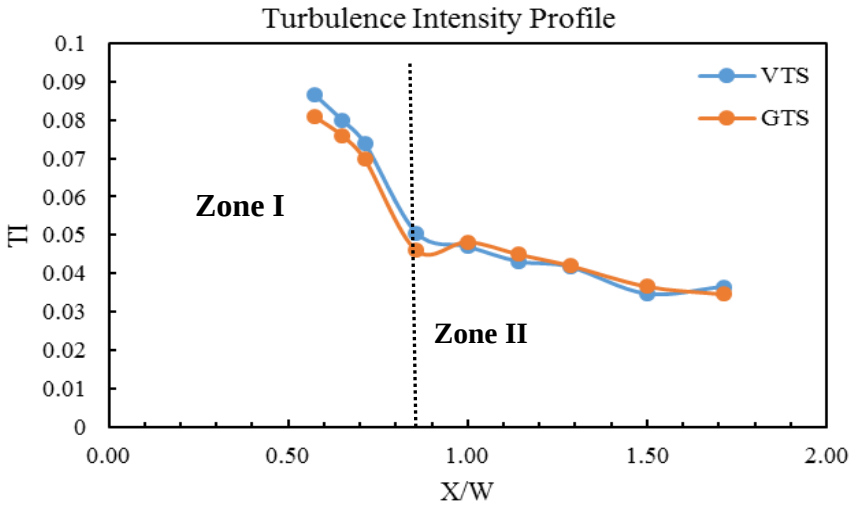

(b)

Figure 4.27(a to b): Profiles of mean velocity (a) and Turbulence Intensity (b), for GTS (Geobag Transect, Cross Section), VTS (void Transect, cross Section) in pre-failure condition.

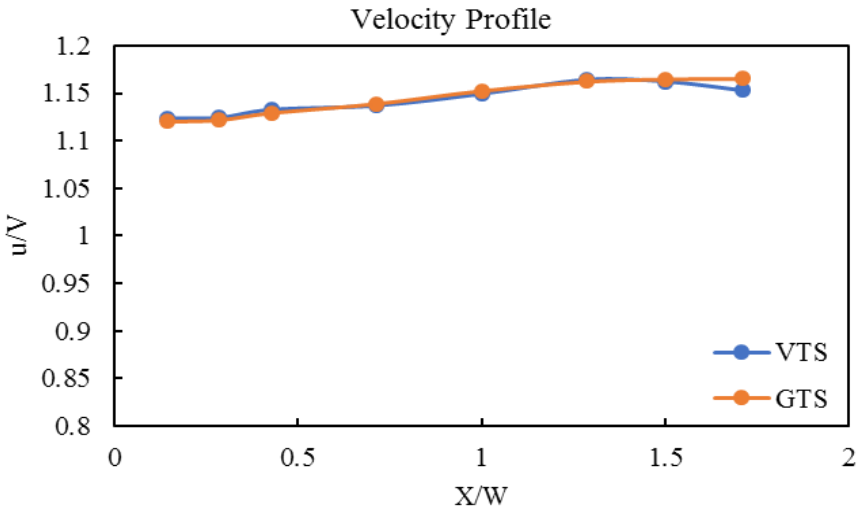

(a)

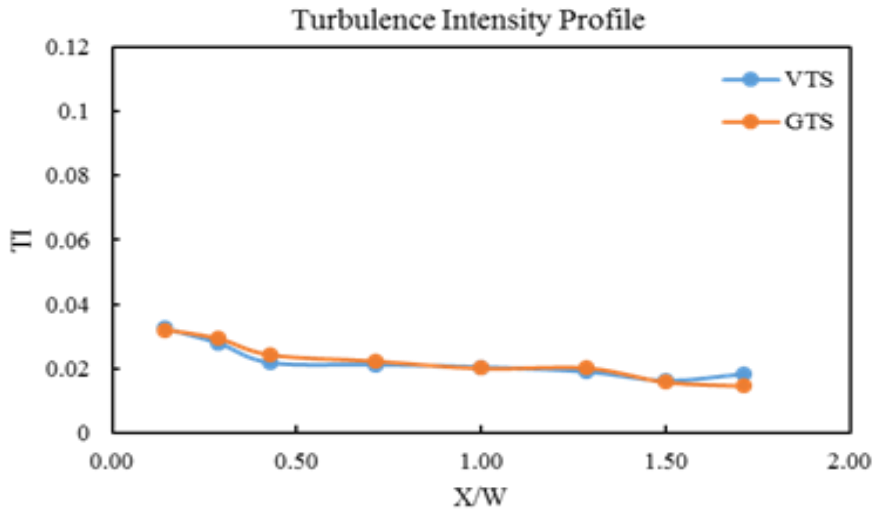

(b)

Figure 4.28(a to b): Profiles of mean velocity (a) and Turbulence Intensity (b), for GTS (geobags), VTS (void between geobags) in post-failure condition.

Turbulent eddies create fluctuations in velocity within time and space. For instance, if u, v and w are the instantaneous velocity components at a point; it should be noted that all three velocities vary in time due to turbulent fluctuations. Hence $\bar{u}$,$\bar{v}$ and $\bar{w}$ are the time-averaged velocity components; and u', v' and w' are the fluctuating components of velocity in the stream-wise, transverse and vertical directions (Figure 4.29) respectively.

For turbulent flow, however, the velocity record includes both a mean and a turbulent component. The flow is decomposed (Reynolds' decomposition) as follows:

$$u(t) = \bar{u} + u'(t) \qquad \text{Equation 4.7}$$

$$v(t) = \bar{v} + v'(t) \qquad \text{Equation 4.8}$$

$$w(t) = \bar{w} + w'(t) \qquad \text{Equation 4.9}$$

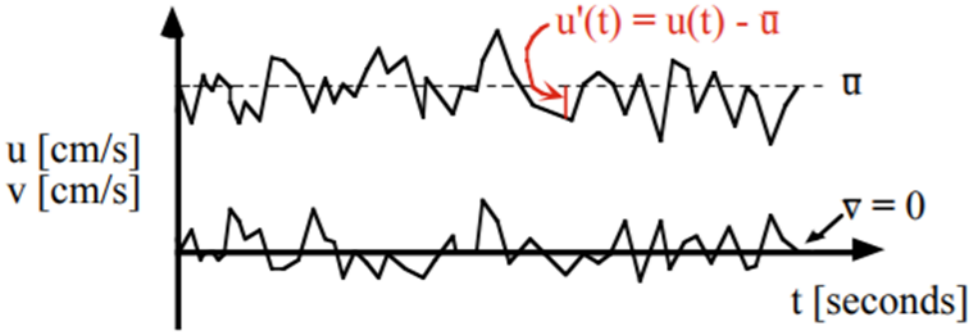

Figure 4.29: Velocity recorded using ADV

4.2.3. *Detailed velocity analysis*

Using the detailed velocity measurement approach detailed in Chapter 3, an analysis of the velocities captured by the ADV yielded the velocity contour plots shown in Figure 4.30 and Figure 4.31. In these figures, u, v and w (which are the velocity components in stream-wise, transverse and vertical direction) are normalised by the mean flow velocity (V) and distances in the x and y directions are normalized by the length (L) and width (W) of a single geobag respectively.

For the case of pre-failure, Figure 4.30a indicates that approaching the revetment results in an increasingly lower value of u/V, with a value of approximately 1 at a distance of Y/W≥0.5. The dense contour lines of u/V (Figure 4.30a) show an increase in the fluctuation of the velocity component in the streamwise direction (u). However, higher values of stream-wise velocity are mostly seen around the voids between bags, which can result in water-pressure differences between the channel side and the geobag lee side.

This can introduce turbulent bursting–induced flow through the revetment voids, which may lead to pullout or ejection of bags in these points. Figure 4.31a indicates no meaningful pattern in the variation of v/V, indicating that the revetment does not have a noticeable impact on the magnitude of v. Figure 4.32a also shows the presence of higher values of positive w/V near the revetment, indicating a small upward current in this vicinity.

In the case of post-failure, the experimental results show how the formation of a failure zone in a revetment can help stabilise the failure processes, this is well illustrated in Figure 4.30b, which shows more uniform distributions of u/V and fewer fluctuations inside the failure zone compared with the pre-failure conditions. From these observations, it can be concluded that the creation of a failure zone diverts and traps flow into the failure zone, resulting in a region of low turbulence which acts to help prevent further failure.

The existence of an area of high values of negative v/V and w/V at the beginning of the hole demonstrates a downward flow towards the revetment (Figure 4.31b and Figure 4.32b). This means that a portion of the flow is diverted from the mainstream toward the failure hole and leads to a reduction of the intensity of the turbulent flow in front of the revetment.

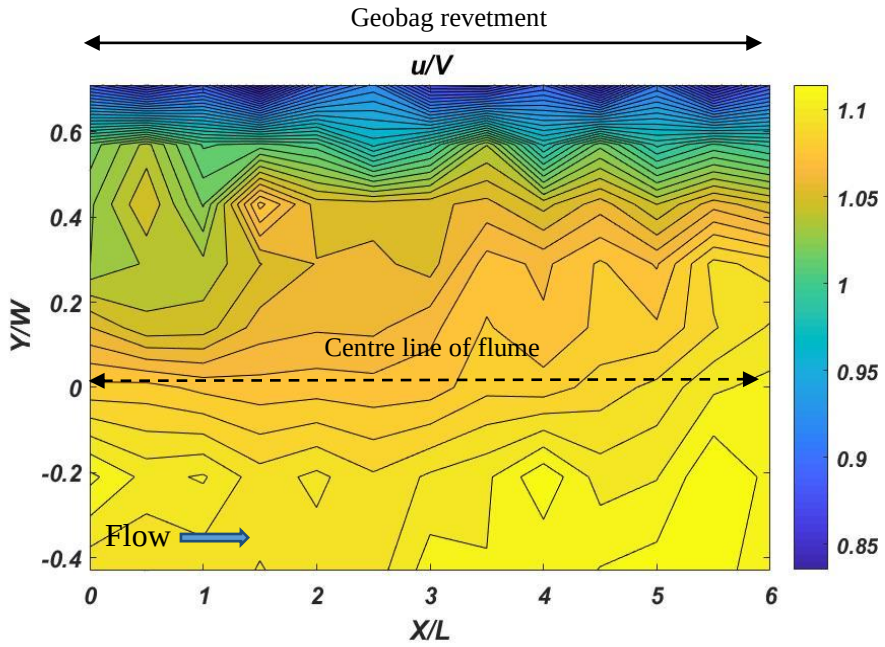

(a) Pre-failure condition

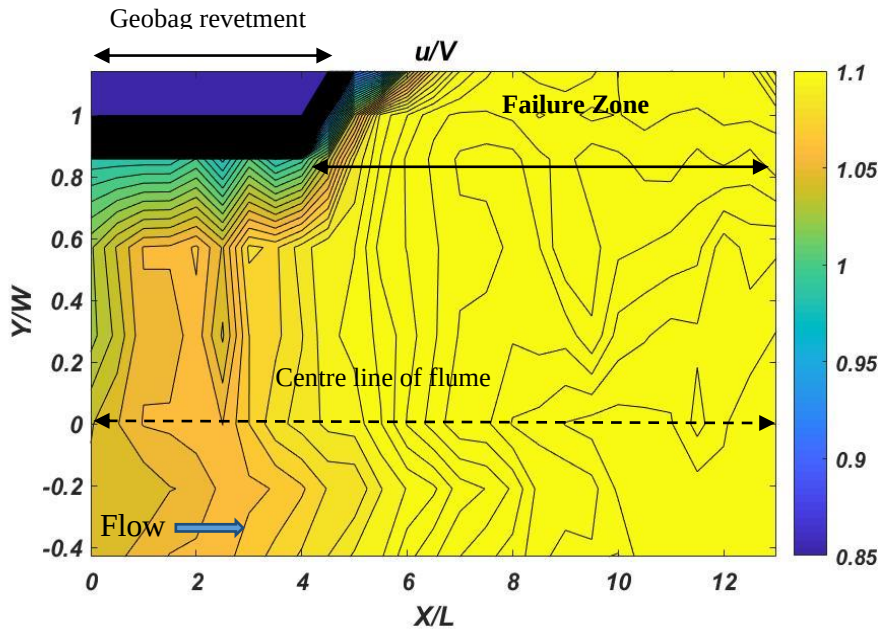

(b) Post-failure condition

Figure 4.30: Contour plots of velocity component *u* for the pre-failure (a) and post-failure (b) conditions in a horizontal plane (Side slope 1V:2H, medium water depth, stack bond)

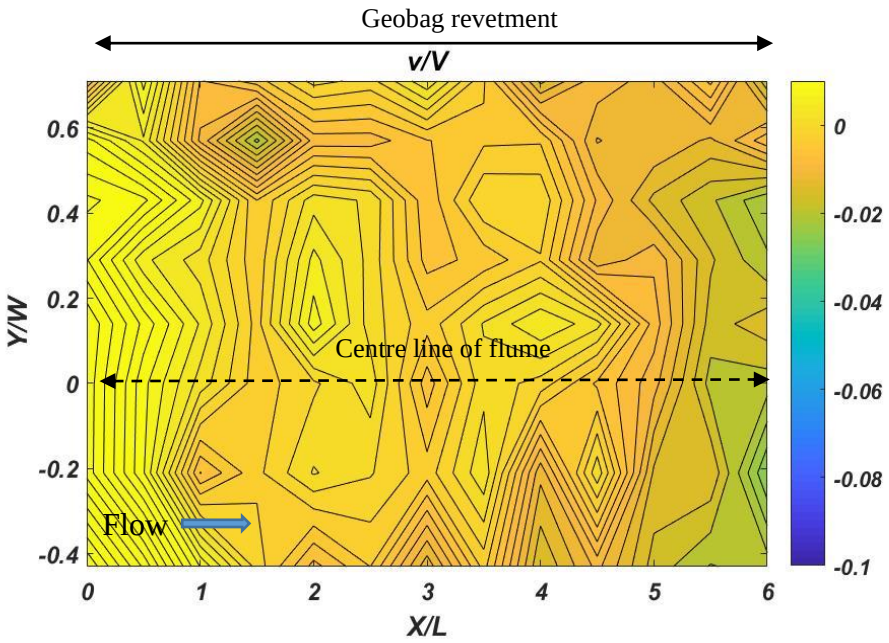

(a) Pre-failure condition

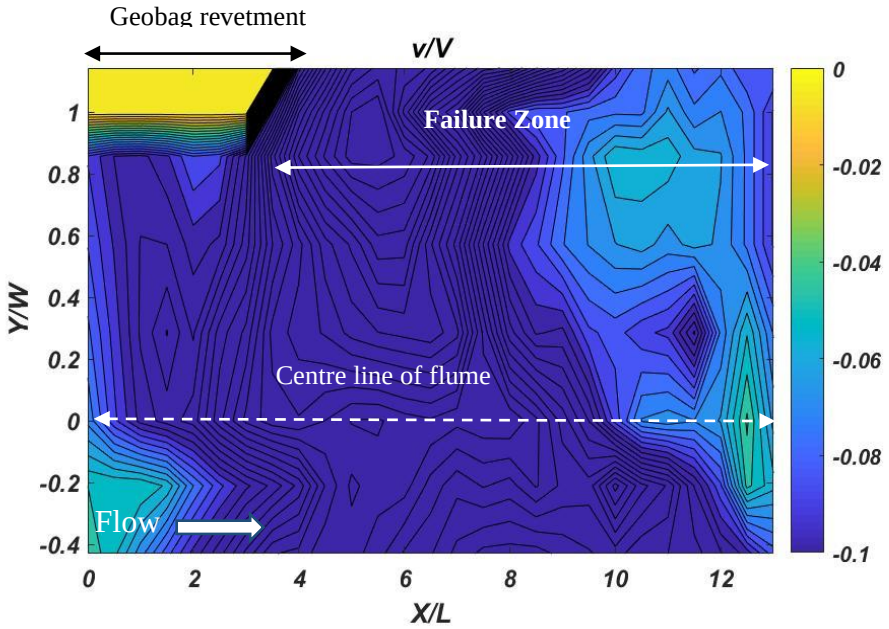

(b) Post-failure condition

Figure 4.31: Contour plots of velocity component *v* for the pre-failure (a) and post-failure (b) conditions in a horizontal plane (Side slope 1V:2H, medium water depth, stack bond)

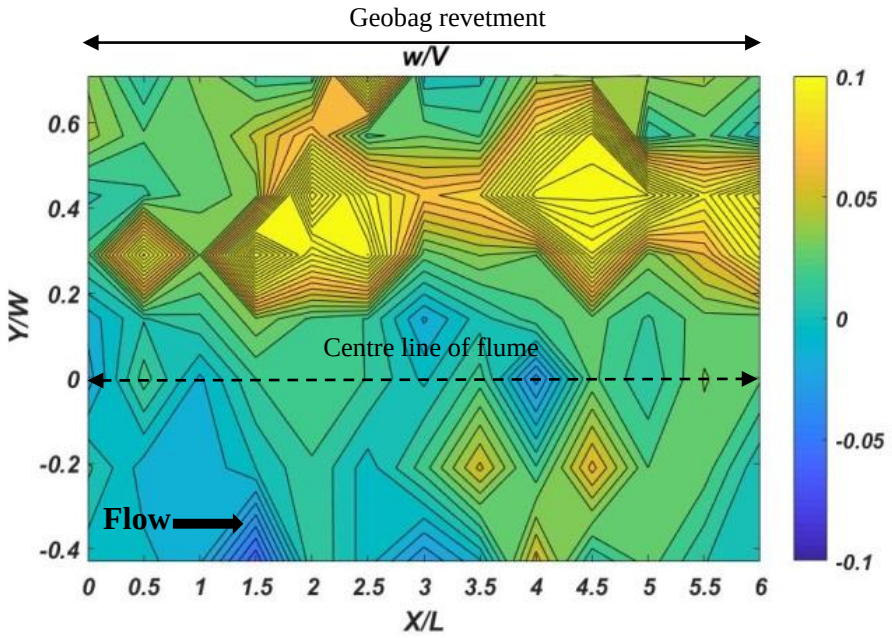

(a) Pre-failure condition

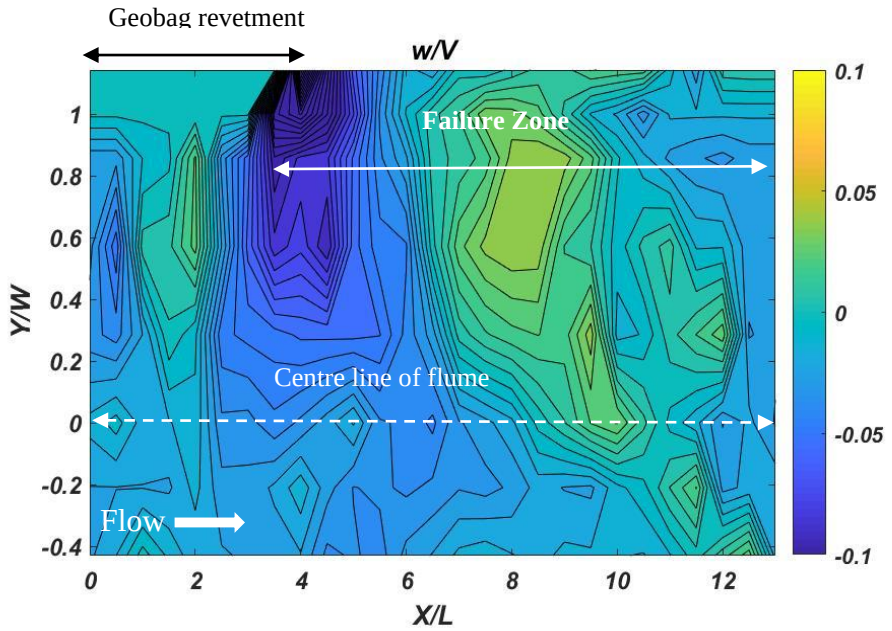

(b) Post-failure condition

Figure 4.32: Contour plots of velocity component *w* for the pre-failure (a) and post-failure (b) conditions in a horizontal plane (Side slope 1V:2H, medium water depth, stack bond)

4.2.3.1. Turbulence intensity components

Since the turbulence associated with eddies moves randomly, they can be characterised by applying statistical concepts. Theoretically, the velocity record is continuous, and the mean can be estimated through integration. However, in practice the measured velocities are a series of discrete points u_i. The overbar shown in Equation 4.10 to Equation 4.13 below is used to denote a time average over the time interval t to t+T, where T is much longer than any turbulence time scale, but much shorter than the time-scale for mean flow unsteadiness.

Mean velocity: $\bar{u} = \int_t^{t+T} u(t)dt$ continuous record; $\overline{u} = \frac{1}{N}\sum_1^N u_i$ discrete, equi-spaced points — Equation 4.10

Turbulent Fluctuation: $u'(t) = u(t) - \bar{u}$ continuous record; $u_i' = u_i - \bar{u}$ discrete points — Equation 4.11

Turbulence Strength: $u_{RMS} = \sqrt{\overline{u'(t)^2}} = \sqrt{\frac{1}{N}\sum_{i=1}^{N}(u_i')^2}$ — Equation 4.12

Turbulence Intensity: $u_{RMS}/\overline{u}$ — Equation 4.13

The subscript 'RMS' stands for root-mean-square. u_{RMS} is defined as the standard deviation of the set of "random" velocity fluctuations u_i'. Similar definitions apply to the lateral and vertical velocities *v*(t) and *w*(t). A larger u_{RMS} shows a higher level of turbulence

Based on the velocity fluctuation components, the total Turbulence Intensity (TI) of the flow in three dimensions can be computed using Equation 4.14.

$$TI = \sqrt{\frac{1}{3}\left(\overline{u'^2} + \overline{v'^2} + \overline{w'^2}\right)} \qquad \text{Equation 4.14}$$

The Root Mean Square (RMS) values of fluctuations of the velocity components demonstrate the turbulence intensity components. In the present study, TI_u in the stream-wise direction and TI_{xyz}, are normalised using the mean flow velocity V. The contour plots of TI_u and TI_{xyz} for the pre-failure are demonstrated in Figure 4.33a and Figure 4.34a, show that the values of TI_u and TI decrease with distance from the revetment. In the case of the post-failure scenario, the contour plots of TI_u and TI_{xyz} shown in Figure 4.33b and Figure 4.34b indicate a significant reduction in both parameters at the failure zone compared with the pre-failure condition. These lower values of TI post-failure indicate fewer fluctuations and accordingly less turbulence in the vicinity of the failure zone, confirming that the formation of a failure zone acts to stabilise the failure process.

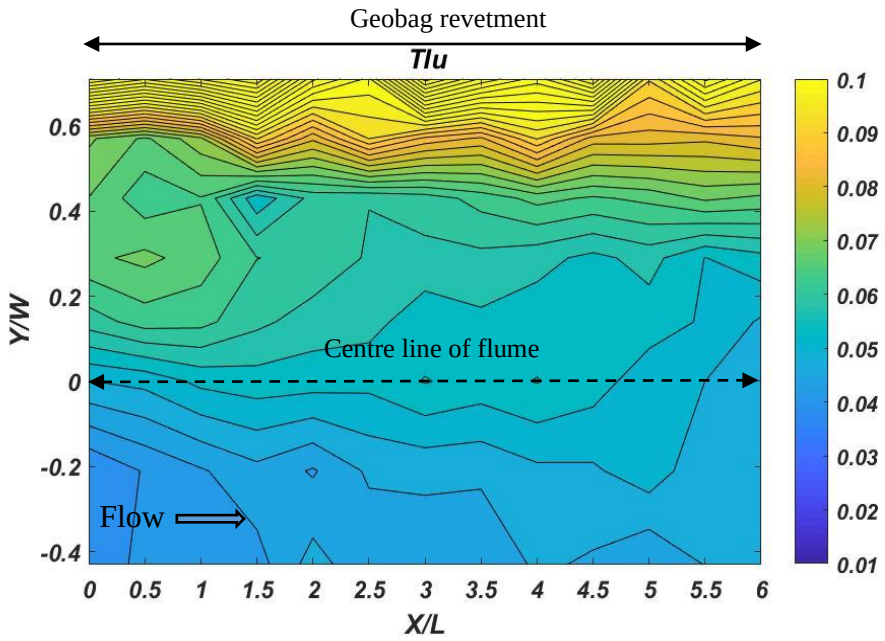

(a) Pre-failure condition

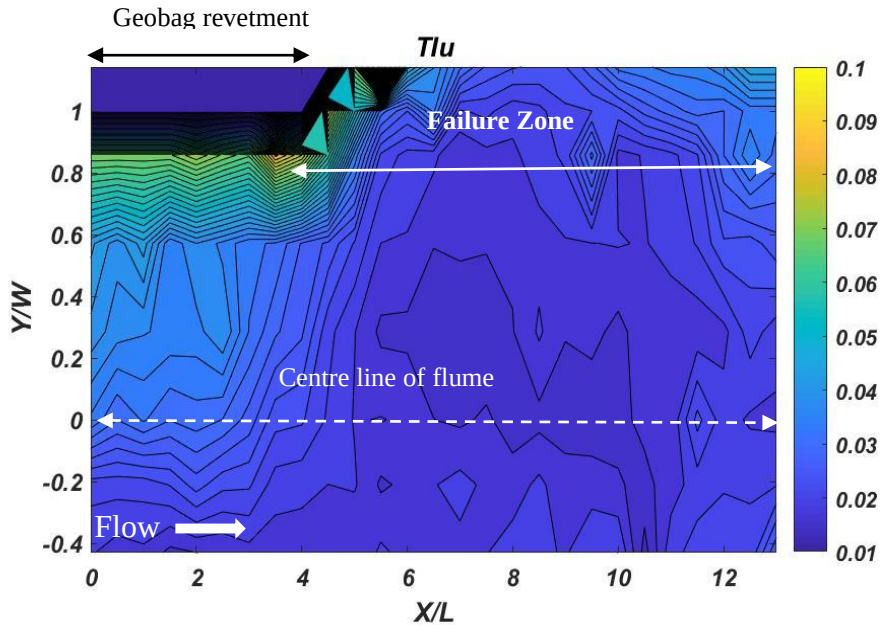

(b) Post-failure condition

Figure 4.33: Contour plots of stream-wise turbulence intensity component TIu, for the pre-failure (a) and post-failure (b) conditions in a horizontal plane (Side slope 1V:2H, medium water depth, stack bond)

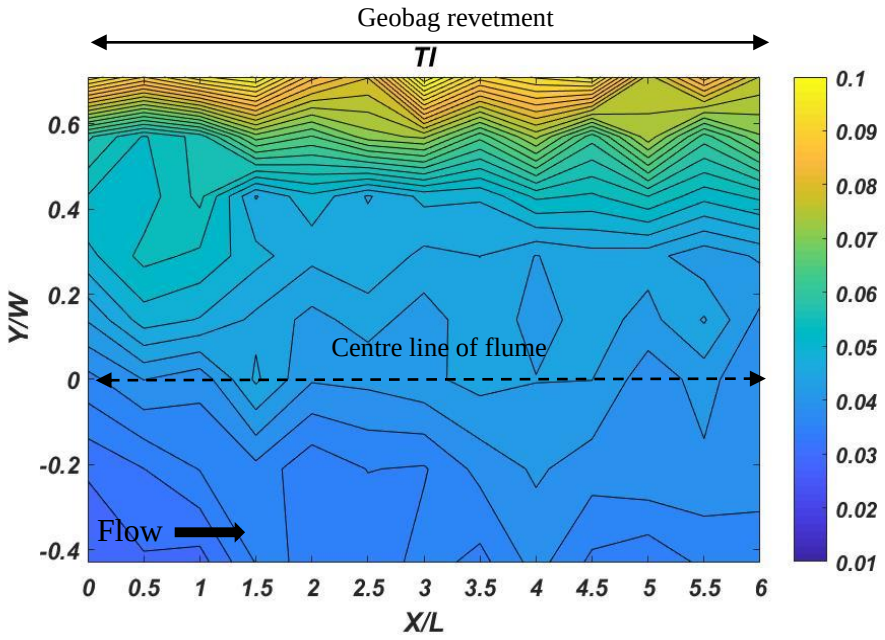

(a) Pre-failure condition

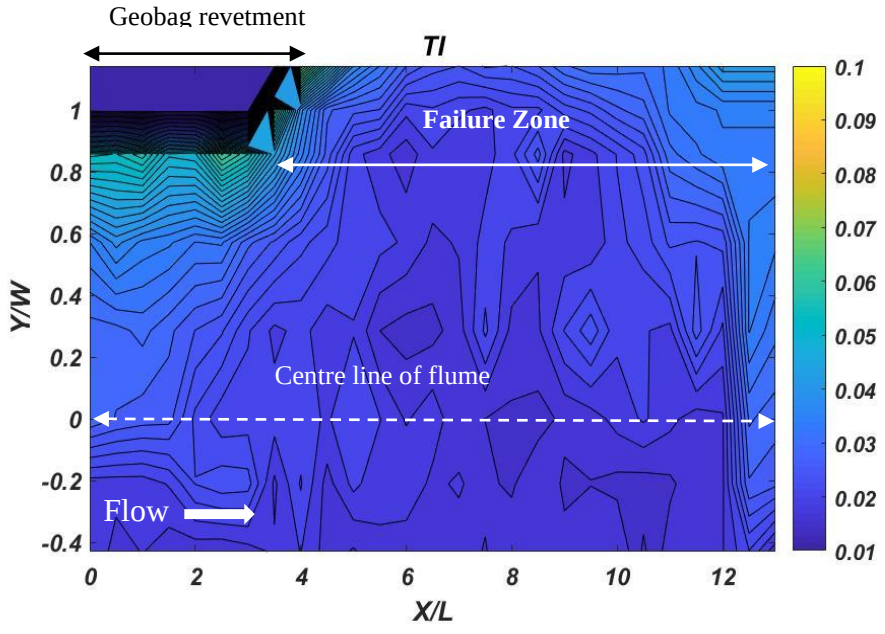

(b) Post-failure condition

Figure 4.34: Contour plots of total turbulence intensity TI/V, for the pre-failure (a) and post-failure (b) conditions in a horizontal plane (Side slope 1V:2H, medium water depth, stack bond)

4.2.5.2 Turbulent kinetic energy

Based on the velocity fluctuation components, the total turbulent kinetic energy (TKE_{xyz}) of the flow in three dimensions can be computed using Equation 4.15.

$$TKE_{xyz} = \frac{1}{2}\left(\overline{u'^2} + \overline{v'^2} + \overline{w'^2}\right) \quad \text{Equation 4.15}$$

Contour plots of TKE/V^2 for the pre- and post-failure case in a horizontal plane are presented in Figure 4.35(a and b). The results from the contour plots show that the distribution of TKE/V^2 is similar to the distribution of turbulence intensity. Although for both cases higher values of turbulent kinetic energy are observed close to the revetment and specifically around the void space between the bags a dramatic reduction of TKE is seen towards the failure zone. The maximum value of TKE/V^2 is approximately equal to 0·015 at the void space between bags.

The results indicate that TKE varies noticeably from the centreline toward the revetment for the pre- and post-failure cases. Considering the detailed velocity measurement approach detailed in Chapter 3 and comparing the contribution to the TKE_{xyz} of different velocity fluctuations (u′, v′ and w′ in x, y and z directions, respectively), average turbulent energy for each line (L.A–L.H) is presented in Figure 4.35(a and b), Figure 4.36 (a and b) and Table 4-2 for conditions pre- and post-failure of the revetment, respectively. According to Table 4-2 it can be found that, the maximum percentage of contribution belongs to the streamwise direction and surprisingly the contribution of vertical flow direction into total kinetic energy is significantly high compared to the lateral direction. Becoming closer to the revetment for post-failure case in the failure zone TKEz is almost equal to TKEx. Therefore, it can be speculated that the role of stream-wise and vertical velocity components on failure processes is more prominent than the lateral velocity component for both pre- and post-failure conditions. Based on the above results the effect of vertical velocity fluctuations cannot be neglected in the progress of failure.

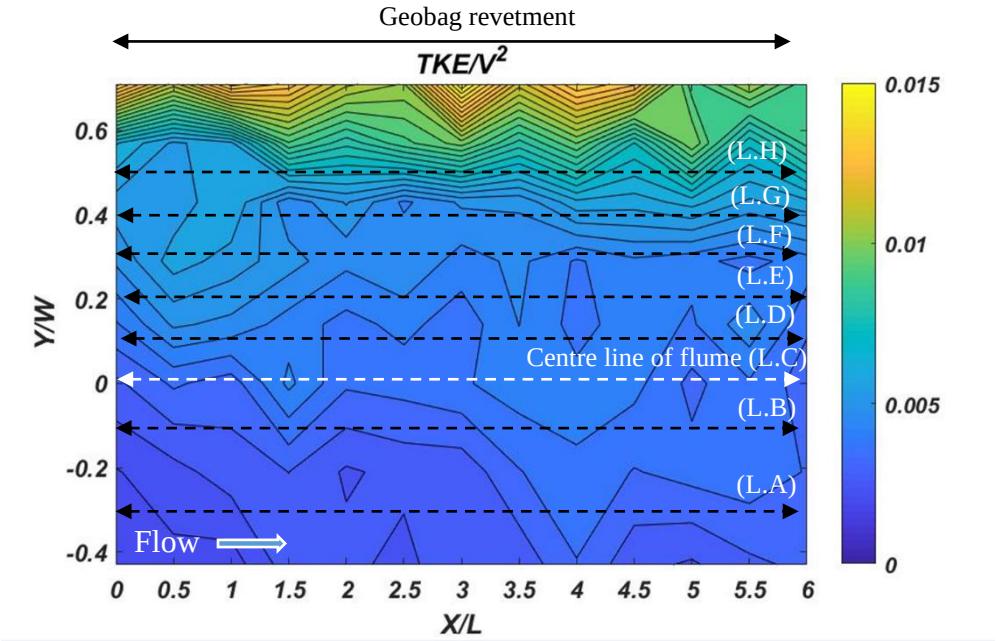

(a) Pre-failure condition

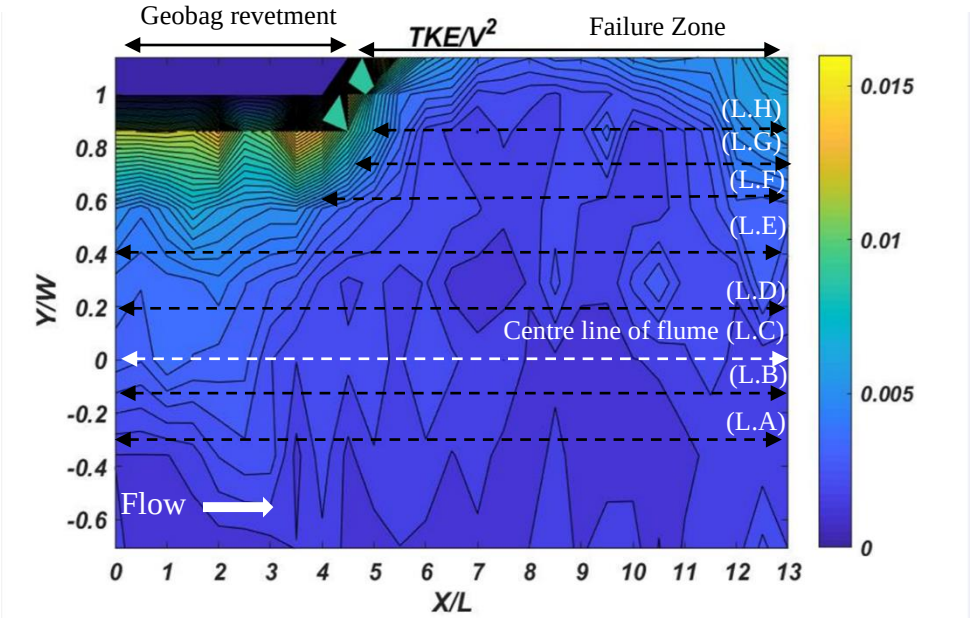

(b) Post-failure condition

Figure 4.35: Contour plots of total turbulent kinetic energy TKE/V^2 for the pre-failure (a) and post-failure (b) conditions in a horizontal plane (Side slope 1V:2H, medium water depth and stack bond)

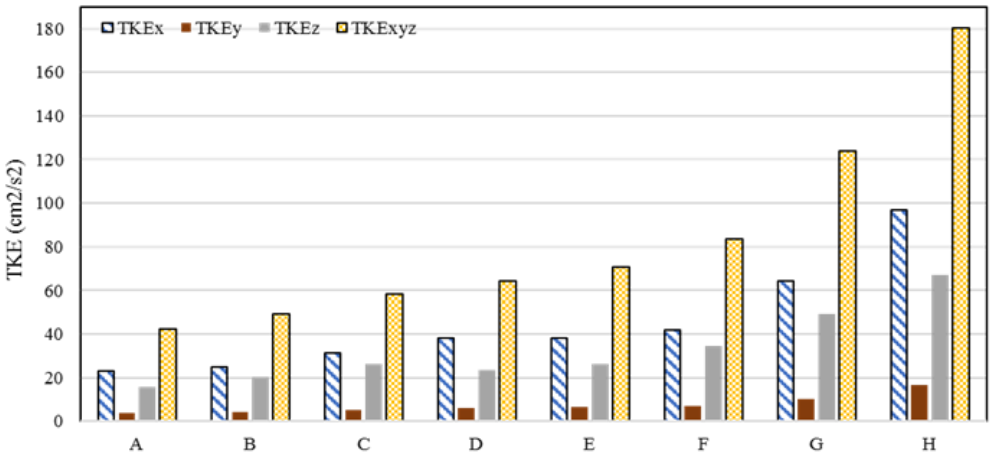

(a) Pre-failure condition

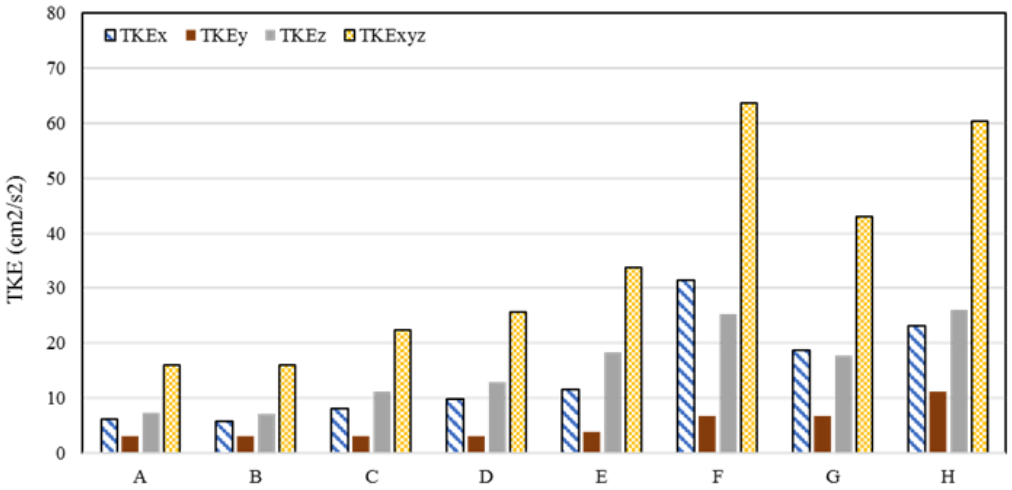

(b) Post-failure condition

Figure 4.36: Averaged longitudinal TKE for pre-failure (a) and post-failure (b) conditions

Table 4-2 Turbulent kinetic energy of flow for pre- and post-failure conditions

Lines	Conditions	TKEx	% contribution	TKEy	% contribution	TKEz	% contribution	TKExyz
A	Pre-failure	22.96	54.07	3.72	8.76	15.79	37.18	42.47
B	Pre-failure	24.87	50.65	4.06	8.26	20.17	41.09	49.10
C	Pre-failure	31.13	53.54	5.09	8.76	26.45	45.49	58.14
D	Pre-failure	38.33	59.76	6.06	9.45	23.32	36.37	64.13
E	Pre-failure	38.16	53.82	6.63	9.34	26.12	36.84	70.90
F	Pre-failure	42.07	50.26	7.20	8.60	34.44	41.14	83.71
G	Pre-failure	64.21	51.92	10.05	8.13	49.41	39.95	123.66
H	Pre-failure	96.68	53.58	16.48	9.13	67.28	37.29	180.44
Average			**53.45%**		**8.80%**		**39.42%**	
A	Post-failure	6.15	38.46	3.01	18.84	7.26	45.39	15.99
B	Post-failure	5.74	36.03	3.02	18.93	7.17	45.04	15.93
C	Post-failure	8.10	36.32	3.01	13.48	11.20	50.20	22.31
D	Post-failure	9.72	37.96	3.05	11.92	12.83	50.12	25.60
E	Post-failure	11.61	34.35	3.88	11.47	18.32	54.19	33.81
F	Post-failure	31.45	49.49	6.77	10.65	25.33	39.86	63.55
G	Post-failure	18.66	43.39	6.64	15.44	17.70	41.17	43.01
H	Post-failure	23.17	38.39	11.18	18.53	25.99	43.08	60.34
Average			**39.30%**		**14.91%**		**46.13%**	

4.2.5.3 Reynolds shear stresses

The fluctuating components can be used to measure the Reynolds stress, which is the total stress tensor in a fluid. The components of the Reynolds stress tensor are generally defined as Equation 4.16:

$$\tau_{uv} = -\rho\overline{u'v'}, \qquad \tau_{vw} = -\rho\overline{v'w'}, \qquad \tau_{uw} = -\rho\overline{u'w'} \qquad \text{Equation 4.16}$$

Reynolds shear stresses are calculated using the streamwise, lateral and vertical components of velocity fluctuation. The values of $-\rho\overline{u'v'}$, $-\rho\overline{u'w'}$ and $-\rho\overline{v'w'}$ have been normalised by ρ~V^2 and ρ represents the mass density of water. The contour plots of Reynolds shear stresses for the pre-and post-failure cases and in the plane XY, XZ and YZ are shown in Figure 4.37, Figure 4.38 and Figure 4.39 respectively. The contour plots demonstrate that, before failure started from upstream to downstream of revetment, the negative Reynolds shear stresses in XY and YZ plane considerably increase by becoming closer to the revetment. Considering $-\overline{u'v'}$ as the lateral advection of streamwise turbulent momentum or more simply the lateral flux of streamwise momentum then $-\overline{v'w'}$ is the horizontal flux of lateral momentum and the sign of the momentum flux terms tell whether the flux is inducing a net increase or decrease in momentum (positive

and negative, respectively).Thus great negative values of these parameters specifically close to the revetment show high streamwise and lateral turbulent momentum in this area. Although the existence of some small areas of low positive Reynolds shear stresses in XZ plane around the voids between the bags display a rapid change in vertical flux of sreamwise momentum in these small areas where the bag motions usually are initiated (Akter, Pender, et al., 2013).

Contour plots of the Reynolds stress values for the post-failure case indicate similar trends but with significantly lower values close to the revetment.

Comparing Reynolds shear stress and turbulent kinetic energy in the areas close to revetment, a high gradient of shear stress and turbulent kinetic energy is observed. Since the high magnitudes of shear stress are located in highly turbulent zones hence as expected the high magnitudes of TKE_{xyz} were observed in these locations (Figure 4.35). Therefore, it can be concluded that approaching the revetment in the transverse direction, the flow situation differs significantly due to fully three-dimensional vortex rotations.

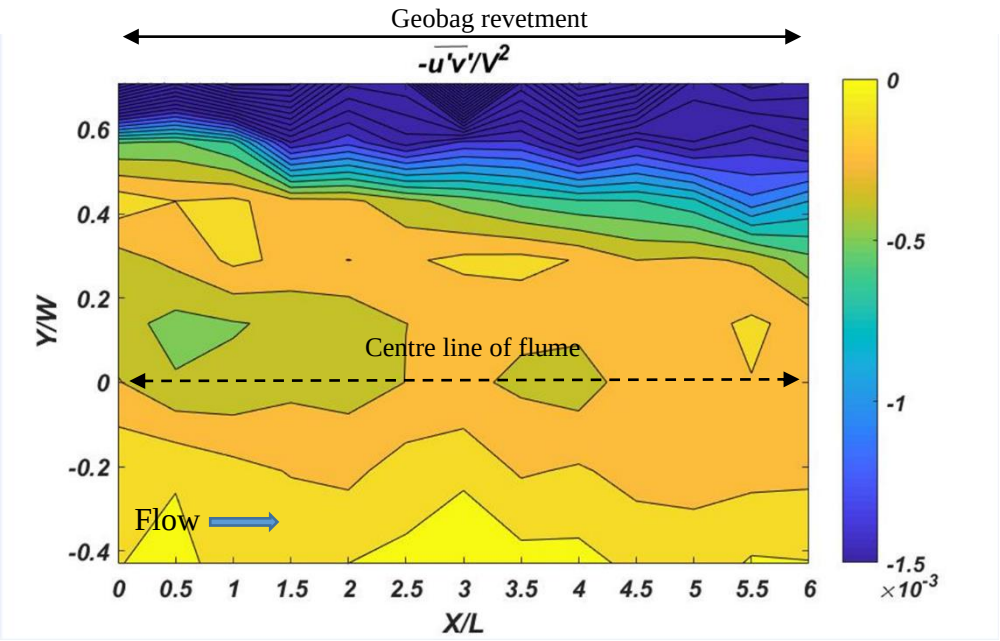

(a) Pre-failure condition

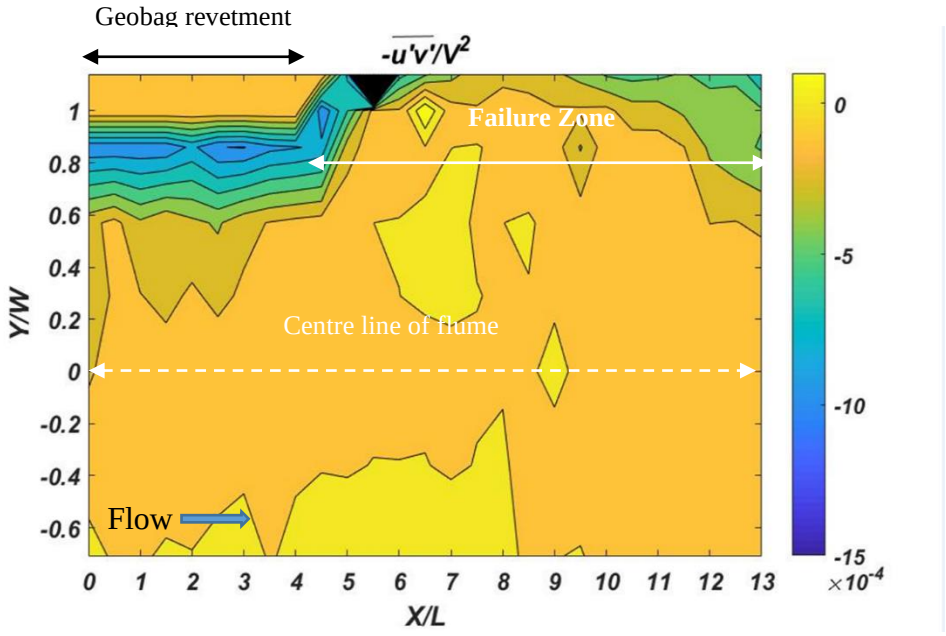

(b) Post-failure condition

Figure 4.37: Contour plots of Reynolds shear stress components in the horizontal plane XY for the pre-failure (a) and post-failure (b) conditions (Side slope 1V:2H, medium water depth and stack bond)

.

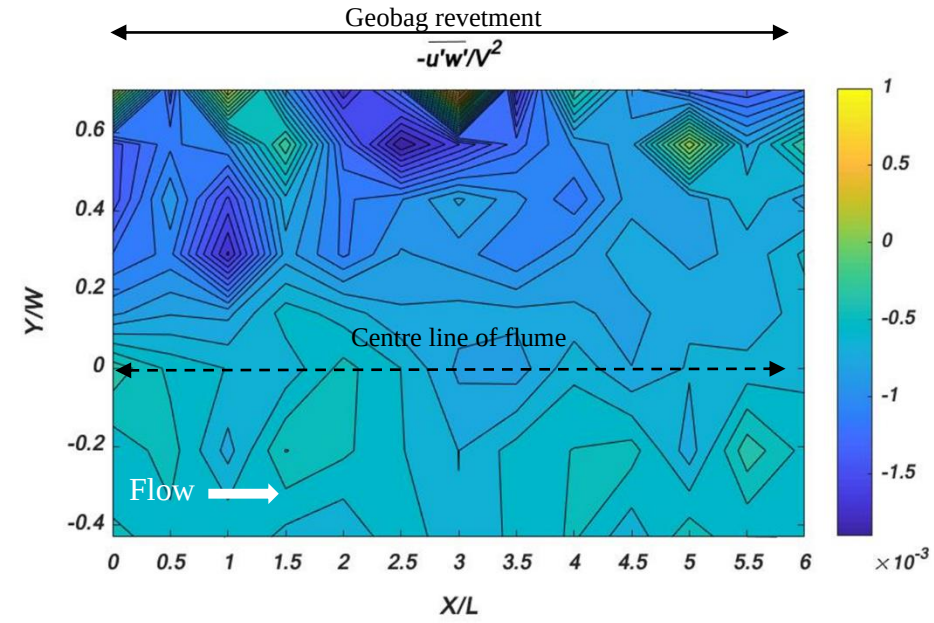

(b) Post-failure condition

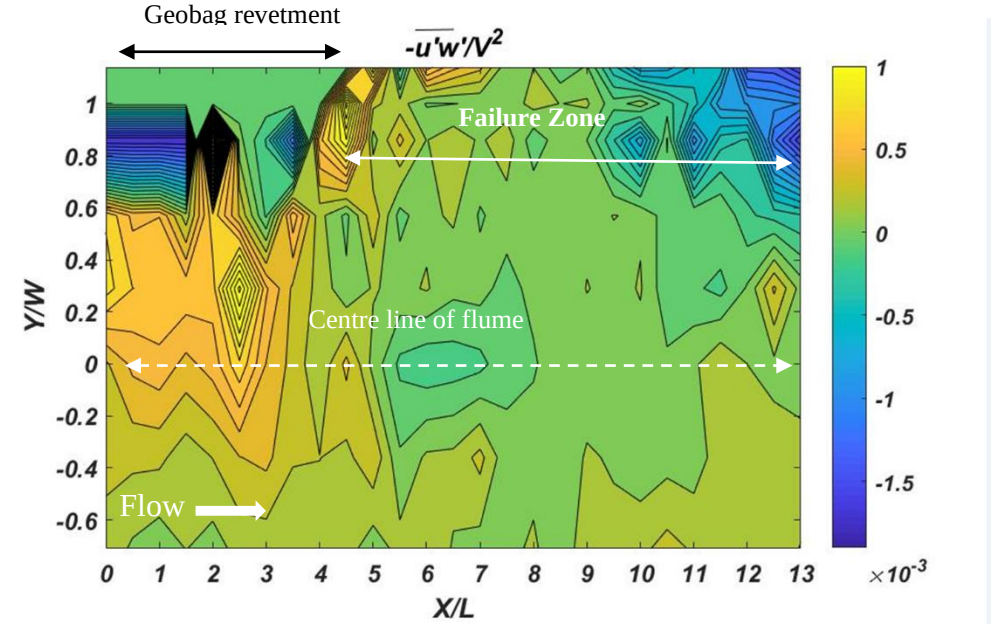

(b) Post-failure condition

Figure 4.38: Contour plots of Reynolds shear stress components in the plane XZ for the pre-failure (a) and post-failure (b) conditions (Side slope 1V:2H, medium water depth and stack bond)

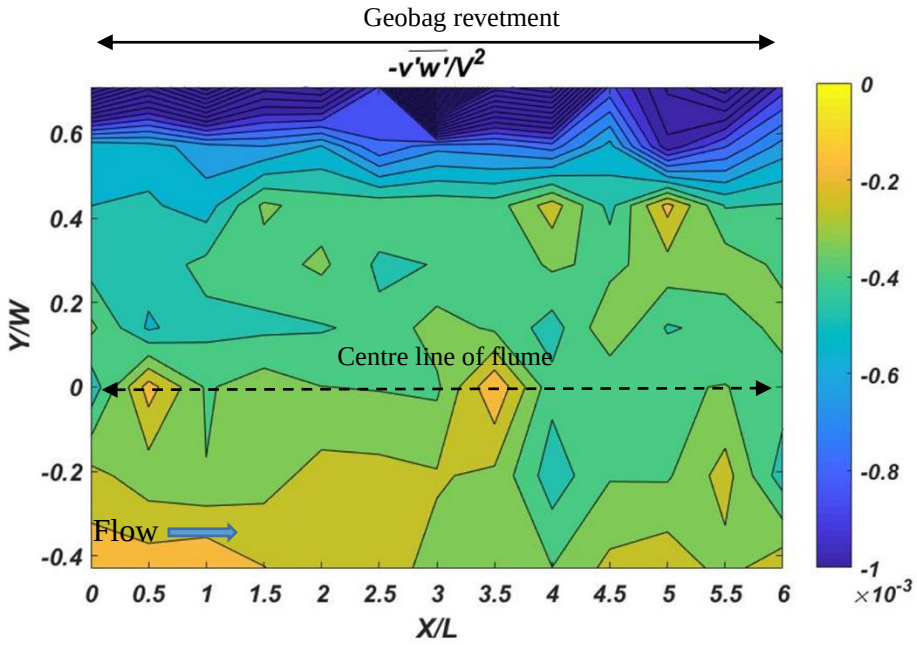

(b) Post-failure condition

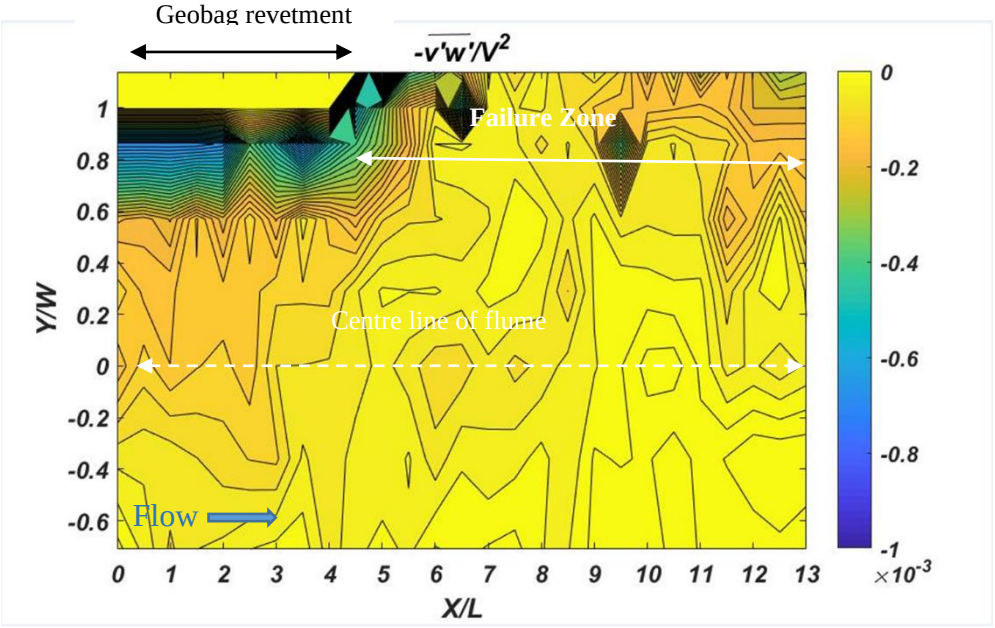

(b) Post-failure condition

Figure 4.39: Contour plots of Reynolds shear stress components in the plane YZ for the pre-failure (a) and post-failure (b) conditions (Side slope 1V:2H, medium water depth and stack bond)

4.2.4. *Summary of the detailed velocity result*

Three-dimensional analysis of flow structures and turbulence characteristics around geobag revetment was undertaken for pre- and post-failure conditions. The results demonstrate that the flow structures around revetment are complicated. Furthermore, the flow structures are affected significantly by approaching the revetment in the transverse direction from the distance of Y/W>0.6. The turbulence characteristics such as turbulence intensity, turbulent kinetic energy and Reynolds shear stresses for the pre-failure case are notably different from those for the post-failure. Results of the present study show that stronger turbulence structures are noticed around the void spaces between bags. Accordingly, it can be concluded that regarding initiation the failure process, voids is the most critical zones at which the revetments experience the highest turbulence, and hence the maximum probability of bag motions can be expected. For the case of post-failure, the results show that the level of turbulence, in particular, TKE decline significantly due to failure hole and it can be the main reason for stopping failure progress.

4.3. Chapter summary

The failure processes in a geobag revetment have been studied in a laboratory flume by using different revetment side slopes and construction bonds. On the revetment, geobags are exposed to the flowing water and they are subjected to the hydrodynamic forces of Lift and Drag caused by the flow over them. However, gravity (body force) is found to be as the main stabilising force which acts against hydrodynamic forces to keep the geobags in place -provided that the side slope of revetment is not too steep, in which case gravity can develop a destabilising force.

The results also indicate that whilst failure mechanisms are highly dependent on water depth and revetment slope. The construction method had no noticeable impact and it was concluded that the dominating factor is the friction between individual geobags which itself is dependent on bag overlap rather than specific construction method. This finding has potentially important implications for revetment construction methods.

Results of the present study show that stronger turbulence structures are noticed around the void spaces between bags. Accordingly, it can be concluded that in terms of what initiate the failure process, voids are the most critical zones at where the revetments experience the highest turbulence and hence where the maximum probability of bag motions can be expected. For the case of post-failure, the results show that the level of

turbulence decline significantly due to failure hole and it can be the main reason for stopping the failure progress. The outcomes from this study have been used to develop a DEM model of geobag revetments. Once validated, the DEM model could be used to develop guidance on the performance of geobag revetments in riverbank situations.

Chapter 5. **NUMERICAL MODEL STUDY**

This Chapter presents the results of a numerical study which attempted to simulate the processes that affect the stability of geobag revetment using numerical simulations.

The first part focuses on a brief description of an open source Discrete Element Model (DEM) code LIGGGHTS which is developed and adapted to simulate geobag structure.

The second part of the Chapter presents the results of the DEM model coupled with hydrodynamic forces to simulate the failure modes observed in Chapter 4 for the geobag – water flow interactions and clarify the role of drag and lift force as two main hydrodynamic forces on different stages of failure processes.

The third part of this chapter aims to use the coupled model to reproduce the observed failures for the geobag – water flow – mobile sand bed interactions represented by (Akter, Pender, *et al.*, 2013). Therefore, the DEM model was developed to simulate the behaviour of revetment mounted on a mobile sand bed and affected by the hydrodynamic forces.

5.1. Basic model setup

5.1.1. *Representing geobags as discrete elements*

The majority of particulate systems taking place in nature or use in industry are made of particles with complex geometric shapes. A DEM model simulates the interaction between the particles as well as the dynamic behaviour of the system accurately when the shape of modelled particles are defined correctly (Parteli, 2013).

Besides the 'single-particle' methods e.g. ellipses/ellipsoids, super-quadrics and polygons/polyhedrons, the multi-sphere method, in which a rigid body is built by combining spheres of different sizes (sphere clump) is extensively used as a method for approximating complex and non-spherical particle shapes in DEM simulations and most popular in the DEM community (e.g. Kafui and Thornton, 2000; Abbaspour-Fard, 2004; Garcia et al., 2009; Ferellec and McDowell, 2010; Grima and Wypych, 2013; Weigler and Mellmann, 2014).

During contacts, in such a composite particle, the relative positions of the inter-connected spheres do not change. The total forces and torques acting on the composite particles are the summation of those acting on the primary spheres relative to the centre of mass of the composite particle. Eventually, trajectories of the composite particle are calculated using these total forces and torques (Favier *et al.*, 1999). The popularity of this method in non-spherical DEM is due to the capability of this method to model any complex particle shape with sufficient accuracy. Furthermore, the most important advantage of the multi-spheres method is that the contact detection and calculation procedures of the contact parameters developed for conventional spherical DEM can be directly used (Lu *et al.*, 2015).

However, as a deficiency of this method, in the most numerical simulations, the mass and moment of inertia of the resulting sphere clumps are incorrectly computed as a result of the contribution of the sphere-sphere overlaps (Parteli, 2013). For the system consists of a large number of particles, and the calculation can become computationally too expensive if the mass and moment of inertia of each clump are numerically calculated (Amberger *et al.*, 2012). Ferellec and McDowell, (2010) proposed to modify the density of the spheres constituting the clumps to achieve the target mass and moment of inertia. However, it is important to use the real density of the particle material in order to model inter-particle collisional forces correctly.

In order to represent the characteristic shape of geobags in a DEM framework, in this study a multi-sphere approach was adopted in which a rigid body representing a bag is built by combining spheres of different sizes. (Akter, Crapper, *et al.*, 2013) also used this method for DEM simulations of geobags with 110 spheres.

Since the non-smooth surface leads to a higher possibility of multiple contacts between two contacting particles, obtaining the sufficient level of surface smoothness requires a large number of primary spheres (Lu *et al.*, 2015). Although using more spheres results in more accuracy and efficiency in force calculations and consequently in simulating the movement of bags, the computational time of simulation increases significantly. Therefore, for this work to represent a single geobag size of 0.103 m × 0.07 m, a model of 178 spheres using four different sizes, 18 spheres of 20 mm diameter, 36 spheres of 15 mm, 72 spheres of 10 mm and 52 spheres of 5 mm diameter was employed to let the software function optimally (Figure 5.1). Within LIGGGHTS, the 178 spheres acted as an individual rigid body and the total contact forces of the geobags were summed over each sphere within a geobag.

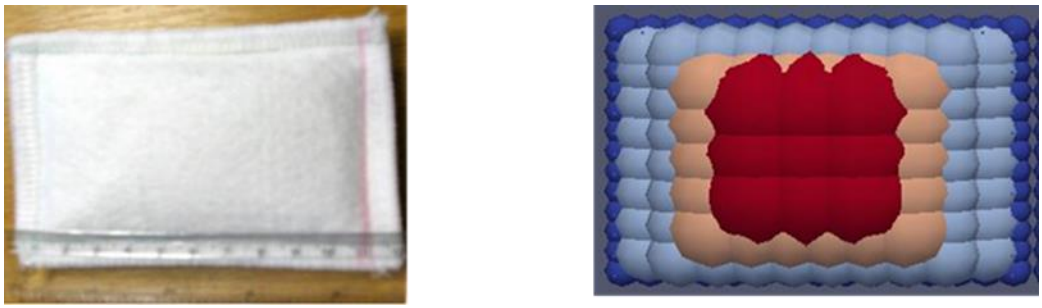

Figure 5.1: Laboratory and DEM representation of a geobag

5.1.2. *Velocity field*

To calculate fluid forces (Drag and Lift) which were exerted on geobags, the required input parameters were water density (998.2 kg/m^3) and viscosity (1.003 × 10-6 m^2/s) (at 20°C) together with the coefficient of drag and lift force for the bags and the local 3-dimensional mean velocity.

In order to have an accurate estimation of local mean velocity over surface geobags, the average 3-D velocities measured by ADV (described in Chapter 3 and 4) were used to predict the mean local velocity over revetment for different flow conditions. The measured streamwise velocity shows an increasing trend with respect to increased water depth and a decreasing trend, approaching the revetment.

The velocity of flow at a certain point is dependent on the distance from that point to the "wall", or the boundary of the fluid region. Previously in chapter 4, it was shown that the ratio of streamwise velocity in each point to the average velocity decreases getting closer to the revetment and 0.95 is the value of this ratio at the closest points to the revetment (Figure 4.30). Akter (2011) used the CES method to predict a mapped streamwise velocity field (Figure 5.2). For the present DEM model, this mapped velocity field was applied to estimate depth-average velocities over the surface geobags in different depths of water with 0.06 m intervals, instead of 0.01m intervals used in the referred study. To achieve a practical numerical model, in this study, average velocities obtained from ADV measurement (detailed in chapter 4) were used as input for the DEM modelling. However, to acquire a sufficient accuracy of the flow velocities over the geobag revetment, the coefficient of 0.95 (described above) was multiplied to these velocities and with considering Akter's mapped velocity field the frequent depth-average velocities close to revetment were estimated. For force calculations, the lateral and vertical component of velocities were taken as the proportions of the stream-wise velocity obtained from the experimental measurements for specific water depth (see Chapter 4,Table 4-1). Furthermore, it was assumed that only the surface bags were exposed to the flow, and the effect of drag and lift on the rear buried geobags was assumed to be negligible. The bag permeability and state of wetness were ignored. Due to the limitations of using ADV to measure the velocity at each geobag, this approach can be applied to predict average velocities at any point over the revetment. Also, this approach seems to be efficient for a limited time and computational budget.

From the quasi-physical model tested in the laboratory it was recognised that for both medium and high-water level conditions the failure process followed the same trend. Therefore, the low and high-water level conditions were applied for the numerical program.

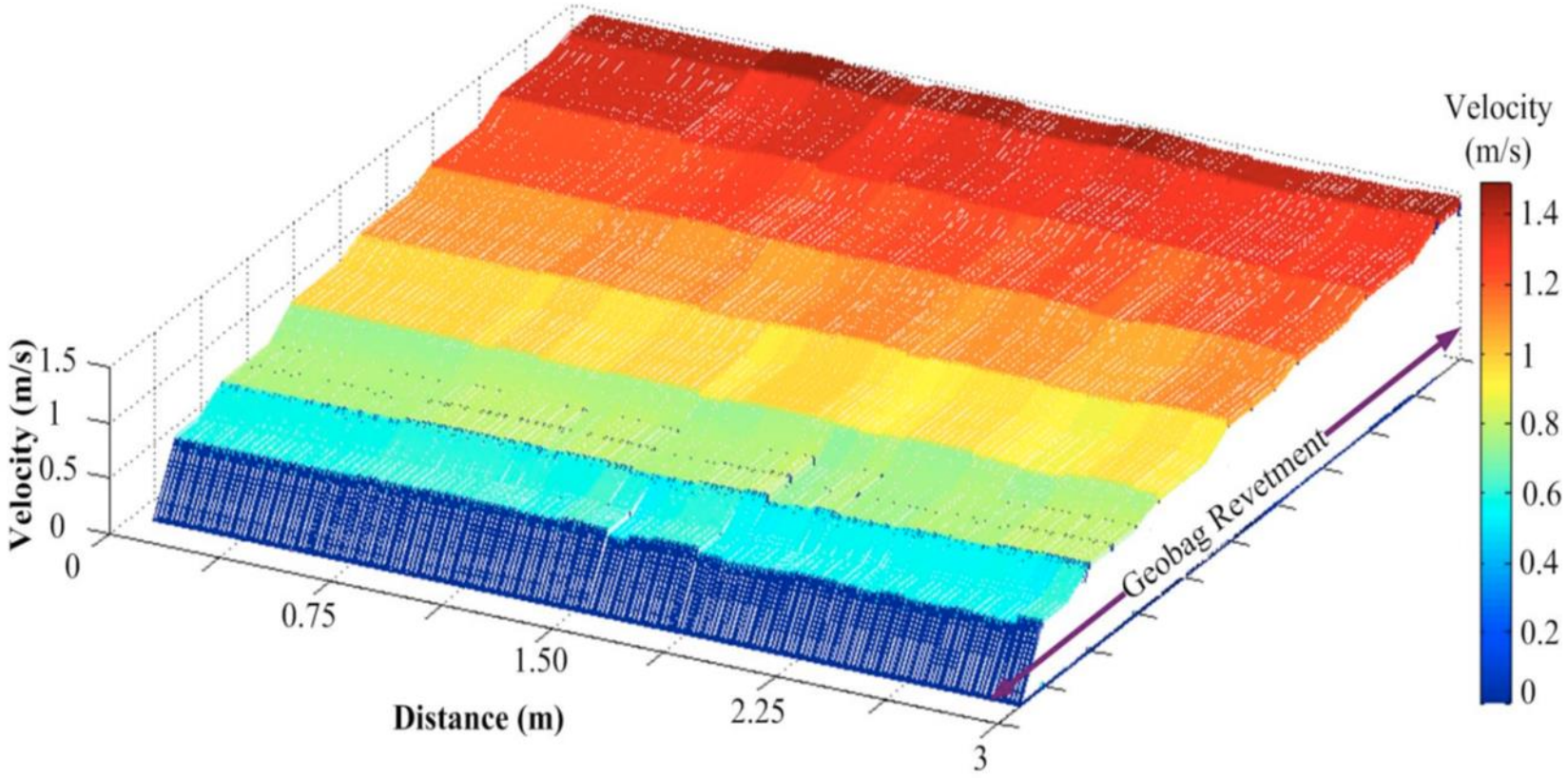

Figure 5.2: CES predicted water velocity data on the geobag surface (Akter et al, 2013)

5.1.3. *Drag and Lift coefficient*

In the LIGGGHTS model the coefficients of drag and lift forces were applied manually by the user to give the best representation of laboratory observations. Since forces were calculated and applied individually to each sphere in the multi-sphere geobag using a constant coefficient drag force formula, a trial and error approach was used to determine a realistic value for the drag coefficient that would yield simulated incipient failure comparable to that observed during experimental testing (coefficient = 0.47 for spherical particles) (Bird *et al.*, 2002; White, 2003). This coefficient was close to the constant drag coefficient of 0.5 which was found by Akter, (2011) to simulate the initial bag motions. Verifying both values, the value of 0.5 was accepted for this study due to the better agreement with the experimental result. For the flow simulations, a constant lift coefficient of 0.8 was employed according to work done by (Akter, Crapper, *et al.*, 2013) which represented the best result compared with laboratory observations. Moreover, the drag and lift coefficients, C_D and C_L were calibrated using data from low water depth conditions and validated using the other water depth condition datasets (Figure 5.3 and Figure 5.4).

5.2. Fixed bed condition

This study attempted to simulate different failure modes through the progression of the failure process and reproduce the complete failure processes of a geobag revetment tested in the laboratory. Afterwards the results of DEM simulation were visually compared with the experimental observation associated with varying water levels different construction methods and different revetment side slopes. For the flow simulations, the drag and lift coefficients, C_D and $C_{L'}$ determined by (Akter, Crapper, *et al.*, 2013) were applied in this study and calibrated using data from low water depth conditions and validated using the other water depth and construction condition datasets (Figure 5.8 to Figure 5.16).

5.2.1. *Drag and Lift force*

Actual model development was undertaken in steps initially focusing on drag force and then adding in a lift force term to help determine the relative importance of each hydrodynamic force in isolation. However, comparison of the laboratory observations and drag-only model results indicated that whilst drag force plays a major role in the

initial stages of the failure process (i.e. when the first bags start moving and pulling out from revetment) it could not alone account for the impact of the void flows resulting from bag displacement. Results compared visually with the corresponding experiments are shown in Figure 5.3 and Figure 5.4. Although applying just drag force as a main hydrodynamic force could predict the position of the initial failure and some failure modes such as sliding and pull-out, it is unable to reproduce bag displacement due to uplifting, and also overestimated the amount of failure in advanced stage. Since exerting lift and buoyancy force does not affect the cost of modelling, for this reason, simulations were carried out incorporating lift force as per Equation 3.13 and buoyancy force to determine their significance. Employing a drag coefficient of 0.5 with a lift coefficient of 0.8 alongside the average flow velocities measured during the experimental work led to simulation results comparable to those observed in the laboratory experiments for complete failure processes of all revetment types (Figure 5.5 to Figure 5.7).

In order to validate DEM model, an open-source tracker software (Tracker) was used to track geobag motion through the process of uplifting in laboratory. Time-average geobag positions in horizontal (X) and vertical (Z) directions were measured using Tracker. For both experiment and DEM model, displacement of upstream outside corner of a geobag was tracked. The simulation results which represent the behavior of a geobag based on DEM model theories were compared to the results obtained from experiment qualitatively (visually comparison in Figure 5.5and Figure 5.6) and quantitively (Figure 5.7).

Figure 5.7 shows the comparison of the vertical and horizontal distances that were travelled by a geobag at different time steps. This figure confirms that the simulation results obtained from LGGGHTS are in good accordance with experimental results.

Results of simulations with drag and lift and buoyancy forces are shown in Figure 5.5 to Figure 5.7. Comparing these results with experimental observations shows that the basic modelling approach replicates the failure very well especially some important failure modes such as uplifting, vertical sliding and dislodgement. Comparisons also show that the model is capable of predicting the position of failure in the revetment in different water depths.

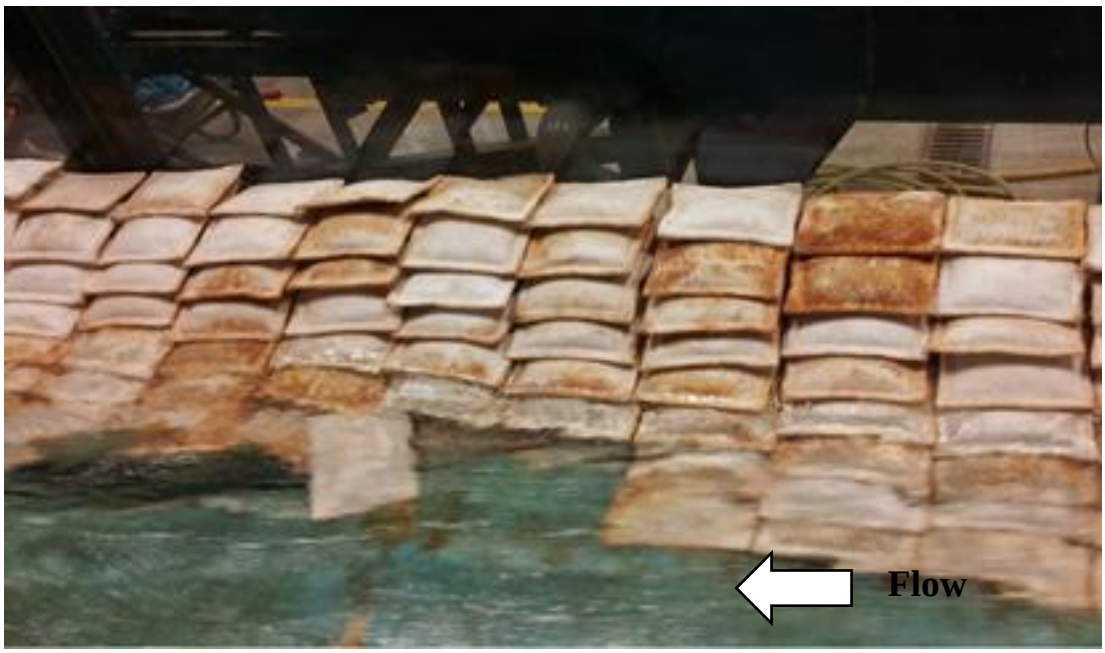

(A1) Laboratory

Partial uplifting observed in the layer nearest to bed while the bag pulled out in the layer nearest to the water surface.

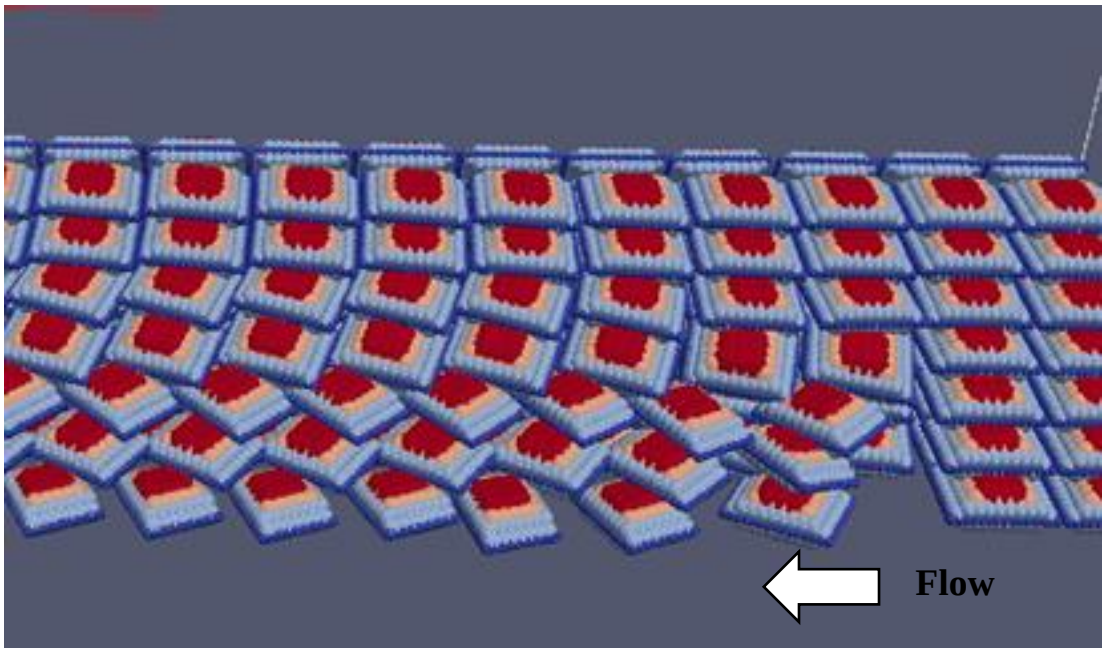

(A2) DEM model

Bag movement observed due to pullout and sliding

Figure 5.3(A1 and A2): Experimental and Numerical results for initial failure modes simulated using a one-way coupling with only drag force, stack bond construction and low water depth.

(A1) Laboratory

Complete failure process

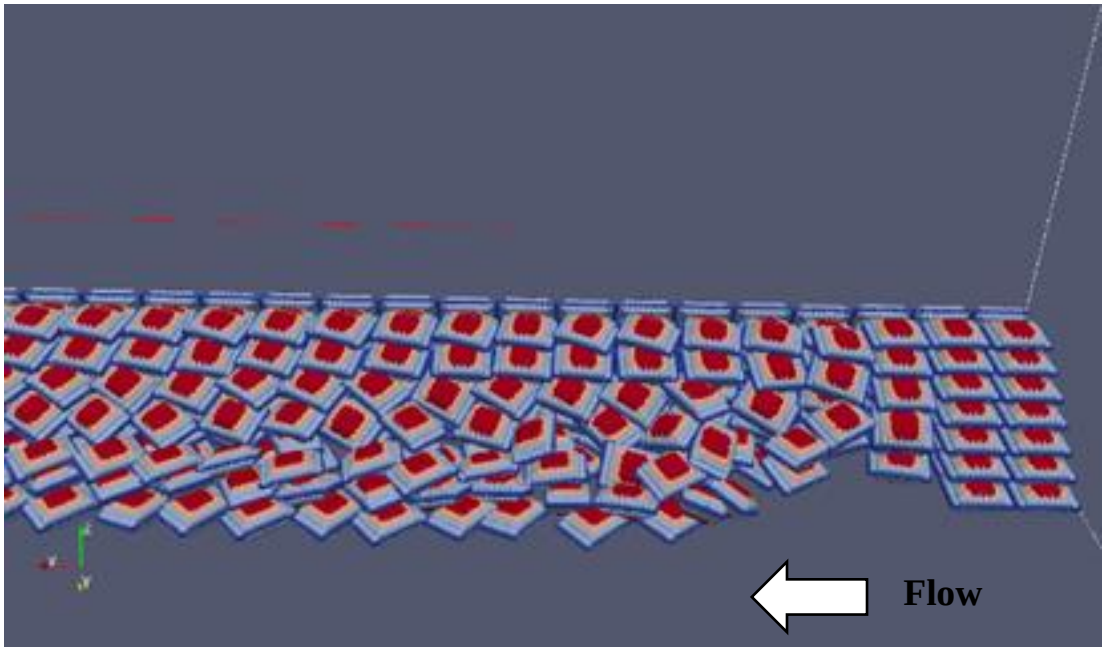

(A2) DEM model

Overestimating the amount of failure in advance stage

Figure 5.4(A1 and A2): Experimental and Numerical results for complete revetment failure simulated using one-way coupling with only drag force, stack bond construction and low water depth.

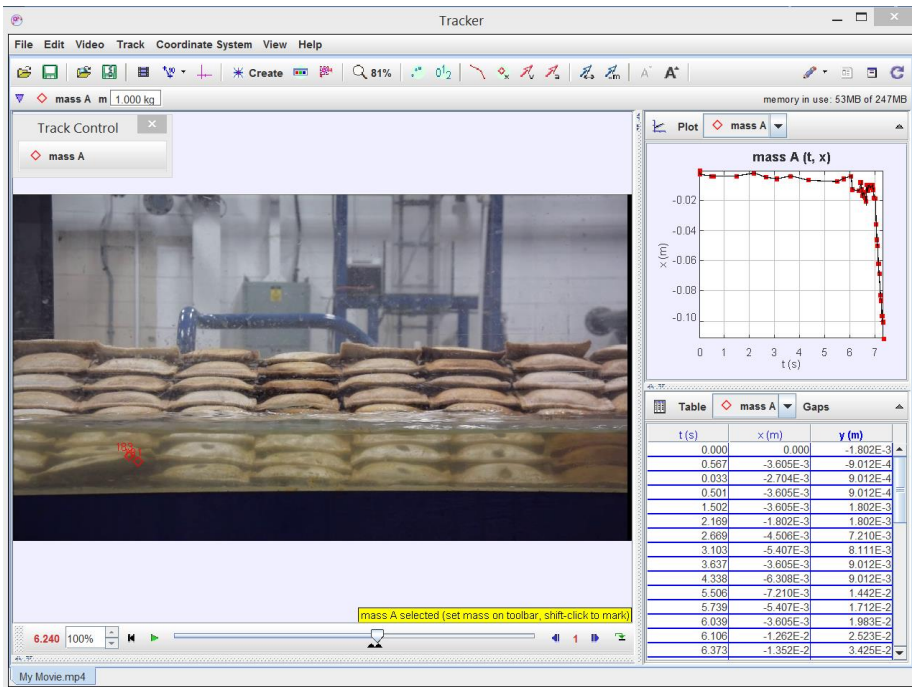

(A1) Track the displacement of a geobag using Tracker (laboratory results)

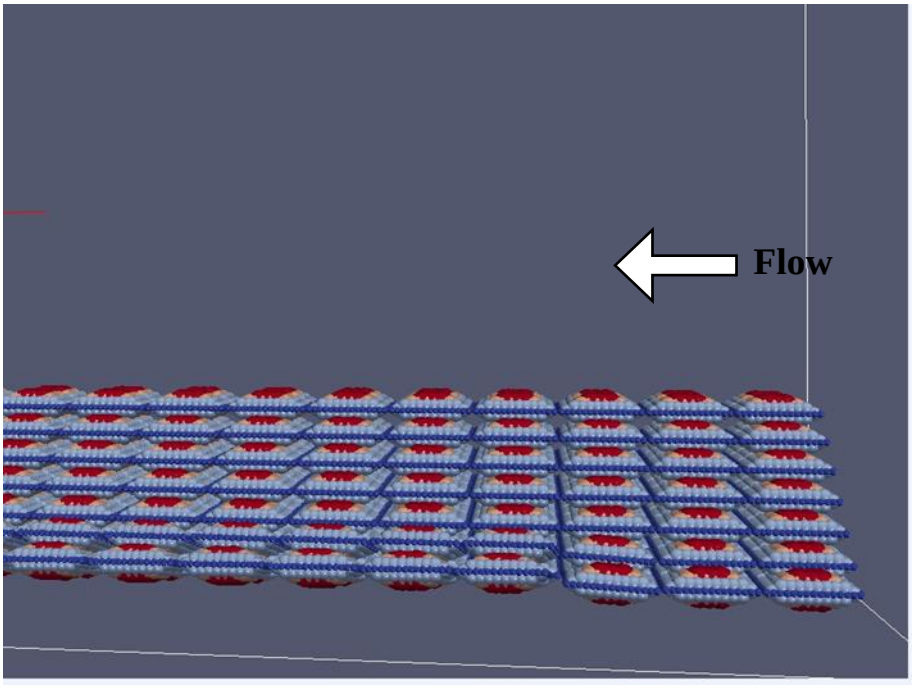

(A2) DEM simulation of initiation of uplifting

Figure 5.5: Initiation of bag failure due to uplifting (A2) laboratory observation and Tracker was used to track geobag displacement, (A2) DEM simulation.

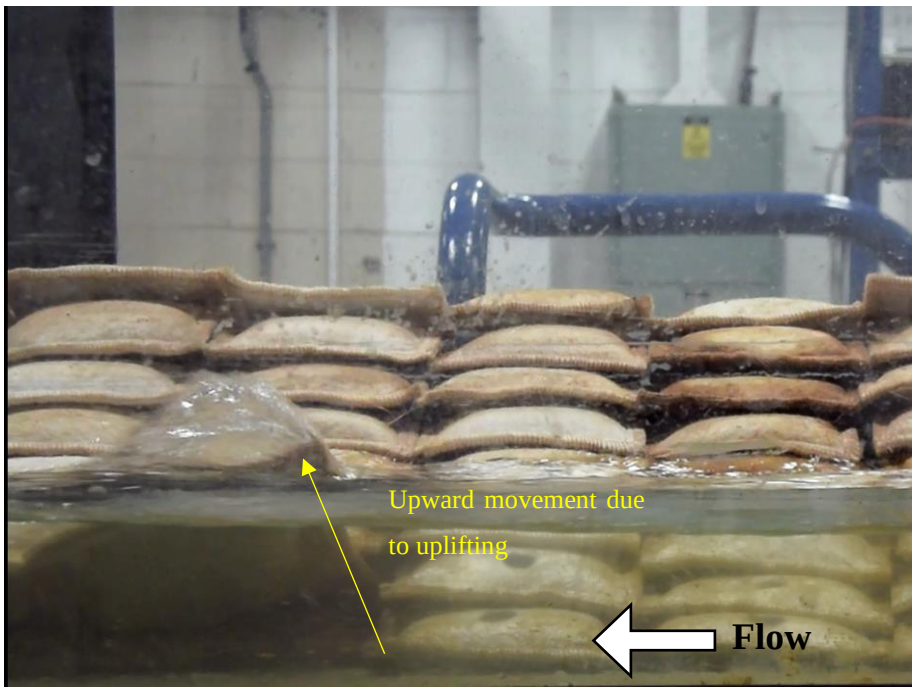

(A1) Laboratory observation

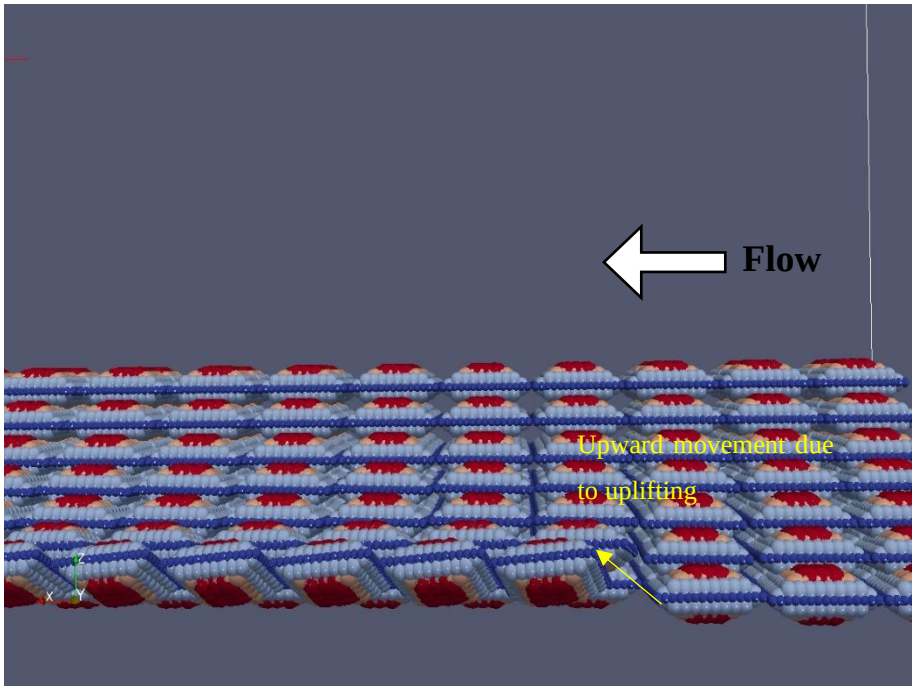

(A2) DEM simulation

Figure 5.6: Validation using visual comparison of (A1)laboratory observation and (A2) DEM simulation.

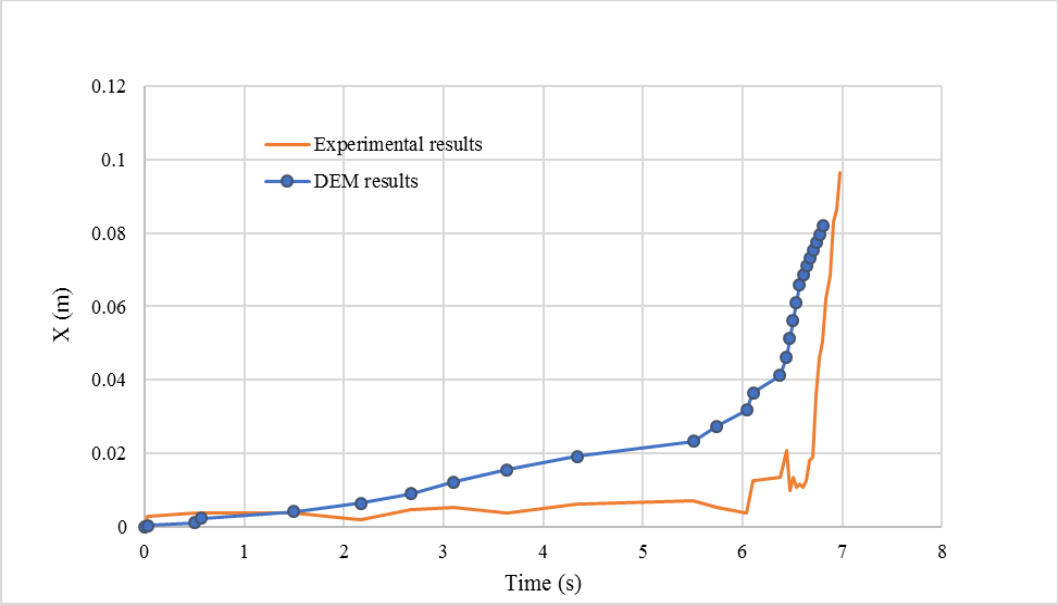

(A1) displacement in streamwise direction (X)

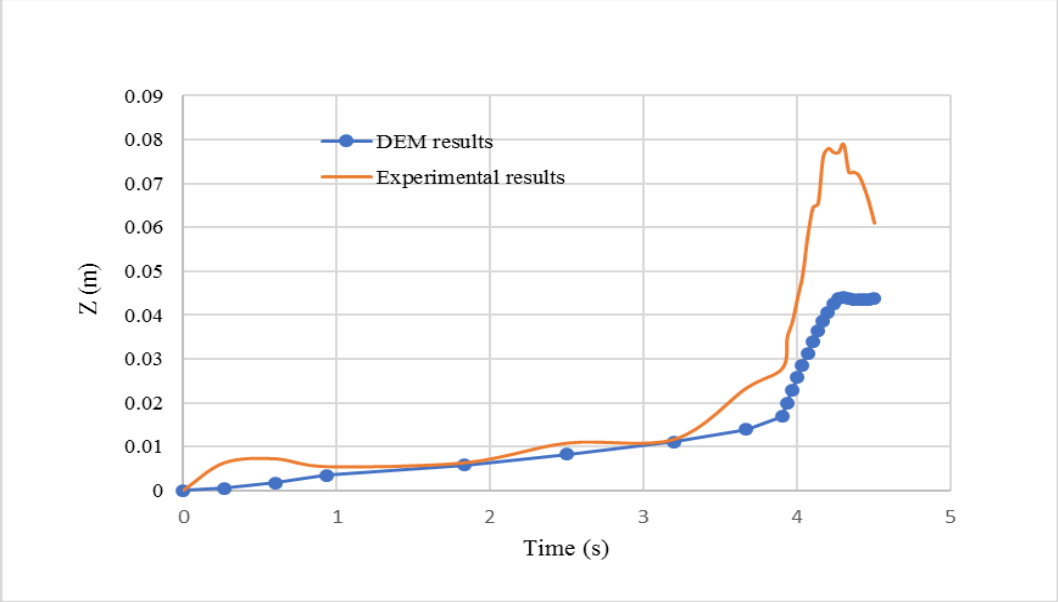

(A2) displace ment in vertical direction (Z)

Figure 5.7: Validation using quantitative approach by compering time-avarage position of geobag in (A1) horizontal and (A2) vertical direction.

5.2.2. *Failure Mechanisms*

Failure progression of the geobag revetment concerning the hydrodynamic forces is represented in Figure 5.8 to Figure 5.16. Theoretically, the DEM model cannot simulate the flow through the gaps between geobags but the presently developed DEM model with drag and lift forces could successfully reproduce partial uplifting which are normally observed in low to moderate flow depth (Figure 5.8A1). The increased flow depth causes partial uplifting in combination with sliding of geobags from the upper layers. In the case of high flow depth, the DEM could also reproduce the laboratory observation very well (Figure 5.9). Regarding observed vertical sliding which mostly occurs in the whole failure progression, the DEM model result showed an excellent agreement with experimental results (Figure 5.9 A1).

DEM results for running bond showed in the low to moderate flow depth the failure initiates due to partial uplifting associated with internal sliding (Figure 5.10). Also, in the high flow depth condition, vertical sliding occurs persistently with the geobags uplifting and pulling out (Figure 5.11).

Similar to the experimental results the outcomes of DEM simulations indicated that the processes of failure and also the observed failure modes are generally independent of construction methods (running bond or stack bond) which were tested in the laboratory.

According to the laboratory observations for all different side slopes, and also DEM results for side slope 1V:2H (Figure 5.8 to Figure 5.11), the construction methods (running bond and stack bond) did not have a noticeable effect on failure process and consequently failure modes, hence, for side slopes 1V: 3H and 1V: 1.25H, the DEM model was run applying only stack bond.

The DEM outcomes support the conclusion drawn from the experimental results for the case of side slope 1V:3H which characterised the failure mode by: (i) Clockwise outward movement and partial uplifting observed in the layer adjacent to the water surface associated with pull out for low water level condition (Figure 5.12) and (ii) the slump of upper layer bags on the bottom layer (Figure 5.13 and Figure 5.13). These results showed the capability of the DEM model to give a distinguishable representation of failure modes observed in the laboratory.

In the numerical model of the revetment similar to laboratory observation, the bag pull-out processes are mostly influenced by higher streamwise velocities. Vertical sliding associated with other modes, characterised the failure process in almost all cases but

mostly accrued in the case steeper slope and in moderate to high water level condition (Figure 5.13).

5.2.3. *Summary*

The main results obtained from DEM models and their implications for the engineering practice can be summarised as follow:

- In the present study, applying a coefficient of friction of 0.55 measured through a dry test by (Akter, Crapper, *et al.*, 2013) gave the best agreement with laboratory observations. This value is close to a coefficient of friction of 0.57 to 0.70 that was published for dry geotextile – sand interaction (Garcin *et al.*, 1995; NAUE GmbH &Co. KG, 2006) and to a coefficient of friction of 0.554 which was determined by Yang *et al.* (2008) for geobag – geobag interaction.
- According to results, the present method employed to approximate average velocities has a promising potential as an estimation approach to estimate the depth – average velocities needed for the numerical model with acceptable accuracy.
- Comparing the results of DEM model applying both drag and lift forces with the experimental observations shows while pull-out (the outward movement of the upstream corner of the bags) is due to drag force on the bags, uplifting and bag displacement due to void flow strongly depends on the lift force.
- A coefficient of drag of 0.5 and the coefficient of lift of 0.8 represented a desirable agreement with laboratory observations in all conditions.
- Although DEM model was unable to replicate the pressure differences between the main flow and void flow it did reproduce the bag movement in the surface level layer and the one adjacent to water surface due to uplifting.
- The validated numerical model can simulate the impact of hydrodynamic forces on a geobag structure with sufficient accuracy particularly regarding failure modes, failure zone and geobag initial velocities.
- The DEM results for different construction methods proved that the construction method does not have a significant impact on the stability of geobag revetments in rivers;
- DEM model showed a good representation of initial bag displacement and failure modes for all tested side slopes and replicated the impact of side slope on the failure process;

- The DEM results for steep slope (1V:1.25H) represented a large number of bags displaced from the revetment due to sliding. During the laboratory test, it was observed that the turbulence reduction and increase in static water pressure in the failure zone led to stopping the process of failure. Although disregard for these facts could allow overestimating the complete failure at the end of the DEM simulation run. Eventually, it satisfied the laboratory observation.

The DEM simulations supported the conclusion drawn from the laboratory observations that the critical slope-geobag on the revetment is the geobag located just below the water surface. Comparing DEM results with experimental observations showed that the modelling approach well represented the complete failure processes for all conditions. The model also has predicted the potential failure modes i.e. uplifting, vertical sliding and dislodgement or pull-out, and failure zone in different conditions tested in the laboratory for a fixed bed.

A1: Partial uplifting and pull-out.

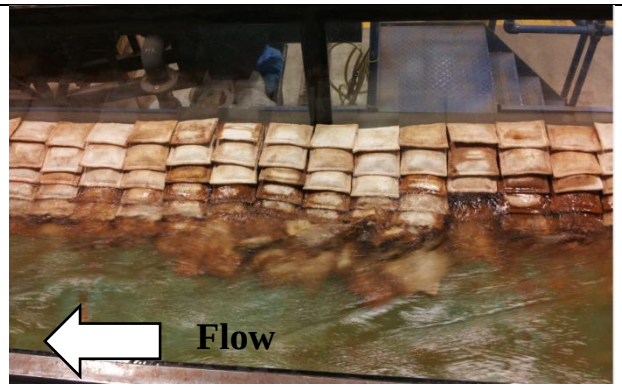

A2: Detail on failure modes.

A3: End of the experiment showing bags displaced in the bottom layers.

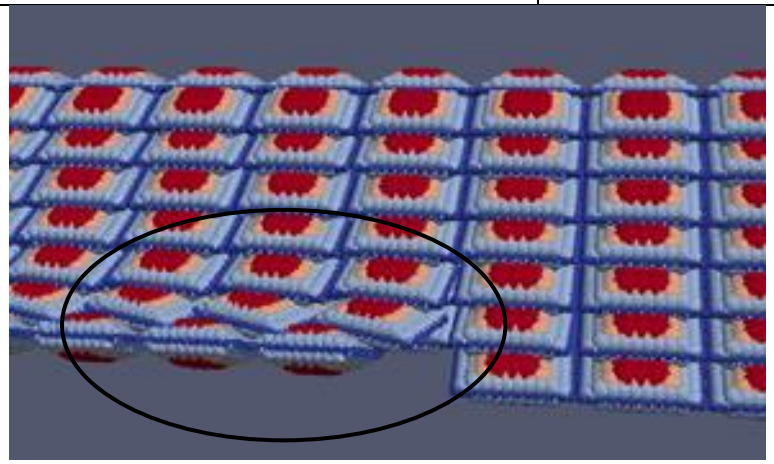

A4: Initial failure mods (partial uplifting and pull-out)

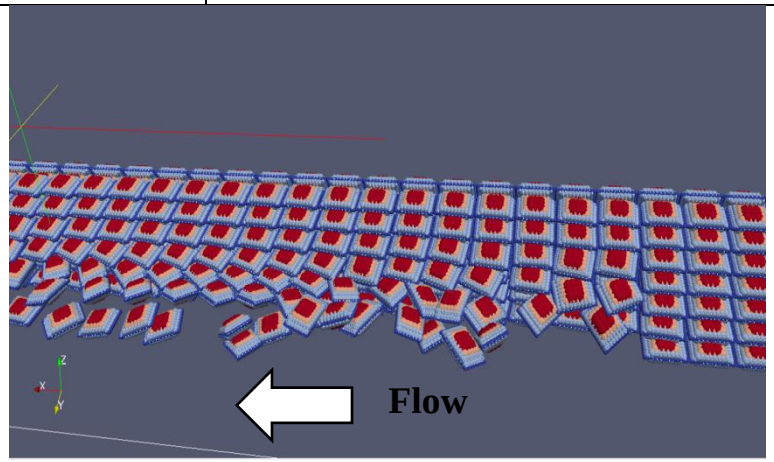

A5: Details of bag displacement. By comparing with **A3**, DEM can be seen to replicate complete failure process.

Figure 5.8 (A1 to A5): Experimental and numerical results for revetment failure processes (Side slope 1V:2H, stack bond construction, low depth)

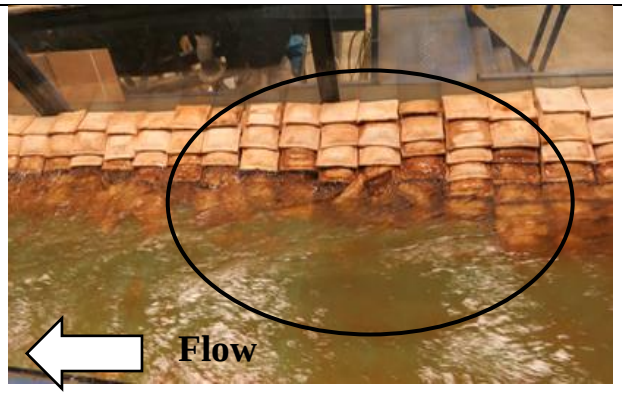

A1: Vertical sliding and pull-out observed adjacent to the water surface.

A2: End of the experiment showing bags displaced from the layers adjacent to the water surface to the bottom layer.

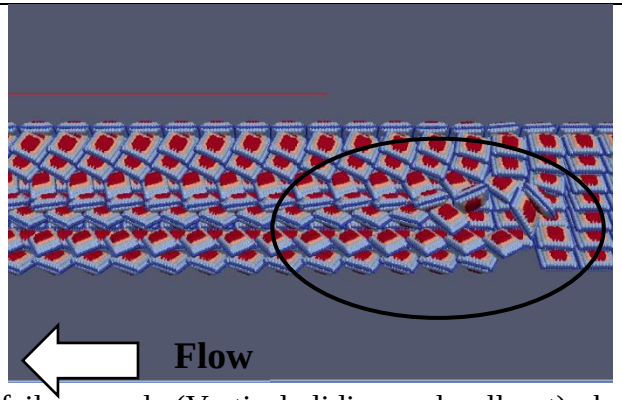

A3: Initial failure mods (Vertical sliding and pull-out) observed from water surface level.

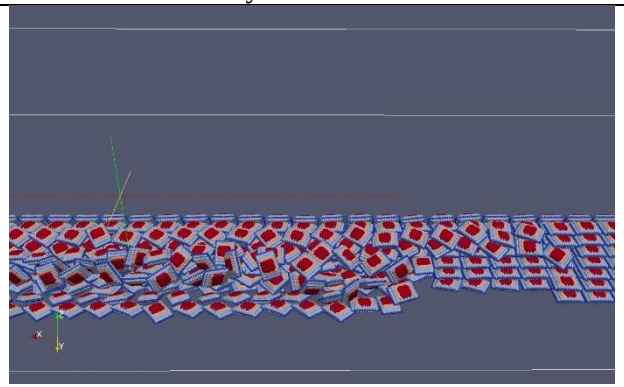

A4: Details of bag displacement. By comparing with **A2**, DEM can be seen to replicate complete failure process.

Figure 5.9 (A1 to A4): Experimental and numerical results for revetment failure processes (Side slope 1V:2H, stack bond construction, high depth

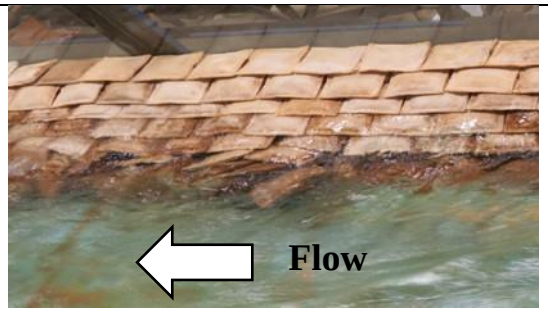

A1: Partial uplifting and pull-out.

A2: Detail on failure modes.

A3: End of the experiment showing bags displaced in the bottom layers.

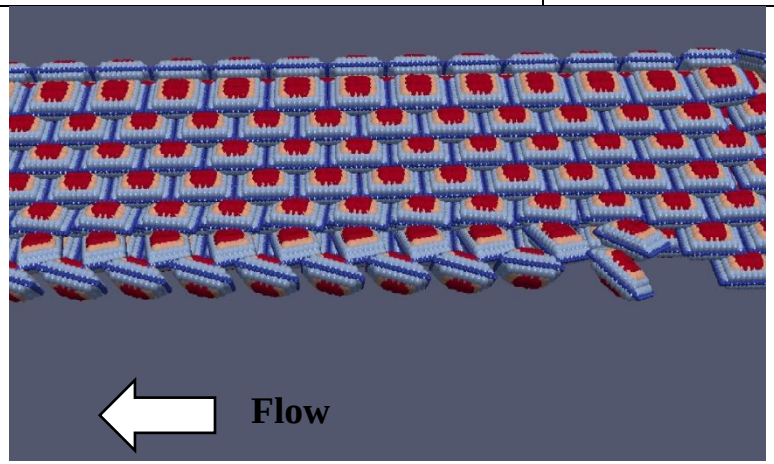

A4: Initial failure mods (partial uplifting and pull-out)

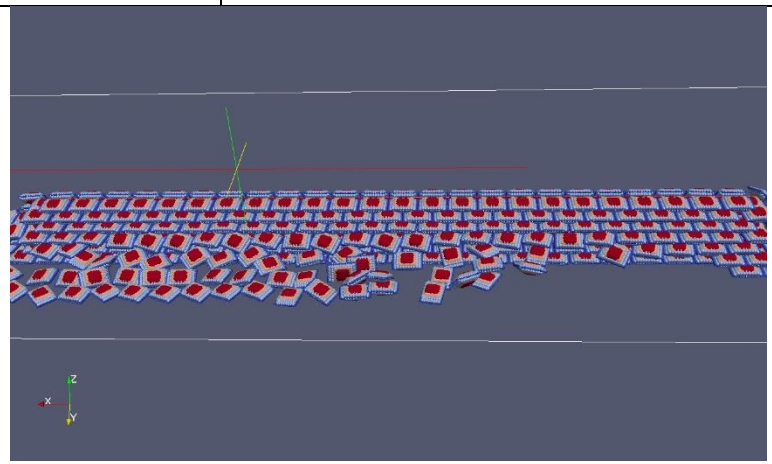

A5: Details of bag displacement. By comparing with **A3**, DEM can be seen to replicate complete failure process.

Figure 5.10(A1 to A5): Experimental and numerical results for revetment failure processes (Side slope 1V:2H, running bond construction, low depth)

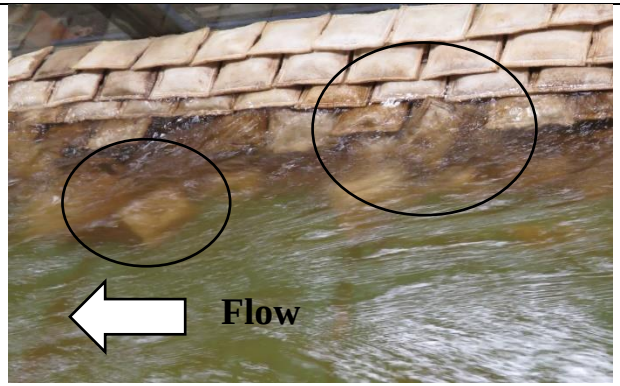

A1: Partial uplifting in the layer adjacent to the water surface, sliding and pull-out f in the bottom layer

A2: End of the experiment showing bags displaced from the layers adjacent to the water surface to the bottom layer.

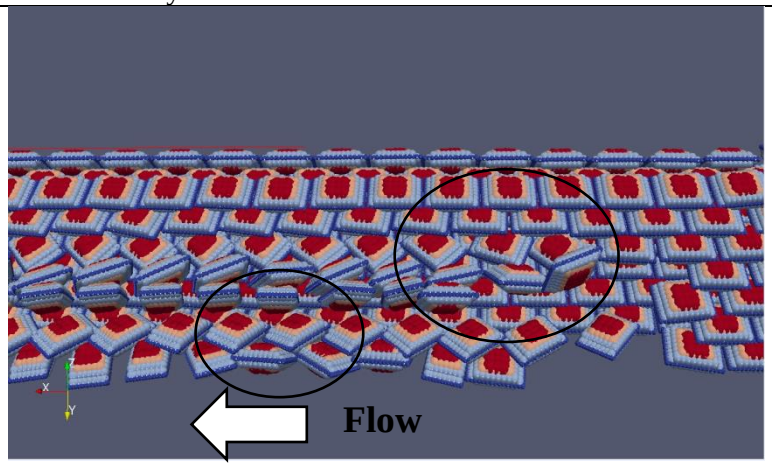

A3: Initial failure mods (partial uplifting, vertical sliding and pull-out) observed from water surface level.

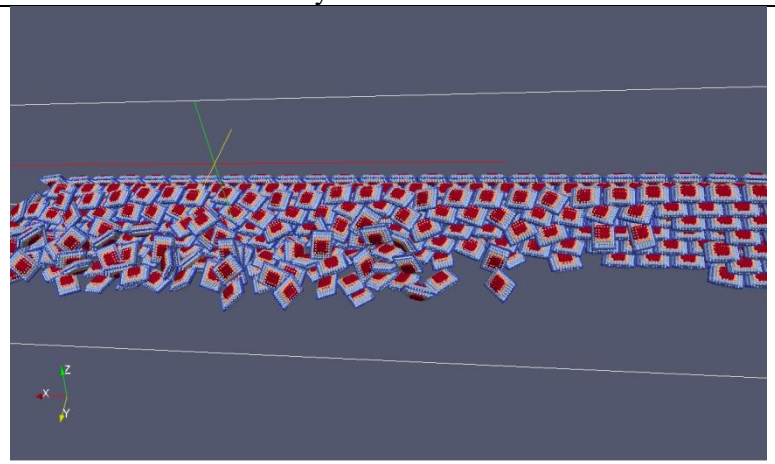

A4: Details of bag displacement. By comparing with **A2**, DEM can be seen to replicate complete failure process.

Figure 5.11 (A1 to A5): Experimental and numerical results for revetment failure processes (Side slope 1V:2H, running bond construction, high depth)

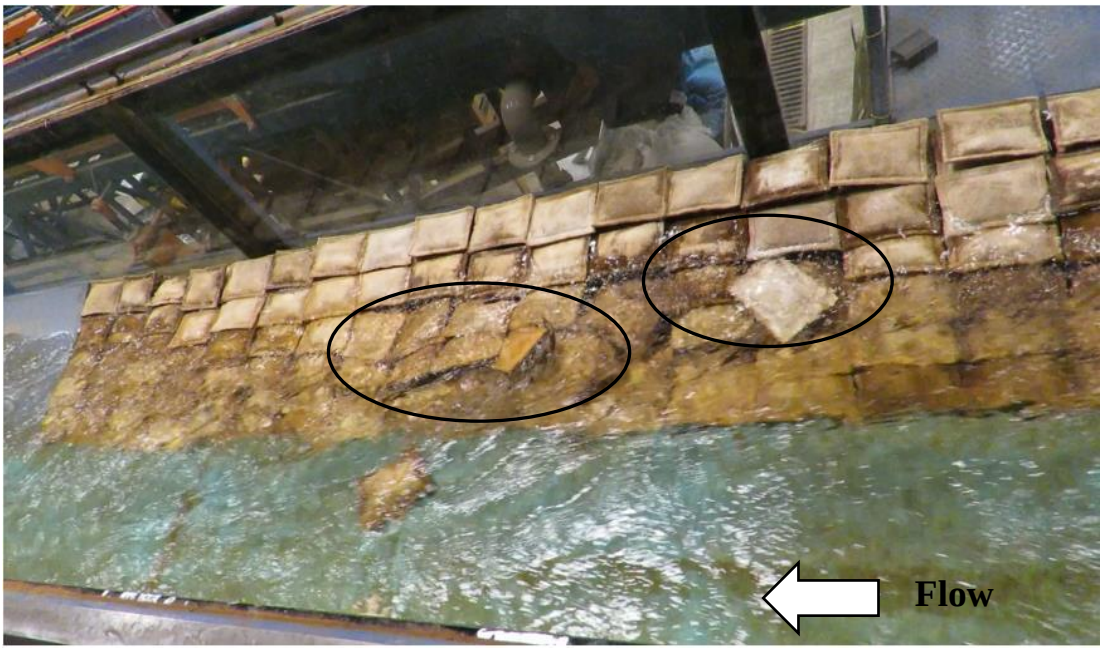

(A1) Laboratory (Initial failure modes)

Clockwise outward movement and partial uplifting observed in the layer adjacent to the water surface.

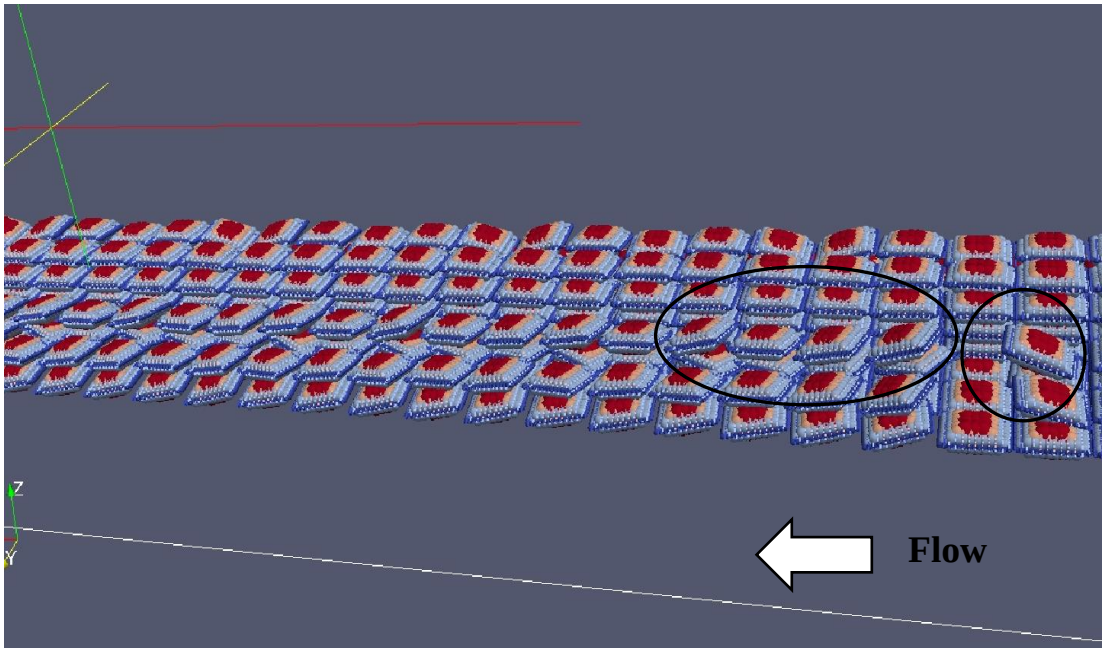

(A2) DEM model (Initial failure modes)

Initial bag movement observed due to partial uplifting and pull out

Figure 5.12(A1 to A2): Experimental and Numerical results for initial failure modes, milder slope (1V:3H), stack bond construction and high-water depth.

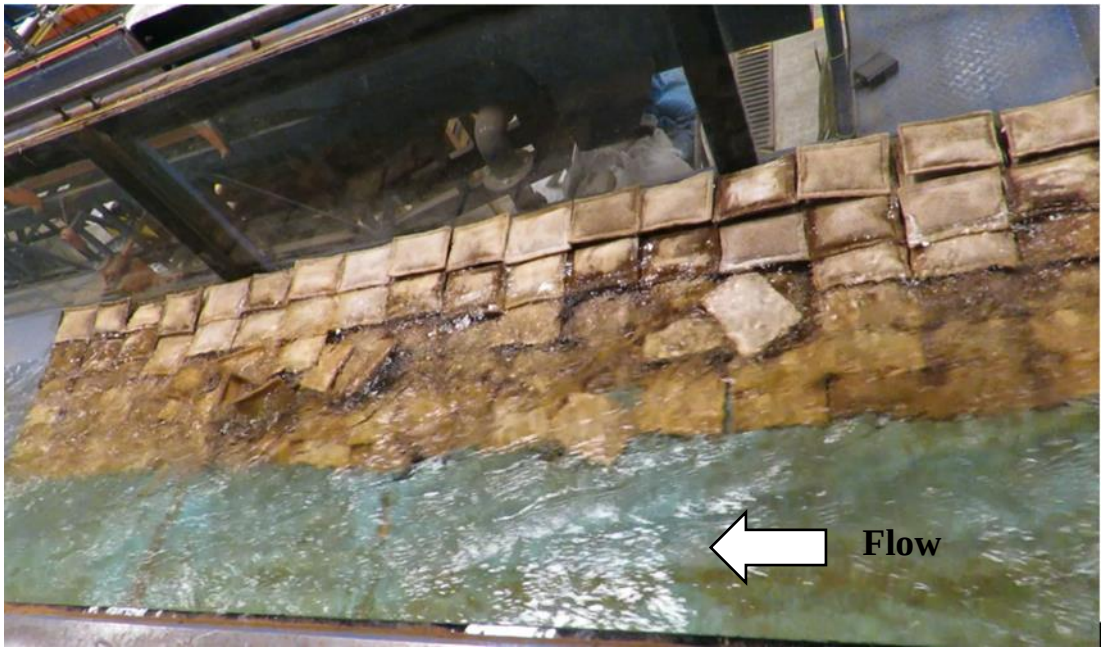

(A1) Laboratory (Failure process)

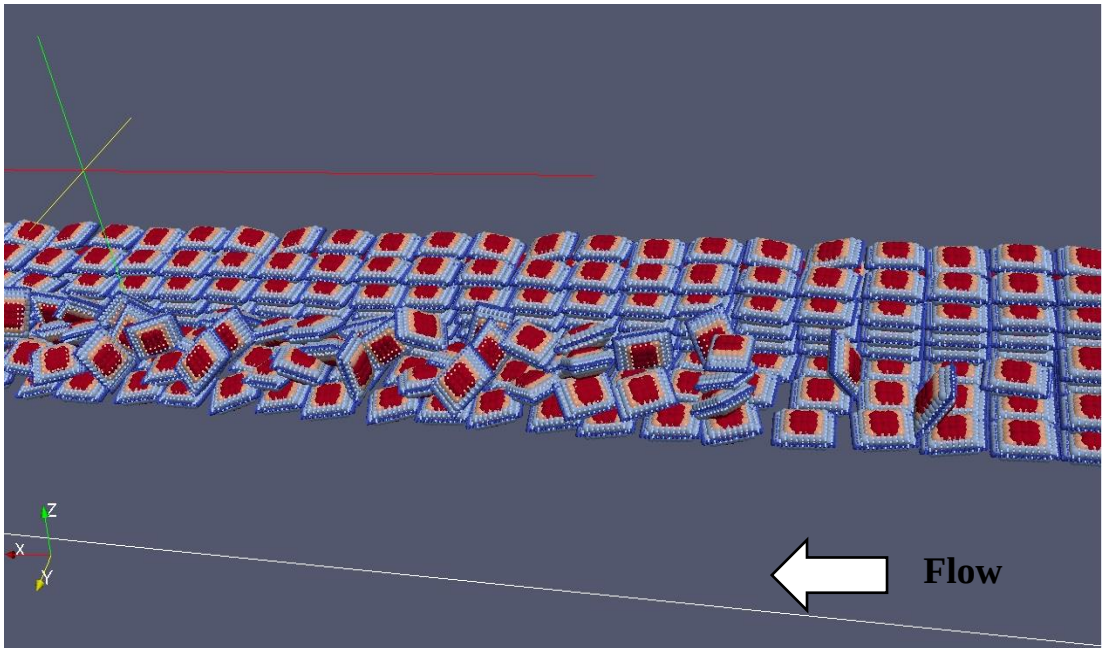

(A2) DEM model (Failure process)

DEM showed similar results to the laboratory observation (the slump of upper layer bags on the bottom layer).

Figure 5.13 (A1 to A2): Numerical results for failure process, milder slope (1V:3H), stack bond construction and high-water depth.

(A1) Laboratory (End of the experiment)

End of the experiment showing bags displaced from the layers adjacent to the water surface.

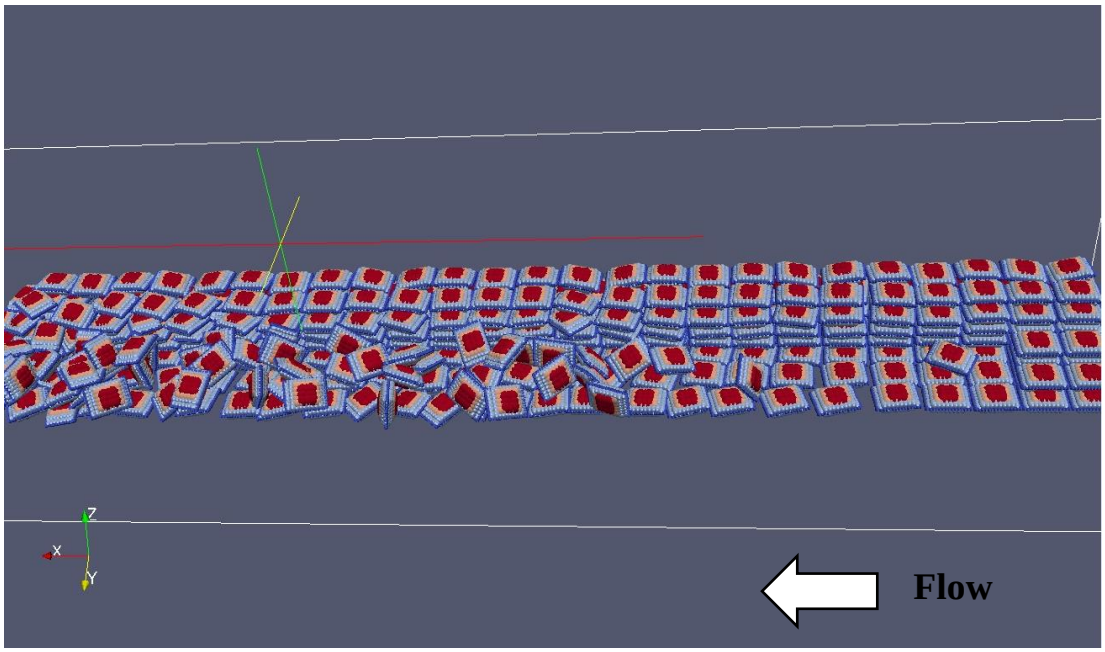

(A2) DEM model (End of the experiment)

Details of bag displacement. By comparing with A1, DEM can be seen to replicate complete failure process.

Figure 5.14(A1 to A2): Experimental and Numerical results for a complete failure, milder slope (1V:3H), stack bond construction and high-water depth.

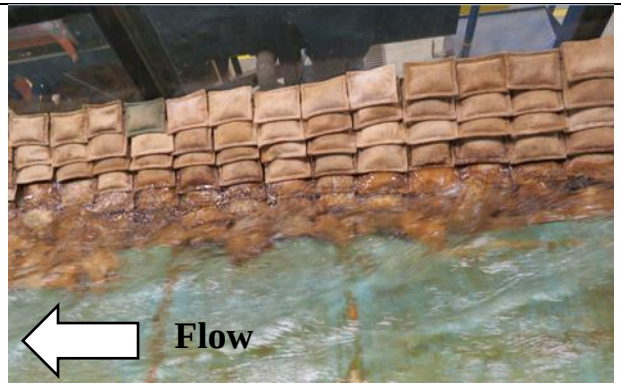

A1: Bag displacement observed due to void flow, pull-out and sliding.

A2: End of the experiment showing bags displaced from the bottom layers.

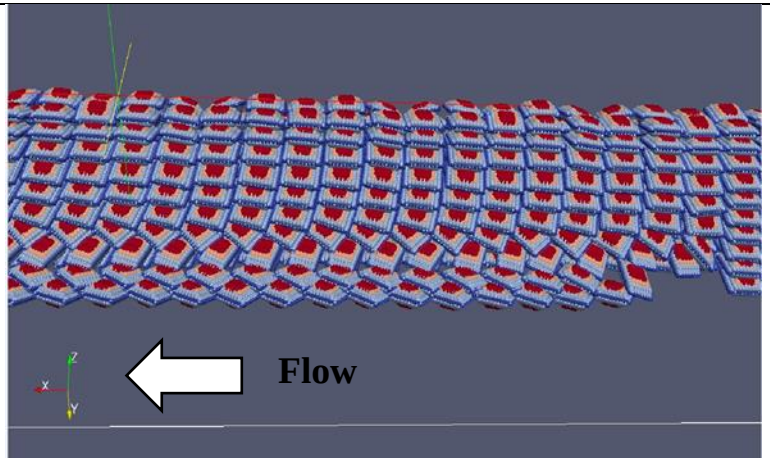

A3: Initial failure mods (Vertical sliding and pull-out).

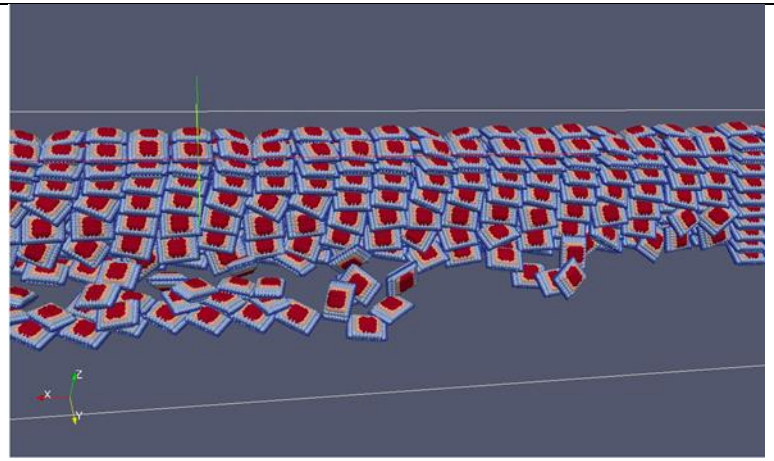

A4: Details of bag displacement. By comparing with **A2**, DEM clearly represented that bags completely displaced from the bottom-most layer at the end of the simulation

Figure 5.15(A1 to A4): Experimental and Numerical results for failure process, steeper slope (1V:1.25H), stack bond construction and low-water depth

A1: Turbulent bursting–induced flow through revetment voids and sliding.

A2: The magnitude of the revetment failure at the beginning of the test due to vertical sliding.

A3: Failure zone after high-water depth condition test.

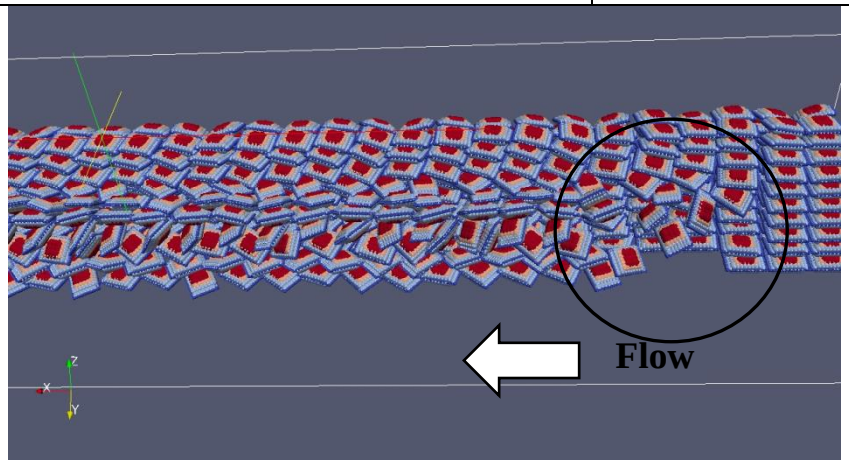

A4: Sliding.

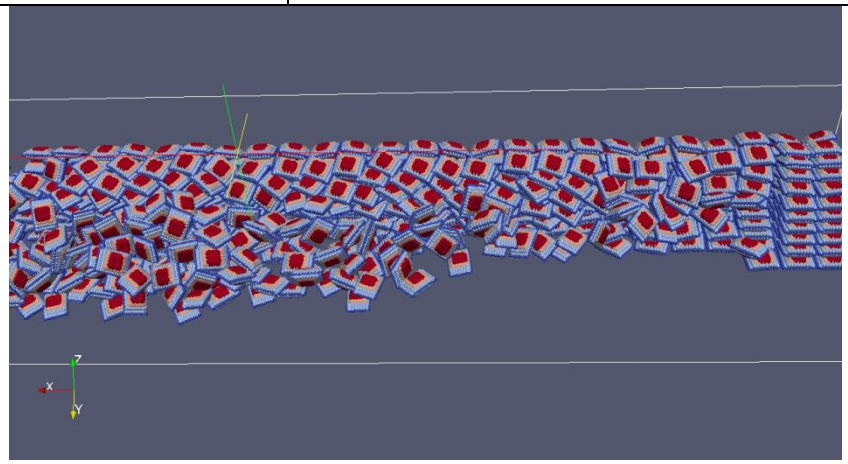

A5: Details of bag displacement. DEM represented the considerable number of bags displaced from the revetment and not only satisfies the **A3** observation but also replicate the significance of sliding due to the steep slope.

Figure 5.16(A1 to A5): Experimental and Numerical results for failure process, steeper slope (1V:1.25H), stack bond construction and high-water depth.

5.3. Mobile bed condition

5.3.1. *Failure mechanisms*

Although the results of the DEM model for mobile bed show similar failure modes to those observed in a fixed bed these results replicate the role of toe scour on the failure processes of the geobag revetment. In the case of mobile bed, failure processes are significantly affected by the sliding of support bags closest to the bed because of scour holes (Figure 5.17 to Figure 5.18). In the laboratory, conducting a series of experimental tests, (Akter, 2011)observed that the bed changes underneath the revetment resulted in a vertical displacement of geobags in the streamwise direction (Figure 5.17 to Figure 5.18). In this study, applying the LIGGGHTS model could reproduce these vertical displacements in addition to uplift, pull-out and internal sliding, which follow the same failure mechanisms as those occurred in fixed bed condition. In the Figure 5.17(A1-A3) to Figure 5.18(A1-A3),the outcomes of the LIGGGHTS model were compared with EDEM results and laboratory observations presented by Akter, Crapper *et al*. (2013).

According to Akter (2011)to simulate the sandbed condition, 265 square of 0.10 m length were used to represent 3 m long, 0.75 m wide and 0.10 m deep sandbed downward or upward movement of the squares was based on the laboratory measured data (Figure 5.17(A3) to Figure 5.20(A3)). Therefore, an accurate method was required to measure the details of bed change along the test section. Although EDEM® could predict the location of failure initiation, LIGGGTS model with a more straightforward setup (see Chapter 3) showed the capability of representing the location of failure initiation as well as some important failure modes e.g. partial uplifting and sliding.

Generally, compared with EDEM® results, LIGGGHTS gave a better representation of initial failure modes in the condition of the mobile bed and the selected water level conditions.

5.3.2. *Summary of results*

The main results can be summarised:

- A coefficient of drag of 0.5 and the coefficient of lift of 0.8 represented a desirable agreement with laboratory observations in all conditions.
- In condition C (65–84% of the geobag revetment height), LIGGGHTS not only predicted the location of failure initiation but it also reproduced some main failure modes such as uplifting, sliding, and pull-out of the geobags. Comparing with EDEM® outcomes from previous work the implementation of the LIGGGHTS model, presented in this study, showed better agreement with experimental results.
- In condition D (85–100% of the geobag revetment height) reported laboratory observation showed that overtopping, sliding and pull-out caused bag displacement from the test section. LIGGGHTS model could replicate these observed incipient failure modes and for this condition, the LIGGGHTS model demonstrated better performance than EDEM®.
- For the case of the mobile sand bed, geobag displacement in the most bottom layer was affected by toe scour underneath the revetment. Downward movement of the sand bed associated with hydrodynamic forces resulted in bag displacement due to sliding. The present LIGGGHTS model showed the capability to reproduce these important laboratory observations.

According to the results obtained from the numerical model for mobile bed condition, the DEM model using LIGGGTHS could reproduce the initial bag displacement and failure modes for conditions C and D which were observed in the laboratory by Akter, Crapper, *et al.* (2013).

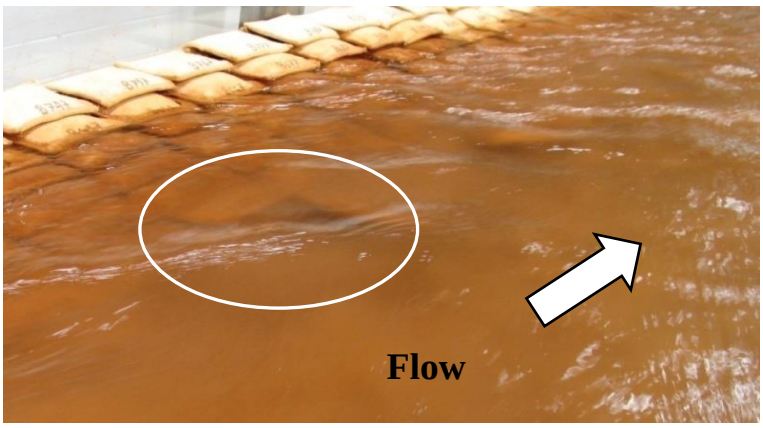

(A1) Bag displacement observed due to void flow, uplifting and sliding (Akter, Pender, *et al.*, 2013)

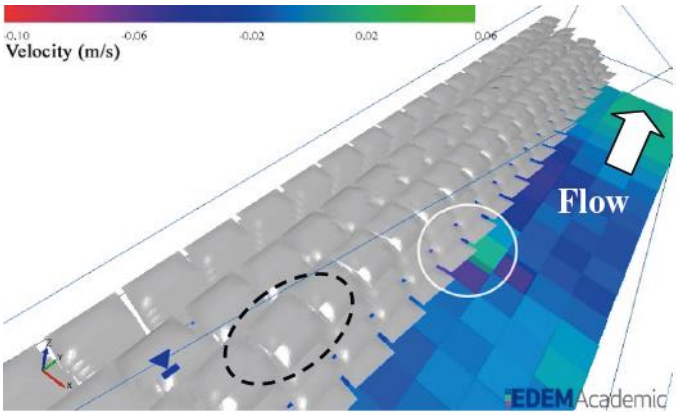

(A2) EDEM® predicted the location of failure initiation (Akter, Crapper, *et al.*, 2013)

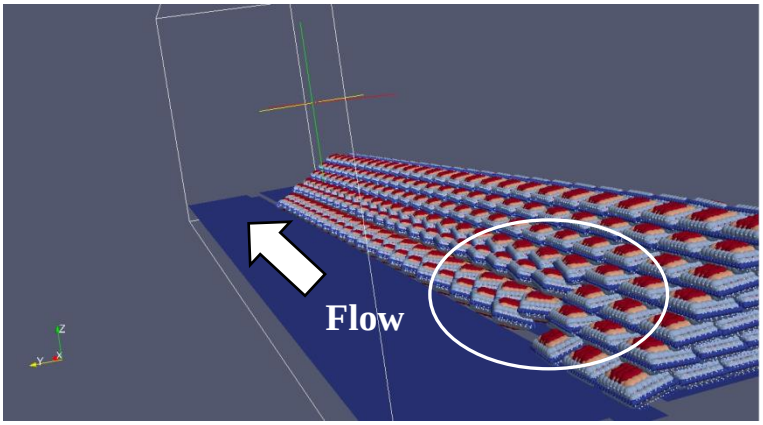

(A3) LIGGGTS outcome shows that failure initiation in the bottom most layer and in the next to the surface water level layer with partial uplifting and sliding.

Figure 5.17**(A1 to A3):** Comparison of laboratory observations, EDEM® and LIGGGHTS outcomes for condition C (incipient bag motion)

(A1) End of the experiment showing failure mostly involved the bottom-most layer.

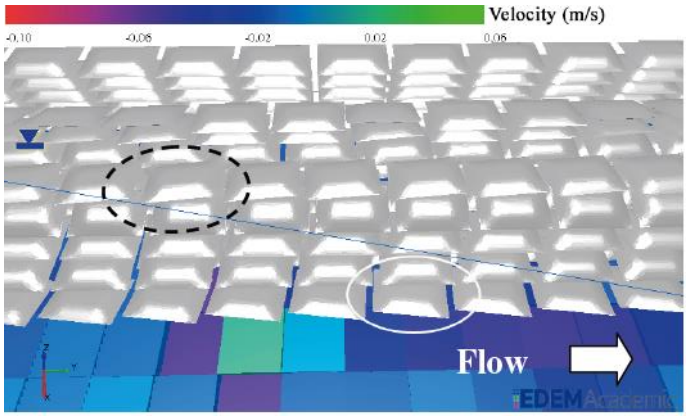

(A2) EDEM® predicted the location of failure initiation (Akter, 2011)

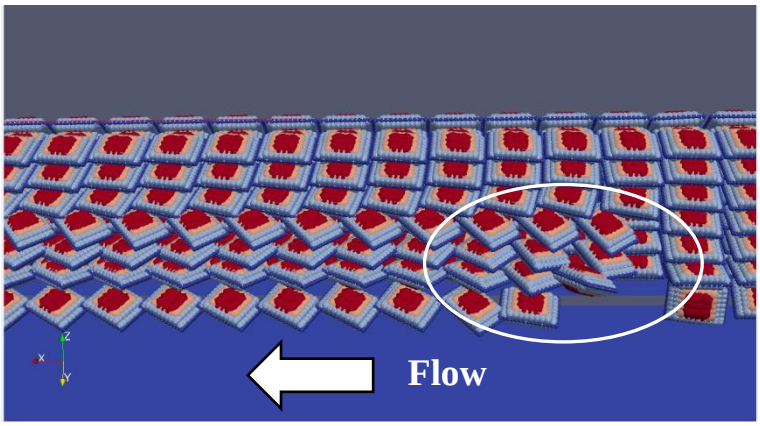

(A3) LIGGGTS outcome replicated the laboratory observations.

Figure 5.18**(A1 to A3)** Comparison of laboratory observations, EDEM® and LIGGGHTS outcomes for condition C (End of Experiment).

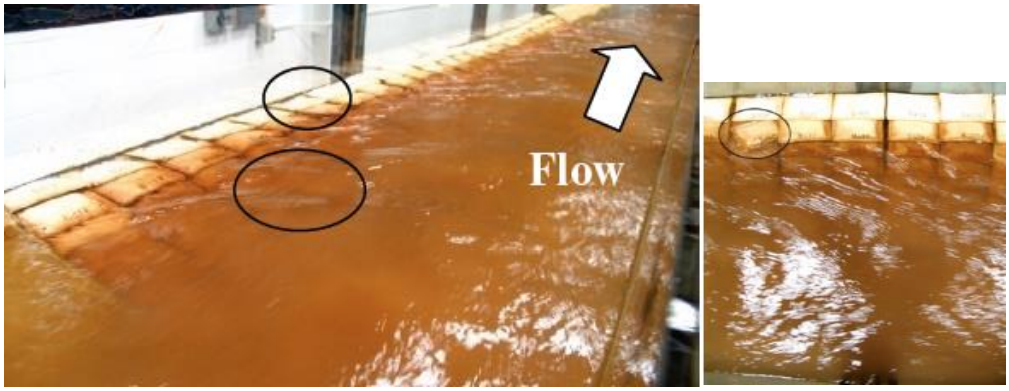

(A1) Uplifting in the bottom layers whilst sliding due to overtopping is observed in the layer adjacent to the water surface (Akter, 2011).

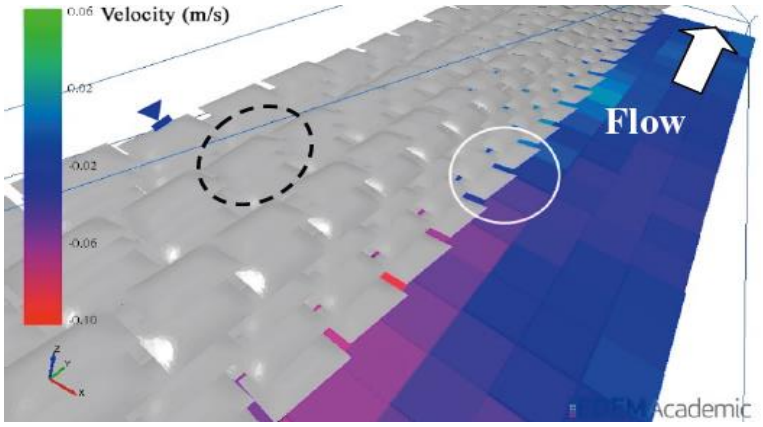

(A2) EDEM® predicted the location of failure initiation (Akter, 2011)

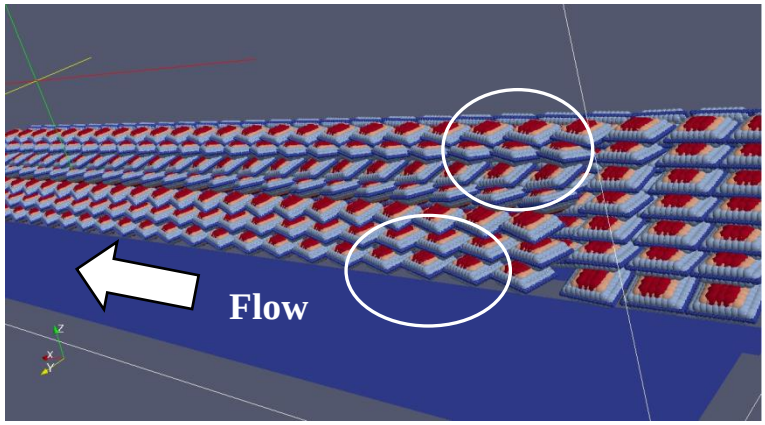

(A3) LIGGGTS shows that failure initiation in bottom most layer and in the next to the surface water level layer with partial uplifting and sliding.

Figure 5.19**(A1 to A3):** Comparison of laboratory observations, EDEM® and LIGGGHTS outcomes for condition D (incipient bag motion).

(A1) End of the experiment, initial bag displacement was observed in the bottom-most layer and the next to the surface water level layer (Akter, 2011)

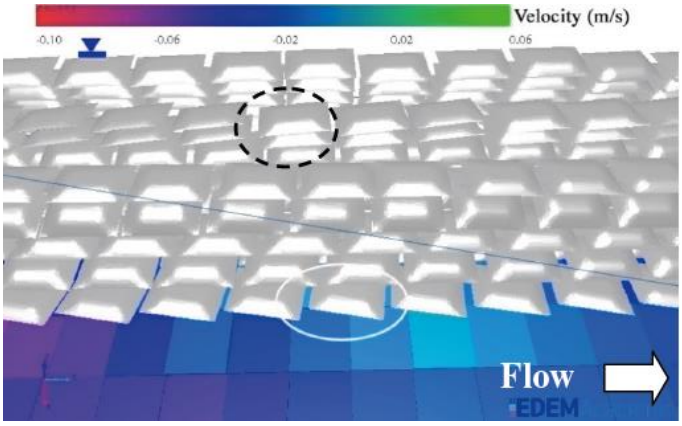

(A2) EDEM® predicted the location of failure initiation (Akter, 2011)

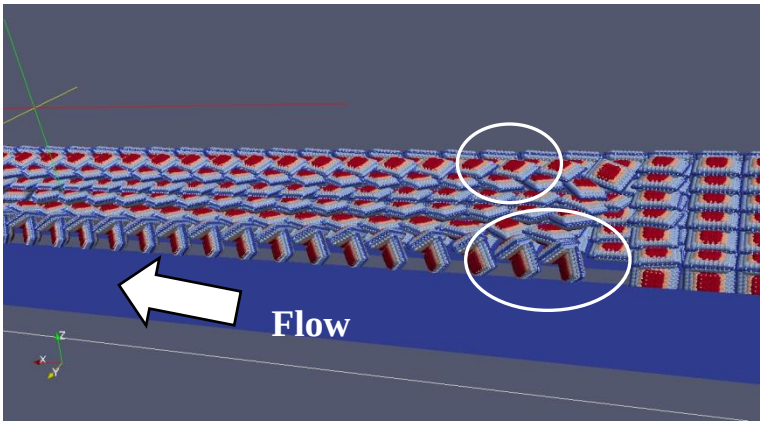

(A3) LIGGGTS showed a good representation of laboratory observations.

Figure 5.20**(A1 to A3):** Comparison of laboratory observations, EDEM® and LIGGGHTS outcomes for condition D (End of Experiment).

5.4. Analysis of numerical model results

Numerical activities which are definitely an advance on the previous work conducted by Akter, Crapper, *et al.*, (2013) and extended the line of study to the representation of complete failure processes of the geobag revetment. The computational demands associated with DEM-only simulations, and the open source nature of the LIGGGHTS code made it an ideal candidate for model development with the non-spherical geobags being modelled using the multi-sphere method.

Comparison the quasi-physical model observations with drag-only DEM model results indicated that while drag force plays a significant role in the initial stages of the failure process it could not alone account for the impact of the void flows resulting from bag displacement. The addition of a lift force term remedied this deficiency. Employing a drag coefficient of 0.5 with a lift coefficient of 0.8 and buoyancy force alongside the average flow velocities measured during the experimental work led to simulation results comparable to those observed in the laboratory experiments for complete failure processes of all revetment types.

In the case of geobag revetments mounted on a fixed bed the DEM model could replicate the laboratory observed incipient failure modes. Generally, comparing DEM results with experimental observations showed that LIGGGHTS well-represented the complete failure processes for all conditions. Furthermore, the LIGGGHTS model can predict the potential failure modes i.e. uplifting, vertical sliding and dislodgement or pull-out, and the most failure-prone location under different water levels conditions and revetment configurations. Thus, for robust geobag revetments in rivers, this result can provide a basis for realistic design guidelines.

Applying geobag revetments on a mobile sediment bed was experimentally tested by Akter (2011). The same DEM model setup used in this study showed a good representation of their laboratory observation. Incipient bag movement due to uplifting and pull-out in the layer close to surface water level and downward geobag displacement due to toe scour in the most bottom layer was reproduced distinguishably using LIGGGHTS model.

Based on the results, the present DEM-only model satisfactorily simulated the complete failure and could be a sufficiently accurate method to predict the performance of geobag revetment. Therefore, there is no evidence to justify requiring a more expensive approach such as a fully coupled solution, which is long and expensive on the computer.

Furthermore, a one-way coupled DEM-CFD might have a potential as an engineering tool to investigate the stability of can be applied in evaluating the performance of other discrete riverbank protective structures, for example, concrete blocks or riprap structures. Any of these structures can be investigated to identify critical areas for the stability, the failure mechanisms or the response of the structure to active forces. However, the DEM models should be calibrated and validated to adapt them to other discrete structures.

Results of this numerical study confirm that the DEM model has the potential for future use in developing design guidelines aimed at the developing world

5.5. Chapter summary

A 3D DEM model of the laboratory experiment was constructed using the LIGGGHTS open source, C++ and MPI parallel DEM code. A one-way coupled CFD-DEM approach with basic drag and lift formulations was applied to evaluate numerically the performance of a geobag revetment on a fixed bed. The outcomes of the numerical model were validated against quasi-physical model observations. It was found that despite its simplicity this validated one-way CFD-DEM model could reproduce the complete failure processes of revetments very well and showed a good representation of revetment failure modes of all experimentally tested conditions.

In the second part of this chapter, the applicability of the LIGGGHTS model to simulate the performance of geobag revetment mounted on a mobile sediment bed was investigated. In this case, The DEM model results were validated against laboratory observations conducted by Akter (2011). The DEM model using LIGGGHTS could represent well the revetment failure modes under the influence of toe scouring associated with different water level conditions.

Chapter 6. **DISSCUSSION**

The importance of using sand-filled geotextile bags (geobags) as a substitution for traditional materials/solutions particularly rock for erosion-protection in rivers is clear (Chapters 1 and 2).. Work to move the state of the art in employing sand filled bags for coastal bank protection to riverbank protection has been reported in the literature, and numerical tools has been shown to be a valuable tool in this regard, together with more conventional experimental work (Chapter 2). In terms of the hydraulic stability of geobag structures for riverbank protection, there are a few available experimental and computational investigations, but much has still to be required to achieve the desired performance of geobag revetments in the fluvial environment. This lack of knowledge is mainly because of difficulty of numerical modelling of the complete failure processes of geobag revetments in river required to develop much-needed revetment design guidelines.

The aim of the present research was to provide practical recommendations on the performance of geobag revetments in rivers. This has been undertaken through a combined experimental direction and numerical approach. The small-scaled model of geobag revetments were investigated using a combination of distorted-scale laboratory experimental work and steady-flow numerical modelling. The Quasi-physical model developed an improved understanding of geobag stability under horizontal (hydrodynamic) loads and also provided the necessary data (Chapter 4) to validate a developed numerical model which is capable of simulating complete failure of geobag revetment (Chapter 5).

The elements of novelty and the key findings of these approaches are discussed in this chapter.

6.1. Elements of Novelty

Throughout the work presented here, several elements of novelty have been introduced. The most relevant is the development of a DEM model for a geobag revetment in river which is capable of simulating the entire processes of failure. However, additional novelty is found in the analysis of the small-scale experimental data.

6.2. Laboratory-Scale model

In the current study described here, an analysis of a distorted-scale laboratory investigation was performed. Other authors, such as Zhu *et al.* (2004), NHC (2006) and Akter *et al.* (2013) performed similar investigations, but the work described here provides the first attempt to analyses the complete failure processes of geobag revetment and determine the position of failure in terms higher shear stress , unlike previous works, e.g. Zhu *et al.* (2004), NHC (2006) and Akter *et al.* (2013), that limited their analyses to study incipient motion of geobag during construction/launching, or incipient motion after revetment construction.

6.2.1. *Failure mechanisms*

The novel failure mechanisms analysis described in Section 4.1.1 provided for the first-time details of different failure modes occurred in a geobag revetment in river, based on hydrodynamic forces analysis. Such analysis helps to predict the behaviour of geobag revetment while it is exposed to different flow conditions and/or construction specifications. In conclusion, both in laboratory and in numerical model, the complete failure mechanisms are characterised by a combination of turbulent bursting, partial or full uplifting, pull-out and sliding which are basically initiated by turbulent bursting, partial or full uplifting. These findings are in line with the conclusions of NHC (2006) and Akter *et al.* (2013) that showed the experience of similar incipient failure mechanisms in the field and laboratory.

6.2.2. *Geobag revetment side slope*

In JMREM project three main lunching practices were distinguished: (i) mass dumping along the eroding riverbank, when needed as emergency protection tools; (ii) main protection dropped from dumping pontoons located on the river, and (iii) adaptive protection extending the work by dumping to greater depth (Oberhagemann and Hossain, 2011). The assumption behind these practices was that geobags are launched on geotechnically stable slopes. According to (Fedinger, 2004, 2006), geotechnically stable slopes are in the order of 1V:2H. Previous laboratory work undertaken by NHC (2006) and Akter *et al.* (2013) used the side slope of 1V:2H as an only revetment side slope for their laboratory setup.

Here an important factor was unknown i.e. the existing (pre-revetment) side slope of any riverbank will be contributing to the formation of the final revetment side slope.

However, it seems reasonable to assume that the final revetment slope may influence the overall stability of a geobag revetment.

A novel approach followed in this study is to evaluate the performance of revetment, considering three different side slopes of 1V:1.25H, 1V:2H and 1V:3H (section 4.1.3). This approach provided new knowledge regarding the impact of side slope on the stability of geobag revetment. According to laboratory observations, sliding happens easily for model geobags on bank slope of 1V:1.25H.Compared with two other slopes, it makes the whole structure significantly unstable. Considering the different geotechnical nature of riverbank in the field, it is recommended that for slopes steeper than 1V:2H, the slope of the riverbank to be flattened to 1V:2H before placing the geobags.

6.2.3. *Construction bonds*

A further element of novelty in the laboratory-scale analysis comprises the impact of construction bonds on revetment performance, were tested in laboratory using two different bonds namely a stack bond (0% longitudinal overlap) and a running bond (50% longitudinal overlap). For both construction bonds, the longest axis of geobags in the streamwise direction and with a transverse overlap varying between 50% to 60% depending on revetment slope (section 4.1.4). The geobag revetment performance made of different construction bonds has been a subject of investigation of initiation of bag failure in previous work undertaken by Akter *et al.* (2013), but this is the first time that it has been studied in the context of complete failure process of geobag revetment.

The outcome of the current study confirmed that although the hydraulic stability of a revetment is strongly dependent on revetment slope, water depth and flow conditions, it is generally independent of construction method (running bond or stack bond). The failure mechanisms of a revetment under any particular slope/depth scenario were found to be dependent on the contact area between individual geobags, which can be influenced by frictional resistance, rather than the precise bond configuration. This finding has important implications for revetment construction methods. Since in the field different placement methods (e.g. riverbank launching, pontoon launching) can lead to a wide range of different construction bonds (Oberhagemann and Hossain, 2011) and there is no precise rule for achieving target construction bonds among revetment while constructed (JMREM, 2006). This finding highlights an important advantage that present launching practices do not affect the hydraulic stability of geobag revetment within this scope.

6.2.4. *Detailed velocity analysis*

The experimental work presented an element of novelty as for the first time 3D flow characteristics were measured using a side looking ADV. In the work described here, an analysis of the Reynolds shear stress and turbulent intensity was performed. Other authors, such as Akter *et al.* (2013), performed similar investigations based on an analytical approach, but the work described here provides the first example of Reynolds shear stress being used as an indicator to determine the position of failure in terms of higher shear stress. Unlike previous work conducted by Akter *et al.* (2013), that limited their analysis to an analytical method by comparing Chow (1959) method with the CES for calculating active shear stress over geobags. The approach followed in this study (Section 4.2) was analysis of three-dimensional flow structures and turbulence characteristics around geobag revetment for pre- and post-failure conditions. The turbulence characteristics such as turbulence intensity, turbulent kinetic energy and Reynolds shear stresses showed that stronger turbulence structures occurred around the void spaces between bags. Accordingly, in terms of initiation of the failure process, revetments experience the highest turbulence and consequently initiation of bag displacement mainly occurs at void spaces.

6.3. DEM Model

The most relevant element of novelty in the work reported here is the introduction of the DEM model to reproduce failure mechanisms in a geobag revetment. It is clear that only a full-coupling DEM-CFD model can replicate incorporate geobag/water feedback mechanism accurately and reliably. Although, due to the high computational demands, this method is not cost effective and practical (Section 3.23). Therefore, in this study an attempt was made to develop a DEM model which reproduce failure processes of a geobag revetment exposed to hydrodynamic forces. The advantages of a DEM only model have been discussed in Section 3.2. However, the lack of work on the topic, as well as the total absence of numerical modelling has been reported (Section 2.5). Accordingly, the model was developed in this thesis represents an important advance compared to the existing literature, and provides a new, effective tool for investigating the performance of geobag revetment in riverbank protection works.

Akter (2011) conducted a numerical study using commercial EDEM® code to replicate the initiation of bag movement for both fixed bed (nonerodable bed) and mobile

sediment bed. But the work described here provides the first example of a Discrete Element Model (DEM) to replicate the complete failure process of geobag revetment observed in the laboratory using an open source DEM code (LIGGGHTS).

The open-source LIGGGHTS model provided a low cost and flexible numerical tool used to extend the knowledge about geobag revetment performance. The 3D LIGGGHTS model showed good agreement with laboratory observation for both geobag–water interaction in subsection 5.3 and geobag–water–mobile bed interaction detailed in subsection 5.4.

Akter (2011) showed that performed simulations using EDEM underlined the importance of predicting the critical locations for bag instability but did not reproduced any failure modes specifically. However, in the current study, three main failure modes (uplifting, pull-out and sliding) observed in the laboratory were simulated numerically and the DEM model was developed to the extent that different bag displacements due to different active forces were distinctively represented. The performance evaluation of a geobag revetment using a 3D representation of geobag revetment is the main significance of this thesis.

6.3.1. *DEM model application in design guideline*

The outcome of this thesis shows that the DEM model is a suitable tool to predict the performance of geobag revetments under different conditions. According to the result of this study (see Chapter 5) DEM model can provide valuable information on bag movement due to hydrodynamic forces. Therefore, the calibrated DEM model can be applied to clarify the processes affecting the stability of the geobag structure i.e. different placement method, revetment side slope and hydraulic condition and eventually used to develop a design guideline employing numerical simulation. DEM models were developed and calibrated in this study was based on the present geobag size and specifications as recommended by the (JMREM, 2006) and Akter (2011). In the recommended bag design specifications manually bag launching was considered. Although it can be appropriate to apply the DEM to show the impact of bag specifications (e.g. weight and size) and hence better justify its use to develop design guidance.

6.3.2. *Field information*

A numerical model would be applicable if it could provide a reasonable prediction on practical conditions. Therefore, the DEM model needs to be modified and developed to some extent so it cab be used to predict the geobag revetment performance in the field. To achieve this aim, field inspection should be undertaken to provide the required information for calibrating the DEM model. For an instant, in Brahmaputra/Jamuna River, field inspection using diver observations and also Bathymetric surveys before and after launching geobag revetment provided necessary information to evaluate the functionality of geobag structures (Oberhagemann and Hossain, 2011). Thus, if in the phase of inspections, the required parameters to calibrate the DEM model would be ascertained, DEM model could be developed sufficiently precise enough to be applied for performance evaluations of geobag revetments constructed in the field.

To use the calibrated DEM model presented in this study for predicting the performance of field geobag revetment following field information is required:

•Systematic water depth and 3D flow velocity measurement.

• A 3D bed profile before and after launching. Moreover, the rate of riverbank erosion and toe scour should be measured and included.

• In addition to all the above parameters, the specific failure modes in geobag revetment need to be identified and considered.

6.3.3. *Recommendations to Enhance the Performance of DEM model*

Although the numerical models used in this study developed to enhance the understanding of following processes associated with the stability of geobag structures:

• Complete failure mechanisms of geobag structures.

• Further clarification on the types of failure modes in a geobag revetment.

• Performance of the geobag structure under different construction specifications such as: (a) the slope angle of the structure and (b) different construction bonds.

One of the main and most important remaining tasks regarding the numerical model is to extend the model to simulate the effect of deformation on the process of failure considering the internal movement of sand inside the geobags. Figure 6.1 presents a primary DEM simulation of a deformed geobag. Pilarczyk (2000) reported that for the flow velocity higher than 1.5 m/s sand could move inside a bag in the same direction as flow. In these cases, a bag could roll because of this movement (Figure 6.1(B)). Due to

the small scale of modeled geobags such sand movement could not be observed in the scale models of geobags in the laboratory, so results presented in Figure 6.1 have not been validated.

Furthermore, to have a more realistic and accurate numerical representation of geobag structure performance, different type riverbanks (straight versus meandering) should be modelled, which may have implications on flow structure and the secondary flows on the spanwise direction. In general bends are the most vulnerable areas in rivers (in terms of erosion). Hence, the numerical model needs to be developed to simulate geobag revetment installed in a riverbend. Figure 6.2 shows a reproduced model of geobag revetment in a riverbend which needs to be calibrated and validated against field observation and laboratory experiments. Therefore, the further applications of DEM model can confirm that the present DEM model is an appropriate numerical tool that can be used to design infrastructure which applies geobags to provide revetment.

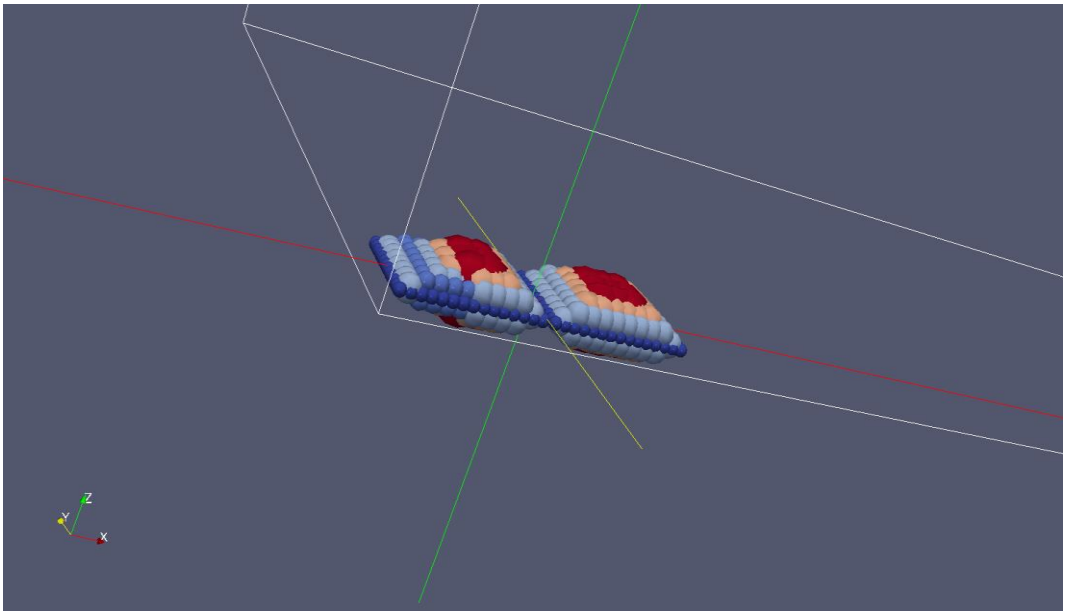

(A) a deformed geobag

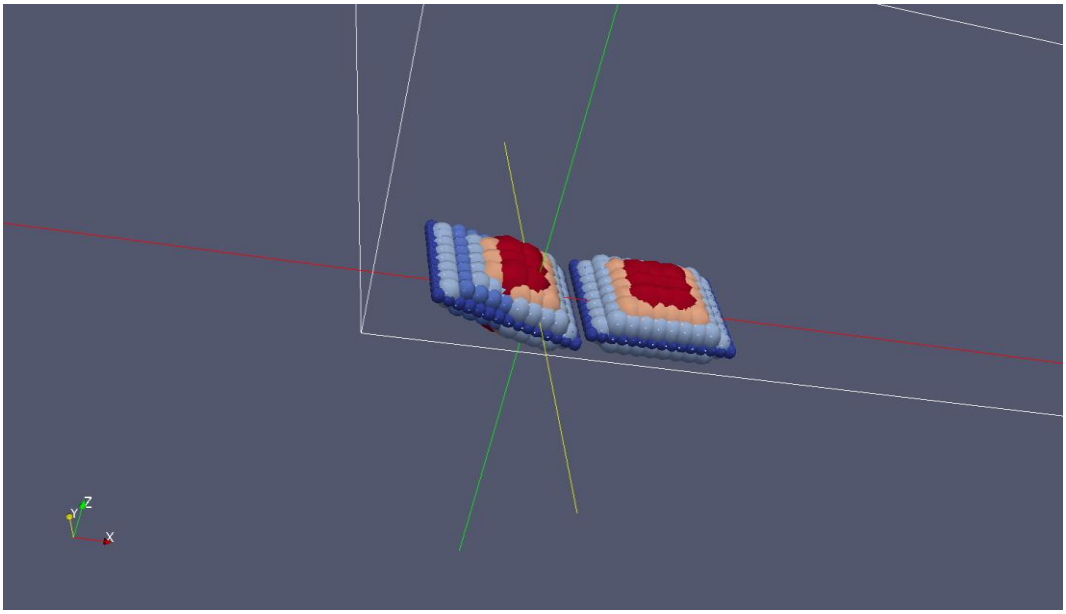

(B) geobag rolls due to deformation

Figure 6.1 (A and B): Primary DEM model of a deformed geobag (A) and rolling of geobag due to the deformation (B).

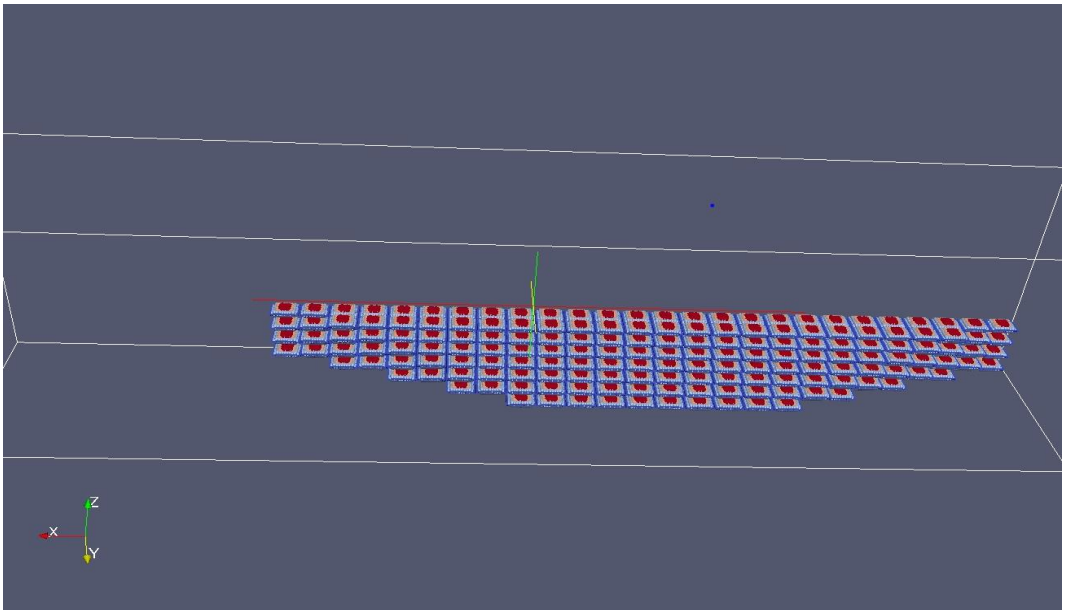

(A)

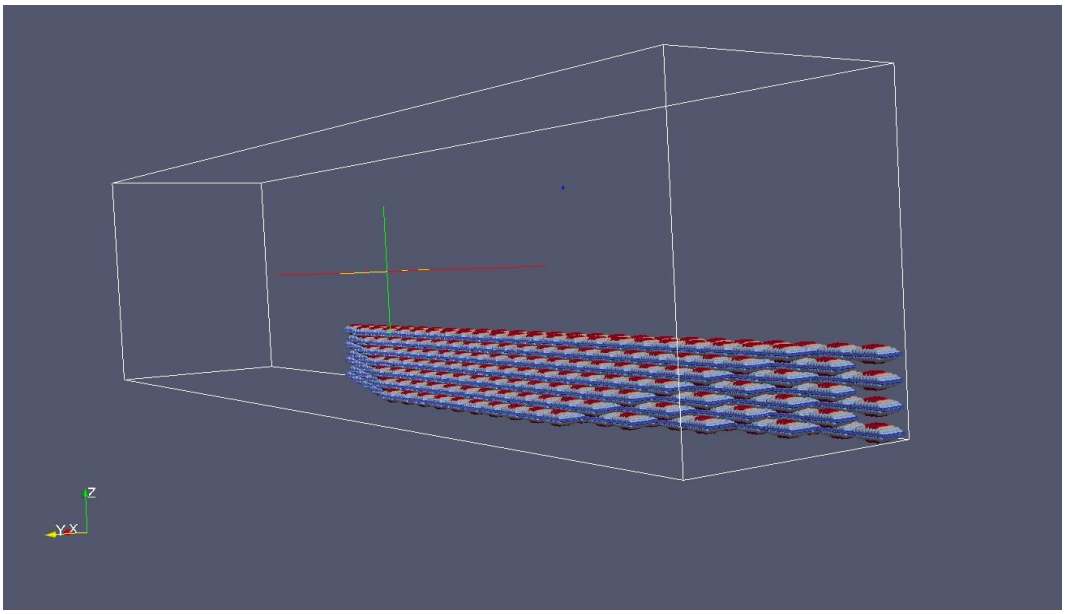

(B)

Figure 6.2: Primary DEM model of a bent geobag revetment.

6.4. Summary

Considering the existence of different flow nature and scouring nature of a riverbank in the field, to some extent the experimental study using a quasi-physical model could provide valuable information on the practical application of geobags.

The methodology and approach used to develop the DEM model can be adapted to any geobag structure in the field considering the actual properties or geometry of the geobags. However, the present LIGGGHTS model is calibrated and validated against information obtained from a geobag revetment tested in the laboratory. By considering the site-specific conditions and properties of the geobags, DEM model could be modified to predict the geobag revetment performances in the field through model calibration. Similar to geobag structures a validated DEM model can be applied for evaluating any riverbank structure made of discrete elements such as rocks and concrete blocks. However, for each type of structure the appropriate force coefficients C_D and C_L should be derived.

Chapter 7. CONCLUSIONS AND RECOMENDATIONS FOR FURTHER WORK

Riverbank protection revetments constructed from sand-filled geotextile bag are increasingly being used in developing countries. Compared to more expensive hard alternatives such as concrete or rubble material, using geobags provides low cost and readily available protections which are also proven to be environmentally advantageous. Despite the extensive research on coastal geobag structures, the processes affecting the hydraulic stability of geobag revetments in rivers are not still clearly understood. Therefore, to improve understanding of the processes involved in the complete failure of geobag revetments, experimental and numerical studies were conducted mainly focusing on: (i) understanding of the processes related to the hydraulic stability of geobag revetment and associated failure modes through a laboratory investigation and (ii) development of a 3D Discrete Element Model (DEM) of a geobag revetment and its application in preparation a design guideline.

Based on the results obtained from different types of experimental and numerical tests, the failure processes associated with geobag revetment were studied with particular emphasis on the impact of side slope and construction bond on revetment performance under different hydraulic loading.

7.1. Summary of Main Results and Conclusions

7.1.1. *Experimental Study*

Firstly, to enhance the understanding of the processes that affect the stability of geobag revetments, several experimental runs were conducted with focusing on some factors which could influence the performance of revetment. The features of the geobag revetment investigated in laboratory were: (i) failure modes, (ii) hydraulic parameters of the flow, (iii) construction method i.e., running bond and stack bond (iv) revetment side slope (v) the magnitude of failure in each condition and (vi) the turbulent properties of flow in pre- and post-failure conditions. Based on the laboratory observation of several types of experimental runs, different failure modes and zones were identified in the geobag revetment for each type of flow condition. On the revetment, geobags are exposed to the flowing water and they are subjected to the hydrodynamic forces of Lift and Drag

caused by the flow over them. However, gravity (body force) was found to be the main stabilising force which acts against hydrodynamic forces to keep the geobags in place - provided that the side slope of revetment is not too steep, in which case gravity can develop a destabilising force hence sliding is the main failure mode. Depending on the water level and construction specifications of revetment (side slope and construction bond) some distinct failure modes were identified. In general, failure processes of the geobag revetments were completed throughout combinations of partial or full uplifting, pullout, and internal sliding.

Experimental results also indicated that, although failure mechanisms are strongly dependent on revetment slope, water depth and flow conditions they are generally independent of construction method (running bond or stack bond) with no mortar-like bonding between individual geobags. The integrity of a revetment under any particular slope/depth scenario was found to be dependent on the contact area between individual geobags, which can be considered a proxy for frictional resistance rather than the precise bond configuration. This finding has important implications for revetment construction methods.

In addition, a detailed velocity measurement using Acoustic Doppler Velocimeter (ADV) was conducted to evaluate the flow field in front of the revetment. A significant limitation noted for the physical model study was the highly turbulent flow in the flume. As this study was focussed on the complete failure processes of the geobag revetment, analysis of detailed velocity measured before and after the failure of revetment showed this limitation is acceptable from an experimental point of view. However, this limitation would still need cautious consideration for field applications. Other than the scale effect in the physical model, a significant challenge in a physical model study is basically related to frequent manual data measurement.

At pre-failure condition, higher values of stream-wise velocity were noticed around the void spaces between bags, and it can be concluded that voids are critical zones where the revetments experience the highest flow turbulence. Therefore, the maximum probability of bag motions can be expected. For the case of post-failure, the results showed that the failure process is self-regulating in that formation of failure zones lead to a decrease in turbulence and subsequent stabilisation of the failure process.

7.1.2. *Numerical Studies*

In the second part of the present study, a 3D Discrete Element Model (LIGHHHTS) is further developed partially coupled and validated to reproduce the range of the hydraulic model tests conducted in the laboratory. Details are described in Chapter 3 and 5. The DEM model could represent a good prediction of failure modes due to geobag–flow and geobag–flow–mobile sediment bed interactions. It also replicated laboratory observations with sufficient accuracy, particularly concerning geobag displacement and geobag velocities. The "one-way coupled" DEM model used in this study has represented geobag displacement due to drag force, lift force and toe scour throughout the complete failure processes. According to the results, a verified and calibrated DEM model could also be capable of evaluating geobag revetment performance in the field.

A 3D DEM model of the laboratory experiment was created using the LIGGGHTS open source, C++ and MPI parallel DEM code. In addition to hydraulic forces, the LIGGGHTS model accounted for geobag self-weight under gravity, sliding friction and tangential and normal forces in collisions using a Hertz-Mindlin soft-sphere collision model. The validated numerical model was applied to predict the performance of geobag revetment in different water depths. According to the results it is found that despite its simplicity, this validated one-way CFD-DEM model could reproduce the complete failure processes of revetments very well including the location and pattern of failure on a fixed bed.

Furthermore, the applicability of the LIGGGHTS model to simulate the performance of geobag revetment mounted on a mobile sediment bed was investigated. In this case, the DEM model results were validated against laboratory observations conducted by Akter, Crapper, *et al.*, (2013). The DEM model using LIGGGHTS could well-represent the revetment failure modes under the influence of toe scouring associated with different water level conditions.

As this thesis aims to contribute to preparing a practical design guideline, the calibrated DEM can be expected to provide reasonable information to identify the desired performance of geobag revetment through prediction of bag displacement considering the active forces.

The main contribution of the thesis is the application of a 3D Discrete Element Model (DEM) in preparation of design guideline for geobag revetment. Results of this numerical

study confirm that the present calibrated DEM model provides a useful tool used to develop guidance on the performance of geobag revetments in riverbank situations.

The DEM model showed promising potential as an engineering tool to investigate the stability of different type of geobag structures. Thus, the calibrated DEM model presented in this study could provide important information needed to prepare a more practical design guideline.

7.2. Further research recommendations

This study has noticeably helped to improve the available knowledge on the hydraulic stability of geobag revetments used in rivers. Despite the results achieved in this study, additional research still is required to understand the geo-hydraulic processes associated with the stability of geobag revetments.

Thus, to achieve a more realistic and accurate prediction of geobag revetment performance in rivers, the numerical models used in this study need to be developed and calibrated to:

- Analyse the effect of deformation of geobag. As the deformations of the geobag could significantly affect the hydraulic stability of geobag structures, the internal movement of sand inside the geotextile bag must be simulated and the impact of consequent deformation on the process of failure need to be understood.
- Represent a numerical model of geobag revetment installed at a riverbend.
- Simulate large-scale models with prototype dimensions to overcome the scaling problem.

Based on the finding of this research study, it is recommended to conduct further investigations on the following topics:

- For prototype geobag structures in the field a comprehensive monitoring programme is needed to investigate an optimum performance over effective design lifetime and also to acquire data required for validating numerical and physical models.
- Scaling of geotextile and fill material is one of the main challenges when designing a small-scale experiment setup on the geobag structure. Therefore,

choosing appropriate materials for the physical models should be based on an exhaustive understanding of the physical and mechanical properties of available materials. So, it is strongly recommended to undertake additional studies to recognise scaling problems associated with geotextile and fill material in the small-scale physical models of the geobag revetment.

Furthermore, due to the lack of reliable stability formula for geobag structures in rivers, systematic numerical and experimental studies are needed to develop an appropriate stability formula. This formula must contain the critical engineering properties of geobags and required force coefficients in the formula, need to be determined for geobags in different locations and configurations.

REFERENCES

Abbaspour-Fard, M. H. (2004) 'Theoretical validation of a multi-sphere, discrete element model suitable for biomaterials handling simulation', *Biosystems engineering*. Elsevier, 88(2), pp. 153–161.

ADB (2002) *Report and Recommendation of the President to the Board of Directors on a Loan Proposed to the People's Republic of Bangladesh for the JamunaMeghna River Erosion Mitigation Projects*.

Akter, A. (2011) *Modelling of geobags for river bank protection*. Heriot-Watt University. Available at: http://hdl.handle.net/10399/2419.

Akter, A., Crapper, M., Pender, G., Wright, G. and Wong, W. (2013) 'Performance of a geobag revetment. ii: numerical modeling', *Journal of Hydraulic Engineering*. American Society of Civil Engineers, 139(8), pp. 877–885.

Akter, A., Pender, G., Wright, G. and Crapper, M. (2011) 'Predicting the hydrodynamic forces on geobag revetments', *Journal of Flood Risk Management*, 4(4), pp. 328–338. doi: 10.1111/j.1753-318X.2011.01117.x.

Akter, A., Pender, G., Wright, G. and Crapper, M. (2013) 'Performance of a geobag revetment. I: Quasi-physical modeling', *Journal of Hydraulic Engineering*. American Society of Civil Engineers, 139(8), pp. 865–876.

Akter, A., Wright, G., Crapper, M. and Pender, G. (2009) 'Failure Mechanism in Geobag Structure', in *Proceedings of the 4th IASME / WSEAS Int. Conference on WATER RESOURCES, HYDRAULICS & HYDROLOGY*.

Amberger, S., Friedl, M., Goniva, C., Pirker, S. and Kloss, C. (2012) 'Approximation of objects by spheres for multisphere simulations in DEM', *ECCOMAS-2012*.

Artieres, O., Lostumbo, J., Watn, A., Bverfjord, M. G. G., Delmas, P., Caquel, F., Grande, L. and Langeland, A. (2010) 'Geosynthetics as eco-friendly defence against erosion in arctic regions', *Geo2010, Calgary, Alberta, Canada*, pp. 634–641.

Bezuijen, A., Adel, H. den, Groot, M. B. de and Pilarczyk, K. W. (2001) 'Research on geocontainers and its application in practice', in *Coastal Engineering 2000*, pp. 2331–2341.

Bezuijen, A., De Groot, M. B., Breteler, M. K. and Berendsen, E. (2004) 'Placing accuracy and stability of geocontainers', in *Proc. EuroGeo*.

Bird, R. B., Stewart, W. E. and Lightfoot, E. N. (2002) 'Transport phenomena. 2nd', *New York*.

Brand, E. W. and Pang, P. L. R. (1991) 'Durability of geotextiles to outdoor exposure in Hong Kong', *Journal of geotechnical engineering*. American Society of Civil Engineers, 117(7), pp. 979–1000.

British Standards Institution (BSI) (1991) 'Methods of test for geotextiles. Determination of sand-geotextile frictional behaviour by direct shear', *BSI London*. London.

British Standards Institution (BSI) (1992) 'Methods of test for nonwovens. Methods of test for nonwovens. Determination of tensile strength and elongation', *BSI London*. London.

British Standards Institution (BSI) (1995) 'Methods of test for nonwovens. Methods of test for nonwovens. Determination of tensile strength and elongation', *BSI London*. London.

British Standards Institution (BSI) (2007) 'Hydrometry. Measurement of liquid flow in open channels using current-meters or floats', *BSI London*.

Carollo, F. G., Ferro, V. and Termini, D. (2002) 'Flow velocity measurements in vegetated channels', *Journal of Hydraulic Engineering*. American Society of Civil Engineers, 128(7), pp. 664–673.

Coastal Area Management Act (CAMA) (2008) *No Title*. Available at: https://deq.nc.gov/about/divisions/coastal-management.

Coghlan, I., Carley, J., Cox, R., Blacka, M., Mariani, A., Restall, S., Hornsey, W. and Sheldrick, S. (2009) 'Two-dimensional physical modelling of sand filled Geocontainers for coastal protection', *Coasts and Ports 2009: In a Dynamic Environment*. Engineers Australia, p. 295.

Crapper, M., Ooi, J., Favier, J. and Golz, P. (2005) 'Coupled Continuum-Discrete Modelling of Solid-Fluid Phase Flow', in *7th World Congress of Chemical Engineering, Glasgow, UK*.

Dassanayake, D. T. and Oumeraci, H. (2007) 'Hydraulic Stability of Coastal Structures Made of Geotextile Sand', *Leichtweiss-Institute for Hydraulic Engineering and Water Resources, Technische Universitaet Braunschweig*, 1(33), pp. 1–14. doi: 10.1260/1759-3131.3.3.135.

Dassanayake, D. T. and Oumeraci, H. (2009) 'Planned research on the hydraulic stability of geotextile sand containers, 7', in *FZK-Kolloquium, Potenziale für die Maritime Wirtschaft", Hannover, Germany*.

Dassanayake, D. T. and Oumeraci, H. (2012a) 'Engineering properties of geotextile sand containers and their effect on hydraulic stability and damage development of low-crested/submerged structures', *The International Journal of Ocean and Climate Systems*. SAGE Publications Sage UK: London, England, 3(3), pp. 135–150.

Dassanayake, D. T. and Oumeraci, H. (2012b) 'Important engineering properties of geotextile sand containers and their effect on the hydraulic stability of GSC-structures', *Terra et Aqua Journal*, 127, pp. 3–11.

DCS Computing (2018). Available at: https://www.dcs-computing.com/.

Favier, J. F., Abbaspour-Fard, M. H., Kremmer, M. and Raji, A. O. (1999) 'Shape representation of axi-symmetrical, non-spherical particles in discrete element simulation using multi-element model particles', *Engineering computations*. MCB UP Ltd, 16(4), pp. 467–480.

Ferellec, J.-F. and McDowell, G. R. (2010) 'A method to model realistic particle shape and inertia in DEM', *Granular Matter*. Springer, 12(5), pp. 459–467.

Gadd, P. E. (1988) 'Sand bag slope protection: Design, construction, and performance', in *Arctic Coastal Processes and Slope Protection Design*. ASCE, pp. 145–165.

García, C. M., Cantero, M. I., Niño, Y. and García, M. H. (2005) 'Turbulence Measurements with Acoustic Doppler Velocimeters', *Journal of Hydraulic Engineering*. American Society of Civil Engineers, 131(12), pp. 1062–1073. doi: 10.1061/(ASCE)0733-9429(2005)131:12(1062).

García, C. M., Cantero, M. I., Niño, Y. and García, M. H. (2007) 'Closure to "Turbulence Measurements with Acoustic Doppler Velocimeters"', *Journal of Hydraulic Engineering*. American Society of Civil Engineers, 133(11), pp. 1289–1292.

Garcia, X., Latham, J.-P., XIANG, J. and Harrison, J. P. (2009) 'A clustered overlapping sphere algorithm to represent real particles in discrete element modelling', *Geotechnique*. Thomas Telford Ltd, 59(9), pp. 779–784.

Garcin, P., Faure, Y. H., Gourc, J. P. and Purwanto, E. (1995) 'Behaviour of geosynthetic clay liner (GCL): laboratory tests', in *Proceedings of the 5th International Symposium on Landfills, Cagliari*, pp. 347–358.

GEOFABRICS (2018) *COASTAL & WATERWAYS SMARTER SOLUTIONS, GEOFABRICS AUSTRALASIA PTY LTD*. Available at: https://www.geofabrics.co.

Goring, D. G. and Nikora, V. I. (2002) 'Despiking acoustic Doppler velocimeter data',

Journal of Hydraulic Engineering. American Society of Civil Engineers, 128(1), pp. 117–126.

Grima, A. P. and Wypych, P. W. (2011) 'Development and validation of calibration methods for discrete element modelling', *Granular Matter*, 13(2), pp. 127–132. doi: 10.1007/s10035-010-0197-4.

Grima, A. and Wypych, P. (2013) 'Effect of Particle properties on the Discrete Element Simulation of Wall Friction'.

Grüne, J., Sparboom, U., Schmidt-Koppenhagen, R., Wang, Z. and Oumeraci, H. (2007) 'Stability tests of geotextile sand containers for monopile scour protection', in *Coastal Engineering 2006: (In 5 Volumes)*. World Scientific, pp. 5093–5105.

Gutman, A. L. (1979) 'Low-cost shoreline protection in Massachusetts', in *Coastal Structures' 79*. ASCE, pp. 373–387.

Heerten, G., Jackson, A., Restall, S. and Saathoff, F. (2000) 'New developments with mega sand containers of non-woven needle-punched geotextiles for the construction of coastal structures', in *27th International Conference on Coastal Engineering, Sydney, Australia, July*.

Heerten, G., Jackson, A., Restall, S. and Stelljes, K. (2000) 'Environmental benefits of sand filled geotextile structures for coastal applications', in *ISRM International Symposium*. International Society for Rock Mechanics.

Heerten, G., Klompmaker, J. and Partridge, A. (2008) 'Design and construction of waterfront structures with special designed non-woven geotextiles', in *Proceedings*.

Heibaum, M. H. (1999) 'Coastal scour stabilisation using granular filter in geosynthetic nonwoven containers', *Geotextiles and Geomembranes*. Elsevier, 17(5–6), pp. 341–352.

Heibaum, M., Oberhagemann, K., Faisal, M. A. and Haque, S. (2008) 'Geotextile bags for sole permanent bank protection', in *Proc. 4. European Conf. on Geosynthetics, Edinburgh*.

Hellevang, K. (2011) 'Sandbagging for flood protection', *NDSU and U.S. Department of Agriculture*.Available at: https://library.ndsu.edu/ir/bitstream/handle/10365/15108/ae626.pdf?sequence=1.

Hölzer, A. and Sommerfeld, M. (2008) 'New simple correlation formula for the drag coefficient of non-spherical particles', *Powder Technology*. Elsevier, 184(3), pp. 361–365.

Hornsey, W. P., Carley, J. T., Coghlan, I. R. and Cox, R. J. (2011) 'Geotextile sand container shoreline protection systems: Design and application', *Geotextiles and Geomembranes*. Elsevier, 29(4), pp. 425–439.

Hornsey, W. P., Jackson, L. A., Restall, S. J. and Corbett, B. (2003) 'Large sand filled geotextile containers as a construction aid over poor quality marine clay', in *Coasts & Ports 2003 Australasian Conference: Proceedings of the 16th Australasian Coastal and Ocean Engineering Conference, the 9th Australasian Port and Harbour Conference and the Annual New Zealand Coastal Society Conference*. Institution of Engineers, Australia, p. 629.

Hudson, R. Y. (1959) 'Laboratory investigation of rubble-mound breakwaters', *Reprint of the original paper as published in the Journal of the Waterways and Harbors Division of ASCE, proceedings paper 2171*. Citeseer.

Hughes, S. A. (1993) *Physical models and laboratory techniques in coastal engineering*. World Scientific.

Ikeda, S. and Kanazawa, M. (1996) 'Three-dimensional organized vortices above flexible water plants', *Journal of Hydraulic Engineering*. American Society of Civil Engineers, 122(11), pp. 634–640.

JACKSON, A., CORBETT, B. and Restall, S. (2006) 'Failure modes & stability modelling for design of sand filled geosynthetic structures', in *30th International Conference on Coastal Engineering*, pp. 1–20.

JMREM (2006) 'Jamuna-Meghna River Erosion Mitigation Project Part B. Special Report 17, Geobag Revetments', *Government of the People's Republic of Bangladesh, Asian Development Bank and Bangladesh Water Development Board.*

Kafui, K. D. and Thornton, C. (2000) 'Numerical simulations of impact breakage of a spherical crystalline agglomerate', *Powder Technology*. Elsevier, 109(1–3), pp. 113–132.

Kim, H. T., Yoo, S. D., Park, S. S., Lee, J. H. and Lee, C. J. (2004) 'A fundamental approach for an investigation of behaviour characteristics of the vegetation structures using seeded sandbags', in *Proc. of the 3rd Asia Regional Conference on Geosynthetics. Seoul, Korea*. Citeseer, pp. 225–232.

Kobayashi, N. and Jacobs, B. K. (1985) 'Experimental study on sandbag stability and runup', in *Coastal Zone'85*. ASCE, pp. 1612–1626.

Korkut, R., Martinez, E. J., Morales, R., Ettema, R. and Barkdoll, B. (2007) 'Geobag performance as scour countermeasure for bridge abutments', *Journal of Hydraulic*

Engineering. American Society of Civil Engineers, 133(4), pp. 431–439.

Kouwen, N., Unny, T. E. and Hill, H. M. (1969) 'Flow retardance in vegetated channels', *Journal of the Irrigation and Drainage Division*. ASCE, 95(2), pp. 329–344.

Krahn, T., Blatz, J., Alfaro, M. and Bathurst, R. J. (2007) 'Large-scale interface shear testing of sandbag dyke materials', *Geosynthetics International*. Thomas Telford Ltd, 14(2), pp. 119–126.

Lawson, C. R. (2008) 'Geotextile containment for hydraulic and environmental engineering', *Geosynthetics International*. Thomas Telford Ltd, 15(6), pp. 384–427.

Lohrmann, A., Cabrera, R. and Kraus, N. C. (1994) 'Acoustic-Doppler velocimeter (ADV) for laboratory use', in *Fundamentals and advancements in hydraulic measurements and experimentation*. ASCE, pp. 351–365.

Lu, G., Third, J. R. and Müller, C. R. (2015) 'Discrete element models for non-spherical particle systems: from theoretical developments to applications', *Chemical Engineering Science*. Elsevier, 127, pp. 425–465.

Matsuoka, H., Liu, S. H. and Yamaguchi, K. (2001) 'Mechanical properties of soilbags and their application to earth reinforcement', in *Proceedings of the international symposium on earth reinforcement, Fukuoka, Japan*, pp. 587–592.

Matsushima, K., Aqil, U., Mohri, Y. and Tatsuoka, F. (2008) 'Shear strength and deformation characteristics of geosynthetic soil bags stacked horizontal and inclined', *Geosynthetics International*. Thomas Telford Ltd, 15(2), pp. 119–135.

Mori, Enrica, Amini, P. L. and Eliso, C. D. (2008) 'Field experiment on a groin system built with sand bags', in *International Conference on Coastal Engineering*, p. 219.

Mori, E, D'eliso, C. and Aminti, P. L. (2008) 'Physical modelling on geotextile sand container used for submerged breakwater', in *Proceedings of 2nd international conference on the application of physical modelling to port and coastal protection, Coastlab08, Bari, Italy*.

Mudiyanselage, D. T. B. D. D. (2013) 'Experimental and Numerical Modelling of the Hydraulic Stability of Geotextile Sand Containers for Coastal Protection'.

Mustoe, G. G. W. and Miyata, M. (2001) 'Material flow analyses of noncircular-shaped granular media using discrete element methods', *Journal of Engineering Mechanics*. American Society of Civil Engineers, 127(10), pp. 1017–1026.

NAUE GmbH &Co. KG (2006) 'No TitleAdvantages of Needle-punched Secutex® and Terrafix® Nonwoven Geotextiles', *NAUE GmbH &Co. KG, Germany*.

Neill, C., Mannerstrom, M. and Azad, A. K. (2008) 'Model tests on geobags for erosion protection', in *Proceedings of the International Conference on Scour and Erosion, Tokyo, Japan*, pp. 5–7.

Das Neves, L., Lopes, M. L., Gomes, F. V. and Pinto, F. T. (2012) 'Physical modeling of sand-filled geosystems for coastal protection', in *2nd European Conference on Physical Modelling on Geotechnics-Eurofuge2012*.

NHC, N. H. C. (2006) 'Jamuna-Meghna River Erosion Mitigation Project Part B. Special Report 11, Physical Model Study (Vancouver, Canada), Final Report, Government of the People's Republic of Bangladesh, Asian Development Bank and Bangladesh Water Development Board.'

NORTEK (2018) *What are the differences between and advantages of side-looking and down-looking Vectrino probes?*, *NORTEK GROUP*. Available at: https://www.nortekgroup.com.

NSW (2011) 'No Title Minister's Requirements under the Coastal Protection Act 1979', *Department of Environment, Climate Change and Water, NSW*. Available at: www.environment.nsw.gov.au.

Oberhagemann, K. and Hossain, M. M. (2011) 'Geotextile bag revetments for large rivers in Bangladesh', *Geotextiles and Geomembranes*. Elsevier, 29(4), pp. 402–414.

Oberhagemann, K., Stevens, M. A., Haque, S. M. S. and Faisal, M. A. (2006) 'Geobags for Riverbank Protection', in *ICSE-3rd International Conference on Scour and Erosion*, pp. 1–3.

Obermayr, M., Vrettos, C., Eberhard, P. and Däuwel, T. (2014) 'A discrete element model and its experimental validation for the prediction of draft forces in cohesive soil', *Journal of Terramechanics*. Elsevier Ltd.

Odgaard, A. J. and Bergs, M. A. (1988) 'Flow processes in a curved alluvial channel', *Water Resources Research*. Wiley Online Library, 24(1), pp. 45–56.

Oumeraci, H. (1994) 'Review and analysis of vertical breakwater failures—lessons learned', *Coastal Engineering*. Elsevier, 22(1–2), pp. 3–29.

Oumeraci, H. (2004) 'Sustainable coastal flood defences: scientific and modelling challenges towards an integrated risk-based design concept', in *Proc. First IMA International Conference on Flood Risk Assessment, IMA-Institute of Mathematics and its Applications, Session*, pp. 9–24.

Oumeraci, H., Hinz, M., Bleck, M. and Kortenhaus, A. (2003) 'Sand-filled geotextile

containers for shore protection', *COPEDEC VI, Colombo, Sri Lanka*.

Oumeraci, H., Kortenhaus, A. and Werth, K. (2009) 'Hydraulic perfomance and armour stability of rubble mound breakwaters with core made of geotextile sand containers: comparison with conventional breakwaters', in *Coastal Structures 2007: (In 2 Volumes)*. World Scientific, pp. 41–52.

Oumeraci, H. and Recio, J. (2010) 'Geotextile sand containers for shore protection', in *Handbook of Coastal and Ocean Engineering*. World Scientific, pp. 553–600.

Padrós, C. B. (2014) 'Discrete element simulations with LIGGGHTS', *College of Engineering in Computational Mechanics. Swansea University*.

Parteli, E. J. R. (2013) 'Using LIGGGHTS for performing DEM simulations of particles of complex shapes with the multisphere method', in *Proc. In: DEM6-6th International Conference on Discrete Element Methods and Related Techniques, Golden USA Google Scholar*.

PIANC (2011) *The Application of Geosynthetics in Waterfront Areas*. PIANC Secrétariat Général (MarCom report 113). Available at: https://books.google.co.uk/books?id=aq7Z6H4jplAC.

Pilarczyk, K. (2000) *Geosynthetics and geosystems in hydraulic and coastal engineering*. CRC Press.

Porraz, J. L., Maza, A., Jose, A. and Medina, R. (1979) 'Mortar-Filled Containers, Lab and Ocean Exeriences', in *Coastal Structures' 79*. ASCE, pp. 270–289.

Rahman, A. (2010) 'Comparative analysis of design and performance of bank protection works of Jamuna River at Titporol and Debdanga'. Department of Water Resources Engineering.

Ray, R. (1977) *A Laboratory Study of the Stability of Sand-Filled Nylon Bag Breakwater Structures.* COASTAL ENGINEERING RESEARCH CENTER FORT BELVOIR VA.

Recio, J. (2008) *Hydraulic stability of geotextile sand containers for coastal structures–effect of deformations and stability formulae*. der Technischen Universität Carolo-Wilhelmina zu Braunschweig. Available at: https://publikationsserver.tu-braunschweig.de/servlets/MCRFileNodeServlet/dbbs_derivate_00004679/ediss.pdf.

Recio, J. and Oumeraci, H. (2009a) 'Hydraulic stability of geotextile sand containers for coastal structures–effect of deformations and stability formulae', in *Coastal Engineering 2008: (In 5 Volumes)*. World Scientific, pp. 3805–3817.

Recio, J. and Oumeraci, H. (2009b) ‘Process based stability formulae for coastal structures made of geotextile sand containers’, *Coastal Engineering*. Elsevier, 56(5), pp. 632–658.

Recio, J. and Oumeraci, H. (2009c) ‘Processes affecting the hydraulic stability of coastal revetments made of geotextile sand containers’, *Coastal Engineering*. Elsevier, 56(3), pp. 260–284.

Recio, J., Oumeraci, H. and Mocke, G. (2010) ‘Stability formula and numerical model for structures made with geotextile sand containers used for coastal stabilization’, in *2nd International Conference on Coastal Zone Engineering and Management (Arabian Coast 2010), Muscat, Oman*.

Restall, S. J., Hornsey, W., Oumeraci, H., Hinz, M., Saathoff, F. and Werth, K. (2005) ‘Australian and German experiences with geotextile containers for coastal protection’, in *Proceedings of the 3rd European Geosynthetics Conference, Munich, Germany, German Geotechnical Society, pp141-146*.

Restall, S. J., Jackson, L. A., Heerten, G. and Hornsey, W. P. (2002) ‘Case studies showing the growth and development of geotextile sand containers: an Australian perspective’, *Geotextiles and Geomembranes*. Elsevier, 20(5), pp. 321–342.

Robin, A. (2004) ‘Paper bag problem’, *Mathematics Today-Bulletin of the Institute of Mathematics and its Applications*. Southend-on-Sea, Essex: Institute of Mathematics and Its Applications, 1996-, 40(3), pp. 104–107.

Roy, A. G., Buffin-Belanger, T., Lamarre, H. and Kirkbride, A. D. (2004) ‘Size, shape and dynamics of large-scale turbulent flow structures in a gravel-bed river’, *Journal of Fluid Mechanics*. Cambridge University Press, 500, pp. 1–27.

Saathoff, F., Oumeraci, H. and Restall, S. (2007) ‘Australian and German experiences on the use of geotextile containers’, *Geotextiles and Geomembranes*. Elsevier, 25(4), pp. 251–263.

Sadik, M. S., Wahed, S. and Mohsina Muhit, S. (2011) ‘Environmental Impact of Using Sand filled Geobag Technology under Water in River Erosion Protection of Major Rivers of Bangladesh’, in.

Scottish Natural Heritage (2000) *Scottish Natural Heritage*. Available at: https://www.nature.scot.

Van Steeg, P. and Klein Breteler, M. (2008) *Large scale physical model tests on the stability of geocontainers*. Delft Cluster.

Van Steeg, P. and Vastenburg, E. W. (2010) *Large scale physical model tests on the stability of geotextile tubes, Deltares report 1200162-000*. Deltares.

Strom, K. B. and Papanicolaou, A. N. (2007) 'ADV measurements around a cluster microform in a shallow mountain stream', *Journal of Hydraulic Engineering*. American Society of Civil Engineers, 133(12), pp. 1379–1389.

TenCate (2018) *TenCate Geosynthetics Asia*. Available at: http://www.tencate.com/apac/geosynthetics/case-studies/hydraulic marine/news-hm4.aspx.

Tilley, R. J. D. (2004) *Understanding solids: the science of materials*. John Wiley & Sons, West Sussex.

Tomlinson, M. and Woodward, J. (2007) *Pile design and construction practice*. Crc Press.

Tran-Cong, S., Gay, M. and Michaelides, E. E. (2004) 'Drag coefficients of irregularly shaped particles', *Powder Technology*. Elsevier, 139(1), pp. 21–32.

US Army Corps of Engineers (2004) 'Sandbagging Techniques', *Northwestern Division, USA.*

Venis, W. A. (1968a) 'Closure of estuarine channels in tidal region, Behaviour of dumping material when exposed to currents and wave action (in Dutch)'', *De Ingenieur,* 50.

Venis, W. A. (1968b) 'Closure of estuarine channels in tidal regions', *Behaviour of dumping material when exposed to currents and wave action, De ingenieur,* 50, p. 1968.

Weigler, F. and Mellmann, J. (2014) 'Investigation of grain mass flow in a mixed flow dryer', *Particuology*. Elsevier, 12, pp. 33–39.

White, F. M. (2003) 'Fluid mechanics. 5th', *Boston: McGraw-Hill Book Company*.

Wouters, J. (1998) *Open Taludbekledingen; stabiliteit van geosystems (Stability of Geosystems), Delft Hydraulics Report H-1930, Annex 7, Delft: Delft Hydraulics. Sewing delays construction time*.

Yang, S. Q., Shu, Y. M. and Yang, X. C. (2008) 'Flume experiment and numerical analysis for bank reinforcement with geocontainer', in *Geosynthetics in Civil and Environmental Engineering*. Springer, pp. 630–636.

Yin, C., Rosendahl, L., Kær, S. K. and Sørensen, H. (2003) 'Modelling the motion of cylindrical particles in a nonuniform flow', *Chemical Engineering Science*. Elsevier, 58(15), pp. 3489–3498.

Zhu, L., Wang, J., Cheng, N.-S., Ying, Q. and Zhang, D. (2004) 'Settling distance and incipient motion of sandbags in open channel flows', *Journal of waterway, port, coastal, and ocean engineering*. American Society of Civil Engineers, 130(2), pp. 98–103.